UNIVERSITI TEKNOGI MARA

FORMULATION, CHARACTERISATION AND EVALUATION OF SUSTAINED RELEASE NICOTINE-LOADED CHITOSAN AND BUTYLGLYCEROL-CHITOSAN NANOPARTICLES INTRANASAL DELIVERY FOR POTENTIAL SMOKING CESSATION THERAPY

WASAN IBRAHIM MOHAMMAD ALWAHSH

PhD

September 2026

UNIVERSITI TEKNOLOGI MARA

FORMULATION, CHARACTERISATION AND EVALUATION OF SUSTAINED RELEASE NICOTINE-LOADED CHITOSAN AND BUTYLGLYCEROL-CHITOSAN NANOPARTICLES INTRANASAL DELIVERY FOR POTENTIAL SMOKING CESSATION THERAPY

WASAN IBRAHIM MOHAMMAD ALWAHSH

Thesis submitted in fulfilment of
the requirements for the degree of
Doctor Of Philosophy
(Pharmaceutics)

Faculty of Pharmacy

September 2026

CONFIRMATION BY PANEL OF EXAMINERS

I certify that a Panel of Examiners has met on 2 July 2026 to conduct the final examination of Wasan Ibrahim Mohammad Alwahsh on her Doctors of Philosophy thesis entitled "Formulation, characterisation and evaluation of sustained release nicotine-loaded chitosan and butylglycerol-chitosan nanoparticles intranasal delivery for potential smoking cessation therapy." in accordance with Universiti Teknologi MARA Act 1976 (Akta 173). The Panel of Examiner recommends that the student be awarded the relevant degree. The Panel of Examiners was as follows:

Lim Siong Meng, Professor, PhD
Professor
Faculty of Pharmacy
Universiti Teknologi MARA
(Chairman)

Meor Mohd Redzuan Meor Mohd Affandi, PhD
Associate Professor
Faculty of Pharmacy
Universiti Teknologi MARA
(Internal Examiner)

Haliza Katas, PhD
Professor
Faculty of Pharmacy
Universiti Kebangsaan Malaysia
(External Examiner)

PROF DR HJH ZURAEDA IBRAHIM
DEAN
Institute of Postgraduates Studies
Universiti Teknologi MARA
Date: 22 September 2026

AUTHOR'S DECLARATION

I declare that the work in this thesis was carried out in accordance with the regulations of Universiti Teknologi MARA. It is original and is the results of my own work, unless otherwise indicated or acknowledged as referenced work. This thesis has not been submitted to any other academic institution or non-academic institution for any degree or qualification.

I, hereby, acknowledge that I have been supplied with the Academic Rules and Regulations for Post Graduate, Universiti Teknologi MARA, regulating the conduct of my study and research.

Name of Student	:	Wasan Ibrahim Mohammad Alwahsh
Student ID. No.	:	2022207462
Programme	:	Doctor of philosophy (pharmaceutics) – ph 964
Faculty	:	Pharmacy
Thesis Title	:	Formulation, characterisation and evaluation of sustained release nicotine-loaded chitosan and butylglycerol-chitosan nanoparticles intranasal delivery for potential smoking cessation therapy.

Signature of Student :

Date : August 2026

ABSTRACT

Cigarette smoking remains a main reason of worldwide death, while present smoking cessation therapies frequently fail to prevent nicotine cravings due to the short duration of action and poor patient adherence. Although intranasal delivery offers rapid onset, current nasal sprays need recurrent dosing. To overcome these limitations, sustained-release nicotine hydrogen tartrate-encapsulated chitosannanoparticles (NHT-loaded CS NPs) and butylglycerol-chitosan nanoparticles (NHT-loaded BG-CS NPs) were developed for intranasal delivery to prolong nicotine effects, which will reduce dosing frequency. Modification of CS by BG attachment was carried out through phthaloylation. Both CS NPs systems were then prepared using ionic gelation with tripolyphosphate (TPP) cross-linking. The physicochemical properties of the NPs, including particle size, zeta potential, encapsulation efficiency (EE%), drug loading (DL%), morphology, and stability, were characterized. Stability of the NPs were conducted at 5 ± 3°C and 25 ± 2°C/60 ± 5% relative humidity (RH) for 90 days. In *vitro* drug release was evaluated using dialysis bag method. Cytotoxicity of the NPs were performed using fibroblast and Calu-3 cells. Finally, in *vivo* pharmacokinetic studies of the intranasal NPs were conducted in male Sprague Dawley rats. For CS NPs, an optimal NHT:CS:TPP ratio of (F2) produced the smallest particle size (120.36 ± 3.23 nm), a positive zeta potential (+36.06 ± 1.70 +mV), high EE% (96.16 ± 0.76 %), and DL% of (15.82 ± 1.93%), with sustained release behavior and stability over 90 days. For BG-CS NPs, formulation F2" achieved a reduced particle size of (69.42 ± 0.72 nm), zeta potential of (+36.93 ± 0.89 +mV), EE% of (93.61 ± 0.34%), and enhanced DL% of (14.14 ± 0.47%), with sustained release behavior for over 5 hours. Both formulations exhibited spherical morphology, an amorphous state, improved thermal stability, and successful nicotine encapsulation. *In vitro* release studies of both CSNPs and BG CSNPs demonstrated sustained nicotine release for 8 hr, drug release was best described by the Korsmeyer–Peppas model. Cytotoxicity studies on fibroblast and Calu-3 human lung epithelial cells (Calu-3) exhibited minimal cytotoxicity with vell viability ≥ 70% for most formulations except, F1″ which show cell viability of (66.42 ± 4.11%) in Calu-3 cells and at the highest concentration of 0.5 mM. However, free nicotine showed cell viability of only 32.77 ± 3.57, indicaing more toxic effects. *In vivo* pharmacokinetic evaluation for F1, F2 , F1" and F2" demonstrated prolonged elimination half-life ($T_{1/2}$) (548.25 ± 110.91), (680.11 ± 313.34), (409.20 ± 105.84) and (278.10 ± 53.90) min respectively than free nicotine (113.60 ± 14.91) min and mean residence time (MRT) (365.61 ± 25.19), (381.38 ± 23.84) , (354.90 ± 36.95) and (513.20 ± 325.70) min resprctively than free nicotine (295.01 ± 25.45) min , consistent with sustained drug release. However, area under the curve (AUC) for F1, F2, F1" and F2" (191.77 ± 38.42), (189.15 ± 47.96), (167.80 ± 16.50) and (147.90 ± 2.78) mg·min/mL respectively lower than free nicotine (625.81 ± 83.23) mg·min/mL. In conclusion, nicotine-loaded CS and BG-CS NPs demonstrated promising physicochemical characteristics, sustained intranasal nicotine release, and favorable pharmacokinetic behavior, supporting their potential as sustained intranasal nicotine delivery systems.

ACKNOWLEDGEMENT

Firstly, I would like to express my deepest thankfulness to Allah for granting me the strength, patience and resolution to embark on and successfully complete this long and PhD journey. Without His blessings and guidance, this achievement would not have been possible. Alhamdulillah. I would like to extend my sincere appreciation and heartfelt thanks to my main supervisor, Associate Professor Dr. Shariza Sahudin, for her invaluable guidance, continuous support, and constructive advice throughout the course of this research. Her dedication, encouragement, and academic excellence have greatly contributed to the successful completion of this thesis. I am also deeply grateful to my co-supervisors, Dr. Hatim Alkhatib, Dr. Mohammad Bostanudin and Dr. Hanish Singh Jayasingh Chellammal, for their insightful comments, technical support and constant motivation, which have enriched this study and strengthened its scientific quality. My sincere appreciation is extended to the laboratory staff and technical team at Universiti Teknologi MARA for their assistance, cooperation and continuous support throughout this research. I would also like to express my deepest gratitude to my beloved husband Mohammad for his endless support, patience and encouragement throughout this journey. Without his unwavering belief in me. I am profoundly thankful to my dear children for their understanding, love and patience during my long periods of absence while pursuing my studies abroad. My sincere appreciation is also extended to my dear brother Dr Mohammad Alwahsh for his tremendous efforts, constant support and invaluable assistance throughout this journey. Finally, I am equally grateful to my beloved parents, my father-in-law, mother-in-law, my sisters and brothers for their prayers, encouragement and unconditional love, which have been a constant source of strength and motivation.

TABLE OF CONTENT

CONFIRMATION BY PANEL OF EXAMINERS **ii**

AUTHOR'S DECLARATION **iii**

ABSTRACT **iv**

ACKNOWLEDGEMENT **v**

TABLE OF CONTENT **vi**

LIST OF TABLES **xi**

LIST OF FIGURES **xiii**

LIST OF PLATES **xviii**

LIST OF SYMBOLS **xix**

LIST OF ABREVIATION **xx**

LIST OF NOMENCLATURE **xxiv**

CHAPTER 1 INTRODUCTION **1**

1.1 Research Background 1

1.2 Problem Statement 7

1.3 Research Objectives 8

1.3.1 General Objective 8

1.3.2 Specific Objectives 8

1.4 Research Question 9

1.5 Significance of Study 9

1.6 Assumption 10

1.7 Ethical Committee 11

1.8 Thesis Scope 11

1.9 Thesis Outline 12

CHAPTER 2 LITERATURE REVIEW **13**

2.1 Introduction 13

2.2 The Effects of Smoking on Health and Society 15

2.3 Problems with Current Smoking Cessation Treatments 16

2.4 The Pharmacology of Nicotine and Its Replacement Treatment 17
2.4.1 Nicotine's Physicochemical and Chemical Characteristics 17
2.4.2 Neuropharmacological Pathways Linked to Nicotine Addiction 19
2.4.3 Metabolism and Pharmacokinetic Profiles of Nicotine 21
2.4.4 Presently Available Treatments for Smoking Addiction 22
2.4.5 Medications used in NRT 24
2.5 Intranasal Drug Delivery for Brain Targeting 26
2.5.1 The Nasal Cavity's Anatomy and Physiology 26
2.5.2 Methods by Which Drugs Reach the Brain (Olfactory, Trigeminal, Systematic) 31
2.5.3 Benefits of Intranasal Administration 32
2.5.4 Challenges and Restrictions of Intranasal Administration 32
2.5.5 Therapeutic Uses of Intranasal Administration in CNS 33
2.6 CS and Its Uses in Drug Delivery 35
2.6.1 Origin, Chemical Composition, and Deacetylation level 35
2.6.2 CS Physicochemical Property 36
2.6.3 Intranasal Delivery of CS: Improving Mucoadhesion, Epithelial Permeation, and Biocompatibility. 36
2.6.4 Application of CS in Intranasal Delivery 37
2.7 CS NPs in Drug Delivery 40
2.7.1 Methods of CS NPs Synthesis 40
2.7.2 Factors Affecting NPs Properties 41
2.7.3 NPs Characterisation 44
2.7.4 Particle Size and Distribution 44
2.8 Drug Release Mechanism from CS 48
2.8.1 Mathematical Modeling Fitting of Drug Release Kinetics 50
2.9 Modified CS Derivatives for Enhanced Delivery 53
2.9.1 Rationale for Chemical Modification of CS 53
2.9.2 Types of CS Modifications 54
2.10 CS and Modified CS Physical Characteristics Comparison 58
2.11 NPs Safety and Biocompatibility 59

CHAPTER 3 RESEARCH METHODOLOGY 62

3.1 Introduction 62

3.2 Materials 62
3.3 Methods 63
3.3.1 Preparation of BG-CS 63
3.3.2 Preparation of CS NPs and BG-CS NPs (Blank and loaded NHT) 67
3.3.3 Preformulation Studies 68
3.3.4 Characterization of CS and BG-CS NPs 69
3.3.5 HPLC Analysis of NHT 70
3.3.6 EE% and DL% of CS and BG-CS NPs 72
3.3.7 Release Studies of CS and BG-CS NPs 72
3.3.8 Stability Studies CS and BG-CS NPs 73
3.3.9 Cytotoxicity Studies of CS and BG-CS NPs 73
3.3.10 In vivo Studies of CS and BG-CS NPs 75

CHAPTER 4 RESULT AND DATA ANALYSIS 79

4.1 Introduction 79
4.2 Preparation of BG-CS 79
4.2.1 Synthesis of Phthaloyl CS 79
4.2.2 Synthesis of BG Phthaloyl CS 80
4.2.3 Synthesis of BG-CS 82
4.3 Preformulation Studies and Development of CS NPs 83
4.3.1 Varying Ratios of CS and TPP 83
4.3.2 Varying Sonication Time 85
4.4 Characterization of CS and BG-CS NPs 86
4.4.1 Particle size, Zeta potential and PDI 86
4.4.2 Transmission Electron Microscopy (TEM) 89
4.4.3 Differential Scanning Calorimetry (DSC) 91
4.4.4 Thermogravimetric Analysis (TGA) 92
4.4.5 X-ray Diffraction (XRD) 93
4.4.6 Fourier Transform Infrared Spectroscopy (FTIR) 95
4.5 HPLC analysis of NHT 97
4.6 EE% and DL% of NPs 99
4.7 Release Studies of NPs 100
4.7.1 First Order Release Model 102
4.7.2 Higuchi Release Model 105

4.7.3 Hixson–Crowell Release Model 108
4.7.4 Korsmeyer-Peppas Release Model 110
4.8 Stability Studies of CS and BG-CS NPs (Blank and NHT-loaded) 112
4.8.1 Stability Studies of CS NPs 112
4.8.2 Stability Studies of BG-CS NPs 118
4.9 Cytotoxicity Studies of CS and BG-CS NPs (Blank and NHT-loaded) 124
4.9.1 Cytotoxicity Studies of CS and BG-CS NPs (Blank and NHT-loaded) using Fibroblast Cells 124
4.9.2 Cytotoxicity Studies of CS and BG-CS NPs (Blank and NHT-loaded) using Calu-3 Cells 126
4.10 *In Vivo* Pharmacokinetic Studies of NHT-loaded CS NPs and NHT-loaded BG-CS NPs 128
4.10.1 Pharmacokinetic Analysis 128
4.10.2 In Vivo Drug Distribution Study 131

CHAPTER 5 DISCUSSION 134

5.1 Introduction 134
5.2 Preparation of BG-CS 134
5.2.1 Synthesis of Phthaloyl CS 134
5.2.2 Synthesis of BG Phthaloyl CS 134
5.2.3 Synthesis of BG- CS 135
5.3 Preformulation Studies and Development of CS NPs 136
5.3.1 Varying Ratios of CS and TPP 136
5.3.2 Varying Sonication Time 137
5.4 Characterization of NHT-loaded CS NPs and NHT-loaded BG-CS NPs 138
5.4.1 Particle size, Zeta potential and PDI 138
5.4.2 Transmission Electron Microscopy (TEM) 141
5.4.3 Differential Scanning Calorimetry (DSC) 142
5.4.4 Thermogravimetric Analysis (TGA) 144
5.4.5 X-ray Diffraction (XRD) 144
5.4.6 Fourier Transform Infrared Spectroscopy (FTIR) 145
5.5 EE% and DL% of NHT-loaded CS NPs and NHT-loaded BG-CS NPs 146
5.6 Release Studies of NHT-loaded CS NPs and NHT-loaded BG-CS NPs 147
5.7 Stability Studies of NHT-loaded CS NPs and NHT-loaded BG-CS NPs 149

5.8 Cytotoxicity Studies of NHT-loaded CS NPs and NHT-loaded BG-CS NPs 150
5.9 *In Vivo* Studies of NHT-loaded CS NPs and NHT-loaded BG-CS NPs 151
5.9.1 Pharmacokinetic Analysis 151
5.9.2 *In Vivo* Drug Distribution Study 155

CHAPTER 6 CONCLUSION AND RECOMMENDATION 158

6.1 Overall Conclusion 158
6.2 Limitation 159
6.3 Future Directions 160
REFERENCES 162
AUTHOR'S PROFILE 247

LIST OF TABLES

Tables	Title	Page
Table 1.1	Medical Cost Related To Smoking In World Health Organization (WHO) Region. WHO (2024)	2
Table 1.2	Some Principal Harmful Compounds Found In Tobacco Smoke.	3
Table 1.3	Benefits Of CS In Nasal Medication Administration.	6
Table 2.1	Intranasal Drug Applications In CNS	34
Table 2.2	Physical Characteristics Of CS And Modified CS.	59
Table 3.1	CS Nps Loaded NHT Formulation	68
Table 3.2	BG-CS Nps Loaded NHT Formulation	68
Table 4.1	Characteristic FTIR, ^{1}H NMR, And ^{13}C NMR Signals Of Phthaloyl CS.	79
Table 4.2	Characteristic FTIR, ^{1}H NMR, And ^{13}C NMR Signals Of BG Phthaloyl CS.	81
Table 4.3	Characteristic FTIR, ^{1}H NMR, And ^{13}C NMR Signals Of BG-CS.	82
Table 4.4	Effect Of CS / TPP Concentrations And Their Ratio On Particle Size, PDI And Zeta Potential Of Nps (N=3).	84
Table 4.5	Particle Size, PDI, And Zeta Potential Of Blank CS Nps (0.05%,0.1%) At Different Sonication Time (N=3).	85
Table 4.6	Particle Size, PDI, And Zeta Potential Of Blank CS And NHT-Loaded CS Nps In Different Concentrations (N=3), 4min Sonication Time.	87

Table 4.7	Particle Size, PDI, And Zeta Potential Of Blank BG-CS And NHT-Loaded BG-CS At Different Concentrations. (N=3), 4min Sonication Time.	89
Table 4.8	EE% And DL% For NHT-Loaded CS Nps (N=3).	99
Table 4.9	EE% And DL% For NHT-Loaded BG-CS Nps (N = 3).	99
Table 4.10	Average Particle Size Of Blank CS And NHT CS Nps At 25 ± 2ºC And 5 ± 3ºC (N=3)	114
Table 4.11	Zeta Potential Of Blank CS And NHT CS Nps At 25 ± 2ºC And 5 ± 3ºC (N=3).	116
Table 4.12	PDI Of Blank CS And NHT CS Nps At 25 ± 2ºC And 5 ± 3ºC (N=3).	118
Table 4.13	Average Particle Size Of Blank BG-CS And NHT-Loaded BG-CS Nps At 25 ± 2 ºC And 5	120
Table 4.14	Zeta Potential Of Blank BG-CS And NHT-Loaded BG-CS At 25 ± 2 ºC And 5 ± 3 ºC (N = 3).	122
Table 4.15	PDI Of Blank BG-CS And NHT BG-CS At 25 ± 2 ºC And 5 ± 3 ºC (N = 3).	123
Table 4.16	Pharmacokinetic Analysis Of Formulations F1, F2 And NHT (N=5).	128
Table 4.17	Pharmacokinetic Analysis Of Cotinine In Formulations F1, F2 And NHT (N=5).	129
Table 4.18	Pharmacokinetic Analysis For Formulations, F1", F2", AndNHT (N =5).	130
Table 4.19	Pharmacokinetic Analysis Of Cotinine For Formulations, F1", F2", And NHT(N=5).	131

LIST OF FIGURES

Figures	Title	Page
Figure 1.1	Structure Of CS	5
Figure 2.1	Nicotine Structure	18
Figure 2.2	Gross Anatomy Of The Nasal Cavity (Chung Et Al., 2022)	27
Figure 2.3	The Nasal Epithelium, Which Lines The Upper Airways And The Nasal Cavity, Is Shown In Microscopic Detail. It Shows The Secretion And Transportation Of Mucus To Cushion The Airways From Dust, Bacteria, And Dehydration (Whitsett, 2018).	30
Figure 2.4	Origin Of CS.	35
Figure 2.5	Diagram Representing The Possible Mechanisms Of Drug Release By Diffusion, Swelling And Erosion Of Polymer (CS) Matrix. Depicted From (Al-Awsi Et Al., 2023).	50
Figure 3.1	Synthesis Of Phthaloyl CS (Protection Of The Amino Groups By The Phthaloyl Groups).	64
Figure 3.2	Synthesis Of BG Phthaloyl CS.	65
Figure 3.3	Synthesis Of BG-CS (Deprotection Of The Amino Groups).	66
Figure 3.4	Preparation Of Nps (Blank And Loaded NHT).	67
Figure 3.5	Release Of NHT-Loaded CS Nps And NHT-Loaded BG-CS Nps	73
Figure 3.6	Treatment Groups	76

Figure 4.1	TEM Micrographs Of (A): Blank CS Nps 0.05%, (B): Blank CS Nps 0.1%, (C): F1, (D): F2, (E): F3, (F): F4, (G): F5 And (H): F6 Nps At Magnification 80x (Scale Bar:500nm).	90
Figure 4.2	TEM Micrographs Of (A): Blank BG-CS Nps 0.05%, (B): Blank BG-CS Nps 0.1%, (C): F1", (D): F2", (E): F3", (F): F4", (G): F5" And (H): F6" Nps At Magnification 80x (Scale Bar:500nm).	90
Figure 4.3	DSC Thermograms Of Blank CS Nps, NHT, TPP, F1, F2, F3, F4, F5 And F6 Nps.	92
Figure 4.4	DSC Thermograms Of Blank BG-CS, NHT, TPP, F1", F2", F3", F4", F5" And F6" Nps	92
Figure 4.5	TGA Thermograms O F Blank CS, NHT, TPP, F1, F2, F3, F4, F5 And F6 Nps.	93
Figure 4.6	TGA Thermog Rams Of Blank BG-CS, NHT, TPP, F1", F2", F3", F4", F5" And F6" Nps.	93
Figure 4.7	XRD Of Blank CS, NHT, F1, F2, F3, F4, F5 And F6 Nps	94
Figure 4.8	XRD Of Pure NHT Powder.	95
Figure 4.9	XRD Of Blank BG-CS, NHT, F1", F2", F3", F4", F5" And F6" Nps.	95
Figure 4.10	FTIR Of Blank CS, NHT, TPP, F1, F2, F3, F4, F5 And F6 Nps.	96
Figure 4.11	FTIR Of Blank BG-CS, NHT, TPP, F1", F2", F3", F4", F5" And F6" Nps.	97
Figure 4.12	NHT Peak.	98
Figure 4.13	Cotinine Peak.	98
Figure 4.14	Average Release % For F1, F2, F3, F4, F5, F6 Nps And NHT.	101

Figure 4.15 Average Release (%) For F1", F2", F3", F4", F5", F6" Nps And NHT. 102

Figure 4.16 First-Order Release Kinetics Of NHT From F1–F6. The Plots Represent The Relationship Between Ln (100 − Qt) And Time (Hr.), Where Qt Means The Cumulative Percentage Of Drug Released At Time T. The Linear Regression Lines Indicate Concentration-Dependent Drug Release Behavior, And The Slope Resembles To The First-Order Release Rate Constant (K_1). 103

Figure 4.17 First-Order Release Kinetics Of NHT From F1"–F6". The Plots Represent The Relationship Between Ln (100 − Qt) And Time (Hr.), Where Qt Means The Cumulative Percentage Of Drug Released At Time T. The Linear Regression Lines Indicate Concentration-Dependent Drug Release Behavior, And The Slope Resembles To The First-Order Release Rate Constant (K_1). 104

Figure 4.18 First-Order Release Kinetics Of NHT. The Plot Represents Ln (100 − Qt) Versus Time (Hr.), Where Qt Is The Cumulative Percentage Of Drug Released At Time T. The Linear Regression Indicates Concentration-Dependent Release Behavior Characteristic Of Free Drug. 105

Figure 4.19 Higuchi Release Model Plots Of NHT-Loaded CS Nps Formulations F1–F6. Cumulative Drug Release (Qt, %) Is Plotted Against The Square Root Of Time (√T, $H^{1/2}$). 106

Figure 4.20 Higuchi Release Model Plots Of NHT-Loaded BG-CS Nps F1"–F6". Cumulative Drug Release (Qt, %) Is Plotted Against The Square Root Of Time (√T, $H^{1/2}$). 107

Figure 4.21 Higuchi Release Model Of NHT. Cumulative Drug Release (Qt, %) Is Plotted Against The Square Root Of Time (√T, $H^{1/2}$). 107

Figure 4.22 Hixson–Crowell Cube-Root Model Plots Of NHT-Loaded CS Nps Formulations (F1–F6). The Cube Root Of The Remaining Drug (100-$Qt^{1/3}$) Is Plotted Against Time (Hr.) 108

Figure 4.23 Hixson–Crowell Cube-Root Model Plots Of NHT Release From NHT-Loaded BG-CS Nps Formulations (F1"–F6"). The Cube Root Of The Remaining Drug (100-$Qt^{1/3}$) Is Plotted Against Time (Hr.) 109

Figure 4.24 Hixson–Crowell Cube Root Plot Of (NHT. The Plot Of (100-Qt1/3) Versus Time Hr. 110

Figure 4.25 Korsmeyer–Peppas Release Model Plots For Formulations F1–F6. 111

Figure 4.26 Korsmeyer–Peppas Release Model Plots For Formulations F1"–F6". Logarithmic Plots Of Log (Mt/M∞) Versus Log(Time). 112

Figure 4.27 Percentage Cell Viability Of Fibroblast Cell Following Exposure To Blank CS Nps, NHT-Loaded CS Nps, And NHT At Different Concentrations (0.5–0.03125 Mm). 125

Figure 4.28 Percentage Cell Viability Of Fibroblast Cell Following Exposure To Blank BG-CS Nps, F1", F2", And NHT At Different Concentrations (0.5–0.03125 Mm). 126

Figure 4.29 Percentage Cell Viability Of Calu-3 Cells After Treatment With Blank CS Nps 0.05%, Blank CS Nps 0.1%, F1, F2 And NHT At Different Concentrations (0.5–0.03125 Mm). 127

Figure 4.30 Percentage Cell Viability Of Calu-3 Cells After Treatment With Blank BG-CS Nps 0.05%, Blank BG-CS Nps 0.1%, F1", F2" And NHT At Different Concentrations (0.5–0.03125 Mm). 128

Figure 4.31	AUC Of Formulations F1, F2 And NHT	129
Figure 4.32	NHT Concentrations In The Brain And Lungs For Formulations F1, F2, And NHT (N=5).	131
Figure 4.33	Cotinine Concentrations In The Brain And Lungs For Formulations F1, F2, And NHT (N=5).	132
Figure 4.34	NHT Concentrations In The Brain And Lungs For Formulations F1", F2", And NHT (N=5).	132
Figure 4.35	Cotinine Concentrations In The Brain And Lungs For Formulations F1", F2", And NHT (N=5).	133
Figure 5.1	Formulation Rationale Scheme.	141

LIST OF PLATES

Plates	Title	Page
Plate 3.1	Rat Brain And Lung.	77
Plate 4.1	Visual Appearance Of Blank CS Nps Prepared At Different CS Concentrations (0.10%, 0.15%, And 0.30%) And TPP Concentration: (A) 0.10%, (B) 0.08, And (C) 0.08 Respectively.	85

LIST OF SYMBOLS

Symbols

C	Concentration
Cs	Solubility Of The Drug
D	Diffusion Coefficient
F	Diffusion Flow
K_0	Zero-Order Release Constant
K_1	First-Order Release Constant
K_{HC}	Hixson-Crowell Constant
K_{KP}	Korsmeyer-Peppas Constant
MHz	Operating Frequency Of The NMR Spectrometer 400
Q_0	Initial Drug Quantity
Qt	Cumulative Drug Release At Time "t"
T	Time
$T_{1/2}$	Half-Life
δ	Chemical Shift Expressed In Parts Per Million (PPM)

LIST OF ABREVIATION

Abbreviations

AUC	Area Under The Curve
AUMC	Area Under The Moment Curve
BBB	Blood Brain Barrier
BG-CS	Butylglycerol CS
Calu-3	Human Lung Epithelial Cell
CDC	Centers Of Disease Control And Prevention
CS	Chitosan
CHD	Coronary Heart Disease
CNS	Central Nervous System
COAs	Critical Quality Attributes
COPD	Chronic Obstruction Pulmonary Disease
CXCL8	C-X-C Motif Chemokine Ligand 8
D	Day
DAC	Dissolution Absorbance Clearance
DDA	Degree Of Deacetylation
DEC	Disposable Electronic Cigarette
DHE	Dihydroergotamine
DMF	Dimethylformamide

DSC	Differential Scanning Calorimetry
EE%	Encapsulation Efficiency
FCTC	Framework Convention On Tobacco Control
FTIR	Fourier Transform Infrared Spectroscopy
GDP	Gross Domestic Product
GH	Galantamine Hydrobromide
IL-1β	Interleukin-1 Beta
IL-6	Interleukin-6
IL-8	Interleukin-8
IVC	Individually Ventilated Cages
KBR	Potassium Bromide
LAFAM	Laboratory Animal Facility & Management
LMICs	Low- And Middle-Income Countries Limit Of Detection
LOD LOQ	Limit Of Quantification
MDZ-CS NPs	Midazolam-Loaded CS NPS
MHb-IPN	Medial Habenula-Interpeduncular Nucleus
MMT	Montmorillonite
MRT	Mean Residence Time
NAc	Nucleus Accumbens
NAChRs	Nicotinic Acetylcholine Receptors

NaCl	Sodium Chloride
NDDS	Novel Drug Delivery Systems
NHT	Nicotine Hydrogen Tartrate
NHT-loaded CS NPs	Nicotine-Encapsulated Chitosan Nanoparticles
NMR	Nuclear Magnetic Resonance Spectroscopy
NPs	Nanoparticles
NRT	Nicotine Replacement Therapy
OLM	Olmesartan Medoxomil
PBS	Phosphate Buffer Solution
PDI	Polydispersity Index
PEG	Polyethylene Glycol
PFC	Prefrontal Cortex
PHT	Phenytoin
PPP	Purchasing Power Parity
QTPP	Quality Target Product Profile
R2	R Square
REC	Rechargeable E-cigarettes
RH	Relative Humidity
SD	Standard Deviation
SEM	Scanning Electron Microscopy
SIT-CS-NPs	Sitagliptin-Loaded CS NPs
TBuOK	Potassium Tert-Butoxide

TEM	Transition Electron Microscope
TGA	Thermo Gravimetric Analysis
THF	Tetrahydrofuran
TNF-α	Tumor Necrosis Factor-Alpha
TPP	Tripolyphosphate
TT	Tetanus Toxoid
UGT	Uridine 5′-Diphospho-Glucuronosyltransferase
U. S	United States
VTA	Ventral Tegmental Area
WHO	World Health Organization
XRD	X-ray Diffraction

LIST OF NOMENCLATURE

Nomenclatures

℃	Celsius
g	Gram
hrs	Hours
KV	Kilovolt
mA	Milliampere
MHz	Megahertz
min	Minutes
μL	Microliter
mm	Millimeter
mM	Millimolar
μm	Micrometer
mV	Millivolt
nm	Nanometer

CHAPTER 1
INTRODUCTION

1.1 Research Background

Novel drug delivery systems (NDDS) have changed the pharmaceutical sciences by enhancing therapeutic efficacy, bioavailability, targeted delivery, and patient adherence, while minimizing side effects (Khadam et al., 2024). A longer duration of action is possible since the innovative drug delivery method can regulate the p lasma drug concentration (Kumar et al., 2023). Smoking is highly correlated with increased mortality from cancer and cardiovascular illnesses, markedly raising the risk of death from all causes. Both daily and nondaily smokers encounter increased health hazards, which intensify with the frequency of daily cigarette smoking (Zhu et al., 2021). The Malaysian Ministry of Health (2003) estimates 20% of the nation's mortality, or to around 10,000 individuals yearly, to smoking (Tan, 2012). According to a 2012 report from the United States Surgeon General's office, approximately 3,800 youth under the age of 18 started smoking every day. This indicates that many young people were taking up smoking at an early age, which can have serious consequences for their health later in life (Onor etal., 2017). According to research conducted by Lim et al. (2018). At least 367 million people worldwide, over the age of 15, use smokeless tobacco, Among the people who used the smokeless tobacco products, 237 million were men and 129 million were women. According to the World Health Organization (WHO) global study on inclinations in the occurrence of tobaccosmoking 2000–2025, over 301 million people, or 82% of the world's total user base, use smokeless tobacco. This usage is prevalent across all regions. In addition, smoking costs over $300 billion in the United States (U.S), with around $170 billion attributed to healthcare expenses related to smoking (Xu et al., 2021). It costs around $269 billion in direct medical costs annually in the Latin American nations (Andrés et al., 2020). As shown in (Table 1.1), themedical cost is related to smoking. The high economic costs and large mortality associated with smoking have driven the implementation of public health works for smoking reduction programs (Adekola et al., 2023)

Table 1.1
Medical Cost Related To Smoking In World Health Organization (WHO) Region. WHO (2024)

WHO Region	Medical Cost related to Smoking (US$ billions)	% of National Health Expenditure	Reference
Africa Region	2.4	Not specified	WHO (2024).
Region of America	356.7	~ 6.7 %	
South East Asia Region	7.0	Not specified	
European Region	163.8	~ 6.6 %	
Western pacificregion	74.6	Not specified	
Eastern Mediterranean	7.8	Not specified	
Globally	612	-	

There are different ways to help peoplequit smoking, like counsellingand drugs such as varenicline, bupropion, cytisine, and nortriptyline. Nicotine replacement therapies (NRTs) have been shown to be cost-effective (Thakur & Choudhari, 2024). The 2015 National Health Interview Survey study found that many people who hadn't quit smoking yet were involved in numerous programs to help them quit. The research conducted by Babb et al. (2017) provides the subsequent statistical information: 68.0% of adult smokers needed to quit, 55.4% had tried to quit in the past year, 7.4% had recently succeeded, 57.2% had obtained counsel from a healthcare professional to quit, and 31.2% had utilized medicine and therapy to help them quit. Healthcare professionals are working hard to help smokers move from thinking about and planning to quit to actually quitting. The goal is to lower smoking rates and improves public health. The Transtheoretical Model of Behavior Variation, often identified as the Stages of Change model, is often used to investigate and encourage changes in behavior, such as quitting smoking (Mundorf et al., 2018). Cigarette smoke dramatically elevates

respiratory, circulatory, and organ diseases due to its high concentration of harmful chemicals (Cha et al., 2023). Smoking causes many changes in the airways of the lungs. Breathing in cigarette smoke can harm alveolar cells and other lung tissues (Kumar et al., 2018). (Table1.2) shows some of the most dangerous compounds in tobacco smoke and how they affect people's health.

Table 1.2
Some Principal Harmful Compounds Found In Tobacco Smoke.

Compound	Target	Disease	Reference
Nicotine	• Nervous system • circulatory	• Vasoconstriction • High blood pressure • Addiction	(Arya et al., 2024)
Carbone monoxide	• Vital organ	• Cardiovascular disease (CVD) • Decrease oxygen	(Zhang et al., 2023) (Bansal et al., 2024)
Formaldehyde	• Respiratory	• Airway Inflammatory • Cancer Risk	(Kang et al., 2022) (Tulen et al., 2023)
Tar	• Respiratory	• Bronchitis • Cancer	(Gupta & Qanungo, 2023)
Arsenic	• Many Organs	• Hyperkeratosis • Skin effect • Bladder effect • Lung cancer	(Shehata et al., 2023)
Hydrogen Cyanide	• Respiratory	• Carcinogenic	(Hikisz & Jacenik, 2023)
Acrolein	• Respiratory	• Irritation • Chronic obstructive pulmonary disease	(Alewel et al., 2023)

People who smoke consume a significantly higher risk of heart stroke, three to five times higher than adults who do not smoke (Ciumărnean et al., 2021). In addition, there

is an improved danger of lung cancer associated with non-smokers (Klebe et al., 2019). Smoking cessation has become an urgent demand to solve the prevalence of related diseases and illnesses from cigarette smoking (Onwuzo et al., 2024). Evidence-based tobacco treatment is not yet the gold standard. Helping people quit smoking is something that the Framework Convention on Tobacco Control suggests (Pipe et al., 2022). Smokers might find relief through a variety of therapies. The most popular method is NRT (Haokip et al., 2020). Nicotine is in tobacco, and when inhaled, it immediately spreads into circulation and changes neurotransmitters, which triggers a lot of different bodily reactions. The primary aim of NRT is to diminish the need to smoke among persons (Shete et al., 2024). NRT can mitigate withdrawal symptoms by enhancing the brain's dopamine synthesis, hence aiding in the management of these symptoms (Patidar et al., 2025). Various types of nicotine products are available for purchase, including chewing gum, sublingual tablets, transdermal patches, and nasal spray. These products are available in different strengths and formulations (Sailer et al., 2019). Nicotine gum dispenses nicotine when retained in the oral cavity for approximately thirty minutes (min) (Sinha et al., 2020). Nicotine gum is offered in dosages of 2 mg and 4 mg. To facilitate full absorption by the body, it is advisable to avoid acidic drinks before to and during its consumption. The recommended daily dosage ranges from 40 to 60 mg (Ziedonis et al., 2024). Negative symptoms, including mouth pain, hiccups, mucosal lesions, and mandibular discomfort, may occur (Sivaramakrishnan et al., 2022; Sivaramakrishnan & Sridharan, 2024). Sublingual pills facilitate the efficient absorption of nicotine into the circulation. The primary distinction between this and chewing gum is that the tablet is allowed dissolve gradually under the tongue rather than being chewed, a process that takes around 20 to 30 min. The impact can be likened to that of 2 mg of nicotine gum (Molander & Lunell, 2001). Nicotine patches provide nicotine transdermally in various amounts to accommodate different levels of dependency. Effortless adherence involvesapplying the patch daily, negating the need for active product use throughout the day (Galge & Pagire, 2022). Nicotine patches are unique among products for their ability to administer nicotine dosages gradually and passively. Conversely, alternative kinds of NRT have a superior success rate for rapid action, although need greater user involvement and effort. Transdermal patches are available in many strengths, from 5 mg to 52.5 mg of nicotine delivered daily. This treatment results in plasma concentrations similar to those found in heavy smokers (Hartmann-Boyce et al., 2018).

Nonetheless, current dosage forms do not provide smokers with the combination of sharp and rapidly rising arterial nicotine levels, together with the immediate pharmacological effects attained by cigarette smokeinhalation. Moreover, these dosage forms fail to sustain an adequately elevated and extended nicotineplasma concentration to avoid the resurgence of cravings at short intervals (Shahab et al., 2013). Nicotine nasal spray is recognized for its fast nicotine absorption relative to other NRTs, achievinga plateau in around 10 min, similar to the nicotine absorption rate seen during a cigarette puff (Prochaska & Benowitz, 2019). A 10 mLspray vial contains the nicotine nasal spray, which is an aqueous nicotine solution; it has a multidose container with a pump mechanism that delivers a dosage of 0.5 mg each 50 μL spray. Every administration comprises a pair of sprays, with one being directed into each nostril; generally, it is a patient-started treatment at a regularity of one or two doses per hr, with the potential to increase to an all-out of 40 doses per day (Jain et al., 2013). This approach will be undesirable to the potential user. Therefore, to facilitate the progression of smoking cessation, it would be therapeutically helpful to develop an improved nasal nicotine replacement formulation that can deliver nicotine rapidly and professionally at the onset, as well as ensure a sustained release of nicotine.

Natural polymers such as CS, N-acetyl-glucosamine, and d-glucosamine, a long-chain polymer obtained from deacetylating chitin (Figure 1.1 Structure of CS) (Satitsri & Muanprasat, 2020; Mura et al., 2022), have mucoadhesive qualities that havebeen shown to be active in the nasal delivery of drugs. There are several reasons why CS is the best material for manufacturing NPs. It is a natural aminopolysaccharide that can break down, is safe, and can kill germs (Egorov et al., 2023). Park et al. (2019) contend that CS demonstrates significant adherence.

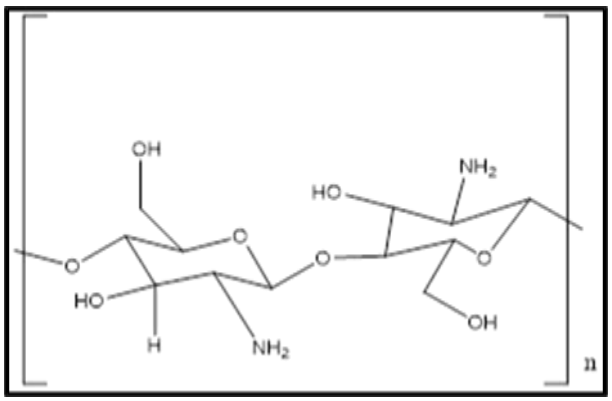

Figure 1.1 Structure Of CS

CS is extensively employed in the improvement of nasal medication delivery systems (Shim & Yoo, 2020; Omidian et al., 2024). (Table1.3) illustrates the advantages of CS in nasal drug delivery.

Even while CS is widely used to provide drugs, it does have some constraints. For instance, it doesn't dissolve well at neutral or basic pH and can't pass several biological membranes (Desai et al., 2023). Changing CS can have several positive effects on the polymer, such as making it more bioactive (Lima et al., 2022). There are many ways to change the physicochemical features of CS, such as chemical alteration (Chen et al., 2022). Changing the physicochemical features of CS can make it more soluble and more stable (Shete, Chavan, et al., 2024). Non-ionic and amphiphilic alkylglycerols can rapidly penetrate endothelial cell membranes, inducing a transient instability and facilitating the passage of the (BBB) for around 3–15 min (Wang et al., 2022). Reports have indicated that alkylglycerols can enhance the penetration of medications via cellular membranes (Erdlenbruch et al., 2003). Using alkyloxirane to chemically change CS with butylglycerol requirescertain labprocedures (Molnár etal., 2010). No published work has been done to ascertain the use of CS NPs or modified CS NPs in providing sustained-release formulation through intranasal delivery for nicotine. Hence, this research aims to fabricate sustained release intranasal nicotine formulation and evaluate its use and aptitude in performing a sustained release design. Due to its mucoadhesive, penetration-enhancing, and sustained-release properties, CS NPs and BG-CS NPs are anticipated to produce a novel formulation of nicotine, which in turn will aid in the treatment for smoking cessation. The need for knowledge and the desire to improve health outcomes through innovative and compassionate thinking drive this.

Table 1.3
Benefits Of CS In Nasal Medication Administration.

CS Property	**Framework**	**Advantages of Nasal Administration**	**Reference**
Mucoadhesion	• Electrostatic adhesion • Formation of the mucin gel	• Extends residence duration • Enhances absorption in mucosa	(Collado-González et al., 2019)
Enhancement of permeation	• Facilitates the opening of tight junctions	• Enables paracellular transfer of	(Marcello & Chiono, 2023)

CS Property	Framework	Advantages of Nasal Administration	Reference
		hydrophilic pharmaceuticals	
Biodegradability and biocompatibility	• Non-toxic natural polysaccharide	• Appropriate for long-term use	(Popescu et al., 2020; Sharma & Bhende, 2024)
Versatility in formulation	• Applicable as a solution, gel, NPs.	• Facilitates controlled and sustained release	(Parhi, 2020; Herdiana et al., 2021)
Nose-to-brain delivery	• Olfactory/trigeminal transmission	• Direct access to the central nervous system (CNS) • Circumventing the blood-brain barrier (BBB) • Minimized systemic adverse effects	(Aderibigbe & Naki, 2019)

1.2 Problem Statement

It is crucial for public health to stop smoking since tobacco usage has many detrimental effects on health. Even though NRT is widely available, the world is still having trouble with smoking addiction. Patches, gums, and oral treatments are not excellent at delivering nicotine quickly and satisfyingly like cigarettes do. Consequently, compliance with these methods diminishes, leading to increased relapse rates. During the earliest and most crucial stages of withdrawal, people experience difficulties due to restricted bioavailability, a slow onset of effects, and an inability to control their cravings.

Formulation scientists have concentrated on nasal distribution since it can avoid the hepatic first-pass impact and quickly reach the CNS and systemic circulation (Pal et al., 2024). The efficacy of this approach is significantly dependent upon the formula tion's capacity to adhere to the nasal mucosa and facilitate the regulated permeation of the medication, while also presenting a potential for minor nasal discomfort. Size, surface charge, CS, nicotine release kinetics, and nasal retention capacity are just a few of the NP properties that have not been studied much in the past. Intranasal drug delivery makes it easy and quick to give people medication to help them quit smoking. But if the existing nasal spray formulations need to be taken too often, patients may be less inclined to follow their treatment plans. A feasible solution to address these restrictions

is the creation of a nasal spray composed of nicotine-encapsulated CS NPs designed for prolonged release. When delivered intranasally, these NPs progressively release nicotine over a prolonged duration, providing a more stable therapeutic impact compared to traditional nicotine replacement treatments.

Their mucoadhesive properties enable prolonged contact with the nasal mucosa, promoting regulated release and enhancing the chance of effective smoking cessation. If the nicotine is released constantly, it will be like smoking, which could aid with withdrawal symptoms and make it easier to quit. There exists a critical deficiency in the advancement of intranasal pharmacotherapies for smoking cessation, from which patients may receive significant benefit, attributable to the current absence of accurate formulation and administration methodologies. CS-based NPs systems will help with mucoadhesion and permeability, but how to best give sustained nicotinic delivery through the nose is still an unknown topic. Hence, the need of this study.

1.3 Research Objectives

This study aims to evaluate CS and BG-CS NPs in producing sustained release nicotine via intranasal route for smoking cessation therapy. This study is a first step towards laying the framework for potential future clinical research, safety and biocompatibility testing to bolster its translational capacity.

1.3.1 General Objective

To formulate, characterize, and evaluate NHT-loaded CS and BG- CS NPs for intranasal nicotine delivery providing sustained nicotine release.

1.3.2 Specific Objectives

i) To synthesize BG-CS via phthaloylation.

ii) To develop CS and BG-CS-loaded nicotine NPs using the ionic gelation method.

iii) To determined the physicochemical and release characteristics (particle size, zeta potential, PDI, EE%, DL%, morphology, chemical interaction, crystallinity, thermal and physical stability) of NHT-loaded CS and BG-CS NPs.

iv) To determine the cell viability and cytotoxicity of the nicotine loaded CS and BG-CS NPs using fibroblast and Calu-3 cells.

v) To determine the pharmacokinetic profiles and in vivo drug distribution towards highly perfused organs (lung and brain) of the nicotine loaded CS and BG-CS NPs using male Sprague Dawley rats.

1.4 Research Question

i) Can NHT -loaded CS NPs and BG-CS NPs be successfully developed using the ionic gelation method?

ii) What are the physicochemical characteristics of the developed NHT- loaded CS NPs and BG-CS NPs?

iii) Do NHT-loaded CS NPs and BG-CS NPs provide a sustained NHT release profile compared with free nicotine?

iv) Are the CS NPs and BG-CS NPs cytotoxic to fibroblast and Calu-3 cells?

v) What are the pharmacokinetics profiles and in vivo organ distribution of CS NPs and BG-CS NPs?

1.5 Significance of Study

A sustained-release intranasal nicotine delivery device is clinically necessary to improve smoking cessation results. In order to improve bioavailability and patient adherence, this project intends to develop a simple, fast-acting formulation using CS NPs. Hence, the goal is to overcome the shortcomings of current NRT. Due to the excellent properties of mucoadhesion, CS NPs-based drug delivery systems and their BG-CS NPs can act by enhancing epithelial permeation. Drug administration in NP form would ensure controlled release, thus lessening the administration frequency of nicotine and encouraging better therapeutic action. Multiple studies conducted towards the end of the last decade have shown that CS NPs have the potential to increase the amount of time a drug remains in the nose and to help it be absorbed systemically. These studies primarily focused on CNS targeted therapies (Obeidat et al., 2025; Frigaard et al., 2022; Sharifi-Rad et al., 2021)

The intranasal route allows nicotine to bypass first-pass metabolism and entering the brain straight from the nose, which is crucial for the diffusion of nicotine's neuroactive effects. An increasing number of studies are linking this approach to improved patient compliance, a considerable decrease in systemic side effects, rapid action onset, and the

ability to cure addiction (Keller et al., 2022; Safarov et al., 2024). The conventional opinion holds that cutting down on nicotine consumption causes withdrawal symptoms, decreased tolerance for current treatments, and poor adherence since the CNS is no longer stimulated quickly (Benowitz, 2008). For controlled and sustained release that matches desire cycles and neurochemical requirements, CS mucoadhesive property prolongs the resident time of NPs within the nasal cavity (Shim & Yoo, 2020).

Targeted administration with fast start and persistent therapeutic activity is necessary for the treatment of additional illnesses affecting the CNS, and this method expands the possibilities for treating such disorders. For example, it could be used to treat pain, epilepsy, depression, or Parkinson disease. These findings add to the expanding paradigm for designing precision drug delivery systems that goes beyond specific drug applications by modifying NPs-related parameters like size, charge and surface chemistry.

The fields of addiction therapy, nanotechnology, and biomaterial science have all developed rapidly in response to rising public health concerns and academic interest (Mahmoudi et al., 2018; Brenner, 2010). The need for effective, long-term, non-invasive treatment techniques has never been greater, the first is that low- and middle-income nations, which have the greatest smoking rates and the fewest effective treatments available, can benefit greatly from this formulation technique. In areas with limited access to healthcare, interventions using reliable, needle-free, and self-administrable intranasal delivery could significantly increase public health outreach and reduce implementation costs.

Last but not least, the results of this study can be used to create new standards for biopolymer-based nasal therapies that will pave the way for a new intranasal formulation of nicotine that can help people quit smoking.

1.6 Assumption

The feasibility and relevance of continuous intranasal nicotine administration utilizing CS-based NPs are supported by the following fundamental assumptions of this study:

a) CS and BG-CS have the right combination of mucoadhesive and permeation-enhancing characteristics for delivering nicotine through the nasal epithelium without causing any irritation or damage.

b) Intranasal administration allows nicotine to be delivered into systemic circulation rapidly and efficiently, bypassing hepatic first-pass metabolism and affording direct nose-to-brain transport, which is a much-needed property when treating cravings and withdrawal symptoms from nicotine.

c) NPs may be engineered to release drugs slowly, which increases therapeutic benefits while decreasing the number of doses needed, thereby improving patient compliance.

d) Particle size, surface charge, and EE% are three of the physicochemical features of CS NPs that may be reliably controlled using the ionic gelation technique.

To improve formulations and predictive design, statistical modeling tools will be used to shed light on the relationships between formulation variables and drug delivery performance. Theoretically, the stated assumptions provide the groundwork for establishing the experimental design and analytic framework. The assumptions are in line with current trends in nanomedicine and intranasal drug delivery systems, and they are supported by literature from the past few years.

1.7 Ethical Committee

The UiTM Committee on Animal Research and Ethics (UiTM CARE) approved the study's procedure and the animals used, ensuring the same standards applied in conformity with national and international guidelines for biomedical research. [Approval No: UiTM CARE (455/2024); 19 April 2024].

1.8 Thesis Scope

The scope of this thesis covers both *in vitro* and *in vivo* studies to assess the NPs stability, safety and efficacy to be used intranasally. The studies are as follows:

a) CS modification and CS NPs synthesis: Chemical modifications (such as phthaloylation) and synthesis of CS NPs are employed to improve their solubility, stability, and nasal permeability.

b) Physical characterization and stability of NPs: Size, zeta potential, PDI, morphology, EE%, DL%, crystallinity and chemical and physical stability of the

particles are determined using Dynamic Light Scattering (DLS), Transmission Electron Microscopy (TEM), Differential Scanning Calorimetry (DSC), Thermogravimetric Analysis (TGA), X-ray Diffraction (XRD) and Fourier Transformed Infra-Red (FTIR).

c) Cytotoxicity studies of nicotine-loaded CS NPs and BG-CS NPs were conducted in fibroblasts and nasal cell model, Calu-3 cells to assess the NPs toxicity

d) *In vivo* studies using male Sprague Dawley rats were performed to determine the drug distribution and pharmacokinetic profiles of nicotine-loaded CS and BG-CS NPs.

e) The statistical analyses were done to identify the formulation variables that significantly affect the efficacy of medication delivery by employing multivariate and univariate regression analysis.

1.9 Thesis Outline

This thesis is composed of five chapters, each of which deals with an important aspect of research on CS and BG-CS NPs for sustained intranasal nicotine delivery.

i) CHAPTER 1 (INTRODUCTION): This chapter gives a general outline of the thesis, research questions, objectives, problem statement, importance and scope.

ii) CHAPTER 2 (LITERTURE REVIEW): This chapter gives information on topics that will help in understanding this study.

iii) CHAPTER 3 (RESEARCH METHODOLOGY): This chapter offers comprehensive information in the material and method used to carry out this study.

iv) CHAPTER 4 (RESULTS AND DATA ANALYSIS): This chapter showcased the results and data analyses of the studies done.

v) CHAPTER 5 (DISCUSSION): This chapter discusses the results obtained with support of other published studies.

vi) CHAPTER 6 (CONCLUSION AND RECOMMENDATION): This chapter concludes the overall results obtained and discusses limitations and future recommendations of the research work.

CHAPTER 2
LITERATURE REVIEW

2.1 Introduction

One of the greatest threats to public health in the modern era is tobacco use (Foll et al., 2022; Hatsukami & Carroll, 2020). According to WHO, tobacco kills more than 8 million people each year. More than 7 million of those deaths are the result of direct tobacco use while around 1.2 million are the result of non-smokers being exposed to second-hand smoke, solidifying tobacco use as one of the leading avoidable reasons of death globally (Tobacco & Public Health, n.d.; World Health Organization ,2024). Despite efforts to reduce tobacco use, several regions continue to have unacceptably high smoking rates (Hampsher-Monk et al., 2024). Around 22% of the world's population uses tobacco in some way, with men being more impacted than women. Approximately 36% of adult men and 7% of women are smokers. With approximately 80% of the world's smokers located in low- and middle-income countries (LMICs), the burden is especially great within these countries (World Health Organization, 2025). Smoking causes an equally shocking amount of death (Jha, 2020 ; Okorare et al., 2023). Chronic obstructive pulmonary disease (COPD), coronary heart disease (CHD), stroke and cancer, all caused by nicotine and the thousands of other dangerous chemicals in tobacco smoke (Hawari, 2018). There were 2,008 fatalities in total, with 347 attributable to (CVD) and 501 to cancer. The risk of death from any cause was 1.5 times higher for people who smoked occasionally butnotdaily compared to those who never smoked. Mortality risk increased with cigarette intake for daily smokers. It was also clear that there was an increased risk of deathfrom (CVD) and cancer. It is worth noting that current smokers have a higher mortality risk compared to former smokers who had quit smoking for at least five years, indicating that quitting minimizes long-term harm. These results highlight the fact that smoking even once a week is associated with a high risk of death, and that efforts to reduce tobacco use should aim at all smoking habits (Zhu et al., 2021).

There is an uneven distribution of the load worldwide. Cigarette taxes, smoke-free legislation, public education campaigns, and other tobacco control initiatives have contributed to a steady drop in smoking rates in high-income nations (World Health

Organization, 2021). Having said that, smoking rates have either remained high or are rising in a number of African, Middle Eastern, and Asian countries (Bilano etal., 2015). For example, out of the world's total smokers, one-third are located in China (approximately 300 million people) (Zhang etal., 2011). It has been shown in numerous researches that smokingcigarettes increases the risk of stroke. Statistics show that 94% of people think smoking causes serious health problems, and 75.5 percent say it causes stroke. In 2018, researchers in Japan and Singapore discovered that smoking rates are lowest in those countries, with Bangladesh, Papua New Guinea, and Bhutan ranked lower than that. On the other hand, the death toll from strokes is highest in Mongolia and Indonesia (Abeysekera et al., 2024). The Centers for Disease Control and Prevention (CDC) utilized the Smoking-Attributable Mortality, Morbidity, and Economic Costs model to assess the yearly impact of smoking-related fatalities in the U.S. According to data from 2005 to 2009, the CDC indicated that cigarette smoking accounted for over 480,000 fatalities annually (Le et al., 2023). Tobacco consumption significantly impacts male mortality in some ASEAN nations, comprising 23.1% of deaths in Malaysia, 22.9% in Thailand, 21.4% in Indonesia, 22.7% in the Philippines, and 26.1% in Vietnam. The economic repercussions are also grave, with the overall cost of smoking in Indonesia estimated at US$44.6 billion, the highest in the region, followed by Thailand (US$6.5 billion), the Philippines (US$5.4 billion), Vietnam (US$3.7 billion), and Malaysia (US$3.6 billion) (Yen & Tan, 2021).

Tobacco use has significant monetary costs in addition to health risks (Makate et al., 2019). From 2010 to 2014, cigarette smoking constituted of 11.7% of yearly healthcare costs in the U.S, amounting to almost USD 225 billion in 2014 based on total personal healthcare spending. Significantly, more than fifty percent of the smoking-related costs were incurred by public health programs like Medicare and Medicaid, with the share attributed to Medicaid rising by over thirty percent throughout this timeframe (Xu et al., 2021). Smoking during pregnancy and lactation considerably modifies the metabolic characteristics of breast milk in women of reproductive age. In Europe, over 10% of women persist in smoking during pregnancy, and while some temporarily refrain, relapse rates are significant, with approximately 67% resuming smoking within three months postpartum and up to 90% by 11 months. Findings from seven research encompassing 614 mothers demonstrate that maternal smoking during gestation and breastfeeding correlates with diminished Interleukin-8 (IL-8) content and increased C-X-C motif chemokine ligand 8 (CXCL8) levels in breast milk (Macchi et al., 2020).

There is an immediate need for effective prevention and cessation programs due to the high prevalence of smoking, smoking related terrible health effects, and the enormous economic cost (Siersbaek et al., 2024). The social, cultural, and economic institutions of many countries continue to support smoking, despite worldwide efforts like the WHO Framework Convention on Tobacco Control (FCTC), which has been ratified by over 180 nations (Siddiqi et al., 2023; Bhatta et al., 2019). This persistent problem emphasizes the need for new nicotine delivery systems to aid in long-term quitting efforts, decrease relapse rates, and lessen the worldwide impact of tobacco -related illnesses (Fathi & Kathuria, 2023).

2.2 The Effects of Smoking on Health and Society

The devastating health and financial effects of tobacco usage have been well-documented in recent years. Lung cancer, ischemic heart disease, stroke, type 2 diabetes, and other serious health problems are greatly increased when non-smokers are exposed to second-hand smoke (Zhang et al., 2024). High healthcare costs associated with smoking-related chronic respiratory disorders like asthma COPD continue to place a heavy financial burden on the U.S (Gu et al., 2024). Although smoking has become less common around the world, it is still a major contributor to many health problems, including poor quality of life and increased risk of death from smoking-related causes (Farcher et al., 2023; Sultan et al., 2024). Direct health expenses andproductivity losses added up to a worldwide economic cost of smoking of $1,436 billion (approximately $1.4 trillion) in 2012, or 1.8% of the world's gross domestic product (GDP) in purchasing power parity (PPP) (Goodchild et al., 2017). An estimated £49.2 billion is spent each year in England on smoking-related expenses. This includes £17.0 billion for lost productivity due to early mortality, £10.7 billion for lower earnings, £9.8 billion for costs associated with unemployment, £8.6 billion for healthcare, and £3.1 billion for social care (Ekpu & Brown, 2015). One of the most significant consequences of smoking is the development of (CVD) (Benowitz & Liakoni, 2021).

CHD and stroke are exacerbated by smoking because it quickens the process of atherosclerosis, increases the likelihood of thrombosis, and peaks blood pressure (Klein, 2022). Cigarette smoking is significantly linked to COPD. Lung function decline, exacerbations, and mortality are all worse for smokers than for non-smokers (Salvi et al., 2020; McRobbie & Kwan, 2020). Smoking also increases the chance of cancer,

which is a serious health concern. Smoking causes cancer in approximately two-thirds of all cases, with lung cancer being the most common type (Hecht & Hatsukami, 2022). A recent worldwide study found that 2.5 million people lost their lives in 2019 due to smoking-related diseases. The most common types of these cancers were lung, trachea, and bronchus cancers (Safiri et al., 2022). New studies have also shown a correlation between smoking and psychological problems. Anxieties and depression are more common in smokers, according to a prospective study, and when people quit, their mental health improves (A. D. Wu et al., 2023). According to these correlations, cigarette smoking is associated with a myriad of health problems that go beyond the usual suspects of chronic illness (Stanton et al., 2016).

2.3 Problems with Current Smoking Cessation Treatments

Over 40 pharmacotherapies have been examined for smoking cessation. The primary first-line agents NRT, bupropion, and varenicline are FDA-approved and provide the foundation of treatment. Evidence indicates that the combination of NRT and varenicline yields the highest cessation rates. Clonidine and nortriptyline are classified as second-line treatments, generally employedwhenfirst-line alternatives are ineffective or inappropriate. Numerous innovative therapies, such as cytisine (cytisinicline), N-acetylcysteine, baclofen, and acetylcholinesterase inhibitors, have demonstrated potential; nonetheless, the majority are still in the experimental stage and necessitate additional assessment (Gómez-Coronado et al., 2017). However, smoking cessation results in the real world are still modest, even though there are numerous pharmacological and behavioural therapy available. There is a high rate of relapse; many people start smoking again within a year of quitting (Jackson et al., 2019; Alboksmaty et al., 2019). Conventional treatment was unsuccessful for many smokers. Among those who did not abstain, the only way to improve quit rates was to increase the dosage of varenicline or combined NRT. Keeping on with the same medication had no effect. Overall, thestudy emphasizes the difficulty of maintaining abstinenceand the high failure rates of first attempts to quit. It also suggests that switching strategies or increasing the dosage may be helpful (Cinciripini et al., 2024). A further study found that nicotine patches, varenicline, and combination NRT did not demonstrate any meaningful differences in stop rates at six or twelve months. The majority of smokers continued to relapse despite receiving treatment. By highlighting the poor long-term success of existing

pharmacotherapies for smoking cessation, our findings highlight the importance of the issue (Baker et al., 2016). A comprehensive analysis discovered that weight gain is a major issue for smokers who are seeking to quit, and that rapid early weight growth predicts long-term relapse in some individuals. Another hurdle that is frequently noted is the fact that weight gain occurs after quitting smoking (Tian et al., 2015). There is also a global concern regarding access to pharmacotherapy. In the case of varenicline, for instance, the recall of the medication owing to nitrosaminecontamination caused a disruption in supply on a global scale, which led to a large decreasein its utilization in smoking cessation programs (Jiménez-Ruiz et al., 2023). Despite the fact that more modern medicines, such as cytisinicline, have been shown to be effective in recent randomized controlled trials, these medications are not yet readily availableor incorporated into cessation clinics (Rigotti et al., 2023). Although the most recent review concluded that nicotine e-cigarettes are more effective than NRT in assisting smokers in quitting, there is still the question of whether or not they are safe to use for an extended period of time and whether or not they can be used in conjunction with traditional cigarettes (Chan et al., 2021). It is essential to recognize that persons who are struggling with mental health disorders face a greater numberof difficulties when attempting to quit smoking (Sharma et al., 2016). Even while there are therapies that work, they aren't always effective because of issues like recurrence, lack of adherence, side effects, hurdles to access, and ongoing inequalities.

2.4 The Pharmacology of Nicotine and Its Replacement Treatment

2.4.1 Nicotine's Physicochemical and Chemical Characteristics

Nicotine, the main psychoactive component of tobacco, is an alkaloid that occurs naturally and is mostly found in Nicotiana tabacum and related species (Sansone et al., 2023). In terms of its molecular composition, it has a bicyclic structure with two rings a pyridine and a pyrrolidine which affects its ability to bind to acetylcholine receptors in the brain Figure 2.1)(. The (S)-isomer of nicotine is the more biologically active and naturally occurring of the two enantiomers; this is also the form that gives nicotine its strong pharmacological and psychoactive effects (Takeda et al., 2021; Trotsko et al., 2024).

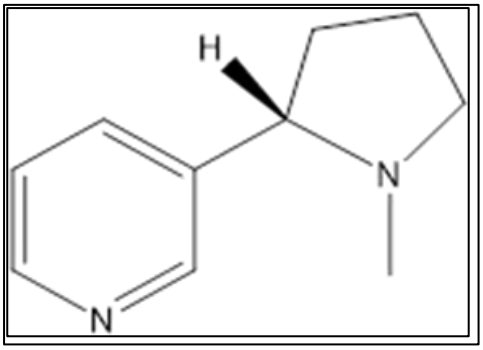

Figure 2.1 Nicotine Structure

The molecular weight of nicotine is 162.23 g/mol, and its density is about 1.01 g/cm³. The liquid is pale yellow in color. This compound's weak basicity is due to the presence of two nitrogen atoms in its structure: one in the pyridine ring and another in the pyrrolidine ring. The ionization potentials of the nitrogen atoms in these compounds are different; at 25 °C, the pyrrolidine nitrogen has a higher pKa value of 8.10, while the pyridine nitrogen has a substantially lower value of 3.41. Nicotine can be distributed in both lipid and water environments since it is water-miscible while being a lipophilic molecule (logP = 1.17). Nicotine can exist in three different forms: di-protonated, mono-protonated, or as the free base, determined by the pH of the medium. Nevertheless, the di-protonated form becomes noticeable only at pH levels below 5.5, and the pyridine nitrogen's contribution to ionization is often insignificant due to its low pKa. To what extent biological membranes allow nicotine absorption and bioavailability is reliant on this pH-dependent ionization profile (Gholap et al., 2020; Clayton et al., 2012). Itmakes up around 95% of the total alkaloid content and accounts for approximately 1.5% by weight in commercial cigarette tobacco, making it the major tobacco alkaloid (Wolff et al., 2016). Nicotine in its salt forms, like nicotinic salt, is very soluble in water (Al-Dahhan et al., 2021). This equilibrium makes it possible for nicotine to partition between aqueous and lipid environments in an efficient manner, which in turn enables quick absorption and widespread dispersion across biological systems. In addition, the moderate lipophilicity is essential for its capability of crossing the BBB, which differentiates it from a great number of hydrophilic medications that have poor penetration into the CNS (Sanap et al., 2023; McKinney & Vansickel, 2016). Tens of seconds are all it takes for nicotine to make its way to the brain after entering the bloodstream primarily through the lungs. At a pH of 7.4, nicotine can be found in

the bloodstream in both charged (69%) and uncharged (31%) forms that are present. It is possible for the uncharged form to traverse lipid membranes and directly influence the signaling that occurs within the cell (Subramaniyan & Dani, 2015). Additionally, its volatility is a significant feature, particularly when it is in the free-base form. Because nicotine in smoke or aerosol particles diffuses into the bloodstream at a quick rate, pulmonary absorption is made possible by the presence of volatility (Panko w, 2001; Maiyo et al., 2022). Nicotine, on the other hand, is easily degraded and prone to chemical instability. In the presence of oxygen, light, and alkaline circumstances, it goes through the processes of oxidation resulting in the formation of cotinine, nicotine-N-oxide, and various other derivatives. Both the potency and the stability of medicinal formulations are compromised as a result of these processes. For example, the liquid nicotine included in electronic cigarette cartridges will darken with time as a result of oxidation (Cañas et al., 2021; Z. Xu et al., 2023; Aldeek et al., 2025).

2.4.2 Neuropharmacological Pathways Linked to Nicotine Addiction

Nicotine addiction is not a straightforward issue of habit; rather, it is the result of intricate interactions between nicotine and brain circuits that regulate reward, reinforcement, and adaptability. Nicotine's effects include the activation, desensitization, andmodification of nicotinic acetylcholine receptors(nAChRs), as well as the modulation of dopamine transmission and the engagement of various neurotransmitter systems. These effects occur at the molecular and cellular levels. (Tiwari et al., 2020; Vallés & Barrantes, 2023). Neuroadaptations, which occur over time, are responsible for the development of tolerance, withdrawal symptoms, and obsessive use, notwithstandingthe negative consequences (Turton & Lingford-Hughes, 2020). Nicotine has the ability to bind to neuronal (nAChRs), particularly receptor subtypes that contain α4β2 and α7 subunits. These receptor subtypes are widely dispersed throughout many parts of the brain, such as the ventral tegmental area (VTA), nucleus accumbens (NAc), prefrontal cortex (PFC), and thalamus (Xiao et al., 2019). In addition to modulating neuronal excitability, binding to presynaptic nAChRs is responsible for promoting the release of neurotransmitters such as dopamine, GABA, and glutamate. After repeated exposure, nAChRs reach a desensitized state, in which they become less responsive. This is then followed by upregulation, which is an increase in the number of receptors, most likely as a compensatory reaction (Arias et al., 2021;

Lovinger et al., 2022). In addition to the conventional α4β2 and α7 subtypes, new nAChR assemblies including α3β4 have been suggested to alter the reinforcing effects of nicotine. In the medial habenula-interpeduncular nucleus (MHb-IPN) pathway, which is associated with nicotine's unpleasant effects, α3β4 receptors are very abundant (Scholze & Huck, 2020). It is possible that activation of this pathway is responsible for the unpleasant responses that are induced by extremely high dosages of nicotine, which counteract the rewarding benefits of the drug when administered in moderate amounts. Dopamine neuron firing and release are tightly connected with α6-containing receptors in the VTA, highlighting the significance that these receptors play in the reinforcing process (Husson et al., 2020; Nguyen et al., 2021).

Nicotine's rewarding effects are completely dependent on the mesolimbic dopamine pathway. The nAChRs on dopaminergic neurons in the VTA are activated by nicotine, which results in an increase in the firing rate of these neurons and the release of dopamine into target locations, particularly the NAc and the PFC. The production of pleasurable sensations and the development of associations with cues and environment are the primary ways in which these events encourage drug taking behavior. (Balfour, 2015; Marcela & Agamennoni, 2024). Chronic nicotine exposure and the related changes in dopamine signaling are factors that lead to cravings and the likelihood of relapse (Wills & Kenny, 2021). It is not just dopamine that is affected by nicotine's influence. GABAergic, glutamatergic, serotonergic, and noradrenergic systems are all modulated by it, which results in the formation of reward, mood, and inhibitory control (Bayassi-Jakowicka et al., 2021). For instance, the release of glutamate that is generated by nicotine can increase the excitatory drive onto dopamine neurons, which in turn causes dopamine responses to become more intense. It is possible that nicotine can reduce the inhibition of GABAergic interneurons, which are responsible for modulating the firing of dopamine neurons. Pathways involving

Serotonin and noradrenaline have been linked to the control of mood as well as the symptoms encountered after withdrawal (Kim & Picciotto, 2023). Changes in neuroadaptive processes, such as increased receptor sensitivity, synaptic remodeling, and altered intracellular signaling (such as changes in gene expression), are triggered by continuous exposure to nicotine. In the process of these adaptations, tolerance develops, which means that higher amounts of nicotine are required to get the same effect. Additionally, withdrawal symptoms, which include anxiety, irritability, and cognitive deficiencies, manifest themselves when nicotine is removed from the body.

Relapse is propelled by these unpleasant states (Schmidt et al., 2018; Nestler & Lüscher, 2019).

2.4.3 Metabolism and Pharmacokinetic Profiles of Nicotine

The addictive potential of nicotine is enhancedby its quick absorption and broad hepatic metabolism (Pickworth et al., 2014; Jain et al., 2021). Because of its moderate lipophilicity and fast transit over BBB, nicotine enters the brain within seconds after inhalation, butfirst-pass metabolism limits its oral administration (StHelen et al., 2015; Kolli, 2023; Tanget al., 2024). It goes through a lot of changes in its biosynthesis, with CYP2A6 being the main enzyme that converts nicotine to cotinine through the nicotine-Δ1′ (5′)-iminium intermediate. Then, aldehyde oxidase and CYP2A6 continue the metabolism to produce trans-3′-hydroxycotinine (3HC). According to Delijewski et al. (2019), cotinine and 3HC are the two most common circulating metabolites that can be used as accurate indicators of nicotine intake. Although they only contribute slightly to total clearance, additional routes involve N-oxidation by flavin-containing monooxygenases and N-glucuronidation mediated by uridine 5′-diphospho-glucuronosyltransferase 2B10(UGT 2B10). Measurements of blood nicotine levels following the administration of a known dose indicate that nicotine has a short plasma half-life of 2 hrs. The average total clearance of nicotine is around 1,200 ml/min. The amount of nicotine eliminated from the bloodstream during each passage through the liver is approximately 70% due to nonrenal clearance, which accounts for approximately 70% of the blood flow via the liver. When compared to cotinine, the clearances of trans-3'-hydroxycotinine are significantly slower, averaging 82 ml/min (Eaton et al., 2018; Perez-Paramo et al., 2022). The amount of nicotine that is excreted by the kidneys depends on the pH of the urine; a higher pH results in less excretion of nicotine by ion trapping, while an acidic pH increases it (Goldberger & Karch, 2022). The pharmacokinetics of nicotine vary greatly from one person to the next; however, the most important factor influencing clearance rate, smoking intensity, and response to treatment is CYP2A6 genetic polymorphisms (Tanner & Tyndale, 2017). Additionally, enhanced CYP2A6 and UGT 2B10 activity speeds up nicotine metabolism during physiological situations like pregnancy, which in turn lowers cotinine levels at equivalent exposures (Taghavi et al., 2017).

2.4.4 Presently Available Treatments for Smoking Addiction

Current pharmacotherapeutics for the treatment of tobacco addiction are categorized into first-line and second-line drugs according to the clinical practice strategies. Mills et al. (2012) included varenicline, bupropion, and nicotine NRT as first-line drugs. The combination of clonidine and nortriptyline is known as second-line medicine (Aubin et al., 2013).

2.4.4.1 Nicotine Replacement Therapy (NRT)

According to research by Giulietti et al. in 2020, NRTs are the most comprehensive and well-established pharmacological strategy for smoking cessation. They are also recommended by major health organizations all over the world as the initial treatment recommendation. According to Kamala et al. (2019), NRTs are offered in a variety of formulations, all of which include transdermal patches, chewing gum, lozenges, inhalers, and nasal sprays. In contrast to gums and lozenges, which allow for flexible, on-demand dosage to manage breakthrough cravings (Hansson et al., 2016), nicotine patches give consistent plasma nicotine concentrations over a period of twenty-four hrs, which helps to suppress cravings over the long term (Rasmussen et al., 2018). They also facilitate long-term craving suppression. According to Kolli et al.'s 2019 research, nasal sprays and oral inhalers deliver nicotine at a faster rate, mirroring certain elements of the pharmacokinetics produced by cigarettes. Cigarette smoke basically works by activating nicotinic receptors in the VTA of the brain, which triggers the release of dopamine, and providing nicotine without other dangerous chemicals. This partially replaces the nicotine that smokers get from tobacco (Flowers, 2016). According to Brown et al. (2013), smokers have more intense withdrawal symptoms and cravings when they attempt to quit nicotine. Regarding the safety of NRT, patients who do not come into contact with other harmful tobacco products can obtain nicotine from NRT, which is a far more reasonable option (Shahab et al., 2014). On the other hand, those who smoke cigarettes absorb nicotine from those cigarettes (Van Amsterdam et al., 2011). When compared to placebo therapy, the effectiveness of all NRT products is double, increasing the likelihood that smokers would be able to quit (Keane, 2013).

However, because to its own limits, NRT was unable to entirely alleviate all symptoms of nicotine withdrawal cravings (Mills et al., 2010). According to Shahab et al. (2013), it takes at least a few min for the nicotine from NRT products to be absorbed into the systemic veins. Nicotine delivered by gum is not instantaneous, and it is not easy to change the dosage (Islam, 2012). The inadequate rate of nicotine release and, by furthermore, the slow beginning of therapeutic benefits, is a drawback of commercially available nicotine gums (Aslani & Rafiei, 2012). Some patients will have a lower success rate with NRT if they are not committed to quitting or if they do not believe they would go through nicotine withdrawal. Additional research on the effectiveness of 42 mg nicotine patch therapy for fast metabolizers of nicotine is necessary (Schnoll et al., 2012; Nelson et al., 2015). When used in conjunction with behavioral support, NRT is typically more effective for heavy smokers who have tried to quit in the past (Rigotti, 2012). Patches and gums or inhalers are two examples of the recommended combination treatments (Caldwell & Crane, 2016; Leung et al., 2019). According to Secades-Villa et al. (2017), when it comes to helping people quit smoking, a combination of medication and positive psychological interventions works better.

2.4.4.2 Electronic Nicotine Delivery Device (e-cigarette)

The marketing of electronic cigarettes began in China in 2003 and moved to the U.S in 2007 (Harrell et al., 2014). Since then, they have been used as a medication delivery device to help people quit smoking in several nations throughout the world (Adkison et al., 2013). Nonetheless, the Therapeutic Goods Administration (TGA) has not given its approval for its usage as a nicotine cessation aid in Australia (Dessaix et al., 2022). Even though nicotine e-liquids have beenbanned in Malaysia since 2015, e- cigarette use was an issue for 15.7% of school-going adolescents who had never used tobacco products. At 21.6%, men were more susceptible than women, who were only 11.1%. The prevalence was highest among Indian teenagers (22.5%) and Chinese adolescents (20.6%), compared to Malays (14.1%), when looking at thedataby ethnicity. Similar vulnerability wasobserved in rural teenagers (16.6% vs. 14.3%) compared to urban teenagers. The results show that teenagers in Malaysia are still susceptible to starting to use e-cigarettes, even if there are regulations in place to prevent it. This highlights the critical need for more extensive prevention programs and specific interventions (Heng et al., 2021).

An electronic cigarette is a battery-operated device that contains a solution of propylene glycol or glycerine, water, and nicotine (BeyazçiÇek et al., 2020). They have a tiny sensor that detects when you breathe in and then uses heat or ultrasound to create a mist of nicotine (Rao et al., 2022). These aerosolizers work with disposable cartridges that contain nicotine in a propylene glycol solution, which acts as a humectant. These tools include a pressure switch, power supply, heating element, and battery (Marcham & Springston, 2019). A disposable electronic cigarette (DEC) is a cigarette-shaped device that uses a battery and an atomizer cartridge to heat a nicotine or non-nicotine solution. Commonly known as e-hookahs, these are disposable once the vapour production ceases and cannot be recharged or filled. An atomizer that heats a nicotine solution is coupled to a rechargeable battery in rechargeable e-cigarettes (REC), which otherwise look identical. You can usually adjust the puff time and the number of puffs in a ro w using these. The pen-shaped, medium-sized rechargeable e-cigarettes have bigger batteries and a more substantial build than regular cigarettes. Prefilled or refillable cartridges are used in these devices, and a manual switch is usually present to let th e user change the puff length and frequency. Big, tank-style rechargeable e-cigarettes have huge refillable cartridges and powerful batteries. Manual switches and replaceable battery cases make them simple to alter (Glantz & Bareham, 2018).

Even though e-cigarettes were first introduced to the public at a relatively early level, there is still a lack of research on their safety inhalation in humans (Marques et al., 2021). Furthermore, the proper dosage of nicotine delivered by e-cigarettes is still up for debate, and the product has not been successful in reducing smoking-related health issues (Farsalinos & LeHouezec, 2015).

2.4.5 Medications used in NRT

2.4.5.1 Bupropion

According to Shewale et al. (2015), bupropion hydrochloride is a viable alternative to nicotine for people looking to quit smoking. As an advantage over quick release, it is best taken orally using a sustained-release formulation (Mendonça et al., 2015). At the moment, bupropion is sold under the brand names Wellbutrin ™ (for the treatment of depression) and Zyban™ (for the treatment of helping people quit smoking). The immediate-release (IR) formulation, which is taken three times daily, the sustained-

release (SR) formulation, which is supplied twice daily, and the extended-release (XL) formulation, which is taken once daily, are the several formulations obtainable. However, the XL formulation is not yet available for use in cases of smoking cessation. Instead, bupropion is only available in the sustained-release version, and for this particular indication, it is necessary to take the medication twice daily (Khan et al., 2016; Disease Interrupted, Tobacco Reduction and Cessation, n.d.). According to Clark et al.'s 2023 research, bupropion, which is a selective reuptake inhibitor of dopamine and noradrenalin, has the potential to minimize and avoid the cravings that are associated with quitting smoking. Based on the findings of King et al. (2011) and Tran et al. (2018), it has been stated that bupropion has the potential to enhance the likelihood of quitting smoking when compared to placebo therapy. However, the mechanism of action of bupropion in the process of smoking cessation remains under investigation. A study conducted by Vázquez-Gómez et al. (2014) found that modest dosages of bupropion have the ability to inhibit the activity of (nAChRs) in the brain, hence potentially diminishing the positive reinforcing effects of nicotine.

It is safe to use in individuals who have (CVD); nevertheless, its use is restricted due to the fact that it can occasionally cause an elevation in blood pressure. This is something that has been found among smokers who have hypertension (Behlke et al., 2020). According to Qin et al. (2024), bupropion effectively lowers the amounts of carbon monoxide in the breath that has been exhaled. According to Patel et al. (2016), the other most prevalent side effects associated with the usage of bupropion include dry mouth and night-time sleepiness.

2.4.5.2 Varenicline

In 2006, Pfizer was the company that brought the medication known as Varenicline (Chantix/Champix®) to the market (Hughes, 2015; Mazurov & Yohannes, 2014). By acting as a partial selective agonist for the α4β2 nAChR subtypes, varenicline has the ability to mediate the reinforcing properties of nicotine in the cerebral segment region of the brain. Furthermore, it significantly enhances oral bioavailability and brain penetration due to its production as a cytisine derivative (Arias et al., 2014; Brunzell et al., 2014). According to Mizoguchi et al. (2018), partial agonists of the α4β2 nicotinic receptor have the potential to prevent the activation of dopamine that is produced by smoking, while simultaneously providing relief from the symptoms of smoking

withdrawal syndrome. Varenicline has two distinct effects: on the one hand, it partially stimulates nAChRs without causing the full effect of nicotine agonist activity, and on the other hand, it blocks nAChRs to prevent nicotine from traveling to them (Borkar et al., 2023). Both of these effects are a result of the drug's ability to inhibit nicotine agonist action. According to Tonstad etal.'s research from 2020, varenicline exhibits a stronger affinity and a less functional effect than nicotine, which results in a smaller release of dopamine. According to Jordan and Xi (2018), varenicline has the ability to alleviate the symptoms of smoking withdrawal syndrome and lower chances of one having a relapse.

According to the findings of Shang et al. (2023), varenicline is a viable choice for quitting smoking that possesses an acceptable safety and tolerability profile. (Benli et al., 2017) found that participants who were using varenicline were more likely to effectively quit smoking than those who were treating themselves with bupropion. Varenicline is known to cause nausea, which is the most significant adverse effect; nevertheless, in the majority of patients, nausea tends to disappear over time with doses that range from mild to moderate (Fouz-Rosón etal., 2017). Additional adverse effects, including headaches, sleeplessness, and gastrointestinal issues, have been reported to be associated with the use of varenicline (Carrillo, 2021). Furthermore, according to Menku et al. (2021), some patients who have been using varenicline have reported experiencing symptoms of sadness, suicidal thoughts, and even suicide, in addition to serious neuropsychiatric symptoms.

2.5 Intranasal Drug Delivery for Brain Targeting

2.5.1 The Nasal Cavity's Anatomy and Physiology

Critical functions of the nasal cavity include inhalation, exhalation, filtration, humidification, thermoregulation, immunological defense, and smell sense (Davraj et al., 2021; Khunt & Misra, 2021). It is exceptionally well-suited for gas exchange efficiency and, in the field of pharmaceutical research, for central and systemic drug delivery because to its complex structure, which includes epithelial, vascular, and neuronal components (Cellina et al., 2020; Bahmanpour et al., 2020).

2.5.1.1 The Nasal Cavity in Gross Anatomy

According to Pagano and Márquez (2022), the nasal cavity is a paired structure that is divided by the nasal septum. It extends from the external nares (nostrils) in the front to the choanae in the back, where it opens out into the nasopharynx. One pair of big irregular cavities can be found within the internal structures of the nose, as shown in Figure 2.2. According to Chung et al. (2022), these bony projections, which are known as superior, middle, and inferior conchae, form narrow channels known as meatuses. These meatuses generate turbulent airflow for the purpose of facilitating air cooling and efficient particle entrapment.

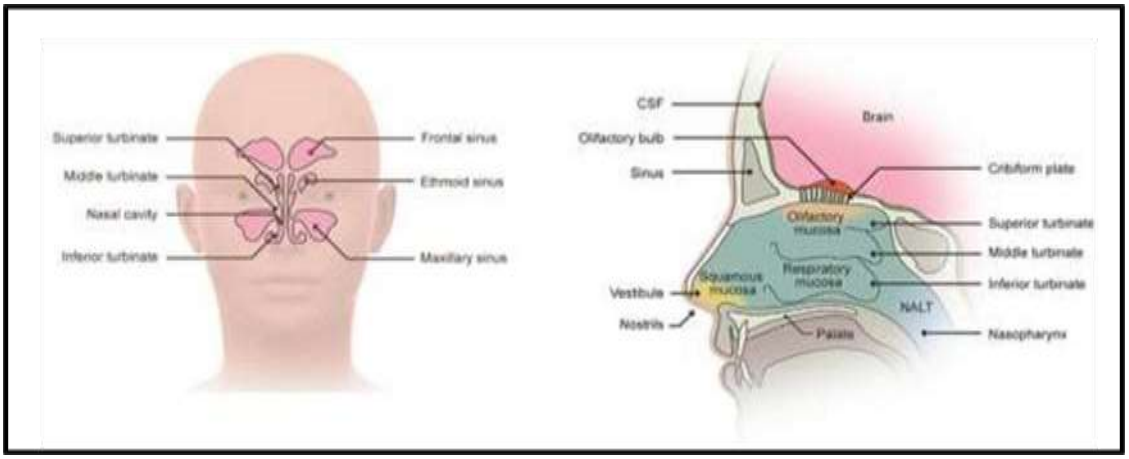

Figure 2.2 Gross Anatomy Of The Nasal Cavity (Chung Et Al., 2022)

In terms of anatomy, the nasal cavity is composed of three separate functional zones, which, when combined, are responsible for performing essential functions related to respiration and sensory perception. A keratinized stratified squamous epithelium that contains vibrissae (coarse hairs) lines the vestibular region, which is situated in the anterior 1.5 centimetres of the nasal passage. This epithelium serves as a primary defense barrier by capturing large particulate matter and debris that are inhaled from inspired air (Peng et al., 2019; Parrilla et al., 2023). This is followed by the respiratory area, which is the biggest portion of the nasal cavity and is lined by pseudostratified ciliated columnar epithelium packed with goblet cells. The respiratory region is located posterior to this. The primary functions of this region include air filtration, humidification, and mucociliary clearance, all of which are procedures that are necessary for preserving the sterility of the respiratory tract and ensuring that inspired

air is properly conditioned (Simukoko, 2021). Specialized olfactory receptor neurons are found in the olfactory area, which is located in the roof of the nasal cavity beneath the cribriform plate of the ethmoid bone (Ilahi & Perry, 2021). These neurons are responsible for the brain's ability to perceive smell by converting odorant molecules into neural impulses. The quadrangular cartilage is locatedanteriorly, the perpendicular plate of the ethmoid bone is located superiorly, and the vomer is located posteriorly. The nasal septum is the structural component that forms the midline barrier that separates the two nasal cavities (Singh etal., 2021). Conchaeare bony projections that are covered by a vascularized mucosal lining that boosts the surface area of the nasal cavity and regulates air temperature and humidity by its vast blood supply (Folkow & Nord, 2022). The superior, middle, and inferior conchae are located on the lateral walls of the nasal canal.

2.5.1.2 The Innervation and Supply of The Vascular System

According to Zbar (2024), the nasal cavity is one of the most highly vascularized parts of the human body. It receives its blood supply from both the internal and exterior carotid artery systems when it is well supplied with blood. According to Bonasia et al. (2019), the origin of the anterior and posterior ethmoidal arteries can be traced back to the internal carotid system. These arteries are branches of the ocular artery and are largely responsible for supplying the upper sections of the nose cavity.

When compared to this, the external carotid system is responsible for contributing through the sphenopalatine, greater palatine, and superior labial arteries. These arteries all originate from the maxillary and facial arteries and perfuse the inferior and anterior portions of the nasal mucosa (Leader et al., 2023). Kiesselbach's plexus, also known as Little's area, is located on the anterior nasal septum. This region is commonly implicated in epistaxis due to its rich vascular density (Smail, 2024). These arterial branches produce vast anastomoses inside the Kiesselbach's apparatus. According to Du et al. (2024), this complicated capillary network performs a critical physiological role in warming and humidifying inspired air. Additionally, its high permeability makes it easier for medications to be absorbed into the systemic circulation when they are supplied intranasally. One of the most important advantages that underpins the use of the intranasal route for targeted brain delivery is the fact that venous drainage of the nasal cavity occurs through the sphenopalatine, facial, and ophthalmic veins. These

veins communicate directly with the cavernous sinus, which provides a potential pathway for rapid drug transport to the CNS.

2.5.1.3 Nasal Mucosa and Mucociliary Drainage

According to Shetty and Archana (2023), the nasal mucosa is mostly lined with pseudostratified ciliated columnar epithelium, with a few goblet cells and basal cells scattered throughout. The epithelial surface is covered with a biphasic mucus layer, which consists of an outer gel layer that acts as a filter for particles and microbes, and an inner sol layer that permits the movement of cilia (Gausterer et al., 2023; Fröhlich, 2022). The distinctive motile cilia of ciliated cells, which are made up of both structural proteins (such dyneins) and motor proteins that control the coordinated directional beating of the cilia, are a telltale sign of ciliated cells (Mitchison & Valente, 2016). Airway ciliated cells sense and respond to both mechanical and irritant stimulation, which is becoming more widely acknowledged, despite the well-established biomechanical roles of multicilia in epithelial cells as an essential part of mucociliary clearance. According to Whitsett (2018), ciliated cells are typically thought of as terminally differentiated cells, however they actually originate from airway basal and club cells. Figure 2.3 R. Zhang et al. (2023) states that the nasal mucosal surface is lined with a highly specialized epithelial barrier that is specifically enginee red for secretion**.**clearance, and protection. An upper, more viscous mucin layer covers the epithelial cells' apical surface, which faces the nasal cavity. This layer acts as a filter for inhaled dust, microbes, and other pollutants. Underneath this, in a thin aqueous layer called pericellular (sol) fluid, the cilia are free to beat and propel mucus toward the nasopharynx (Hill et al., 2022). Hewitt and Lloyd (2021) identified many cell types inside the airway epithelium, all of which play a role in maintaining mucosal defense and homeostasis. In order to maintain a wet surface and to trap inhaled particles, goblet cells release mucins, which are the main structural components of mucus (Wagner et al., 2018). Located along the basement membrane, basal cells are progenitor cells or stem-like cells that are in charge of epithelial regeneration and injury repair (Li et al., 2023). Epithelial integrity and local immune defense are both helped by the detoxifying enzymes and protective proteins secreted by club (Clara) cells (Raith & Swoboda, 2023).

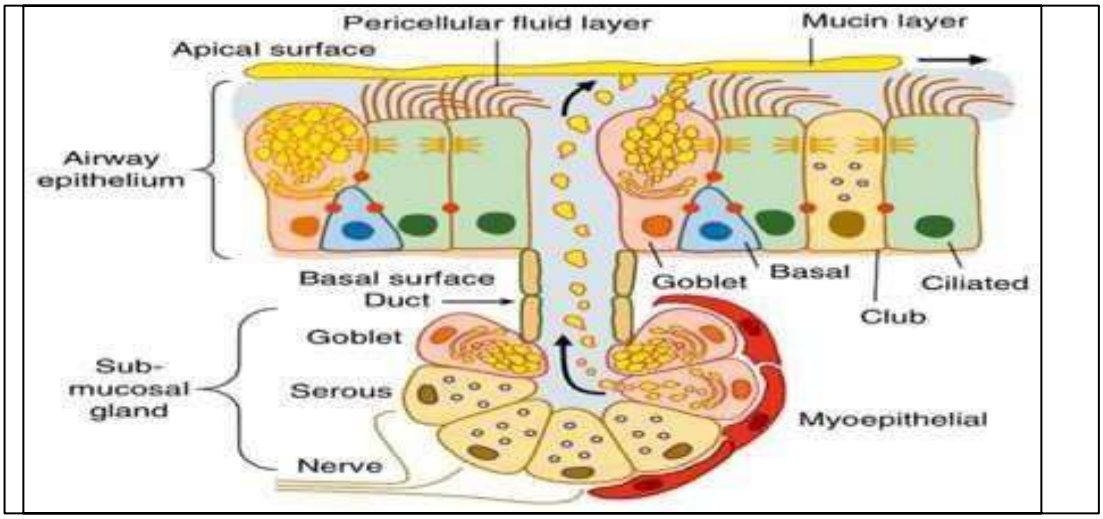

Figure 2.3 The Nasal Epithelium, Which Lines The Upper Airways And The Nasal Cavity, Is Shown In Microscopic Detail. It Shows The Secretion And Transportation Of Mucus To Cushion The Airways From Dust, Bacteria, And Dehydration (Whitsett, 2018).

2.5.1.4 Air Conditioning and Nasal Physiology

According to Ottaviano (2023), the nasal cavity is responsible for conditioning inspired air which includes warming, humidifying, and filtering the air before it reaches the lower respiratory tract. This is one of the fundamental physiological functions of the nasal cavity. When the air reaches the nasopharynx, the temperature is changed to beclose to the temperature of the body, which is approximately 37 degrees Celsius, and the humidity is close to 100 percent (Dong et al., 2024). According to Smith et al. (2018), the quick conditioning process is made easier by the presence of a generous submucosal vascular plexus as well as a wide surface area of the turbinates. There are numerous immune cells, such as macrophages, dendritic cells, and T lymphocytes, that are found within the lamina propria of the nasal cavity. These immune cells collectively contribute to innate and adaptive defensive mechanisms (Shoufy et al., 2024). The nasal cavity serves as a first-line immunological barrier. According to Ainurofiq et al. (2023), the nasal cavity is a suitable route for systemic and brain -targeted medication administration. This conclusion was reached from the perspective of the pharmaceutical industry. Because of the strong vascularity and relatively large surface area of the epithelium, fast absorption is possible. Additionally, the absence of first-pass hepatic metabolism contributes to an increase in bioavailability (Maurya et al., 2024). The olfactory and trigeminal neuronal pathways are also capable of providing drugs with

direct access to the brain, allowing them to circumvent the blood–brain barrier. In order to optimize residence time and absorption efficiency, it is necessary to overcome challenges such as enzymatic degradation, limited dosing volume (ranging from approximately 100 to 200 µL per nostril), and mucociliary clearance. This can be accomplished by employing formulation strategies, such as mucoadhesive polymers, NPs, and bioadhesive gels, as stated by Kashyap and Shukla (2019) and Bayer (2022).

2.5.2 Methods by Which Drugs Reach the Brain (Olfactory, Trigeminal, Systematic)

According to Crowe et al. (2017), intranasal drug administration has the potential to utilize numerous transport channels in order to reach the brain. These pathways include particularly the olfactory and trigeminal nerve routes, as well as systemic absorp tion, which can then be followed by the bridging of the BBB under specific circumstances. There are several ways that drugs can reach the brain: through the olfactory pathway, which runs directly from the nasal epithelium to the olfactory bulb, via axonal transport within cells, or through perineural or paracellular pathways that empty into the cerebrospinal fluid (CSF) and eventually reach brain tissue (Hirlekar & Momin, 2018; González, 2023). An alternative route to the brainstem and forebrain structures are provided by the trigeminal nerve pathway, which innervates the respiratory and olfactory mucosa through branches of the ophthalmic (V1) and maxillary (V2) divisions. Drugs may travel through this pathway through either perineural or transcellular transport (Terrier et al., 2022; Lochhead & Davis, 2019). After that, a portion of the intranasally administered agents enter the systemic circulation through the highly vascularized nasal mucosa. From there, a portion may cross the BBB through conventional mechanisms such as diffusion, transporters, and receptor -mediated uptake. However, this method is typically less effective than direct neural pathways (Dholakia et al., 2021; D. Wu et al., 2023). Together, these three pathways olfactory, trigeminal, and systemic support the vision of targeting delivery to the CNS while avoiding many of the constraints that are associated with traditional administration (Patel & Patel, 2017).

2.5.3 Benefits of Intranasal Administration

The intranasal route of drug administration provides a number of compelling features, which make it an appealing alternative for targeting both the CNS and the systemic nervous system (Crowe & Hsu, 2022). According to Sharma et al. (2021), the nasal mucosa has a highly vascularized surface and a large absorptive area (about 150 cm^2), which enables the quick absorption of drugs straight into the systemic circulation. Additionally, this results in a beginning of effect within min, which is comparable to the administration of the drug intravenously (Tai et al., 2022). The avoidance of hepatic first-pass metabolism is yet another significant benefit. This is because medications that are absorbed by the nasal mucosa enter the systemic circulation through the superior and middle meatus venous drainage into the systemic venous pool, so avoiding the liver (Lombardo et al., 2021; Shrewsbury, 2023).

Furthermore, intranasal delivery makes it possible for therapeutic molecules, such as peptides, proteins, and NPs, to circumvent the BBB, which is one of the most significant barriers to the delivery of drugs to the CNS (D'Souza et al., 2021). this is accomplished through the olfactory and trigeminal neural pathways. The non-invasive aspect of nasal delivery further improves patient compliance (Zhang et al., 2022). Non-invasive nasal delivery provides a painless, self-administered method that lowers the need for trained staff and sterile settings (Alabsi et al., 2022; Qin et al., 2021).According to Stielow et al. (2023), the reduction in the amount of dosage required as a result of increased bioavailability helps to reduce the severity of systemic adverse ef fects.

2.5.4 Challenges and Restrictions of Intranasal Administration

According to Fortuna et al. (2022), intranasal medication delivery is affected by a number of substantial biological and physicochemical barriers, which restrict its efficiency and reproducibility. This is despite the fact that it offers a multitude of benefits. According to Adolf and Heilbronner (2022), one of the most significant issues is the enzymatic degradation that occurs within the nasal cavity. Several metabolic enzymes, such as cytochrome P450 isoforms, carboxylesterases, peptidases, and proteases, are expressed by the nasal mucosa. These enzymes have the ability to breakdown sensitive compounds, such as peptides, proteins, and nucleic acids, prior to their absorption (Torres et al., 2024). Due to the fact that this enzymatic activity considerably decreases the drug's bioavailability, it is necessary to employ enzyme

inhibitors, protective excipients, or encapsulation within polymeric in order to enhance the drug's stability (Naki et al., 2025; R. Patel et al., 2020; Weng et al., 2022). Another significant constraint is the mucociliary clearance system, which is a natural defensive mechanism that eliminates inhaled particles and germs by moving mucus toward the nasopharynx (Tufail et al., 2024; Jiao & Zhang, 2022).

Furthermore, formulations that are high in viscosity or contain particle matter may further limit diffusion through the mucus layer and hinder uniform distribution across the nasal epithelium (Ganger & Schindowski, 2018). Tight junctions between nasal epithelial cells restrict the paracellular transport of hydrophilic and high-molecular-weight compounds, while lipophilic cell membranes limit the permeation of polar drugs (Hansen et al., 2024; Clementino et al., 2025). This presents a significant challenge because the epithelial barrier itself is a significant barrier. Significant heterogeneity in drug absorption can be attributed to a number of physiological factors, including nasal diseases (such as rhinitis, sinusitis, and polyps), variations in mucus viscosity, and anatomical abnormalities between individuals (Eliyan et al., 2023).

Additionally, there are obstacles that are associated with formulation. It is crucial to maintain the physiological pH range (5.5–6.5) and isotonicity in order to prevent irritation and guarantee the stability of the medicine. However, many active chemicals are unstable at this pH (L et al., 2017). Pednekar et al. (2022), stated that mucus rheology and medication dispersion can be affected by ambient factors that are volatile, such as humidity and temperature. Finally, it is difficult to achieve sustained therapeutic levels in the systemic circulation or CNS without frequent administration or advanced delivery systems (Ruiz & Scioli-Montoto, 2024). This is because non-volatile formulations have a relatively small surface area and a short residence time, which makes it difficult to achieve these levels.

2.5.5 Therapeutic Uses of Intranasal Administration in CNS

A new non-invasive method of administering treatments directly to the CNS, intranasal administration has the potential to overcome the BBB and produce a fast onset of action for medications (Mignani et al., 2020). Evidence suggests it may be useful in treating a variety of CNS issues, such as addiction, neurodegenerative illnesses, epilepsy, pain, migraines, and mental health issues (Table 2.1).

Table 2.1
Intranasal Drug Applications In CNS

Classification of Therapeutic Items	Drugs	Mechanism	Outcomes	Reference
Neur Odegenerative disorders	Donepezil	Facilitates cholinergic activation	Effects on Alzheimer's models of memory, cognition, and synaptic activity ameliorated	(Craft, 2011)
	Rivastigmine			(Kaur et al., 2020)
	Insulin	improved glucose metabolism in the brain		(Guo et al., 2024)
Parkinson's disease	Levodopa	Dopamine substitution	Accelerated onset, circumvents hepatic metabolism, diminished peripheral adverse effects	(Wen & Ren, 2024
	Apomorphine	MAO-B inhibition		(Pathak & Akhtar, 2016)
	Rasagiline			(Mittal et al., 2014)
Epilepsy	Midazolam	The limbic system is targeted by GABA receptor agonists.	Ending seizures effectively	(Mula, 2014)
	Diazepam		Quick CNS supply	(Boddu & Kumari, 2020)
	Lorazepam			
			Rapid analgesia	(Kienitz et al., 2022)
			Enhanced patient adherence	(Isfahani et al., 2022)
Analgesic for pain	Ketamine			(Seak et al., 2021)
	Fentanyl			
	Morphone NMDA			
HT1B/ID receptors induce cerebral casoconstriction		Resesptopr antagonism	Swift alleviation of headaches	(Menshawy et al.,2017)
		Opioid receptor stimulation		
		Sumatriptan Agonists of the 5-	Less Nausea	
Sleep Disturbances	Melatonin	Regulation of circadian rhythms	Improved sleep and initiation and quality	(Priprem et al., 2017)
	Orexin antagonists			(Calva & Fadel, 2018)
Psychiatric conditions	Oxytocin	Regulates glutamate and oxytocin pathways	Quickly alleviates depression and anxiety	(Grossman-Giron et al., 2023)
	Ketamine and Esketamine			(Boudieu et al., 2023)

Nicotine receptors	Stimulation of nicotinic	Quick reduction of cravings and avoidance of relapse	(Cheng, 2002) (N. Benowitz et al., 1

(MAO-B: Monoamine Oxidase B)

2.6 CS and Its Uses in Drug Delivery

2.6.1 Origin, Chemical Composition, and Deacetylation level

An alkaline deacetylation process can be used to generate CS, a naturally occurring polysaccharide. Chitin (Figure 2.4) is mainly found in crustacean exoskeletons (e.g., shrimp, crab and fungal) (Kumari & Kishor, 2020). CS is made up of β-(1→4)-linked units of N-acetyl-D-glucosamine and D-glucosamine. According to Sivashankari and Prabaharan (2016), the degree of deacetylation (DDA) h a s significant impact on its physicochemical qualities. According to Pellis et al. (2022), the percentage of free amino groups throughout the polymer backbonedetermines the degree of deacetylation, which usually falls between 50% and 100%. There are a number of benefits to increasing the DDA, including improved solubility in acidic environments, improved mucoadhesion, and the ability to interact electrostatically with negatively charged biological membranes or crosslinkers like TPP (Xu et al., 2019; George & Abraham, 2006).

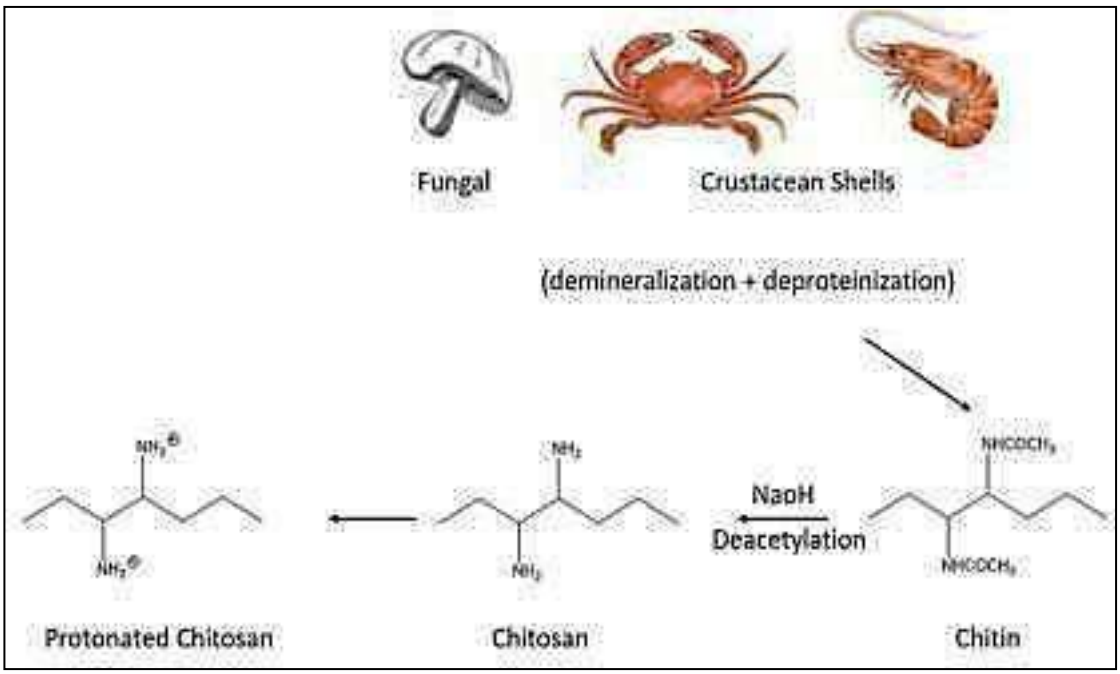

Figure 2.4 Origin Of CS.

2.6.2 CS Physicochemical Property

According to Alwahsh et al. (2024), CS possesses unique physicochemical properties that render it exceptionally well-suited for mucosal and nanoparticle-based drug delivery, particularly in the context of intranasal applications. The presence of primary amino groups along the polymer backbone is that which determines its solubility, which is dependent on the pH of the solution. Because of the significant intermolecular hydrogen bonding and hydrophobic interactions that occur between acetylated residues, CS is incapable of dissolving under conditions that are either neutral or alkaline (pH greater than 7). According to Ardean et al. (2021) and Mourya and Inamdar (2008), when CS is exposed to acidic conditions with a pH below 6.5, the amino groups begin to undergo protonation, resulting in the transformation of CS into a water-soluble cationic polyelectrolyte. According to Kumar et al. (2004), the polymer possesses an intrinsic pKa value of roughly 6.3–6.4. This numerical value indicates that at the healthy nasal pH range of approximately 5.0–6.5, a significant fraction of $–NH_2$ groups undergo protonation to $–NH_3^+$, hence introducing a powerful positive charge to the molecule. According to Svensson et al. (2006), the presence of a cationic charge in CS makes it possible for it to connect electrostatically with mucins that are negatively charged on the surface of the nasal epithelium. This interaction results in good mucoadhesive characteristics that extend the duration of residency and inhibit mucociliary clearance. Additionally, the positive charge makes it possible for tight junctions between epithelial cells to be opened in a reversible manner, which temporarily increases the permeability of the paracellular space and makes it easier for macromolecules to move through the mucosa (Yeh et al., 2011). Ionic cross-linking with multivalent anions, in particular TPP, is another way in which the protonated amino groups participate. This process makes it possible to create stable NPs that have a high EE% (Abdelgawad & Hudson, 2019; Koukaras et al., 2012).

2.6.3 Intranasal Delivery of CS: Improving Mucoadhesion, Epithelial Permeation, and Biocompatibility.

CS is one of the most useful polymers for intranasal drug delivery, particularly for nose-to-brain transport (Bahadur et al., 2020). CS possesses exceptional mucoadhesive and permeation-enhancing properties, which position it as one of the most valuable polymers. According to Fidan et al. (2024), the mucoadhesive behavior of this substance

is a result of the protonation of primary amine groups on the D-glucosamine units when the nasal environment is acidic and physiological (with a pH ranging from around 5.0 to 6.5). This provides the substance with a powerful cationic surface charge. According to Sogias et al. (2008), this enables electrostatic interaction with negatively charged sialic acid and sulfate residues that are present in mucus glycoproteins. This results in the formation of a powerful polymer mucus complex that significantly extends the duration of the formulation's residence time on the nasal mucosa and reduces the amount of mucociliary clearance. CS has the ability to modulate epithelial tight junction proteins, temporarily loosen tight junctions (occludin, claudins, ZO-1), and increase paracellular permeability without causing lasting structural damage (Smith et al., 2004). CS is also capable of boosting paracellular permeability. The positive charge of CS in NPs systems also facilitates the formation of ionic complexes with polyanions (such as TPP), which ultimately leads to NPs that exhibit exceptional encapsulation efficiency, stability, and controlled release behavior (Al-Nemrawi et al., 2018; Janes et al., 2001). Moreover, in addition to these functional advantages, CS exhibits a remarkable biodegradability, biocompatibility, and safety profile, which are all required for intranasal pharmaceutical applications (Iacob et al., 2021). Formulation scientists are able to design CS to release pharmaceuticals over regulated periods since its degradation rate is influenced by the DDA and the molecular weight of the CS (Jennings, 2016). It has been proved time and time again through toxicological testing that CS has a low level of cytotoxicity (Choi et al., 2015).

2.6.4 Application of CS in Intranasal Delivery

While intranasal delivery is convenient and has a high bioavailability, it does necessitate the use of mucoadhesive nanocarriers. CS NPs that were stable and cytocompatibility were developed by using 2,6-pyridinedicarboxylic acid as a biocompatible crosslinker. These NPs were then compared to NPs that were prepared with TPP. The NPs that were produced, which had a size of around 150 nm and a net charge of +10.3 ± 0.9 +mV, exhibited no notable changes in size or surface charge when subjected to temperatures of 4 °C, 32 °C, and 37 °C. Good biocompatibility was demonstrated through *in vitro* cytocompatibility tests conducted on SH-SY5Y neuroblastoma and RPMI-2650 nasal epithelial cells. According to these findings, the crosslinked CS NPs that were proposed are a viable platform for the delivery of drugs through the intranasal route (Gagliardi et

al., 2023). In order to improve the intranasal delivery of dihydroergotamine (DHE) for the treatment of migraines, this study investigated the use of CS NPs: CS NPs loaded with DHE were synthesized using the process of ionotropic gelation. These NPs had a high encapsulation effectiveness of 95 ± 13 %, while also exhibiting regulated drug release. In vivo, the injection of intranasal NPs resulted in a considerable increase in the bioavailability of DHE, with a value of 82.5 ± 12.3%, as compared to the intran asal solution, which had a value of 53.2 ± 7.7%. According to these findings, CS NPs have the potential to enhance systemic absorption and are a promising carrier for the delivery of DHE through the intranasal route (Alastal et al., 2023). A recent study developed a thermosensitive CS-based hydrogel (CS/HTCC/gelatin) as a carrier for the delivery of insulin through the intranasal route. Following optimization of the hydrogel composition, the final formulation (consisting of 2% CS, 1% HTCC, and 0.5% gelatin) exhibited appropriate gelation duration, swelling behavior, mucoadhesion, and structural stability. In this study conducted by Bahmanpour et al. (2020), it was shown that hydrogels loaded with insulin exhibited regulated release, releasing around 65 % of insulin throughout a span of 24 hrs. This suggests that these hydrogels have the potential to serve as a noninvasive alternative to subcutaneous insulin injections. Another study looked into intranasal CS NPs through the use of ionotropic gelation, with the purpose to enhance the bioavailability of olmesartan medoxomil (OLM), an antihypertensive medication that is poorly absorbed, having a high entrapment effectiveness (75–83%) and demonstrating efficient penetration over nasal mucosa. The NPs were spherical in shape and measured between 240 and 344 nm, according to the findings of their pharmacokinetic studies, the bioavailability of CS NPs loaded with intranasal OLM was raised by 11.3 times when compared to oral suspension, the pharmacodynamic study conducted on hypertensive rats demonstrated that the drug was effective in lowering both blood pressure and heart rate, while also preventing any injury to the nasal tissue, the results of this study suggest that CS NPs have the potential to serve as a carrier for the intranasal systemic distribution of OLM (Hassan et al., 2022). Midazolam-loaded CS NPS (MDZ-CS NPs) were developed for the purpose of improving nose to brain transport in the event of an emergency seizure. Ionotropic gelation was used to generate MDZ-CS NPs, which exhibited the desired size, drug loading, and controlled release characteristics. When compared to intranasal MDZ solution and intravenous administration, MDZ-CS NPs obtained significantly higher brain exposure (Cmax and AUC) after intranasal administration. Additionally, they

demonstrated greater drug targeting efficiency and higher direct nose to brain transport. The findings of this study suggest that intranasal MDZ-CS NPs significantly enhance the transport of midazolam to the brain and may present a promising non-invasive therapy option for the treatment of status epilepticus (Shrestha et al., 2020). For the purpose of avoiding the gastrointestinal adverse effects that are associated with oral administration, new study produced NPs based on CS for the purpose of intranasal delivery of galantamine hydrobromide (GH). The preparation of GH-loaded CS NPs and CS–alginate complex NPs was accomplished using the process of ionic gelation. These NPs exhibited significant loading efficiencies, with a range of 67% and 70%, respectively. Additionally, the particle diameters ranged from approximately 240 to 286 nm. In release studies, persistent GH release was seen for up to 8 hrs, and the NPs were stable for a period of one year at a temperature of 5□ C (Georgieva et al., 2023). These data suggested that CS NPs have the potential to serve as a carrier for the intranasal administration of galantamine. Another research produces CS–lecithin NPs for the intranasal delivery of phenytoin (PHT) in order to imp rove brain targeting for the treatment of epilepsy, in addition, Nanoprecipitation was used to create the NPS, which exhibited a spherical morphology, high stability, and an encapsulating efficiency of more than 60%. In comparison to the intraperitoneal or intranasal solution controls, the intranasal injection of the optimized formulation led to increased levels of PHT in the brain as well as sustained release. The results of this study suggest that intranasal delivery of PHT-loaded NPs is a potential technique for nose-to-brain transfer in the therapy of epilepsy (Yousfan et al., 2020). Using a nose-only exposure device in recent study examined the effectiveness of NHT–loaded CS NPs as a controlled-release dry powder inhalation system in C57BL/6 mice. With a flow rate of 0.9 litters per min and an exposure time of five min, the optimal aerosol distribution was accomplished. NPs formulation did not impair nicotineactivity, as demonstrated by the results of locomotor activity tests, which revealed that inhaled NHT-CS NPs (0.88 mg) caused behavioural effects that were comparable to those produced by inhaled NHT (0.59 mg) and subcutaneous injection (0.5 mg/kg). Histopathology of the lungs revealed that there was no evidence of tissue injury following inhalation. In general, inhaled nicotine appears to be a safe and promising technique for the development of innovative nicotine inhalation therapies for the purpose of smoking cessation (H. Wang et al., 2020). In a variety of formulations (solutions, gels, NPs), CS and its derivatives have demonstrated encouraging results in terms of enhancing nasal bioavailability. CS NPs, due to their

mucoadhesion and the ability to transiently open tight junctions, further boost nose to brain transport than simple CS formulations, which are known to improve systemic absorption (Casettari & Illum, 2014).

2.7 CS NPs in Drug Delivery

2.7.1 Methods of CS NPs Synthesis

2.7.1.1 Ionic Gelation Method

Ionic gelation is one of the most extensively used processes for synthesizing CS NPs because of its ease of use, gentle processing conditions, and the fact that it does not require the use of organic solvents (Hoang et al., 2022). In this approach, CS is first dissolved in a weak acidic solution (usually acetic acid), which protonates its amino groups ($–NH_3^+$), giving the polymer a positive charge (Sacco et al., 2021). After that, a multivalent crosslinking agent that is negatively charged, such as TPP, is added drop by drop while the mixture is continuously stirred (Hamidi et al., 2021). Khoerunnisa et al. (2021) stated that the electrostatic interaction among the positively charged CS chains and the negatively charged phosphate groups of TPP causes spontaneous self-assembly and gelation, which results in the formation of nanosized CS–TPP complexes. According to Obeidat et al. (2022), the NPs size, zeta potential, and EE% are all directly influenced by major formulation parameters. These parameters include the concentration of CS, the concentration of TPP, the ratio of CS to TPP, the pH in the mixture, and the stirring speed. It is possible to include drugs into NPs by either dissolving them in the CS solution before crosslinking or by loading them into the NPs that have been created (Gooneh-Farahani et al., 2020; Pedroso-Santana & Fleitas-Salazar, 2020). Ionic gelation is particularly well-suited for applications involving intranasal and nose-to-brain drug administration because it produces NPs that are stable and have mucoadhesive characteristics (Hard et al., 2023; Koo et al., 2024).

2.7.1.2 Spray-drying

NPs of CS can be efficiently and scalable produced using the spray -drying process. This is especially true when getting dry, flowable powders that are good for nasal or inhalation distribution is the aim (Albetawi, 2022). This technique involves dissolving

the drug-to-be-encapsulated in a polymer solution after dissolving CS in a weak acidic solution (usually hydrochloric or acetic acid) (De La Paz et al., 2021). It is possible to induce ionic connections prior to atomization by adding crosslinking agents such TPP, or crosslinking can happen while the material is drying (Antoniraj et al**.,**2019). A spray dryer is used to quickly expose the feed solution to a stream of hot air by atomizing it through a nozzle into fine droplets (Szczap & Jacobs, 2022; Binesh et al., 2023). Particle size, shape, encapsulation effectiveness, and moisture content are dictated by crucial factors, including inlet/outlet temperature, atomization gas flow, feed rate, and polymer concentration (Piñón-Balderrama et al., 2020; Homayoonfal et al., 2022). Spray-drying creates dry Nano powders that are highly dispersible, allows for continuous manufacture, and protects thermolabile medications against high-temperature deterioration (Pardeshi et al., 2021).

2.7.1.3 Emulsion crosslinking

NPs of CS are typically prepared using the emulsion crosslinking technique when exacting control over particle shape and size is required (Ribeiro et al., 2020). Hydrophilic or hydrophobic drugs can be dissolvedor disseminated within the CS phase using this method, which involves protonating the amino groups of dissolved CS in an acidic water solution (Naskar et al., 2018; Shi et al., 2020). To create a stable water-in-oil (W/O) emulsion, the aqueous phase is gradually added to an organic solvent that is immiscible with water and contains a surfactant, such Span 80, while being vigorously stirred or sonicated (Riegger et al., 2017). Chen et al. (2017) states that following crosslinking, the NPs are either filtered or centrifuged to remove any remaining solvent or surfactant. They are then either dried or resuspended according to the situation.

2.7.2 Factors Affecting NPs Properties

2.7.2.1 Polymer Ratio

According to Mohammed et al. (2017), the polymer ratio, which can be, for example, the ratio of CS to crosslinker (such as TPP) or the ratio of polymer to drug, is an important parameter that influences the physicochemical properties of NPs. Oudh et al.

(2023) and Sreekumar et al. (2018) stated that increasing the concentration of CS typically results in greater particle size. This is because the higher viscosity and enhanced polymer–polymer interactions that occur during the production of NPs are directly responsible for this phenomenon. Similarly, an increase in the ratio of CS to CS leads to an increase in the availability of protonated amino groups ($–NH_3^+$). This, in turn, leads to an increase in the positive zeta potential, which in turn improves the stability of NPs through electrostatic repulsion and enhances mucoadhesion to negatively charged mucosal surfaces (Amin & Boateng, 2022; Feng et al., 2015). On the other hand, increasing the quantity of crosslinker (for example, TPP) promotes tighter ionic crosslinking, which may reduce particle size up to an optimal point but may also cause aggregation if enough of it is present (Pan et al., 2020; Huang & Lapitsky, 2016). According to Huang and Lapitsky (2016), the ratio of polymer to drug was found to have a significant impact on both the EE% and the drug loading. Generally speaking, larger polymer ratios are associated with an increase in EE% because of the increased availability of bindingsites. On the other hand, low polymer ratios may result in drug leakage (Yun et al., 2021; Zhou et al., 2016). Additionally, the polymer ratio has an effect on the behavior of drug release. NPs that have a larger polymer content or stronger crosslinking exhibit slower and more sustained drug release, whereas NPs with lower polymer ratios frequently result in rapid diffusion and burst release (Pinto et al., 2017).

2.7.2.2 Crosslinker

Critical criteria affecting the physicochemical properties of CS NPs include the choice and concentration of the crosslinking agent (Vandana & Sahoo, 2009). One of the most common crosslinkers is TPP. It's utilized a lot since it's biocompatibleand may ionically connect with CS positively charged amino groups ($-NH_3^+$) in mild water (Qian et al., 2020; Silvestro et al., 2020). NPs with controllable size, zeta potential, and EE% are generated through this electrostatic interaction (Gan et al., 2005). According to Gierszewska and Ostrowska-Czubenko (2016) and Shu and Zhu (2002), the density of ionic crosslinking is greatly influencedby the structure andconcentration of multivalent phosphates, which in turn alters the mechanical strength and release characteristics of CS-based systems. On the other hand, genipin and glutaraldehyde are covalent

crosslinkers that strengthen mechanical stability and network rigidity by creating permanent links between CS chains (Mi et al., 2005). In a similar vein, Jayakumar et al. (2009) found that glutaraldehyde effectively crosslinks CS, however caution is needed to avoid cytotoxicity. When it comes to drug delivery systems, the structural integrity, surface charge, and stability of the NPs are all affected by the type of crosslinker, which can be either ionic or covalent (Liu et al., 2008)

2.7.2.3 pH

Because it influences the ionization state of the amino groups in CS and the strength of interaction with the crosslinker, the pH of the reaction medium is vital for the production, physicochemical properties, and stability of CS NPs (López-León et al., 2004). A weak polybase, CS solubility is determined by the protonation of the $-NH_2$ groups on the D-glucosamine units; its pKa ranges from about 6.3 to 6.5. During the creation of NPs, CS becomes more soluble and capable of electrostatically interacting with multivalent anions like TPP when the pH drops below its pKa (Blagodatskikh et al., 2023; Atay, 2019). Wu et al. (2017) and others have shown that CS-TPP NPs structural compactness andionic crosslinking effectiveness are significantlyaffected by pH. The protonation of CS amino groups ($-NH_3^+$) is enhanced when the pH is lowered, which in turn strengthens the electrostatic contact with TPP and causes denser, more uniform NPs production. On the other hand, according to research by L. C. Wang et al. (2008) and Ding et al. (2018), increasing the pH decreases protonation, weakens ionic bonding, and leads to larger and less stable aggregates.

For protein delivery, researchers looked into ionic gelation with TPP to create low-molecular-weight CS NPs. In order to create NPs, the results showed that CS solubility and crosslinking effectiveness were highly pH dependent. Accelerated protonation of CS amino groups ($-NH_3^+$) in acidic environments enhanced electrostatic interaction with TPP, leading to the production of NPs and the encapsulating of proteins. Weak crosslinking and fewer stable particles were the outcomes of diminished protonation at a pH close to neutral. The results showed that maintaining particle homogeneity, stability, and efficient protein entrapment during CS NPs formation requires careful regulation of pH (Janes & Alonso, 2003).

The formation, size, stability, and drug encapsulation effectiveness of sitagliptin -loaded CS NPs (SIT-CS-NPs) are all greatly affected by pH during their manufacture. During

ionic gelation, CS amino groups, which have a pKa of approximately 6.3 -6.5, get protonated ($-NH_3^+$) at acidic pH, enabling significant electrostatic interaction with the negatively charged TPP ions. This process produces tiny, stable, and evenly distributed NPs that have a high zeta potential and effectively entrap drugs. At pH levels close to or above neutrality, protonation diminishes, which weakens the contacts between CS and TPP. This, in turn, causes the aggregates to become bigger and less stable, and the encapsulation effectiveness to drop. According to Wilson et al. (2020), in order to get the best NPs quality and consistent physicochemical properties, it is crucial to keep the SIT-CS NP preparation environment slightly acidic, at a pH range of 4.5 to 5.5**.**

2.7.3 NPs Characterisation

2.7.4 Particle Size and Distribution

Determination of particle size and size distribution is a critical step in the characterization of CS NPs, as these parameters directly influence drug loading, release kinetics, mucosal permeability, and overall biological performance (Büyük etal., 2020; Vaezifar et al., 2013; R. Jha & Mayanovic, 2023). DLS is one of the most widely used techniques for evaluating the hydrodynamic diameter and PDI of NPs in suspension (Danaei et al., 2018). It measures the fluctuations in scattered light intensity caused by the Brownian motion of particles, allowing calculation of average size and distribution uniformity (Hassan et al., 2014). A PDI below 0.3 generally indicates a narrow and homogeneous particle population suitable for pharmaceutical applications (Masarudin et al., 2015; Mandal et al., 2014). In contrast, Transmission Electron Microscopy (TEM) provides direct visualization of NPs morphology, shape, and surface characteristics at the nanometer scale (Wang, 2003). TEM images reveal the actual particle size (often smaller than DLS values because DLS includes the solvation layer) and confirm the spherical and discrete structure of CS NPs (Zia, 2025; Yeap et al., 2018). The combination of DLS and TEM offers complementary insights: DLS gives rapid quantitative size distribution in solution, while TEM verifies morphology and dispersion uniformity (Parashar et al., 2025).

2.7.4.1 Zeta Potential

According to Pochapski et al. (2021), zeta potential is an important physicochemical metric for assessing the surface charge and colloidal stability of CS NPs. It is usually measured by electrophoretic light scattering using devices, such as a Zetasizer, and it reflects the electrical potential at the sliding plane around the scattered particles (Uskoković, 2012). According to Lowry et al. (2016), NPs with Zeta potential values above +30 mV or below -30 mV have a sufficient surface charge to avoid aggregation due to repulsive interactions and maintain high suspension stability. NPs made of CS get their positive surface charge mostly from the protonated amino groups ($-NH_3^+$) of CS in slightly acidic environments. According to Thambiliyagodage et al. (2023), variables like pH, CS molecular weight, degree of deacetylation, and crosslinker concentration impact the amplitude of the zeta potential. NPs having a higher zeta potential interact with mucin's negatively charged sialic acid residues to increase retention duration on nasal or mucosal surfaces, which improves mucoadhesive characteristics (Dhawan et al., 2004). According to Dudhani and Kosaraju (2010), zeta potential study is a crucial part of characterizing CS NPs formulations for the purpose of forecasting their physical stability and bioadhesion.

2.7.4.2 Encapsulation Efficiency (EE%) and Drug Loading (DL%)

Important characterization metrics for evaluating the drug entrapment capacity and loading capability of CS NPs are EE% and DL%. NPs made of alginate and CS showed excellent trapping performance when tested for the delivery of quercetin. The formulation successfully integrated the hydrophobic chemical into the polymeric matrix, as evidenced by its high EE% of 82.4% and drug loading capacity of 46.5%.These findings support the idea that NPs made of alginate and CS offer a great way to transport hydrophobic bioactives, such as quercetin (Nalini et al., 2019).
Since high DL% is more difficult to get than EE%, optimizing both in CS NPs is still a daunting task. Crystallization or covalent/coordinate contacts produce a better loading efficiency than physical adsorption, which typically leads to a low EE%. The efficient procedures are crucial for high-content nanomedicines, which is why CS NPs are being designed to enhance drug incorporation, stability, and loading per formance (Herdiana

et al., 2024). In addition, research on CS NPs loaded with nicotine demonstrated that the drug loading was directly proportional to the nicotine content, indicating that the polymer matrix effectively entrapped the drug. According to Wang et al. (2017), the dry powder inhaler formulation showed improved drug incorporation and delivery effectiveness when the loading was increased, which also led to an increase in the fine particle dose. The conjugation of nicotine with stearic acid greatly increased the drug loading capability of solid lipid NPs loaded with nicotine, a method called ultrafiltration was used to measure the EE%, which was found to be 46.45 ± 1.53%. In this process, unencapsulated nicotine was separated using 10 kDa centrifugal filters and then quantified using UV-Vis spectroscopy. The conventional equations were used to compute the starting and free drug content difference, which in turn determined the EE% and loading capacity. Renukuntla et al. (2023) found that compared to free nicotine gel formulations, the results show that the solid lipid NPs matrix effectively incorporates the nicotine-stearic acid conjugate, which supports better drug retention and sustained release.

2.7.4.3 Other Analytical Methods

The interior molecular structures can be identified using FTIR, which is based on the vibrational and rotational motions of atoms. In addition to helping us understand how inorganic, organic, and biological molecules are extracted, it is crucial for describing separation materials like solid sorbents and liquid extractants. Food research, environmental analysis, clinical and forensic medicine, analytical chemistry, and FTIR's sensitivity and flexibility make it a popular tool in many domains (Gong et al., 2024). Functional group and structural feature examination of CS-based NPs is a common use of FTIR. In a typical spectrum, CS has a broad 3400-3500 cm^{-1} peak that corresponds to -NH_2/-OH stretching, an amine band about 1540 cm^{-1}, and a strong carbonyl band at 1654 cm^{-1} (C=O-NHR). In the range of 1000-1200 cm^{-1}. According to Boonsongrit et al. (2007), the FTIR spectra of dried CS micro/NPs displayed the predicted bands without any notable changes. This suggests that the chemical structure of the CS was unaltered and that no new interactions between functional groups occurred during NPs production.

By studying the diffraction patterns formed when X-rays reflect off periodically organized atoms, XRD may reveal the crystallinity, lattice structure, and phase

composition of materials. Information on grain size, degree of crystallinity, and structural order can be gleaned from the locations and intensities of peaks in both crystalline and partially amorphous systems. XRD is a popular tool in the field of materials research, particularly for the characterization of catalysts, nanocomposites, polymers, and NPs (Khan et al., 2020). The produced CS NPs structural features were validated by XRD analysis. Ionic crosslinking with TPP disturbs the native polymer packing and decreases crystallinity, as shown by the diffractogram, which typically displays the broad, diffuse peaks linked with amorphous CS. As is typical for CS NPs made by ionic gelation, the lack of strong diffraction peaks indicates the creation of a mostly amorphous polymeric network. Minor peaks at specific 2θ positions may still be visible when a crystalline drug is integrated into an otherwise amorphous CS matrix; these peaks indicate residual crystalline domains of the drug (Ullah et al., 2022).

Essential thermal parameters including glass transition temperature, heat capacity, enthalpy changes, and melting point can be found via DSC. In order to accommodate melting transitions, including asymmetric or overlapping peaks, an analytical DSC model was devised, despite the fact that standard DSC analysis is susceptible to experimental and sampling artifacts. This method enhances the accuracy of assessing phase transitions and thermal behavior in complicated binary systems as well as in pure materials (Ghanbari et al., 2023). As a result of its high solubility for water, CS usually exhibits an endothermic peak in DSC analyses. These thermal transitions change and the TPP melting peak goes away when CS is crosslinked with TPP to make NPs, which means that the ionic connection was successful. Due to changes in the structure of the polymer and its ability to bind water, CS NPs frequently exhibit new or changed endothermic peaks. Molecular weight, deacetylation level, and preparation techniques are the three main factors that cause CS and CS NPs to have different thermal profiles (Villegas-Peralta et al., 2020).

To better understand thermal processes like oxidation and decomposition, TGA tracks the mass change of a substance as its temperature rises. The method relies on precisely calibrated equipment, well-prepared samples, and regulated heating. Both the parameters of the instrument and the characteristics of the sample might affect the TGA curves. Its composition and thermal stability can be evaluated by scientists in many different domains (Akash & Rehman, 2025). At around 213 to 380 °C, CS undergoes significant decomposition as a result of the breaking of OH and NH bonds as well as etheric connections, as revealed by TGA analysis, which follows an initial weight loss

caused by dehydration. The reduced heat stability of CS-TPP NPs, brought about by structural disruption andthe presence of phosphategroups, wasevident in their early and lower overall weight loss. In comparison to the pure polymer, CS heat stability is reduced due to crosslinking and NP production, as shown by the TGA profiles (Kahdestani et al., 2020).

For in-depth examinations of surface morphology, topography, and composition, scanning electron microscopy (SEM) produces high-resolution pictures. One of the most important tools for material characterization is SEM, which uses a high-energy electron beam to show the structure, size, surface roughness, and shape of particles (Akhtar et al., 2018). Imaging using a SEM showed distinct morphological characteristics of the CS nanocomposites, including surface imperfections and particle clustering. The presence of aggregates and surface structures became more apparent at greater concentrations, in contrast to the tiny specks seen at lower concentrations. These findings emphasize the importance of SEM in evaluating the surface properties and morphology of NPs (Aziz, 2017).

2.8 Drug Release Mechanism from CS

The release of drugs from CS NPs is regulated by a complex interaction of diffusion, polymer swelling, ionic interactions, and matrix erosion, all of which enhance their ability for controlled and sustained delivery (Lucio & Martínez-Ohárriz, 2017; Gupta & Kumar, 2000). When exposed to aqueous physiological media, water swiftly infiltrates the CS matrix, resulting in partial hydration of the polymer chains and the relaxation of ionic crosslinks usually established between the protonated amino groups of CS ($–NH_3^+$) and multivalent anions like TPP. The initial hydration induces a distinctive burst release, where drug molecules adsorbed on or adjacent to the nanoparticle surface disperse fast (Karoyo & Wilson, 2021; Zenget al., 2011; Bhumkar & Pokharkar, 2006). Ostrowska-Czubenko et al. (2015) found that CS strong hydrophilicity and pH-responsive protonation enable deeper water penetration as swelling develops. This, in turn, creates larger diffusion channels that the medication can gradually escape through. Stronger interactions, such as hydrogen bonding, ionic attraction, or hydrophobic embedding, can delay drug release; the rate of this sustained diffusion phase is dependent on the drug-polymer affinity, degree of deacetylation, CS molecular weight, and crosslinking density (Lim et al., 2021; Varma et al., 2004). With

extended exposure, the CS network experiences matrix relaxation and progressive degradation, especially in slightly acidic environments where protonation interferes

$$F = -D \, \partial c/\partial x \qquad (2.1)$$

with inter-chain ionic bonds(Feyisa et al., 2023). This degradation affects the structural integrity of the NPs, facilitating the gradual release of encapsulated drugs retained within the inner core (Perrigue et al., 2021). Drug release from CS NPs mostly transpires via polymer swelling, diffusion, and degradation. Initial burst release outcomes result from the quick diffusion of surface attached drugs and the early development of pores. Figure 2.5. Release kinetics frequently adhere to Fick's law equation (2.1):

In this model, F denotes the diffusion flow, C signifies the drug concentration, and D represents the diffusion coefficient. Fick’s law presupposes pseudo-steady-state conditions, sufficient sink conditions in the surrounding media, and that the diffusion channel length through the polymer matrix exceeds the solute diameter (Kuen & Masarudin, 2022).

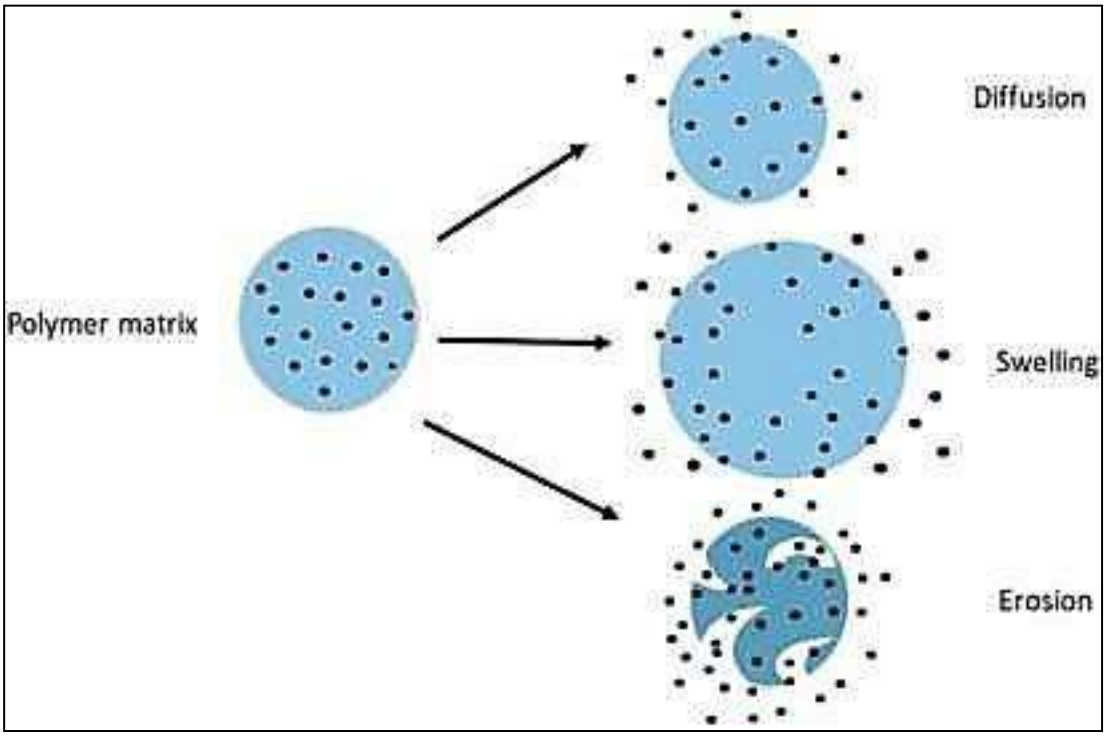

Figure 2.5 Diagram Representing The Possible Mechanisms Of Drug Release By Diffusion, Swelling And Erosion Of Polymer (CS) Matrix. Depicted From (Al-Awsi Et Al., 2023).

2.8.1 Mathematical Modeling Fitting of Drug Release Kinetics

Drug release from CS NPs may transpire by diffusion, polymer swelling, or erosion of the CS-TPP matrix. Due to variations in NPs composition and drug–polymer interactions, it is crucial to determine the most common release mechanism for regulated delivery. Standard kinetic models: zero-order, first-order, Higuchi, Korsmeyer–Peppas, and Hixson Crowell are used to characterize and fit the release dynamics from the CS NP system (Adepu & Ramakrishna, 2021; Ata et al., 2019)

2.8.1.1 Zero-Order

A drug delivery system exhibiting a zero-order release profile is theoretically ideal and sought by researchers to achieve a low dosage rate with a consistent release profile, devoid of initial burst release throughout the full period (Talevi & Ruiz, 2021). The related mathematical equation is presented in Equation (2.2):

$$Qt = Q0 + K0t \quad (2.2)$$

where Q0 represents the initial drug quantity; Qt is the cumulative drug release at time "t"; K0 is the zero-order release constant.

The removal of zero-order kinetics occurs at a constant rate throughout a linear elimination phase when the system reaches saturation, irrespective of plasma concentration (Mircioiu et al., 2019). In actuality, there are other release models, including the first-order model, Higuchi model, Hixson-Crowell model, and Korsmeyer-Peppas model, which have been modified (Askarizadeh et al., 2023).

2.8.1.2 First Order

The first-order model was initially proposed by Gibaldi and Feldman in 1967 and subsequently by Wagner in 1969 (Mhlanga & Ray, 2014). The mathematical equation is presented in Equation (2.3):

$$\log Qt = \log Q0 + K1t \quad (2.3)$$

Q_t represents the cumulative percentage of medication released at time t; Q_0 denotes the starting drug amount; K1 signifies the first-order release constant; t indicates time.

It has been frequently utilized to delineate the absorption and/or excretion of several medicinal drugs. The elimination in first-order kinetics is contingent upon the concentration of a single reactant drug, with the drug being eliminated at a constant percentage per unit of time (Savva, 2019).

2.8.1.3 Higuchi Model

The Higuchi model, defined by Higuchi in 1961, relates to his investigation of the release kinetics of ointment bases (Siepmann & Peppas, 2011). The Higuchi model's mathematical equation is delineated in Equation (2.4):

$$Qt = \sqrt{D}\ (2C - Cs)\ Ct \qquad (2.4)$$

Where, Qt represents the quantity of drug released per unit area at time t, C denotes the initial concentration of the medication, Cs signifies the solubility of the drug, and D indicates the diffusion constant (Jain & Jain, 2016).

This example emerged as one of the most renowned and commonly employed frameworks for cargo release from matrix systems (Lee, 2011).

2.8.1.4 Hixson-Crowell Model

Conversely, the Hixson-Crowell model is a prominent release model introduced by Hixson and Crowell in 1931, based on the finding that a fixed area of a collection of particles is proportional to the cube root of its volume. The corresponding mathematical equation is expressed as Equation (2.5):

$$\sqrt[3]{Qt} - \sqrt[3]{Q0} = KHCt \qquad (2.5)$$

Q_t represents the cumulative percentage of drug released at time t; Q_0 is the initial amount of drug at time t; K_{HC} is the Hixson-Crowell constant (Abid et al., 2019).

This model is frequently employed in pharmaceutical systems, such as tablets, where the dissolving rate corresponds to the surface area of the dose form (Williams et al., 2002).

2.8.1.5 Korsmeyer-Peppas Equation

The Korsmeyer–Peppas model is derived from the Power law, serving as a more comprehensive framework for characterizing drug release from a polymeric system. This model was formulated by Korsmeyer et al. in 1983 to characterize the exponential correlation between drug release and time, as represented in Equation (2.6):

$$Qt = KKPtn \qquad (2.6)$$

Qt represents the cumulative percentage of drug released at time t; K_{KP} denotes the Korsmeyer-Peppas constant; n signifies the release exponent that characterizes the drug release mechanism (Patil et al., 2013).

2.9 Modified CS Derivatives for Enhanced Delivery

2.9.1 Rationale for Chemical Modification of CS

The chemical modification of CS is a strategic approach to overcome the inherent limitations of its native structure and to improve its performance in advanced drug delivery systems (Brasselet et al., 2019). Although CS is a promising polymer for NPs fabrication, its native form exhibits poor solubility at physiological pH, limited charge density tunability, structural rigidity, restricted accessibility of functional groups, and inadequate stability under biological conditions, all of which limit its pharma ceutical applications (Bashir et al., 2022; Boominathan & Sivaramakrishna, 2021). Therefore, advanced chemical modifications, including selective N- and O-substitution and controlled cross-linking, have been employed to enhance solubility, tailor reactivity, improve compatibility with therapeutic payloads, and provide precise control over NPs formation, stability, and drug release (Li et al., 2022). Moreover, modified CS derivatives have demonstrated improved suitability for intranasal drug delivery by enhancing mucoadhesion, regulating residence time, and increasing permeability (Wang et al., 2020). Consequently, chemical modification has become an effective strategy for developing sustained-release nanocarriers with improved pharmaceutical performance (Weng et al., 2023). Furthermore, chemical modification enhances the potential of CS for nose-to-brain delivery by improving its interaction with the nasal mucosa and facilitating transport across the BBB (Ojeda-Hernández et al., 2020). Since the BBB and olfactory epithelium preferentially permit the diffusion of mildly hydrophobic molecules, the intrinsic hydrophilicity of native CS limits its passive transcellular transport and interaction with lipid-rich epithelial membranes (Rajput et al., 2022; Cohen & Poverenov, 2022).

2.9.2 Types of CS Modifications

2.9.2.1 Trimethyl CS (TMC)

TMC is a cationic, water-soluble polymer that facilitates the addition of a positive charge regardless of pH, derived from CS. The TMC represents the most basic form of quaternized CS, achievable through the continuous methylation of CS using methyl iodide and a base such sodium hydroxide in organic solvent conditions (Zhao et al., 2020). TMC designed to enhance solubility, charge density, and epithelial permeability relative to native CS. Its robust mucoadhesion, capacity to open tight junctions, and stability under physiological conditions facilitate enhanced antigen absorption and mucosal administration. TMC demonstrates significant adjuvant action similar to traditional adjuvants, putting it as a suitable platform for sophisticated vaccine and antigen-delivery systems (Malik et al., 2018). It is examined for biological applications owing to its superior compatibility and functional adaptability. Conventional synthesis depends on hazardous alkyl halides or dimethyl sulfate, which presents safety and environmental issues (Wu et al., 2017). TMC is a chemically altered derivative of CS, engineered to address the inadequatesolubility of native CS, hence exhibiting markedly enhanced solubility across a broad pH spectrum and superior absorption-enhancing characteristics. The improved solubility, alongwith its capacity to facilitate paracellular transport, renders TMC a potent and dependable excipient for the delivery of big or hydrophilic medicines in non-invasive pharmaceutical applications (Silva et al., 2018). The research created tristearin nanostructured lipid carriers (NLCs) that were surface-modified with N, N, N-trimethyl TMC to produce mucoadhesive mNLCs for the nasal transport of ropinirole to the brain. The TMC coating significantly enhanced bioadhesion, and pharmacokinetic tests validated improved brain uptake through the olfactory route, indicating the promise of mNLCs for Parkinson's treatment (Pardeshi & Belgamwar, 2019). A study illustrates the significant immunoadjuvant efficacy of TMC nanospheres for the nasal administration of tetanus toxoid (TT), a prototype vaccine antigen. TT-loaded TMC NPs elicited significantly improved systemic IgG and mucosal sIgA responses following intranasal treatment. Mixed cross-linked dextran microspheres, utilized as an absorption enhancer, greatly intensified these immunological responses. TMC functioned as the principal catalyst for enhanced nasal

immunogenicity, underscoring its efficacy as a nanocarrier for vaccine administration (Kabiri et al., 2021).

2.9.2.2 Glycol CS

Glycol CS is an improved and more versatile hydrophilic derivative of CS that is made by adding glycol groups to chitin during processing. Becaue of its high concentration of reactive amine and hydroxyl groups, glycol CS is amenable to a wide variety of chemical modifications and drug delivery systems. According to Kim et al. (2017), glycol CS is a versatile platform for pioneering biomedical and pharmaceutical applications due to its low acetylation level, excellent biocompatibility, and stability throughout molecular-weight ranges. The process of producing farnesylated glycol CS involved linking the amine groups of glycol CS with the aldehyde groups of farnesal in a reductive amination reaction. By using the glycol CS -to-farnesal feed ratios (12:1, 6:1, and 4.5:1), the level of farnesylation could be precisely modulated, enabling the regulation of hydrophobic substitution (Ho et al., 2018). Coating NPs with glycol CS, a combination of CS and ethylene glycol, allows for efficient steric stabilization and full water solubility across physiological pH. With these benefits in mind, glycol CS was employed to alter nanostructured lipid carriers for asenapine intrana sal delivery; this improved brain targeting, stability, and contact with the mucosa (Singh et al., 2017).

New developments in mucosal nucleic acid vaccination have brought attention to the requirement for nanocarriers that can transport genetic material across the respiratory mucosa while keeping it protected, glycol CS is a potential carrier for DNA and mRNA vaccine nasal delivery since it is water soluble, has a changeable backbone, significant mucoadhesive and stabilizing qualities (Tang et al., 2022). According to Petkova et al. (2022), glycol CS shows promise as a noninvasive vehicle for delivering genetic material to specific areas of the brain. In order to enhance cisplatin-loaded melanin NPs (MNPs), this study emphasizes the use of hydrophilic glycol CS as a surface modification. With their glycol CS coating, MNPs maintained great compatibility with cisplatin and displayed ideal nano-size (100-200 nm), high drug loading, and outstanding EE. Crucially, when contrasted with free cisplatin, glycol CS improved NPs stability, regulated release via polymer relaxation and swelling, and extended anticancer

activity. The significance of glycol CS in developing nanocarriers that are both safer and more effective in delivering chemotherapy is highlighted by these findings (Atik et al., 2023).

2.9.2.3 PEGylated CS

In drug-delivery systems, polyethylene glycol (PEG) is highly regarded for its adaptable capacity and excellent safety profile; it is also an FDA-approved polymer (D'souza & Shegokar, 2016). Although CS shows promise as a nucleic acid carrier, its limitations include low transfection effectiveness, mucus trapping, and poor solubility; by adding PEG chains to the polymer, PEGylated CS improves solubility, mucus penetration, and stability of the produced nanocomplexes, thus overcoming these disadvantages. A more effectiveapproach for delivering gene-editing tools is PEGylated CS, which is modified to preserve DNA from degradation, enhance movement through airway mucus, and achieve greater transfection efficiency (Zhang et al., 2018). To improve the administration of resveratrol for glaucoma treatment, PEGylated CS NPs were created. Unlike unmodified CS NPs, which stayed on the surface, PEG-modified NPs were able to penetrate the cornea and reach deeper ocular tissues (Pandian et al., 2016). Stabilizing montmorillonite (MMT) for drug administration was achieved by adsorbing onto and intercalating inside the clay layers with PEGylated CS, this resulted in PEG-rich nanosheets that disperse very well under physiological conditions. The multi-layered forms demonstrated improved doxorubicin loading and regulated intracellular release, and the nanosheet structure was altered as the PEGylated CS content increased. According to Huang et al. (2022), PEGylated CS significantly enhanced the stability of MMT and made it possible to employ it as a platform for drug delivery. (Cao et al., 2019). The BBB is very narrow, making it challenging to deliver medications to the brain, one important way to improve the stability, circulation time, and BBB penetration of NPs is to PEGylate them. This helps to decrease surface fouling, protein adsorption, and fast clearance; NPs treated with PEG have properties that allow them to accumulate more effectively in the brain, such as increased hydrophilicity and prolonged blood residency. Highly promising platforms for CNS drug delivery exist in PEGylated nanocarriers due to their antifouling and increased transport efficiency (Rauf et al., 2019).

2.9.2.4 Alkylglycerol-modified CS

Alkylglycerol-modified polysaccharides have emerged as notable carbohydrate-based nanocarriers for brain delivery due to the ability of short-chain alkylglycerols to facilitate drug access to the brain. This principle has been applied to polymers such as dextran and CS, which, when functionalized with alkylglycerol groups, yield amphiphilic NPs that demonstrate enhanced endothelial uptake and increased permeability across BBB mimicking models. Further modification with butylglycidyl ether results in butylglycerol-CS (BG-CS) derivatives that self-assemble into stable Nano systems, improving the loading capacity for hydrophobic or efflux-prone molecules. The release profiles of these systems are typically characterized by Higuchi or Korsmeyer–Peppas kinetics, underscoring the potential of alkylglycerol- and butylglycerol-modified polymers as effective platforms for brain-targeted drug delivery (Bostanudin et al., 2020). Alkyl-modified CS has been identified as an effective carrier, as the incorporation of hydrophobic alkyl groups converts CS into an amphiphilic substance, thereby enhancing drug transport capabilities. Recent research indicates that alkylated CS, synthesized using 2-tert-butoxymethyloxirane, was formulated into NPs exhibiting slower drug release and enhanced membrane penetration compared to unmodified CS. The NPs exhibited increased hydrophobicity while maintaining biocompatibility. Diffusion studies indicated nearly double the skin permeation and improved antimicrobial activity of the encapsulated drug. The results indicate that alkylation enhances the efficacy of CS as a transdermal delivery system (Bostanudin et al., 2023). Alkylglyceryl modification imparts CS with a distinctive equilibrium of flexibility and membrane interaction that is challenging to attain with the native polymer.

The incorporation of alkyl chains onto the CS backbone enhances the polymer's compatibility with lipid-rich biological surfaces, thereby strengthening its interaction with mucosal membranes and facilitating more efficient carrier cell contact. This modification stabilizes NPs structures and enhances tissue penetration, providing alkylglyceryl-CS systems with a significant advantage in delivering therapeutic molecules across complex physiological barriers, including those in CNS pathways (Caprifico et al., 2020). Alkyl and butyl modifications have notably enhanced the functional versatility of CS for targeted delivery to the brain. Researchers have synthesized lipid-interactive derivatives by grafting alkylglycerol or butylglyceryl groups onto the CS backbone, resulting in increased membrane affinity and enhanced

capacity to cross restrictive biological barriers. Hydrophobic substitutions enhance NPs stability and improve compatibility with endothelial and neural tissues, facilitating more efficient transport to the brain. Alkyl-modified CS derivatives, when utilized as NPs matrices or surface coatings, enhance charge presentation, facilitate cellular uptake, and prolong circulation time. This results in improved delivery efficiency of sensitive therapeutics across the BBB, circumventing the limitations of unmodified CS (Curcio et al., 2020). The BBB plays a critical role in maintaining brain homeostasis while significantly limiting the passage of numerous therapeutic agents, thereby complicating treatment strategies for the CNS. NPs based strategies have garnered attention, particularly CS decorated systems, which demonstrate significant potential in enhancing BBB penetration and facilitating the treatment of disorders including Alzheimer's disease, Parkinson's disease, gliomas, and stroke. Utilizing the interaction of CS with endothelial surfaces, the decoration of NPs enhances transport across the BBB and elevates drug availability in the brain (Cortés et al., 2020).

2.10 CS and Modified CS Physical Characteristics Comparison

Table 2.2 summarises and compares the properties and applications of both CS and Modified CS in drug delivery.

Table 2.2
Physical Characteristics Of CS And Modified CS.

Parameter	CS	Modified CS	Reference
Solubility	• pH-dependent • CS is insoluble at neutral and basic pH levels.	• pH-independent • PEGylated CS achieves significant aqueous solubility. • Glycol CS is soluble in water.	(Sung et al., 2012) (Parchen et al., 2025)
Release Rate	• Rapid • Moderate and Lower EE%	• More sustained • Higher EE%	(Lu et al., 2019)
Hydrophilicity	• High hydrophilicity	• Tunable depending in substitution	(B. Wang et al., 2011)
Water uptake	• Low to moderate •	• Higher than CS •	(Sun et al., 2006)

PLGA NPs.

2.11 NPs Safety and Biocompatibility

CS-based NPs enhance drug bioavailability to the brain by enhancing permeability across the BBB and facilitating direct nose-to-brain transport. Their biocompatibility, biodegradability, andmucoadhesive characteristics facilitate safe and effective transport while minimizing systemic exposure and adverse consequences. Nonetheless, despite largely favorable cytocompatibility in short-term investigations, long-term safety issues, including chronic neurotoxicity, accumulation, and clearanc e, have not been adequately assessed. CS NPs demonstrate significant potential for secure and effective brain-targeted delivery; however, extensivelong-term safety investigations are required for clinical application (Ezzaki et al., 2025). The assessment of cytotoxicity is essential for evaluating the suitability of CS NPs for intranasal and nose-to-brain transport, ensuring that the formulation is non-toxic to both the nasal epithelium and underlying neuronal tissues (Duarte et al., 2024). CS is a naturally sourced, biodegradable, and

biocompatible polysaccharide, with NPs produced from CS typically demonstrating low inherent cytotoxicity (Rizeq et al., 2019). Multiple investigations utilizing various cell models including fibroblasts, Calu-3 airway epithelial cells, Caco-2 cells, and respiratory or brain cell lines have shown that CS NPs generally preserve excellent cell viability within pertinent dosage ranges (Grenha et al., 2007). Nonetheless, highly cationic NPs may interact more intensely with cellular membranes, potentially compromising membrane integrity and diminishing metabolic activity when administered in excessive quantities (Saei et al., 2017; Fröhlich, 2012).

Nose-to-brain administration passes through the BBB; however, NPs inducedtoxicity in the nasal mucosa presents a significant challenge. Current efforts mitigate this risk by optimizing particle size, charge, and surface characteristics to diminish irritation and inflammation. The utilization of biocompatible materials minimizes tissue damage, hence enhancing the safety of intranasal NPs delivery for CNS therapy (Gandhi et al., 2024).

Calu-3 lung epithelial cell line serves as a prevalent *in vitro* model for nasal delivery owing to its significant similarity to human airway physiology. It facilitates research on drug transport, aerosol deposition, controlled-release dynamics, and possible drug–drug interactions for inhaled treatments. Calu-3 cells offer a consistent platform for investigating the interaction of inhaled medications with airway barriers; however, more sophisticated systems are required to comprehensively elucidate pulmonary absorption and metabolism. Calu-3 continues to be an essential instrument for the advancement of safer and more efficacious inhaled drug-delivery systems (Ong et al., 2013). Although formulations containing CS are widely considered to be non -immunogenic and have outstanding mucosal compatibility (Kruczkowska et al., 2024), the fact that CS is a positively charged biopolymer with strong mucoadhesive characteristics means that its interaction with nasal epithelial surfaces must be carefully evaluated to avoid undesirable inflammatory reactions or irritation (Luppi et al., 2010). Histopathological investigation of epithelial integrity, assessment of the number of goblet cells, evaluation of ciliary function, and quantification of pro -inflammatory cytokines such as Interleukin-6 (IL-6), Interleukin-1 beta (IL-1β) , and Tumor Necrosis Factor-alpha (TNF-α) are all typical components of research investigating irritation of the nasal mucosa (Adivitiya et al., 2021; Szekely et al., 2025). Maintaining the formulation at physiological pH and osmolarity further decreases irritation and protects the mucociliary clearance process, which is critical for maintaininggood nasal function

(X. Chen, 2025; Javed et al., 2018). The use of CS NPs that have been properly tuned maintains a high level of mucoadhesion without causing any structural damage. This allows for an extended period of residence time and also ensures that the mucosal safety is preserved. While previous studies have studied CS NPs for intranasal drug delivery, limited information is available regarding BG-CS NPs for sustained intranasal nicotine delivery. Thus, this study aimed to develop and evaluate this novel delivery system to address this research gap.

CHAPTER 3
RESEARCH METHODOLOGY

3.1 Introduction

This chapter covers the materials and methods employed for the development and evaluation for NHT-loaded CS NPs and NHT-loaded BG-CS NPs. Included in this chapter are the preparation steps for modified CS, development of CS NPs and BG-CS NPs, characterization of the NPs using DLS, TEM, DSC, TGA, XRD AND FTIR, determination of the NPs EE% and DL%, stability, in *vitro* cytotoxicity and in *vivo* pharmacokinetic studies.

3.2 Materials

CS (CAS 9012-76-4) (Sigma-Aldrich/CHINA), (DDA): 85%, TPP (CAS 7758-29-4) (Sigma-Aldrich/USA), and NHT (CAS 65-31-6) were purchased from Fisher Bioreagents (Fisher Scientific, USA). Cotinine (CAS 486-56-6), phthalic anhydride (CAS 85-44-9), alkyloxirane (n-butyloxymethyloxirane) (CAS 1-2426-08-6), and potassium tert-butoxide (tBuOK) (CAS 865-47-4) were bought from Sigma-Aldrich (USA). Human normal skin fibroblasts (CDD-1064SK) and Calu-3 human airway epithelial cells (HTB-55™) supplied from The American Type Culture Collection (ATCC, Manassas, VA, USA). Acetic acid glacial MW: 60.05 g/mol supplied from (Friendeman Schmidt); acetic acid 50% HPLC grade MW: 60.05 g/mol from (Sigma-Aldrich/USA). Potassium bromide (KBR) from Sigma-Aldrich (USA). Anhydrous Dimethylformamide (DMF), Tetrahydrofuran (THF) and Hydrazine monohydrate from (Sigma-Aldrich/ Germany). Individually ventilated cages (IVC) were bought from Tecniplast (Italy). Sterile 26-gauge needles were acquired from BD Biosciences (USA). K_2-EDTA blood collection tubes were provided by (BD Vacutainer/(USA). Hexagonal containers made of glass for organ preservation were procured from (Duran /Germany). Capillary tubes were acquired from Hirschmann Laborgeräte (Germany). The MTT reagent was gained from Sigma-Aldrich and all other reagents and solvents in analytical grade.

3.3 Methods

3.3.1 Preparation of BG-CS

3.3.1.1 Synthesis of Phthaloyl CS (protect amino groups (NH2) by the phthaloyl groups)

A solution of phthalic anhydride (14.40 g) in anhydrous DMF (140 mL) was refluxed under nitrogen atmosphere, while CS (5.00 g) was added slowly over a period of 2 hrs. Following reflux for a duration of 18 hrs, the resultant reaction mixture underwent a transformation into a solution of yellow-brown color with a high viscosity. Subsequently, this solution was transferred into a container containing 1 liter of cooled water. The resulting precipitate was subjected to filtration and subsequently rinsed with ethanol and ether to ensure thorough purification. Additional purification was accomplished using Soxhlet extraction using ethanol as the solvent. The resultant pure product was subjected to drying and isolation, solid material with a beige coloration were found (Molnár et al., 2010). Figure 3.1

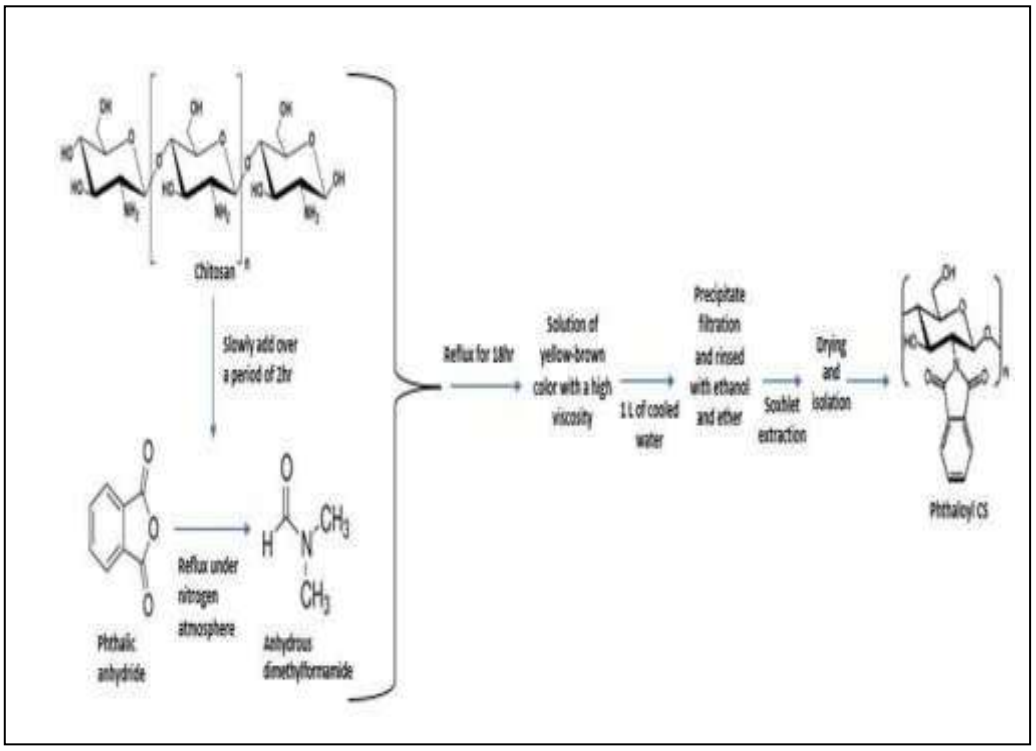

Figure 3.1Synthesis Of Phthaloyl CS (Protection Of The Amino Groups By The Phthaloyl Groups).

3.3.1.2 Synthesis of BG Phthaloyl CS

A solution of phthaloyl CS (1.20 g) in anhydrous DMF (120 mL) was prepared under a nitrogen atmosphere. The resulting solution was added dropwise over a period of 30 min to a mixture of t-BuOK in anhydrous THF (3.29 g) in (10% v/v). A solution of alkyloxirane (n-butyloxymethyloxirane; 29.30 mmol) in DMF (15 mL) was gradually introduced drop by drop over a duration of 30 min, while maintaining constant stirring. The reaction mixture was subjected to stirring at ambient temperature overnight, after which it was subsequently transferred into a container containing 500 mL cool water. Rotary evaporator to evaporate the solvent, and the resulting brown solid was reconstituted in water and subjected to dialysis against deionized water for a duration of 4 days. The final products were obtained as light beige powders through the process of freeze-drying of the dialyzed solution (Molnár et al., 2010). The synthesis process is depicted in Figure 3.2

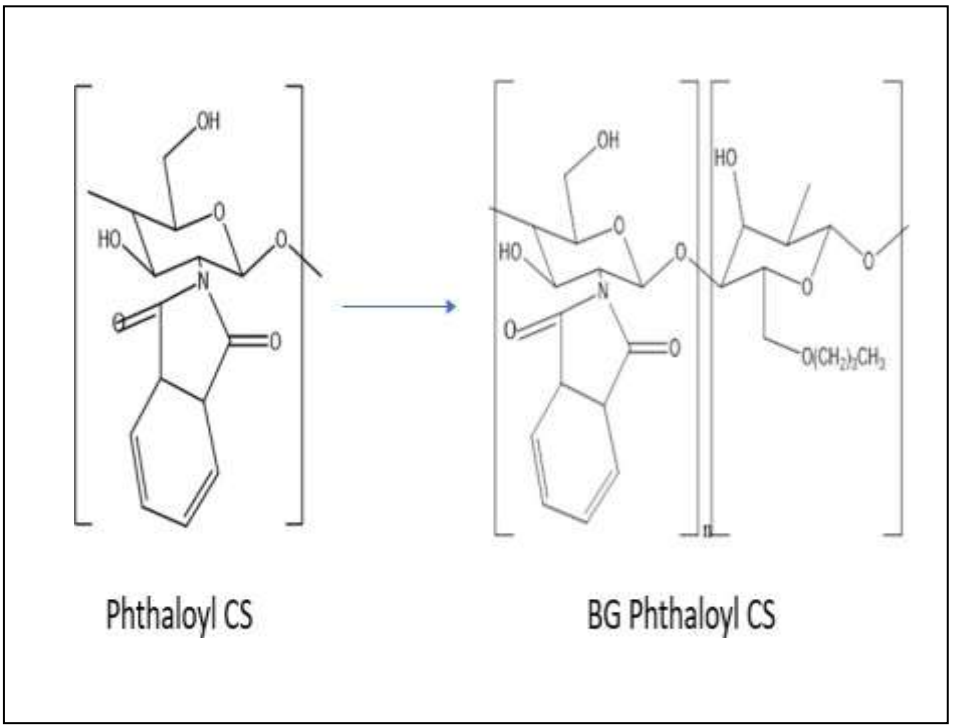

Figure 3.2 Synthesis Of BG Phthaloyl CS.

3.3.1.3 Synthesis of BG- CS

A suspension of 4 g of BG phthaloyl CS was prepared in a solution mixture of 45 mL hydrazine monohydrate and 90 mL of water. The resulting mixture was subjected to reflux for a duration of 15 hrs. Following the cooling process, the reaction mixture underwent dilution with 10 mL of deionized water. The residue obtained after evaporation was washed three times with 20 mL portions of water, with the solvent removed by evaporation after each wash. This washing process was repeated until the total removal of hydrazine was achieved. The product was subjected to additional purification by dispersing it in water and subsequently dialyzingthe resulting suspension against deionized water for a duration of 4 days. Followingcentrifugation at 1000 g for 15 min and subsequent freeze-drying, two distinct materials were produced in the form of beige powders (Molnár et al., 2010). The synthesis process is depicted in Figure 3.3.

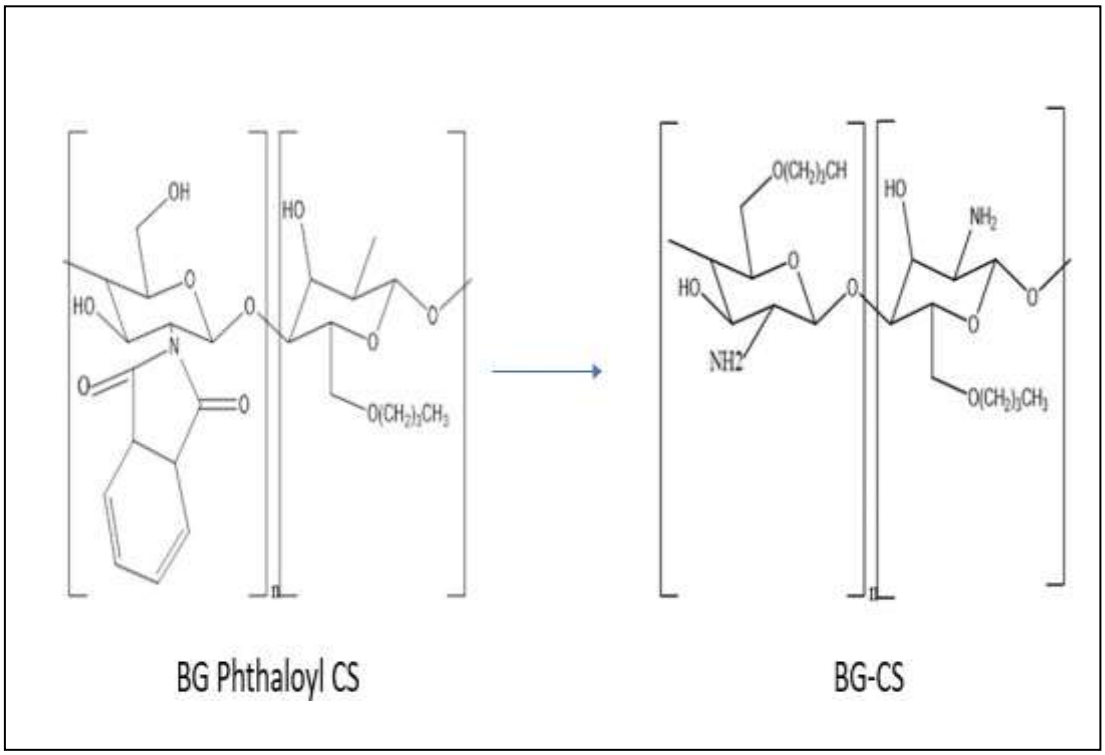

Figure 3.3 Synthesis Of BG-CS (Deprotection Of The Amino Groups).

3.3.1.4 Nuclear Magnetic Resonance Spectroscopy (NMR) Analysis of BG-CS

Using a Bruker Avance III 300 spectrometer with a ^{13}C resonance frequency of75.5 MHz, solid-state ^{13}C CP-MAS (cross-polarization magic angle spinning) nuclear magnetic resonance spectra were recorded from both the original CS and the freeze-dried BG-CS. At a speed of 5 kHz, the samples were compressed into zirconia rotors that were 7 mm in diameter. An external standard was tetramethylsilane at a concentration of 0 ppm. A variable amplitude was used with contact pulse of 1.5 ms duration, 16384 scans, a 4 s repetition rate, and SPINAL-64 decoupling to obtain the spectra (Denis & Gagnon, 2022).

3.3.1.5 Fourier Transformed Infrared (FTIR) Analysis of BG-CS

A Fourier transform infrared spectrophotometer (Spectrum 100; Perkin Elmer, USA) was used to collect the spectra. A transparent solution was prepared by mixing approximately 1-2 mg of CS, phthalic anhydride, and BG-CS with 87 mg of KBR and then being compressed. It was transmitted-scannable within the 4000-400 cm-1 spectral band (Mamand and colleagues, 2024).

3.3.2 Preparation of CS NPs and BG-CS NPs (Blank and loaded NHT)

Usingthe ionic gelation method, the CS NPs and BG-CS NPs were prepared with TPP as a cross-linker (Ding et al., 2018; Sharma et al., 2025). At concentrations of 0.05% and 0.1% (w/v) CS solutions were prepared by dissolving CS in 2% (v/v) aqueous acetic acid with magnetic stirring until a transparent solution was achieved. TPP at concentrations of 0.05 and 0.1% (w/v) was dissolved in deionized water, after the CS and TPP solutions were prepared, the TPP solution (2mL) was slowly added to the CS solution (8mL), probe sonicated for 4 min using a high-intensity ultrasonic processor (VCX 600 Vibra Cell, USA) to ensure complete crosslinking of the NPs. Furthermore, to ensure that no temperature was raised during probe sonication, all samples were placed in an ice bath. Predetermined amounts of NHT (0.025, 0.05, and 0.1% w/v) were incorporated into the CS solution before the synthesis of NPs. Upon dropwise addition of 2 mL of TPP solution to 8 mL of CS solution, NPs were formed. The NPs were then sonicated. The NPs were separated by rotating them in an ultracentrifuge (Optima Max-TL, Beckman Coulter, USA) set at 25°C for 30 min at 30,000 rpm. The NPs were then washed with deionized water and centrifuged at 3000 rpm for 5 min to remove any unencapsulated NHT and TPP before lyophilized (Scanvac Cool Safe 110, Chemo Science, Thailand) for 24 hrs at −90°C. The NPs were freeze-dried directly without the addition of any cryoprotectant prior to lyophilization. Lyophilized NPs were redistributed in deionized water and then subjected to all characterization analyses. (Figure 3.4). The optimum ratios of NHT:CS:TPP and NHT:BG-CS:TPP to give the best size, zeta potential and PDI was then determined. The ratios of NHT, CS, BG-CS and TPP used in our formulation are summarized in Tables 3.1 and 3.2.

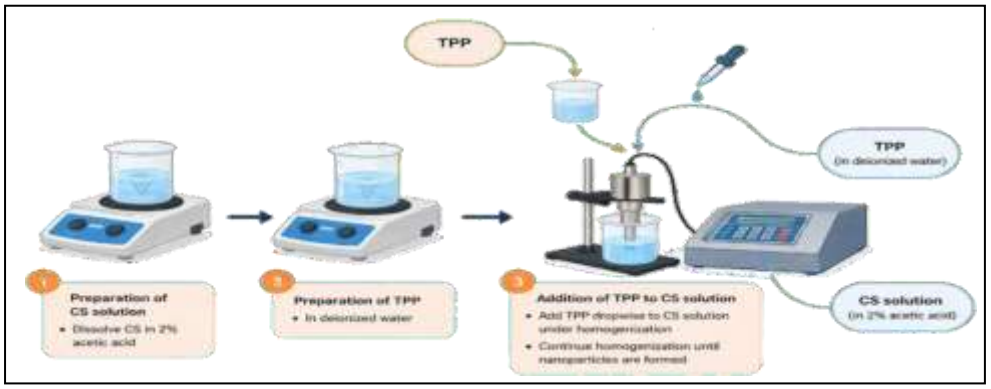

Figure 3.4 Preparation Of Nps (Blank And Loaded NHT).

Table 3.1
CS Nps Loaded NHT Formulation

Formulation	NHT %	CS %	TPP%
F1	0.025	0.050	0.050
F2	0.025	0.100	0.100
F3	0.050	0.050	0.050
F4	0.050	0.100	0.100
F5	0.100	0.050	0.050
F6	0.100	0.100	0.100

Table 3.2
BG-CS Nps Loaded NHT Formulation

Formulation	NHT %	BG-CS %	TPP%
F1”	0.025	0.050	0.050
F2”	0.025	0.100	0.100
F3”	0.050	0.050	0.050
F4”	0.050	0.100	0.100
F5”	0.100	0.050	0.050
F6”	0.100	0.100	0.100

3.3.3 Preformulation Studies

3.3.3.1 Varying Ratios of CS and TPP

CSNPs and BG CSNPs were synthesized via the ionic gelation method using different concentrations (0.05% – 0.3%) of CS and TPP with (CS:TPP) volume ratios (Table 3.1 and Table 3.2).

3.3.3.2 Varying Sonication Time

Sonication time effects on the NPs average particle size, PDI and zeta potential was determined for NPs containing 0.05% and 0.1% CS concentrations, at different sonication time intervals (1,2,4,8 min) using the ultrasonic processor at a measured power of 120 Wwith wave amplitude 20%. NPs with 0.05% and 0.1% CS concentrations were chosen due to its smaller size, good PDI and zeta potential which was obtained from the study done in Section 3.3.2.1.1.

3.3.4 Characterization of CS and BG-CS NPs

3.3.4.1 Particle size, zeta potential and PDI

The size distribution, zeta potential, and PDI of the NPs were determined by employing DLS technique using a Zetasizer (Malvern, UK). Folded capillary cells were filled with a diluted sample according to the manufacturer's instructions using double-distilled water. 30 µL of double-distilled water was added to the NPs, with gentle mixing before being transfered into the folded capillary cell. As demonstrated by Stetefeld et al. (2016), a laser Doppler anemometer. The PDI and mean size measurements were taken at 25°C. Each sample was measured in triplicate, and the results were reported as mean ± standard deviation (SD).

3.3.4.2 Transmission Electron Microscopy (TEM)

High-resolution TEM (Hitachi H-8100 TEM) was used to examine NPs, operated at an acceleration voltage of 60 kV. A small quantity of NPs suspension was applied onto a copper grid, with a 200-mesh size, which had been coated with a layer of carbon. The grid was allowed to dry at ambient temperature. The use of this method enabled the assessment of both the particle size and morphology, as described by Zhang (S. Zhang et al., 2015).

3.3.4.3 Differential Scanning Calorimetry (DSC)

DSC calorimeter (Perkin Elmer Model, USA) recorded the DSC thermograms of the NPs. The precisely weighed samples (± 3mg) sealed into an aluminium pan. An empty,

apply sealed aluminium pan as a reference and heated range (27° C to 400° C), (heating rate: 10 ° C /min) (Abioye et al., 2015).

3.3.4.4 Thermogravimetric Analysis (TGA)

TGA was carried out utilizing a Perkin Elmer Model from the U.S. The sample was taken using a balance system-equipped sample pan within a temperature range of 25° C to 800° C at a flow rate of 10° C/min, with a concentration of 1 -2mg. A constant recording of the sample's mass as according to Rodrigues et al. (2020), temperature is affected (Rodrigues et al., 2020).

3.3.4.5 X-ray Diffraction (XRD)

XRD (Rigaku Ultima IV XRD) was determined the crystalline or amorphous character of CS, BG-CS, NHT, NHT-loaded CS NPs and NHT-loaded BG-CS NPs. A Cu anode operating at 40 kV monochromatic voltage was used for data collecting. The area $20 < 2$ was used to determine the diffraction pattern. It was carried out with a 40- kV voltage and a 40-mA generator (Yun et al., 2018).

3.3.4.6 Fourier Transform Infrared (FTIR)

A FTIR spectrophotometer (Spectrum 100; Perkin Elmer, USA) was used to obtain the FTIR spectra. To manufacture transparent pellets, 2 mg of CS, BG-CS, NHT, NHT-loaded CS NPs and NHT-loaded BG-CS NPs were combined with 87 mg of KBr in a little amount and then compressed. These a spectral area spanning 4000 -400 cm^{-1} was examined in transmission mode (Jozanikohan & Abarghooei, 2022).

3.3.5 HPLC Analysis of NHT

A C18 reverse-phase column (150 × 4.6 mm) and UV detection at 259 nm were used in an Agilent 1260 Infinity HPLC system to determine the NHT concentration. The sodium acetate: methanol (88:12 v/v) solution with 0.05 M sodium acetate and 0.5% triethylamine made up the mobile phase. Glacial acetic acid was used to bring the pH level down to 4.2, and the system was set to run at a flow rate of 1 mL/min. A 1 mg/mL aqueous solution of the medication NHT was prepared for the purpose of plotting

standards and calibration curves. Water, a phosphate buffer solution (PBS) (pH 7.4), and a 2% v/v solution of acetic acid (pH 3) were the solutions used to make the standard solutions for the variousdilutions. After transferring the solution to a vial, it was injected into the HPLC to be analyzed. According to the research of Chen and Chen (2022), the linear regression method was used to determine the correlation coefficient (Chen & Chen, 2022).

Nicotine and cotinine concentration in rat plasma were determined using HPLC analysis. Plasma samples (200 µL) were diluted with 200 µL of NaOH solution (5 M) mixed with sodium chloride (NaCl) solution (1 M) and methanol (20 µL) to a concentration of less than 500 ng/mL of nicotine and cotinine. Following that, the aqueous solutionwas extracted usingdichloromethane (700 µL). After that, the organic layers were dehydrated using reduced pressure and subsequently mixed again with 25 µL of methanol. Injecting a 2 µL portion into the HPLC apparatus was described by Shaik et al. (2019).

Samples of lung and brain tissue were homogenized for 30 seconds each in acetone and hexane before being subjected to HPLC analysis. Each sample weighed around 0.08 g. After the homogenate was centrifuged at 10,000 rpm for 5 min at 4°C, the pellet was discarded. The remaining liquid was reconstituted with 90 µL of mobile phase and 10 µL of methanol after being evaporated to dryness with a mild nitrogen stream (Chik et al., 2022).

3.3.5.1 Linearity

Various quantities of NHT were used to prepare standard solutions. The correlation coefficient (R^2) was calculated after constructing a calibration curve by graphing peak area versus concentration (Li et al., 2022).

3.3.5.2 Limit of Detection (LOD) and Limit of Quantification (LOQ)

The following equations [(3.1) and (3.2)] were used to compute LOD and LOQ:

$$LOD = 3.3\ (\sigma/S) \qquad (3.1)$$

$$LOQ = 10\ (\sigma/S) \quad (3.2)$$

Where σ is the standard deviation of the response and S is the slope of the calibration curve (N et al., 2025).

3.3.6 EE% and DL% of CS and BG-CS NPs

To determine the quantity of entrapped drug, NHT-loaded CS NPs and NHT-loaded BG-CS NPs were weighed and dissolved in 2% (v/v) aqueous acetic acid. The concentration of NHT was determined in the supernatant by an Agilent HPLC system after ultracentrifuge (Optima Max-TL, Beckman Coulter, USA) for 30 min at 15,000 rpm. The separation was achieved on a reverse-phase column (C18). The NHT EE% and the NHT DL% of the NPs were calculated using equations (3.3) and (3.4):

$$EE\% = \frac{(\text{Total amount NHT} - \text{Free amount NHT})}{(\text{Total amount NHT})} \times 100 \quad (3.3)$$

$$DL\% = \frac{(\text{Total amount NHT} - \text{Free amount NHT})}{(\text{Total amount NPs weight})} \times 100 \quad (3.4)$$

The formula "Total amount NHT" represents the total amount of nicotine hydrogen tartrate, "Free amount NHT" represents the amount of free nicotine hydrogen tartrate in the filtrate, and "Total amount NPs weight" represents the weight in the formulation (Soltanzadeh et al., 2021).

3.3.7 Release Studies of CS and BG-CS NPs

The dialysis bag was soaked in PBS for 12 hrs before use to prevent sudden osmotic changes or pH shifts during dialysis. Then 25 mg of NHT-loaded CS NPs/ NHT-loaded BG-CS NPs and 5 mL (PBS) (pH 7.4) were added into the dialysis bag (Biotec CE-Tubing, 500-1000D) (donor phase) (Tao et al., 2023). The membrane was then soaked in 100 mL PBS (acceptor phase) at 37°C and shaken at 75 rpm in an orbital shaking. At

specified time intervals (0.5, 1, 2, 3, 4, 5, 6, 7, 8, and 24 hrs), 3 mL of medium was removed from the acceptor phase and replaced with 3 mL of fresh medium of PBS. The release of NHT was identified by HPLC and calculated as the percentage release (Bohrey et al., 2016), shown in Figure 3.5.

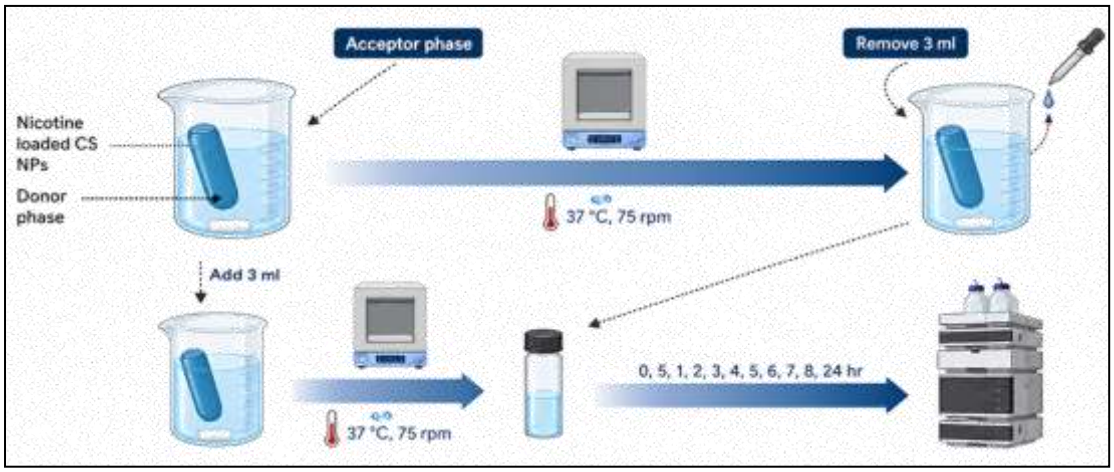

Figure 3.5 Release Of NHT-Loaded CS Nps And NHT-Loaded BG-CS Nps (Dialysis Bag (Biotec CE-Tubing, 500-1000D)

3.3.8 Stability Studies CS and BG-CS NPs

A specified amount of NPs was suspended in a PBS solution (pH 7.4) to evaluate the represent the physicochemical stability of NPs as a suspension for a nasal spray application. All samples were deposited in tubes and wrapped in aluminium foil. Each sample of NPs was stored at 5 ± 3°C and 25 ± 2°C/60 ± 5% (RH) according to ICH Q1A(R2) guidelines. Samples were analyzed at predetermined intervals of 0, 2, and 5 days, and then weekly for up to 90 days. Variations in particle size, PDI, and zeta potential were monitored, which is relevant to the projected intranasal application (Tolentino et al., 2020). Particle size, PDI, and zeta potential data were evaluated by one-way ANOVA to determine statistically significant variations ($p < 0.05$).

3.3.9 Cytotoxicity Studies of CS and BG-CS NPs

3.3.9.1 Cytotoxicity Studies Using Fibroblast Cells

Fibroblast cells were supplemented with 10% fetal bovine serum (FBS), 1% penicillin-streptomycin, and 1% L glutamine, fibroblasts were seeded into T75 flasks (SPL Life Sciences Co., Korea). The cells were incubated at 37°C for 24 hrs in a humidified

incubator containing 5% CO_2. To identify the metabolic activity of live cells, the MTT-3-(4,5-dimethylthiazol-2-yl)-2,5-diphenyltetrazolium bromide assay was employed. Serial dilutions of NHT and the formulations were prepared (0.5, 0.25, 0.125, 0.0625 and 0.03125 mM), and 10 μL aliquots were transferred into the 96 wells and incubated in a humidified 5% CO_2 incubator at 37°C for 24 hrs. Then, 10 μL of MTT reagent was added to each well, followed by incubation at 37°C in 5% CO_2 and 95% humidity for a further 4 hrs. Subsequently, 100 μL of detergent reagent (stop solution) was added to each well, and it was placed in an incubator for 2 hrs. The absorbance was then recorded at 570 nm using a Synergy™ HTX Multi-Mode Microplate Reader (BioTek, USA) (Kamiloglu et al., 2020). Cell viability was calculated using the following equation (3.5):

$$Cell\ viability\% = \frac{(\text{Mean absorbance of treated cells})}{(Mean\ absorbance\ of\ control\ cell)} \times 100 \qquad (3.5)$$

3.3.9.2 Cytotoxicity Studies Using Calu-3 Cells

Calu-3 cells were exposed on Day 7 to the test solutions, including selected formulations (F1, F2, F1", F2") and NHT. Serial dilutions of both NHT and NP formulations were prepared at concentrations of (0.5, 0.25, 0.125, 0.0625, and 0.03125 mM). Subsequent to treatment, the Transwell membranes were rinsed twice with PBS. MTT reagent (1 mg/mL in PBS; 500 μL) was introduced into the apical compartment and incubated in the dark for 3 hrs at 37 °C. The MTTsolution was thereafter eliminated, and formazan crystals were solubilized by introducing 500 μL of extraction solution (0.04 N NaOH in isopropyl alcohol). After one hr, the solutions were amalgamated, and absorbance was quantified at 540 nm and 690 nm utilizing a VERSA max microplate reader (Molecular Devices, Sunnyvale, CA, USA). % Cell viability was determined using equation (3.5), which is based on the ratio of the optical density of treated cells to that of the negative control (Jeong et al., 2019).

3.3.10 In vivo Studies of CS and BG-CS NPs

3.3.10.1 Nasal Administration

Healthy Male Sprague dawley rats from 200g to 300g was fasted for 12 hrs. prior to the experiment, with water beingmade available atall times in individually ventilated cages (IVC) housed in the Laboratory Animal Facility & Management (LAFAM), Faculty of Pharmacy, UiTM. The Committee on Animal Research and Ethics UiTM (UiTM CARE) approved the research protocol and the use of animals (455/2024; (19 April 2024)). The animal investigation was followed as per the regulations and guidelines of Animal Research: Reporting of *In vivo* experiments (Du Sert et al., 2020), and it complied with the scientific research on animal utilization delineated by European Union recommendations (Directive 2010/63/EU) (Guillén et al., 2013). A total of 36 rats allocated into six distinct groups, each group (n=6) (Hamman et al., 2002). Sample size calculation was done according to the equation (3.6):

$$Corrected\ sample\ size = \frac{\text{Sample size}}{(1 - \%\ \text{of attrition})} \tag{3.6}$$

consider attrition is 10%

= [5 / (1-0.1)]

= 5 / 0.9

= 5.55 Sample size was 6.

Six (6) groups of animals were used in this experiment. Hence the number of rates used were 36 rats. The groups are as follows:

a) Control group receiving (PBS)
b) Group receiving free NHT
c) Group receiving NHT loaded CS/TPP NPs [NHT:CS:TPP] ratio (F1)
d) Group receiving NHT loaded BG-CS/TPP NPs [NHT:BG-CS:TPP] ratio (F1”
e) Group receiving of NHT loaded of CS/TPP NPs [NHT:CS:TPP] ratio (F2)
f) Group receiving NHT loaded BG-CS/TPP NPs [NHT:BG-CS:TPP] ratio (F2”)

The group selection is indicated in Figure 3.6. The rats were anesthetized using intraperitoneal administration of ketamine and xylazine, with a dosage of 40 mg/kg for ketamine and 5 mg/kg for xylazine, injected using a 26 -gauge needle (Shoyaib et al., 2019). The NHT-loaded CS NPs/BG-CS NPs were administered at a dose of 1 mg/kg in 50 µL through the intranasal route (Khafagy et al., 2023). Blood samples of 100-500 µL (Jintapattanakit et al., 2010) were extracted by retro -orbital bleeding, which was collected in a heparinized tube at specific time intervals (5, 15, 30 min, 1, 2, 4, and 6 hrs) following administration. Subsequently, the resultant plasma was isolated using centrifugation at 12,000 rpm for a duration of 5 min. The plasma samples were kept at - 22°C until analysis. After blood collection, the animals were euthanized in a CO_2 chamber, and the required tissues which were the lung and brain (Plate 3.1) were isolated in ice-cold condition.

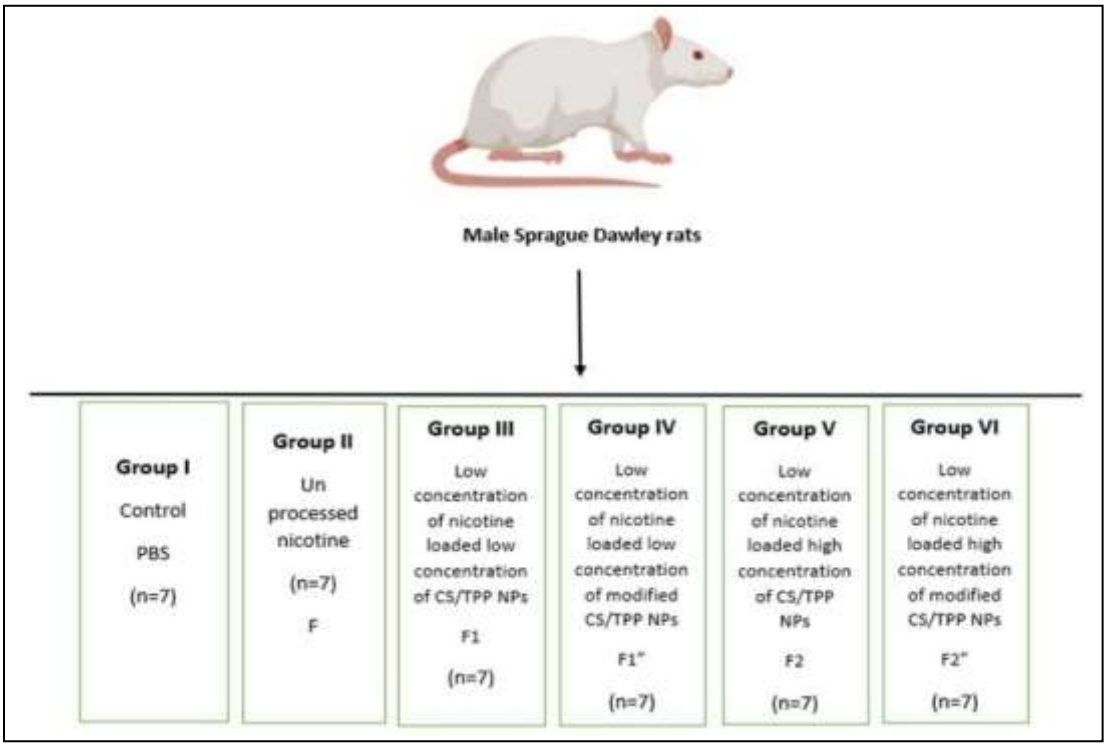

Figure 3.6 Treatment Groups

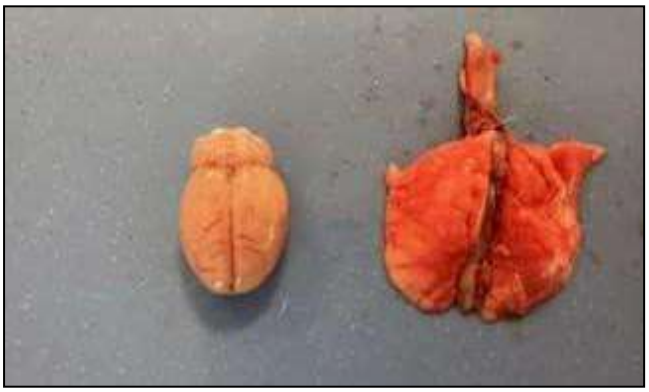

Plate 3.1 Rat Brain And Lung.

3.3.10.2 Pharmacokinetic Analysis

The terminal elimination rate constant (β) for NHT after intranasal delivery was determined usinglinear regression analysis. The calculationof the equivalent T½ ($T_{1/2}$ß) of NHT was performed using the relationship 0.693/ß (Uemura et al., 2005). The calculation of the AUC for plasma concentration versus time and the area under the moment of the curve (AUMC) for plasma NHTconcentration versus time was performed using the usual trapezoidal approach (Schrag & Regal, 2013), following equations (3.7) and (3.8):

$$AUC = \frac{(\mathrm{C1} + \mathrm{C2})}{2} \times (t2 - t1) \tag{3.7}$$

$$AUMC = \frac{((\mathrm{C1} \times \mathrm{t1}) + (\mathrm{C2} \times \mathrm{t2}))}{2} \times (t2 - t1) \tag{3.8}$$

The calculation of the mean residence time (MRT) in the plasma involves the division of the AUMC by the area under the concentration-time curve (AUC), shown in Equation (3.9):

$$MRT = \frac{\mathrm{AUMC}}{\mathrm{AUC}} \tag{3.9}$$

The AUC for cotinine was determined by employing the trapezoidal method to compute the AUC value (Gisleskog et al., 2020). Nicotine has a rapid clearance rate, so measuring cotinine at the same time is required to confirm the metabolic conversion of NHT after delivery and reduces variability (Giratallah etal., 2021). Nicotine content was determined using the same HPLC method previously described for NHT (section 3.3.4)

CHAPTER 4
RESULT AND DATA ANALYSIS

4.1 Introduction

This chapter presents the results of the studies done as described in Chapter 3. The results include the preparation of modified CS, development of CS and BG-CS NPs, physicochemical properties of CS and BG-CS NPs such as particle size, PDI, zeta potential, EE%, DL%, shape, crystallinity, thermal and physical stability and chemical interaction. Results of the NPs release behavior, in *vitro* cytotoxicity and in *vivo* pharmacokinetic studies of NHT-loaded CS NPs and NHT-loaded BG-CS NPs are also depicted.

4.2 Preparation of BG-CS

4.2.1 Synthesis of Phthaloyl CS

FTIR, ^{1}H NMR and ^{13}C NMR spectra confirming the attachment of phthaloyl group onto the CS backbone are presented in Appendices A1, A2 and A3 respectively. Table (4.1).

Table 4.1
Characteristic FTIR, ^{1}H NMR, And ^{13}C NMR Signals Of Phthaloyl CS.

Technique	Peak (cm^{-1} or δ, ppm)	Assignment
FTIR	3587.60 cm^{-1}	O–H stretching
	2347.30 cm^{-1}_ 2301.08 cm^{-1}	Atmospheric CO_2 absorption
	1745.58 cm^{-1}	C=O stretching of phthaloyl (imide) carbonyl
	1548.84 cm^{-1}	Amide II (N–H bending coupled with C–N stretching)
	1446.61 cm^{-1}	N–H deformation (Amide II)
	1373.32 cm^{-1}	Aromatic C=C stretching

	1220.94 cm^{-1}	C–H deformation (CH_3CO)
	1074.38 cm^{-1}	C–O–C stretching (glycosidic linkage)
	945.12 cm^{-1}	C–O–C stretching (glycosidic linkage)
	775.38 cm^{-1}	C–H deformation of aromatic phthaloyl group
^{1}H NMR	δ 1.9 ppm	CH_3 acetyl (multiple)
	δ 2.8–3.3 ppm	Pyranose ring CH protons (multiple)
	δ 7.5–7.9 ppm	Aromatic protons of phthaloyl group (4H, multiple)
^{13}C NMR	δ 31.24 ppm	CH_3 acetyl carbon
	δ 38.24 ppm	Carbon signals (2 C)
	δ 39.40 ppm	Carbon signals (3 C)
	δ 39.47 ppm	Carbon signals (6 C)
	δ 39.64 ppm	Carbon signals (4 C)
	δ 39.97 ppm	Carbon signals (5 C)
	δ 40.47 ppm	Carbon signal (1 C)
	δ 131.25 ppm	Aromatic carbon
	δ 162.79 ppm	Carbonyl carbon of the phthaloyl group

4.2.2 Synthesis of BG Phthaloyl CS

FTIR, ^{1}H NMR and ^{13}C NMR spectra confirming the attachment of BG group to onto the phthaloyl-CS backbone is shown in Appendices B1, B2 and B3 respectively. Table (4.2)

Table 4.2
Characteristic FTIR, ^{1}H NMR, And ^{13}C NMR Signals Of BG Phthaloyl CS.

Technique	Peak (cm^{-1} or δ, ppm)	Assignment
FTIR	3419.79 cm^{-1}	O–H stretching (glycerol hydroxyl group)
	2918.29_2861.30 cm^{-1}	C–H stretching (pyranose ring and alkyl groups)
	1774.51_1710.85 cm^{-1}	Asymmetric and symmetric C=O stretching of the phthaloyl (imide) group
	1523.76 cm^{-1}	N–H deformation (Amide II)
	1485.10_ 1442.75 cm^{-1}	Aromatic C=C stretching vibrations
	1379.10 cm^{-1}	C–H deformation (CH_3CO)
	1060.84 cm^{-1}	C–O–C stretching (glycosidic linkage)
	748.02_721.37_648.08 cm^{-1}	Aromatic C–H deformation of the phthaloyl group
^{1}H NMR	δ 0.92_ 1.40_1.55 ppm	Alkyl group protons (multiple)
	δ 2.60–4.52 ppm	Pyranose ring and glycerol protons (multiple)
	δ 7.60–8.27 ppm	Aromatic protons of the phthaloyl group (multiple)
^{13}C NMR	δ 14.19_ 19.30_ 27.67_ 31.80 ppm	Alkyl group carbons

	δ 40.51 ppm	CH_3 acetyl carbon
	δ 46.38 ppm	Carbon signals (2 C)
	δ 61.78 ppm	Carbon signals (6 C)
	δ 69.25–70.00 ppm	Glycerol carbons
	δ 70.72 ppm	Carbon signals (3 C)
	δ 70.94 ppm	Carbon signals (5 C)
	δ 72.04 ppm	Carbon signals (4 C)
	δ 78.70 ppm	Carbon signal (1 C)
	δ 79.04–130.60 ppm	CS backbone
	δ 166.07, 168.51 ppm	Carbonyl carbons of the phthaloyl (imide) and acetyl groups

4.2.3 Synthesis of BG-CS

FTIR, 1H NMR and 13C NMR spectra of BG-CS is shown in Appendices C1, C2 and C3 respectively. Table (4.3)

Table 4.3
Characteristic FTIR, ^1H NMR, And ^{13}C NMR Signals Of BG-CS.

Technique	Peak (cm^{-1} or δ, ppm)	Assignment
FTIR	3369 cm^{-1}	O–H stretching (glycerol hydroxyl group)
	2873.95 cm^{-1}	C–H stretching (pyranose ring)
	1657.07 cm^{-1}	N–H bending (primary amine, NH_2)
	1592.12 cm^{-1}	N–H deformation (Amide II)

	1378.13 cm^{-1}	C–H deformation (acetyl CH_3)
	1152.94_1083.48_ 611.81 cm^{-1}	C–O–C stretching (glycosidic linkage)
^{1}H NMR	δ 0.98_ 1.33_ 1.55 ppm	Alkyl group protons (multiple)
	δ 1.90 ppm	Acetyl CH_3 protons (multiple)
	δ 2.60 ppm	CH_2 protons (singlet, 2H)
	δ 2.78–3.38 ppm	Pyranose ring and glycerol protons
	δ 4.14–6.87 ppm	Proton assigned to hydroxyl (multiple, 1H)
^{13}C NMR	δ 14.25_19.29_20.84_ 70.58 ppm	Alkyl group carbons
	δ 31.78 ppm	Acetyl CH_3 carbon
	δ 38.87 ppm	Carbon signals (2 C)
	δ 70.68 ppm	Carbon signals (6 C)
	δ 71.02 ppm	Glycerol carbons (multiple)
	δ 76.68 ppm	Carbon signals (4 C)

4.3 Preformulation Studies and Development of CS NPs

4.3.1 Varying Ratios of CS and TPP

Table 4.4 summarizes the impact of CS concentration and CS:TPP ratio on NPs properties. In general, formulations made with lower concentrations of CS and TPP (0.05% and 0.1%) showed better results than those made with higher concentrations of CS (0.15% and 0.3%). The effect of the CS:TPP concentration fluctuated based on the concentration of CS. At a concentration of 0.05% CS, TPP concentration 0.01% yielded the smallest particle size (119.7 ± 3.60 nm), whereas the CS concentration 0.05%, TPP concentration 0.05% exhibited the lowest PDI (0.195 ± 0.01). At a concentration of 0.10% CS, TPP concentration 0.05%: yielded the smallest particle size of (115.5 ±

10.53) nm, accompanied by a comparatively low PDI of (0.219 ± 0.04). Consequently, no individual CS:TPP concentration excelled across all evaluated parameters, and the choice of formulation was determined by a comprehensive equilibrium among particle size, PDI, and zeta potential. At higher CS concentrations, particularly at 0.3% bigger particle sizes and higher PDI was observed.

Table 4.4
Effect Of CS / TPP Concentrations And Their Ratio On Particle Size, PDI And Zeta Potential Of Nps (N=3).

CS Concentration (%)	TPP Concentration(%)	Size (nm)	PDI	Zeta potential(+mV)
0.05	0.01	119.7±3.60	0.352±0.03	+44.3±2.30
0.05	0.03	165.0±5.75	0.260±0.10	+48.5±0.55
0.05	0.05	180.4±8.69	0.195±0.01	+48.2±1.60
0.10	0.03	176.0±9.10	0.391±0.10	+58.7±1.97
0.10	0.05	115.5±10.53	0.219±0.04	+38.4±4.77
0.10	0.10	177.8±17.29	0.190±0.02	+51.1±2.24
0.15	0.04	195.8±6.61	0.350±0.01	+38.5±2.53
0.15	0.08	188.6±15.86	0.212±0.02	+22.2±9.23
0.15	0.15	227.5±14.19	0.396±0.03	+50.9±1.64
0.30	0.08	574.3±9.65	0.378±0.01	+49.7±1.15
0.30	0.15	407.1±13.68	0.536±0.12	+17.6±0.45
0.30	0.30	267.8±4.33	0.475±0.26	+34.4±0.25

Plate 4.1 shows the visual appearance of blank CS NPs prepared at different CS concentrations (0.1%, 0.15%, and 0.3%) and TPP concentration: (a) 0.1%, (b) 0.08, and (c) 0.08 respectively. At the lower concentration (0.1%), the dispersions appear relatively clear and homogeneous, indicating the formation of smaller and more uniformly distributed NPs. As the CS concentration increased to 0.15% and 0.3%, the formulations became progressively more turbid with visible sedimentation, suggesting the formation of larger particles and aggregation. This observation is consistent with the increase in particle size, PDI, and zeta potential at higher polymer concentrations. Additionally, increasing the TPP proportion further contributed to particle aggregation

and instability, as evidenced by the opaque appearance and phase separation. These findings indicate that both higher CS concentration and higher crosslinker content lead to increased particle size, broader size distribution, and changes in surface charge, reflecting reduced colloidal stability.



Plate 4.1 Visual Appearance Of Blank CS Nps Prepared At Different CS Concentrations (0.10%, 0.15%, And 0.30%) And TPP Concentration: (A) 0.10%, (B) 0.08, And (C) 0.08 Respectively.

4.3.2 Varying Sonication Time

Regardless of the sonication time (1, 2, 4 and 8 min), particle size dropped when sonication was performed from 1 to 4 min, suggesting better dispersion. However, the reductions in particle size and PDI between 1,2, and 4 min were not statistically significant ($p > 0.05$). The PDI also dropped when sonication was done up to 4 min, which is indicative of improved homogeneity. However, at 8 min sonication, there were changes of NPs size at CS concentrations of 0.05% (**** $p \leq 0.0001$). PDI and zeta potential at both concentrations ($p > 0.05$), on the other hand remained constant. Among all the sonication time used, 4 min was selected because it consistently produced the lowest mean particle size, lower PDI, and stable Zeta potential (Table 4.5).

Table 4.5
Particle Size, PDI, And Zeta Potential Of Blank CS Nps (0.05%,0.1%) At Different Sonication Time (N=3).

Particle Size (nm)

Sonication time	**Blank (0.05%)**	**Blank (0.1%)**
1 min	103.3 ± 2.47	130.1±2.43
2 min	104.2 ±2.60	128.9±0.56

4 min	100.9±3.15	115.4±2.68
8 min	150.2±14.21	138.7±2.19
PDI		
Sonication Time	**Blank (0.05%)**	**Blank (0.1%)**
1 min	0.43±0.03	0.53±0.02
2 min	0.39±0.06	0.45±0.04
4 min	0.38±0.11	0.46±0.05
8 min	0.57±0.08	0.52±0.03
Zeta potential (+mV)		
Sonication Time	**Blank (0.05%)**	**Blank (0.1%)**
1 min	40.4±5.65	+32.6±3.32
2 min	37.9±4.25	+49.2±5.35
4 min	34.4±0.96	+44.5±5.30
8 min	37.6±3.74	+37.8±8.70

4.4 Characterization of CS and BG-CS NPs

4.4.1 Particle size, Zeta potential and PDI

Particle size and size distribution of blank CS (0.05% / 0.1%) and NHT-loaded CS NPs from F1 to F6 were obtained using DLS (Table 4.6). The average diameters of NPs ranged from 104.30 ±3.60 to 338.10 ± 21.85 nm. The NHT-loaded CS NPs were significantly larger than blank CS NPs (0.05%), and their size increased with increasing ratios of NHT to CS. As depicted in Table 4.6, blank CS (0.05%) showed particle size of 104.30 ± 3.60 nm, which was significantly smaller than F1 (155.83 ± 6.28 nm) (***$p \leq 0.001$), F3 (261.40 ± 19.52 nm) (***$p \leq 0.001$), and F5 (294.40 ± 31.67 nm) (***$p \leq 0.001$).

In dissimilarity, blank CS (0.1%) presented a particle size of 191.90 ± 5.75 nm, which was significantly different from F2 (120.36 ± 3.23) (***$p \leq 0.001$), F4 (341.40 ± 13.34 nm) (***$p < 0.001$), and F6 (338.10 ± 21.85 nm)(***$p \leq 0.001$).The average size of NPs in formulation F2 was found to display the lowest average diameter of 120.36 ±

3.23 (** $p \leq 0.01$). Formulation F6 showed a much higher average diameter of 338.1 ± 21.85 (**** $p \leq 0.0001$), which was twice the size of the blank CS NPs.

The PDI significantly ranged from 0.21 to 0.48, blank CS (0.05%) showed a PDI of 0.25 ± 0.003, which was significantly lower than F1 (0.40 ± 0.007), F3 (0.37 ± 0.020), and F5 (0.48 ± 0.007) (***$p \leq 0.001$). Blank CS (0.1%) showed a PDI of 0.21 ± 0.006, which was significantly lower than F2 (0.26 ± 0.020) (**$p \leq 0.01$), F4 (0.34 ± 0.005), and F6 (0.43 ± 0.010) (***$p \leq 0.001$), indicating that the NPs had less propensity to agglomerate in suspension. The zeta potential measured of blank CS (0.05%) NPs was +59.83 ± 1.09 +mV, which was significantly higher than F1 (+30.66 ± 2.51 +mV), F3 (+15.66 ± 0.87 +mV), and F5 (+22.10 ± 0.79 +mV) (****$p \leq 0.0001$). Blank CS (0.1%) NPs showed a zeta potential of +59.33 ± 2.10 +mV, significantly higher than F2 (+36.06 ± 1.70 +mV), F4 (+24.16 ± 0.37 +mV), and F6 (+17.06 ± 1.95 +mV) (****$p \leq 0.0001$). The values reported in Table 4.6 differ slightly from those presented in Table 4 .5 because they were obtained from a new set measurement performed during the optimization study.

Table 4.6
Particle Size, PDI, And Zeta Potential Of Blank CS And NHT-Loaded CS Nps In Different Concentrations (N=3), 4min Sonication Time.

NPs	Average size (d, nm)	PDI	potential (+mV)
Blank CS (0.05%)	104.30 ±3.60	0.25 ± 0.003	+59.83 ± 1.09
Blank CS (0.1%)	191.90 ±5.75	0.21 ± 0.006	+59.33 ± 2.10
F1	155.83 ± 6.28	0.40 ± 0.007	+30.66 ± 2.51
F2	120.36 ± 3.23	0.26 ± 0.020	+36.06 ± 1.70
F3	261.40 ± 19.52	0.37 ± 0.020	+15.66 ± 0.87
F4	341.40 ± 13.34	0.34 ± 0.005	+24.16 ± 0.37
F5	294.40 ± 31.67	0.48 ± 0.007	+22.10 ± 0.79

NPs	Average size (d, nm)	PDI	potential (+mV)
F6	338.10 ± 21.85	0.43 ± 0.010	+17.06 ± 1.95

The particle size and size distribution of BG-CS (0.05 and 0.1%) and NHT-loaded BG-CS NPs from F1"to F6" are summarized in Table 4.7 The NPs have an average diameter ranging from 69.42 ± 0.72 to 218.63 ± 4.60 nm. Blank BG-CS (0.05%) showed particle size of 182.53 ± 7.65 nm, which was significantly higher than F1" (83.64 ± 1.73 nm) (****p ≤ 0.0001), F3" (139.4 ± 4.46 nm) (****p ≤ 0.0001), and lower than F5" (218.63 ± 4.60nm) (****p ≤ 0.0001). In contrast, blank BG-CS (0.1%) presented a particle size of 103.36 ± 4.22 nm, which was significantly different from F2" (69.42 ± 0.72) (****p ≤ 0.0001), F4" (209.7 ± 5.32 nm) (****p < 0.0001), and F6" (200.7 ± 7.639 nm) (****p ≤ 0.0001). NPs formulated from F2" had the smallest average diameter of 69.42 ± 0.72 (****p ≤ 0.0001). F5" had a much higher average diameter of 218.63 ± 4.6 (****p ≤ 0.0001). The PDI of the NPs ranged from 0.29 to 0.44. Blank BG-CS (0.05%) showed a PDI of 0.31 ± 0.025, which was significantly lower than F1" (0.43 ± 0.020) (**p ≤ 0.01), F3" (0.44 ± 0.034) (**p ≤ 0.01), and non-significantly different with F5" (0.39 ± 0.034). Blank BG-CS (0.1%) showed a PDI of 0.432 ± 0.033, which was significantly higher than F2" (0.32 ± 0.033) (*p ≤ 0.05), F4" (0.29 ± 0.036) (**p ≤ 0.01), and non-significantly different F6" (0.44 ± 0.040). indicating the high degree of uniformity of the NPs, with low tendency of agglomeration in suspension (Ullah et al., 2022).

The zeta potential of the NPs indicated that blank BG-CS (0.05%) had a zeta potential of +38.26 ± 1.79 +mV, which was significantly higher than F1" (+31.93 ± 0.68 +mV) (***p≤ 0.001), F3" (+33.1 ± 1.479 +mV) (**p ≤ 0.01), and F5" (+30.86 ± 1.51 +mV) (****p ≤ 0.0001).Blank BG-CS (0.1%) showed a zeta potential of +40.86 ± 0.96 +mV, significantly higher than F2" (+36.93 ± 0.89 +mV), F4" (+29.46 ± 0.25 +mV), and F6" (+30.53 ± 1.25+mV) (****p≤ 0.0001), blank BG-CS (0.05 and 0.1%) and NHT- loaded BG- CS NPs were positively charged and the surface charge decreased marginally when NHT was incorporated. The surface charge decreased with increasing drug loading, indicating that the positive charge diminishes as the surface coverage of the NPs with NHT increases. Surface zeta potentials of all particles decreased with increasing size,

likely due to drug loading, suggesting that particle surface positive charges are concealed with increased adsorption of NHT (Marsalek, 2014).

Table 4.7
Particle Size, PDI, And Zeta Potential Of Blank BG-CS And NHT-Loaded BG-CS At Different Concentrations. (N=3), 4min Sonication Time.

NPs	Average size (d,nm)	PDI	Zeta potential (+mV)
Blank BG-CS (0.05%)	182.53 ± 7.65	0.31 ± 0.025	+38.26 ± 1.79
Blank BG-CS (0.1%)	103.36 ± 4.22	0.43 ± 0.033	+40.86 ± 0.96
F1”	83.64 ± 1.73	0.43 ± 0.020	+31.93 ± 0.68
F2”	69.42 ± 0.72	0.32 ± 0.033	+36.93 ± 0.89
F3”	139.40 ± 4.46	0.44 ± 0.034	+33.1 ± 1.479
F4”	209.70 ± 5.32	0.29 ± 0.036	+29.46 ± 0.25
F5”	218.63 ± 4.60	0.39± 0.034	+30.86 ± 1.51
F6”	200.70 ± 7.639	0.44 ± 0.040	+30.53 ± 1.25

4.4.2 Transmission Electron Microscopy (TEM)

Blank CS NPs displayed a spherical and semi spherical shape with a diameter ranging from 82.46 to 245.50 nm and a smooth surface (Figure 4.1). The CS NPs have a core–shell structure, with denser skirts and looser interiors. Also, blank BG-CS (0.05 / 0.1%) and NHT-loaded BG-CS NPs exhibited a nearly spherical shape with a diameter ranging

from 56.5 to 290 nm (Figure 4.2). The TEM results concord with the DLS data, and the nano-sized formulation would be advantageous for the transport of NHT intranasally.

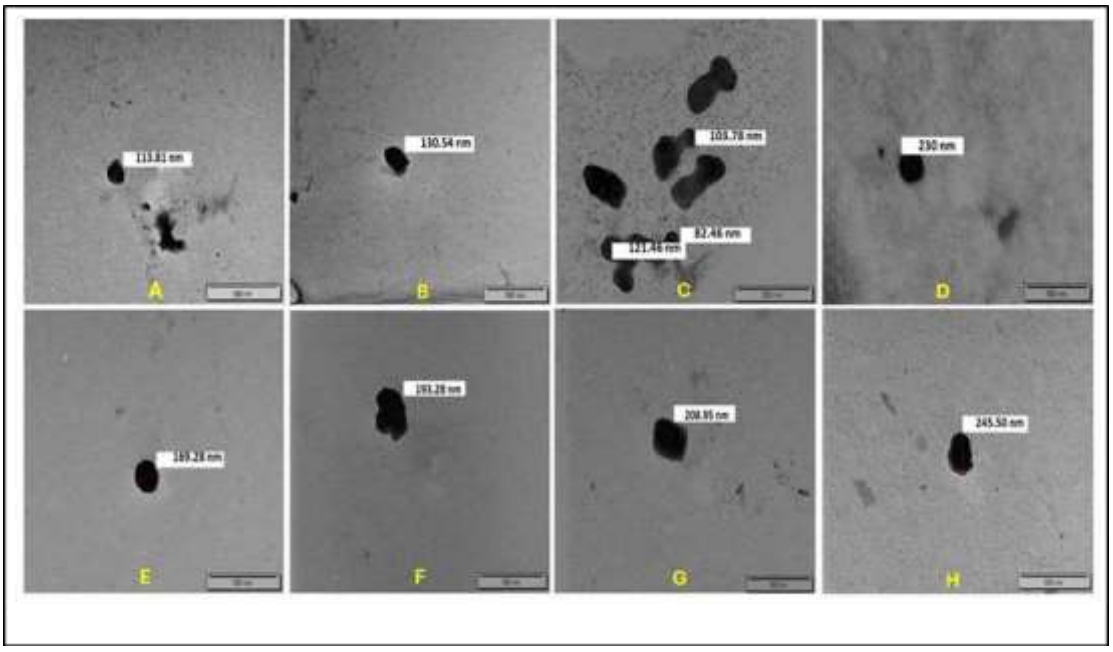

Figure 4.1 TEM Micrographs Of (A): Blank CS Nps 0.05%, (B): Blank CS Nps 0.1%, (C): F1, (D): F2, (E): F3, (F): F4, (G): F5 And (H): F6 Nps At Magnification 80x (Scale Bar:500nm).

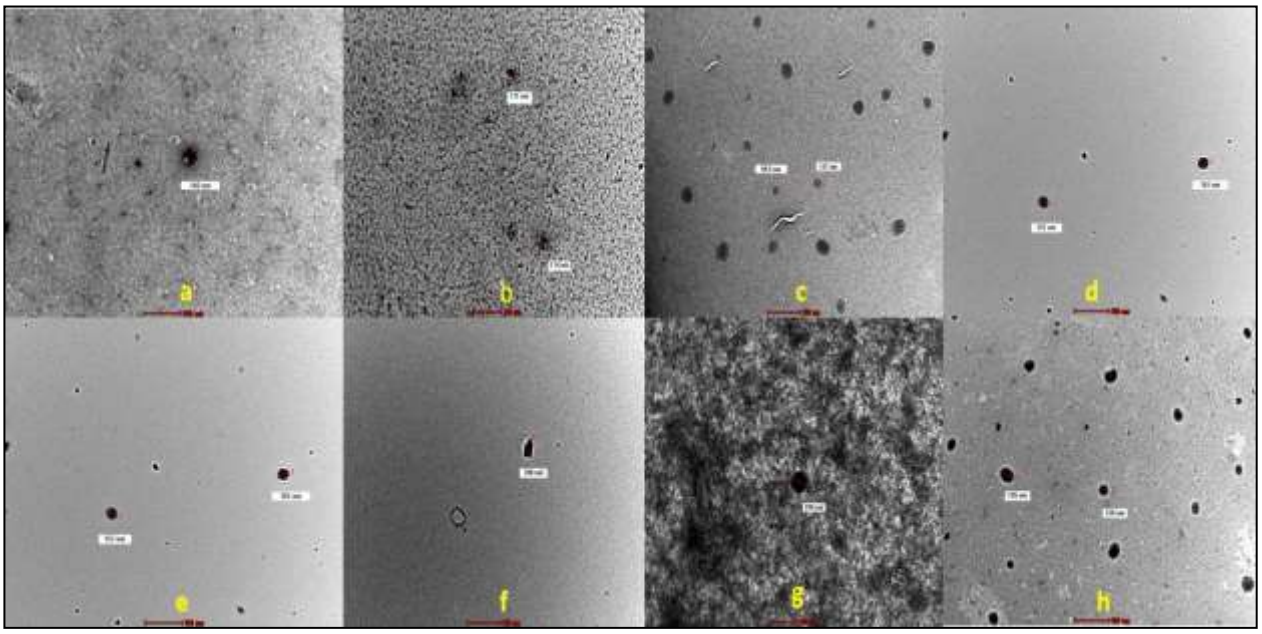

Figure 4.2 TEM Micrographs Of (A): Blank BG-CS Nps 0.05%, (B): Blank BG-CS Nps 0.1%, (C): F1", (D): F2", (E): F3", (F): F4", (G): F5" And (H): F6" Nps At Magnification 80x (Scale Bar:500nm).

4.4.3 Differential Scanning Calorimetry (DSC)

The DSC thermograms of the blank CS, pure NHT and NHT-loaded CS with different drug to polymer weight ratios F1, F2, F3, F4, F5 and F6 are shown in (Figure 4.3). A broad endothermic peak of CS NPs found to be onset at 83.741 °C, corresponding to loss of bound water from CS NPs (Mucha & Pawlak, 2004). Pure NHT showed a sharp endothermic peak at 90.22 °C due to a crystalline melting point (Riggs & Perfetti, 2001). However, this peak disappeared during the cool/reheat circle. The deep changes in drug thermal behavior were found in thermograms of NHT-loaded CS NPs, as the typical peaks of NHT disappeared in terms of NHT:CS: TPP mass ratios between F1, F2, F3, F4, F5 and F6. The NHT after heating appears to be liquid rather than crystalline under the microscope (Yu, 2001). As illustrated in Figure 4.4, the DSC thermograms of the blank BG-CS, pure NHT, and NHT-loaded BG-CS NPs with various drug to polymer weight ratios are as follows: F", F2", F3", F4", F5", and F6".

According to the findings, the endothermic peakof BG-CS NPs was discovered to begin at 88.962 °C, which corresponds to the loss of bound water from BG-CS NPs. At 90.8°C, pure NHT displayed a distinctive endothermic peak. On the other hand, this peak vanished whenever the cool/reheat cycle was performed. The thermograms of NHT-loaded BG-CS NPs revealed significant alterations in the thermal behavior of the drug. This was evidenced by the disappearance of the characteristic peaks of NHT in terms of the mass ratios of NHT:BG-CS: TPP between F1", F2", F3", F4", F5", and F6". The endothermic peaks, which were comparable to the peaks from the BG-CS transition, moved to a lower temperature when the NHT-loaded BG-CS NPs were present.

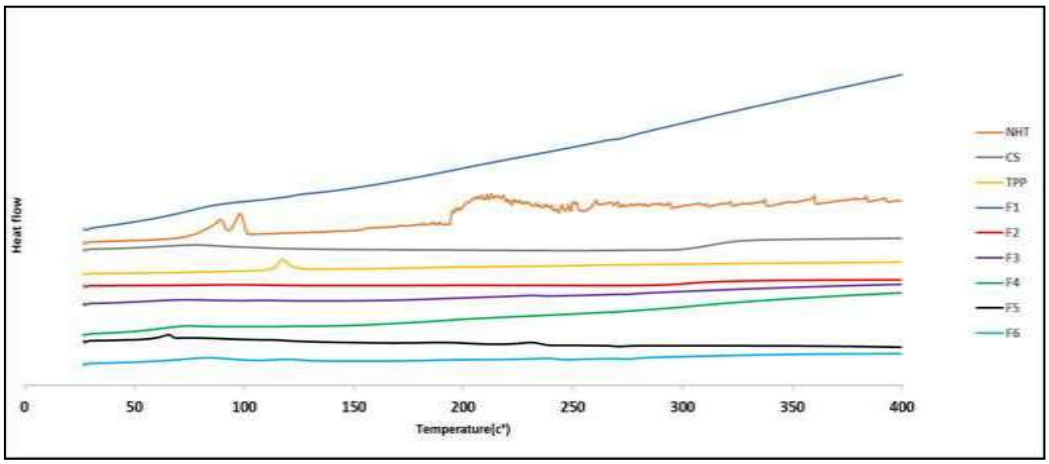

Figure 4.3 DSC Thermograms Of Blank CS Nps, NHT, TPP, F1, F2, F3, F4, F5 And F6 Nps.

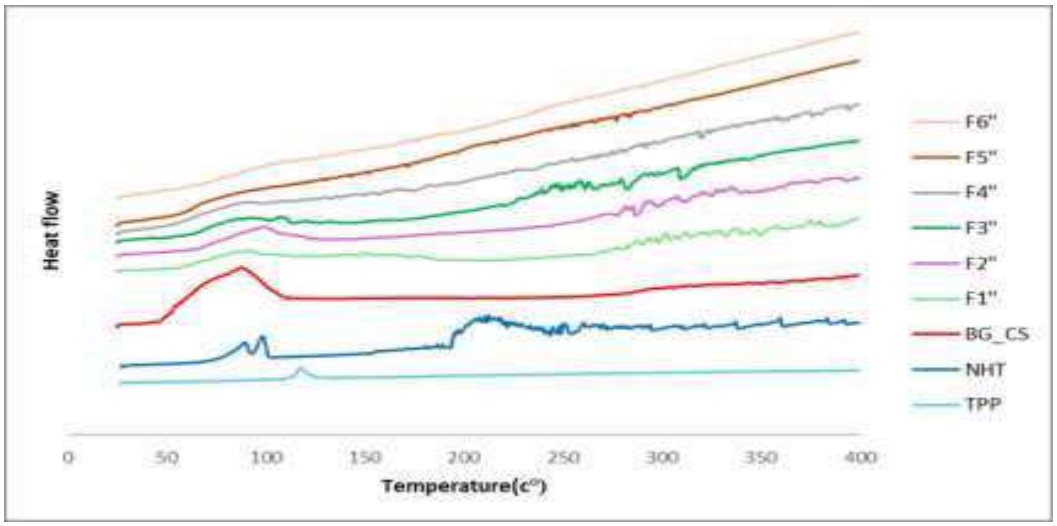

Figure 4.4 DSC Thermograms Of Blank BG-CS, NHT, TPP, F1", F2", F3", F4", F5" And F6" Nps

4.4.4 Thermogravimetric Analysis (TGA)

TGA is a method for investigating the thermal stability and weight changes in samples (Liu & Yu, 2005). According to the TGA thermograms (Figure 4.5), CS, and NHT-loaded CS NPs exhibited weight losses. The initial weight losses of CS and loaded CS NPs, observed in the range of 25 to 150 °C, demonstrated the evaporation of absorbed water (Hong et al., 2007). The weight losses shown in the temperature range of 150 to 800 °C .TGA thermograms of blank BG-CS NPs, NHT, TPP, F1", F2", F3", F4", F5" and F6" shown in Figure 4.6 indicated that due to the evaporation of physically adsorbed

and bound water, blank BG-CS and NHT-loaded BG-CS NPs showed an initial weight loss in the temperature range of 25-150 °C.

Weight loss occurs in two stages, the first stage, between 150 and 300 °C, is caused by the thermal breakdown of the polymer backbone. The second stage, throughout the BG-CS matrix, is the breakdown of intermolecular connections (Neto et al., 2005). The quick weight loss observed at lower temperatures in the presence of pure NHT suggests that the free drug is not very thermally stable. In contrast, BG-CS NPs loaded with NHT showed a slower and more staggered pattern of weight loss, proving that the nicotine was more thermally stabilized after being encapsulated in the BG-CS NPs matrix.

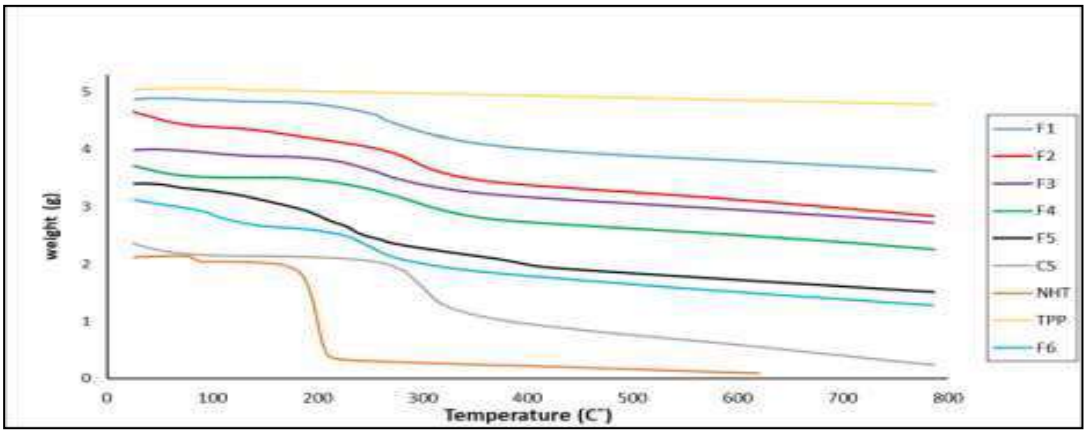

Figure 4.5TGA Thermograms OF Blank CS, NHT, TPP, F1, F2, F3, F4, F5 And F6 Nps.

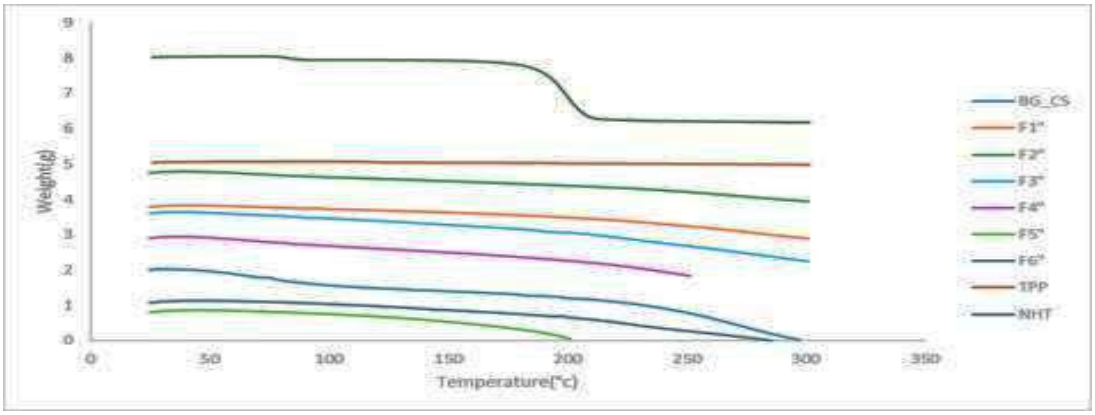

Figure 4.6 TGA ThermogRams Of Blank BG-CS, NHT, TPP, F1", F2", F3", F4", F5" And F6" Nps.

4.4.5 X-ray Diffraction (XRD)

Figure 4.7 shows the XRD patterns of blank CS and NHT-loaded CS NPs. There was only a broad peak in the diffractogram of blank CS at 2θ at 19.94°, which was characteristic

of CS as an amorphous polymer. The region under the broad peak was related to the amorphous phase. In the X-ray diffractogram of pure NHTpowder (Figure 4.8), several sharp peaks were seen at the angle of 2θat 17.97°, 17.98°, 18° and 18.02°, implying that the NHT was crystalline material. XRD patterns of blank BG-CS, NHT-loaded BG-CS NPs, and NHT are illustrated in (Figure 4.9). The diffractogram of blank BG-CS shows only a broad peak at 2θ 20.32°, indicating an amorphous nature. The area under the wide peak is associated with the amorphous phase (F1"at 21.84°, F2"at 20.62°, F3"at 19.5°, F4"at 22.12°, F5"at 20.76°, and F6"at 22.86°). The X-ray diffractogram of pure NHT powder displays sharp peaks at 2θ angles of 17.97°, 17.98°, 18°, and 18.02° indicating that NHT is crystalline material. Salt synthesized using D-tartaric acid has one of the highest melting points for a crystalline NHT solid reported to date (Angevine et al., 2023). The XRD patterns show qualitative differences in the crystal structure (Bates et al., 2006). The solubility of drugs in amorphous form is much higher than that in the crystalline form (Kaushal et al.,2004).

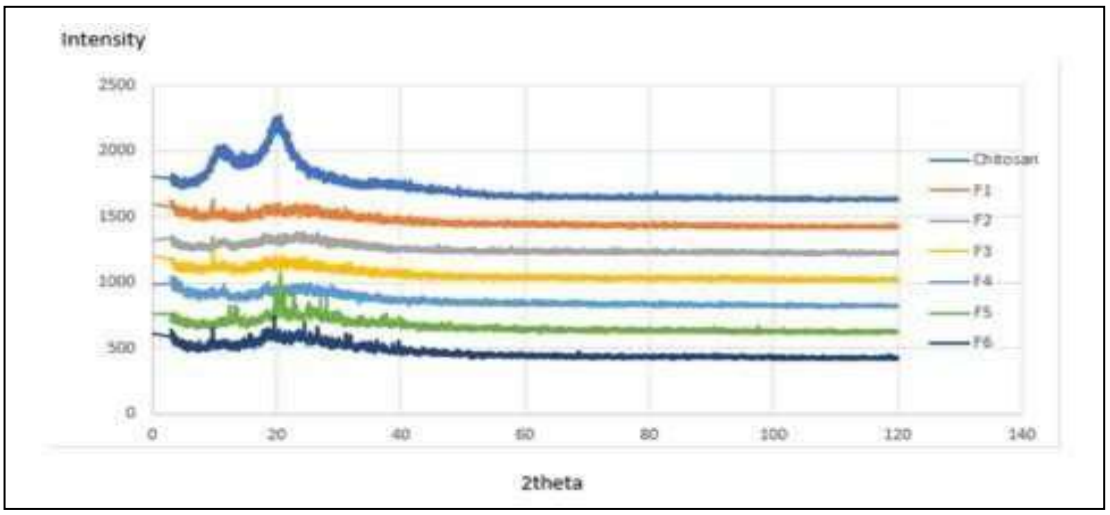

Figure 4.7 XRD Of Blank CS, NHT, F1, F2, F3, F4, F5 And F6 Nps

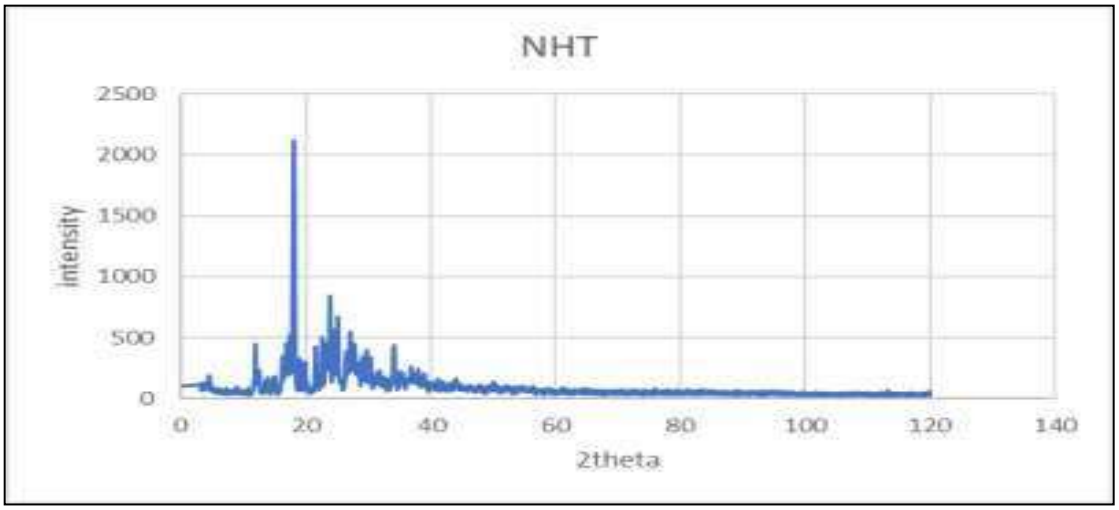

Figure 4.8 XRD Of Pure NHT Powder.

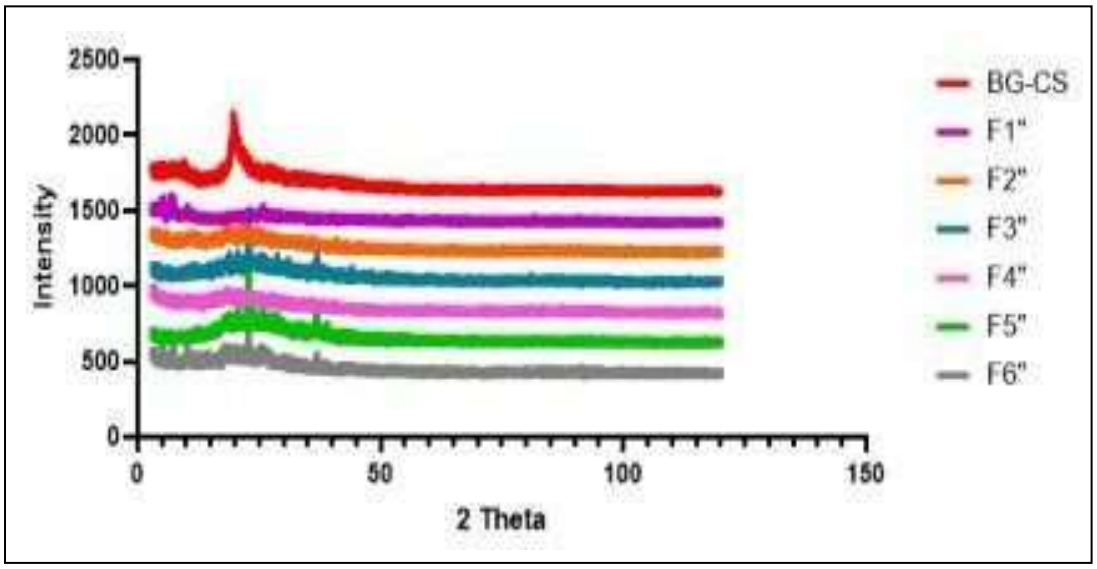

Figure 4.9 XRD Of Blank BG-CS, NHT, F1", F2", F3", F4", F5" And F6" Nps.

4.4.6 Fourier Transform Infrared Spectroscopy (FTIR)

Several characteristic bands of CS can be seen in absorbance FTIR spectra (Figure 4.10). The overlapped peaks of the OH and N-H stretching existed at 3432.9 cm^{-1}. At 2877.55 cm^{-1}, the peak of CH_2 stretching vibration was recorded, which corresponded to a pyranose ring. The characteristic peaks of CS were at 1647.4 cm^{-1} and 1601.7 cm^{-1} with high intensity and were attributed to the vibration of the amide I (C=O) and amide II (N-H) bands, respectively, from the residual N-acetyl groups of chitins. We assigned the peak of asymmetric stretching of the C-O-C bridge at 1155.11 cm^{-1} and the skeletal

vibration involving the O-C-O stretching at 1087.22 cm^{-1} and 1027.42 cm^{-1} to its polysaccharide structure (Zawadzki & Kaczmarek, 2009). The characteristic absorbance of C=N stretching, usually ranging between 1600 and 1700 cm^{-1}, was not seen, and this may be related to overlapping with the amide I band. Theinfrared spectrum of TPP revealed peaks at ranges 1212.38 cm^{-1} and 1098.02 cm^{-1} that can be attributed to P=O stretching, while other peaks found in the TPP IR spectrum at 895.53 cm^{-1} contributed to P-O along with P-O-P (Silvestro et al., 2020).

The FTIR spectra for NHT exhibited an absorption band at 1727.6 cm^{-1}, which was the characteristic band (C=O) of –COOH from NHT. The presence of -COO caused a specific band at 1562.05 cm^{-1}. The absorption bands of 1410.61 cm^{-1}, 1264.68 cm^{-1}, 1134.99 cm^{-1}, and 1076.39 cm^{-1} were related to C-O stretching. The entrapment of NHT into CS NPs was also investigated by FTIR analysis of NHT-loaded NPs with different mass ratios of NHT:CS: TPP. F1, F2, F3, F4, F5, and F6 showed carboxyl peaks of NHT slightly shifted after encapsulation with CS. The FTIR spectra (Figure 4.11) for NHT exhibited an absorption band at 1727.6 cm^{-1} characteristic of COOH (C=O). The COO also gives rise to a band at 1562.05 cm^{-1}. Absorption bands at 1410.61, 1264.68, 1134.99, and 1076.39 cm^{-1} are related to O−H and C−O stretching. The entrapment of NHT was also investigated by FTIR analysis of NHT-loaded BG-CS NPs

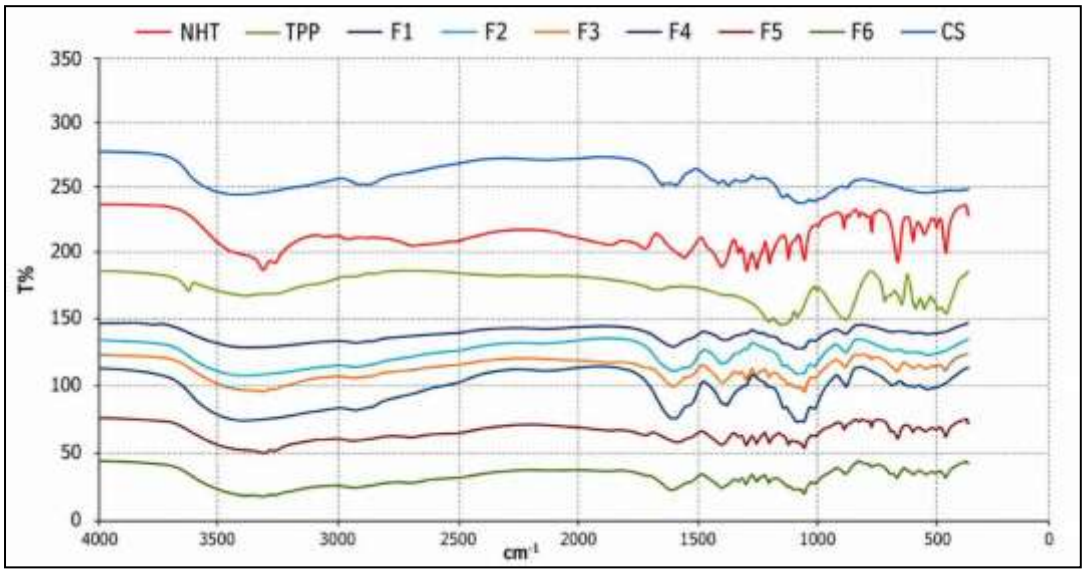

Figure 4.10FTIR Of Blank CS, NHT, TPP, F1, F2, F3, F4, F5 And F6 Nps.

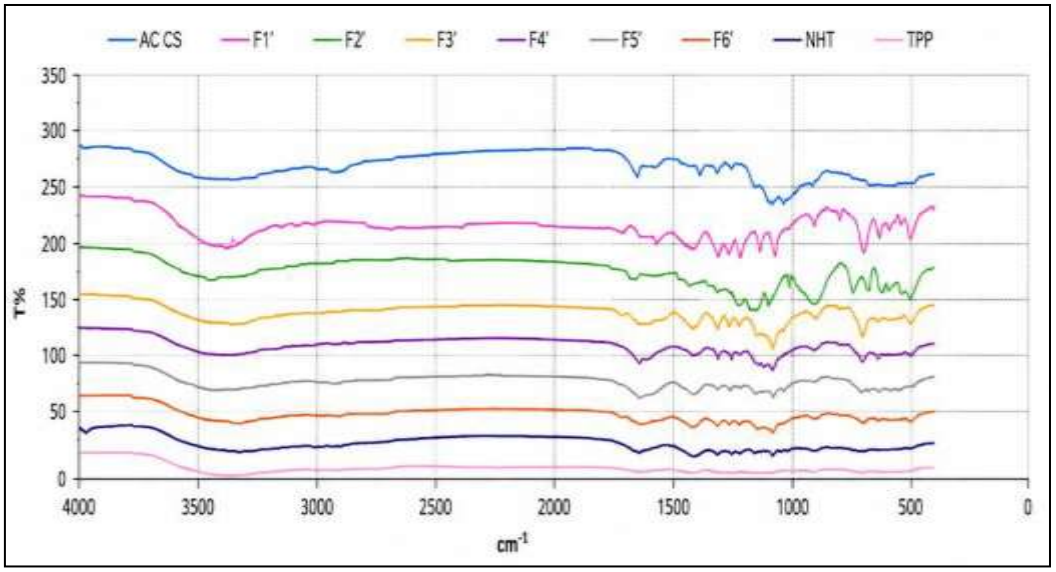

Figure 4.11 FTIR Of Blank BG-CS, NHT, TPP, F1", F2", F3", F4", F5" And F6" Nps.

4.5 HPLC analysis of NHT

HPLC chromatogram of NHT is shown in Figure 4.12 The chromatographic separation was carried out at a flow rate of 1 mL/min, and the detection wavelength was 259 nm. NHT was identified as a distinct and clearly defined peak at retention time of 2.516 min. A correlation coefficient of 0.9999 was found between thecalibration curves at the concentration range of 0.008–0.07 mg/mL, demonstrating that the linearity of the calibration curves was excellent. Atsignal-to-noise ratios of 3:1 and 10:1, the (LOD) and (LOQ) were determined to be 0.00180 mg/mL (1.80 µg/mL) and 0.00547 mg/mL (5.47 µg/mL), respectively. These values were determined by calculating the standard deviation of the intercept (SD = 0.1935) and the slope of the calibration curve (354.36). These findings provide further evidence on the suitability and accuracy of the HPLC method in determining the amount of NHT and cotinine present in the formulations.

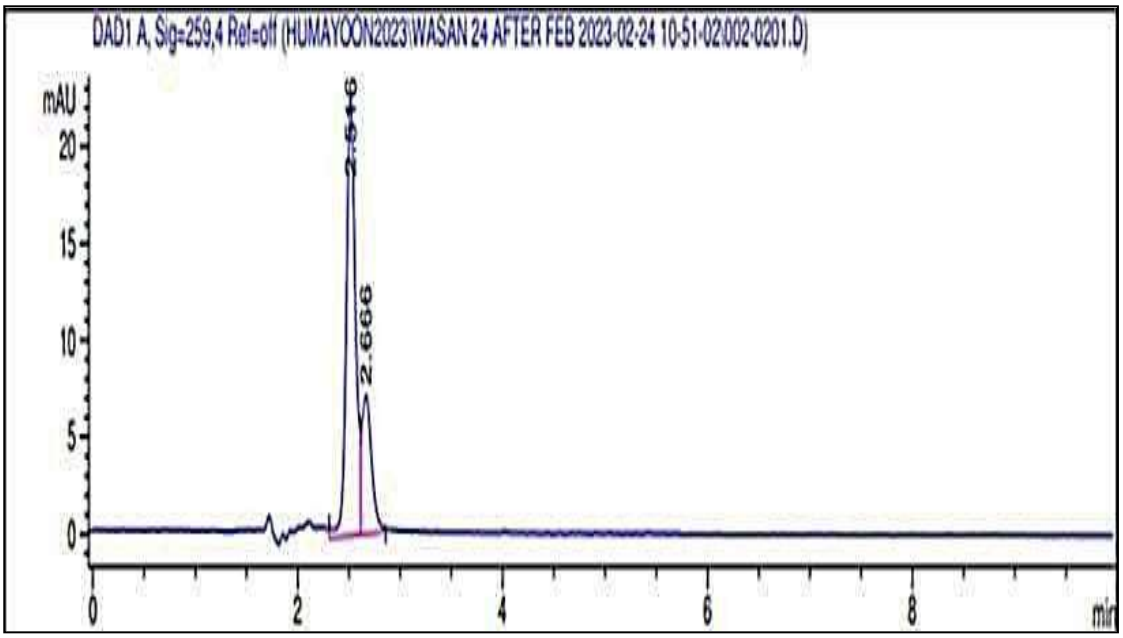

Figure 4.12NHT Peak.

The cotinine HPLC chromatogram is shown in Figure 4.13 Under the given chromatographic conditions, a clear and sharp peak was seen with a retention period of about 1.20 min. Since cotinine is more polar than nicotine, it elutes from the chromatographic column earlier, which agrees with this retention time. The established HPLC approach is appropriate for cotinine detectionand identification based onthe clear separation and well-defined peak. The solvent front or trace contaminants might be responsible for the small signals seen at early retention times.

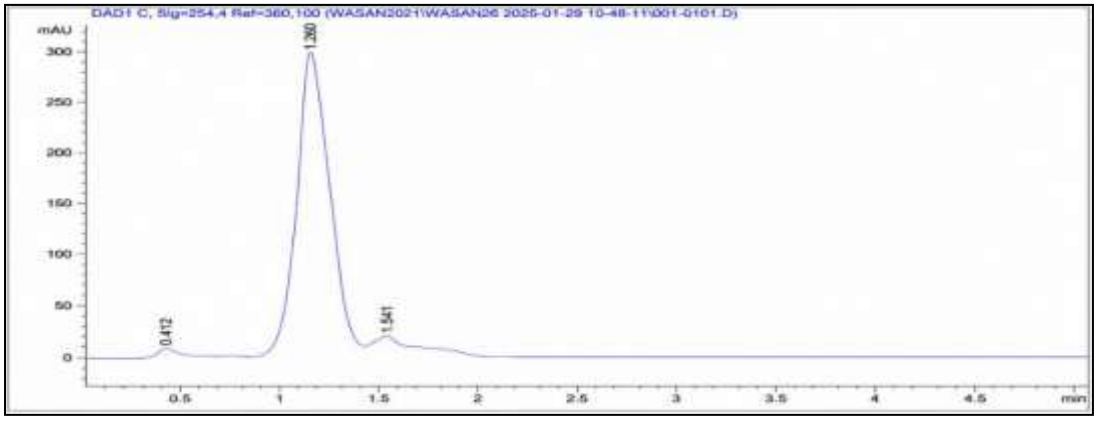

Figure 4.13Cotinine Peak.

4.6 EE% and DL% of NPs

The results of EE% and DL% for NHT-loaded CS NPs are presented in Table 4.8. The amount of encapsulated NHT inside CS NPs was found to be in the range of 92.67 % to 98.76 %. F4 exhibited a highest EE% (98.76%), followed by F1 and F2, 96.88 % and 96.05 %, respectively. From Table 4.6, F1 and F2 provided the highest zeta potential values with the second highest EE%. However, the DL% of NHT-loaded CS NPs was in the range of 15.82 % to 51.78 %. The DL% increased by increasing the concentration of NHT and polymer ratio (Wang et al., 2020). The highest DL% was seen for F5 and F6, which was 51.78 % and 40.86 %, respectively, with the highest NHT concentration and highest CS:TPP ratio.

Table 4.8
EE% And DL% For NHT-Loaded CS Nps (N=3).

NPs	EE%	DL%
F1	96.88 ± 0.09	18.56 ± 2.32
F2	96.05 ± 0.12	15.82 ± 1.93
F3	89.52 ± 0.20	31.51 ± 0.89
F4	98.76 ± 0.05	17.17 ± 0.33
F5	92.67 ± 0.14	51.78 ± 1.35
F6	95.39± 0.06	40.86 ± 0.34

The results for EE% and DL% of NHT-loaded BG-CS NPs are shown in Table 4.9. The quantity of EE% of NHT within BG-CS NPs, varied from 85.65% to 95.70%. Maximum EE% (95.70%) was obtained for F4", followed by F1" and F2". The DL% for NHT-loaded BG-CS NPs was in the range of 14.14%−45.81%. F5" had the highest loading. The DL% increased at higher NHT concentration. DL% was generally higher with lower CS proportions in F1", F3", and F5" formulations compared to F2", F4", and F6".

Table 4.9
EE% And DL% For NHT-Loaded BG-CS Nps (N = 3).

NPs	EE%	DL%
F1"	95.40±0.09	22.31±1.81
F2"	93.89±0.23	14.14±0.47
F3"	91.67±0.06	32.47±0.58
F4"	95.70±0.10	16.14±0.76
F5"	86.17±0.16	45.81±1.31

NPs	EE%	DL%
F6”	85.65±0.11	36.73±0.50

4.7 Release Studies of NPs

NHT release from CS NPs was determined using the HPLC analytical method. The percentage of drug released from the particle formulations is shown in Figure 4.14 Compared to the NHT release profile, it was apparent that entrapment of NHT in the CS particles can affect NHT release. F4 showed the slowest drug release in the first hrs of 19.41 ± 5.01% (****$p \leq 0.0001$), followed by F6 at 20 ± 0.87 % (****$p \leq 0.0001$), F2 at 21.45 ± 3.34 % (****$p \leq 0.0001$), F3 at 28.37 ±8.59%% (****$p \leq 0.0001$), F1 at 34.25 ± 3.09 % (****$p \leq 0.0001$) and F5 at 34.65 ± 12.59 %% (***$p \leq 0.001$). These results suggest that the initial quantity released depends on the ratio of CS to TPP. It should be mentioned that CS is not soluble in phosphate-buffered media, and the primary amine protonation process is responsible for CS solubility in aqueous acidic environments (Aranaz et al., 2021).

After 5 hrs. the amount released from F1, F5, and F3 increased to the maximum (84.81 ± 0.58% , $p > 0.05$), (54.49 ± 4.64 %,****$p \leq 0.0001$) and 64.93 ± 3.33 %,****$p \leq 0.0001$) respectively, while the corresponding values for F2, F4, and F6 were (30.88 ± 1.80 %,****$p \leq 0.0001$), (36.11 ± 4.79 %, ****$p \leq 0.0001$) and 43.53 ± 10.16%, ****$p \leq 0.0001$) respectively. At longer times, formulations with higher drug loading exhibited a faster drug release from the NPs due to a greater diffusional driving force (De Castro et al., 2020). In contrast, formulation F2, which had a lower drug loading (28.27%), showed the lowest drug release, reaching only 38.01 ± 1.79% after 8 hours (****$p \leq 0.0001$).

At the end of the release period, all NHT-loaded CS NPs (F1, F2, F3, F4, F5, and F6) achieved the maximum cumulative % release (91.83±5.54%, $p > 0.05$), 49.21±3.04%, ****$p \leq 0.0001$), 73.01±4.10%, ****$p \leq 0.0001$), 56.08 ±4.58%, ****$p \leq 0.0001$), 68.35±17.28%%,****$p \leq 0.0001$) and 55.60±2.89%%, ****$p \leq 0.0001$) respectively.

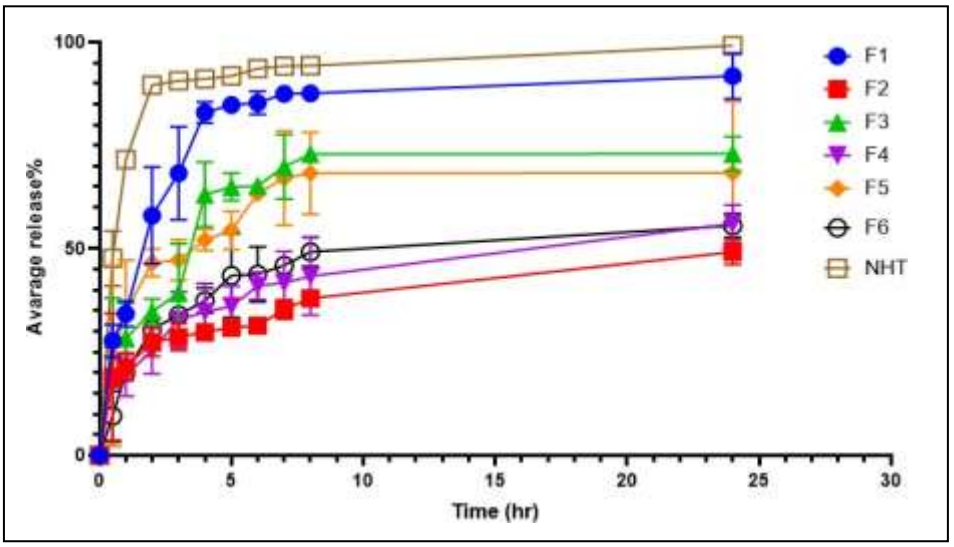

Figure 4.14Average Release % For F1, F2, F3, F4, F5, F6 Nps And NHT.

NHT release from BG-CS NPs is shown in Figure 4.15 During the initial hr of release, the formulations exhibit unique profiles indicative of their content. At first hr, F2" has the most gradual release at 28.43 ± 8.61% because of its elevated concentrations of CS and TPP, which create a dense matrix that impedes early drug diffusion. Conversely, F6" exhibits a release of 61.15±1.32%, the highest amongthe formulations, indicating a more porous or less retentive matrix. Alternative formulations, including F1" (54.88±2.24%, ****p ≤ 0.0001), F3" (55.52±1.58, ****p ≤ 0.0001%), and F5"(54.99±8.07, ****p ≤ 0.0001%), demonstrate rapid release, most likely due to reduced CS ratios. F4" has an intermediate release of 46.03±1.54% (****p ≤ 0.0001), consistent with its modest drug loading and comparatively elevated CS content. At 5 hrs release values rise for all: F2" (65.16±6.45%, ****p ≤ 0.0001), F4" (50.65±1.07%****p ≤ 0.0001), F6" (72.73±2.41%, ****p ≤ 0.0001), F1" (78.55±5.68%, **p ≤ 0.01), F5" (62.55±0.24%, ****p ≤ 0.0001), and F3" (69.03±2.45%, ****p ≤ 0.0001). F2" continues to exhibit the slowest cumulative release, thus sustaining its sustained release capacity. F1" exhibits a significant increase to 78.55%, whereas F3" and F6" nearly 70%, indicating a more rapid progression beyond the initial hr.

After 8 hrs, the cumulative release particularly differentiates the profiles: F1" (87.02±1.99%), F4" (55.52±1.13%, p > 0.05), F5" (65.65±1.46%, ****p ≤ 0.0001), F2"(75.39±9.2%, ****p ≤ 0.0001), F6" (74.59±7.75%, ****p ≤ 0.0001), and F3"(72.26±1.84%, ****p≤ 0.0001). F1″ achieved nearly complete release within 8 hrs, whereas F2″, F3″, and F6″ exhibited slower and more sustained release profiles, making

them more suitable for prolonged nicotine delivery. F4″, despite exhibiting the highest EE%, demonstrated the slowest release at 8 hrs (55.52%), which may be attributed to the higher degree of ionic crosslinking between CS and TPP, forming a denser polymeric network that restricted NHT diffusion. The lower DL% of F2″ and F4″ may have contributed to their slower release by reducing the drug concentration gradient; however, the denser CS:TPP crosslinked matrix was considered the main factor restricting NHT diffusion.

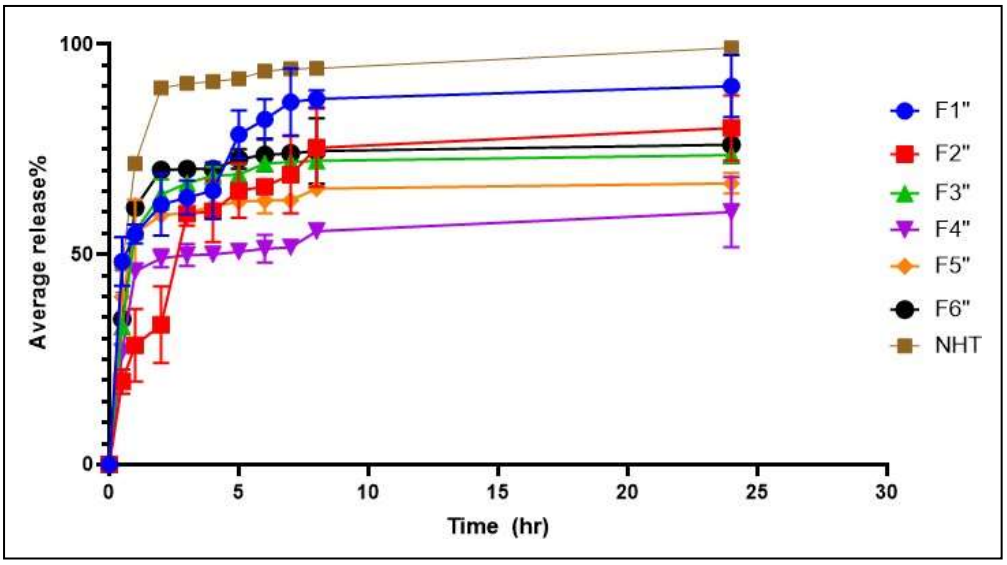

Figure 4.15Average Release (%) For F1", F2", F3", F4", F5", F6" Nps And NHT.

4.7.1 First Order Release Model

According to zero order model, all formulations with R^2 less than 0.5 and do not go throw this model. To assess the first-order release behavior for F1-F6, the cumulative % of drug released at time (Qt) was plotted against time, and the formula ln (100 − Qt) was used (Figure 4.16). The release rate correlated with the residual drug concentration, since all formulations followed a general linear declining pattern in the first-order plots. Over the examined time range the profiles showed good linearity, with the exception of a few early time points where there were small leavings from linearity. F2(R^2=0.741) and F4(R^2=0.752) demonstrated intermediate conformity to first-order kinetics, as indicated by the relatively better arrangement of experimental data with the fitted regression line, compared to the other formulations. But there was substantial scatter around the regression line for F1(R^2=0.562), F3(R^2=0.500), F5(R^2=0.493), and F6(R^2=0.615), suggesting that they only partially complied with the first-order model.

According to these results, there is a concentration -dependent component to the drug release from the NPs formulations, but other parameters, such the dispersion of the polymeric matrix and the structural features of the NPs, also impact the release mechanism.

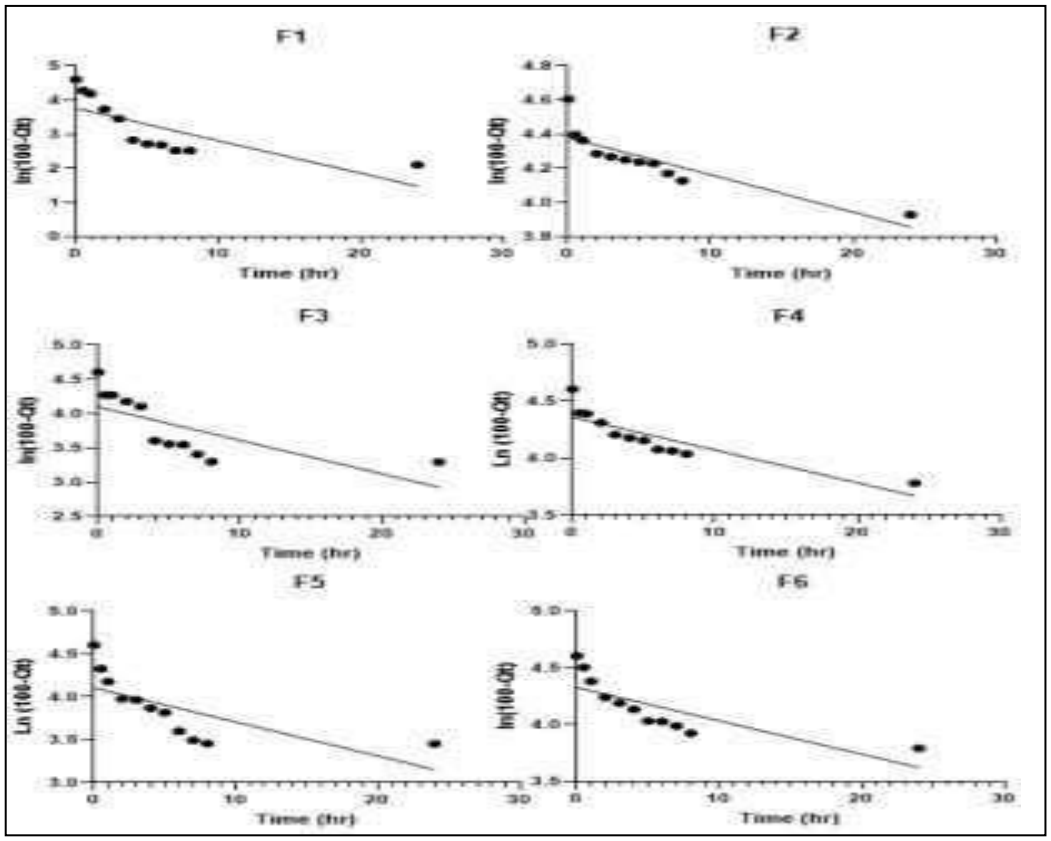

Figure 4.16First-Order Release Kinetics Of NHT From F1–F6. The Plots Represent The Relationship Between Ln (100 − Qt) And Time (Hr.), Where Qt Means The Cumulative Percentage Of Drug Released At Time T. The Linear Regression Lines Indicate Concentration-Dependent Drug Release Behavior, And The Slope Resembles To The First-Order Release Rate Constant (K_1).

NHT-loaded CS NPs (F1-F6) were compared with the NHT-loaded BG-CS NPs (F1”-F6″) by plotting ln (100 − Qt) vs time, which allowed for the evaluationof the first-order release profiles of the compounds (Figure 4.17). The presence of a concentration-dependent release component was confirmed by the downward linear trend that all changed formulations exhibited. Nevertheless, formulations F1”-F6″ exhibited better linearity and less data point scatter around the regression lines compared to (F1-F6), especially for F1” (R^2=0.610) and F2″(R^2=0.629), suggesting intermediate with first-order kinetics, compared to the other formulations. But there was substantial scatter

around the regression line for F3" (R^2=0.320), F4" (R^2=0.392), F5" (R^2=0.294), and F6" (R^2=0.295), suggesting that they less complied with the first-order model.

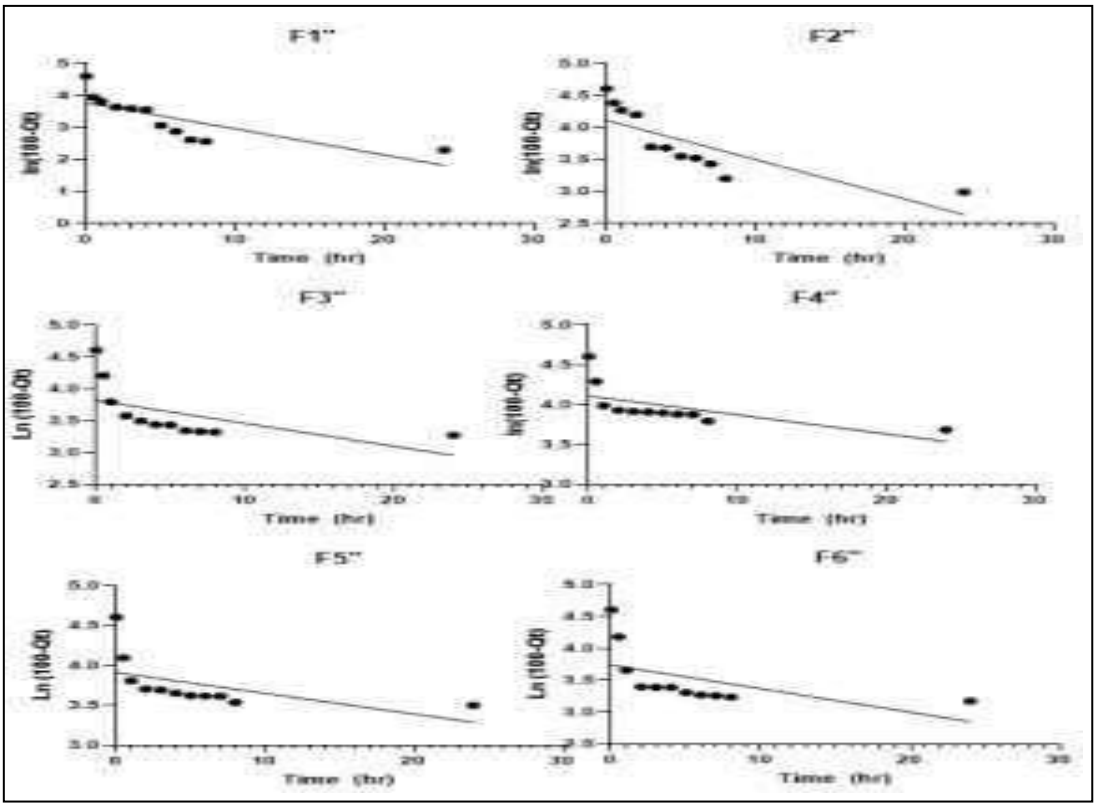

Figure 4.17First-Order Release Kinetics Of NHT From F1"–F6". The Plots Represent The Relationship Between Ln (100 − Qt) And Time (Hr.), Where Qt Means The Cumulative Percentage Of Drug Released At Time T. The Linear Regression Lines Indicate Concentration-Dependent Drug Release Behavior, And The Slope Resembles To The First-Order Release Rate Constant (K_1).

NHT first-order release profile was assessed by graphing ln (100 − Qt) against time (Figure 4.18). Good agreement with first-order kinetics which displays a robust linear relationship with little data point scatter during the time (R^2=0.750). It is evident from this behavior that the rate of NHT release is influenced by the amount of drug still in the system. Unlike the NPs-based formulations, no polymeric matrix or carrier was present to modulate drug diffusion, resulting in a rapid and predictable concentration-dependent release. The lack of diffusion barriers and the rapid release of the free drug are demonstrated by the strong linearity in the NHT profile.

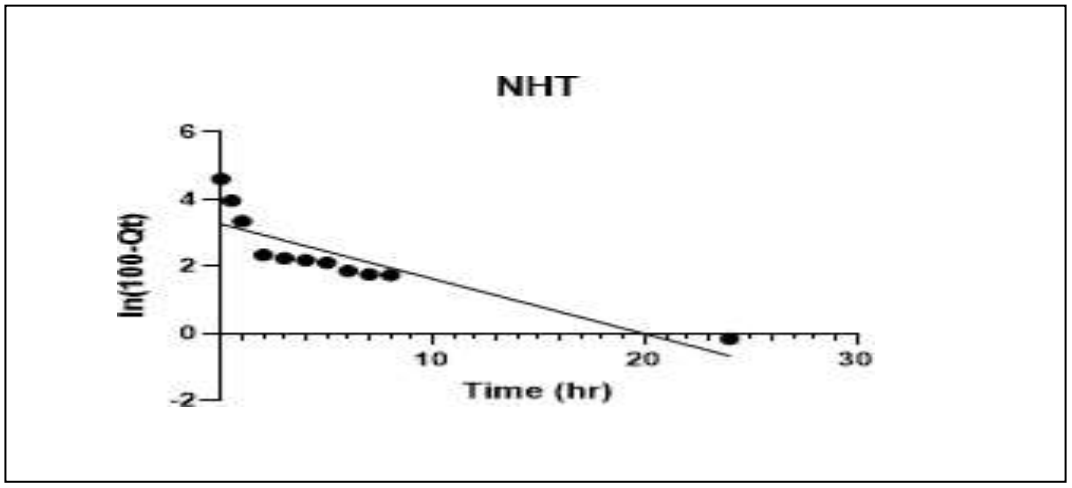

Figure 4.18First-Order Release Kinetics Of NHT. The Plot Represents Ln (100 − Qt) Versus Time (Hr.), Where Qt Is The Cumulative Percentage Of Drug Released At Time T. The Linear Regression Indicates Concentration-Dependent Release Behavior Characteristic Of Free Drug.

4.7.2 Higuchi Release Model

By graphing the cumulative drug release (Qt, %) against the square root of time (√t), the Higuchi release model was used to assess diffusion-controlled drug release from of NHT-loaded CS NPs (F1-F6) (Figure 4.19). The Higuchi plots demonstrated that the drug release was mostly controlled by diffusion via the NPs matrix, since all formulations followed a linear relationship. F2(R^2=0.884) and F4(R^2=0.906) adhered more closely to the Higuchi diffusion mechanism since they were the most linear and had the least amount of dispersion around the regression lines. On the other hand, at larger √t values, F1(R^2=0.710), F3(R^2=0.740), F5(R^2=0.739), and F6(R^2=0.832) displayed small deviations from linearity.

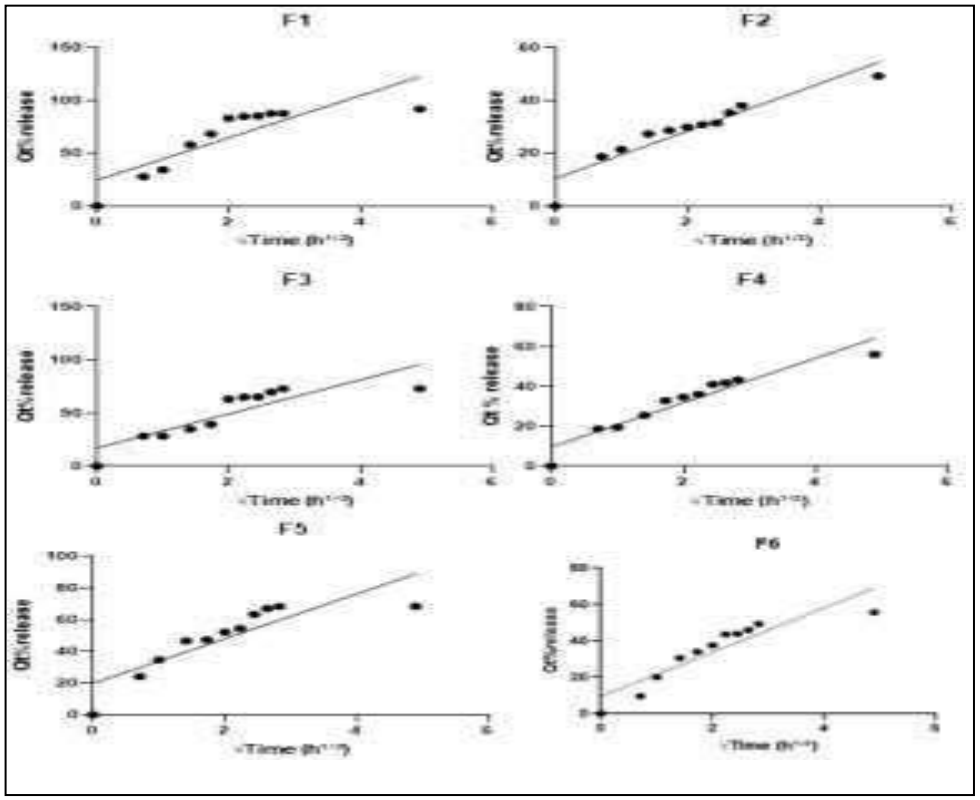

Figure 4.19Higuchi Release Model Plots Of NHT-Loaded CS Nps Formulations F1–F6. Cumulative Drug Release (Qt, %) Is Plotted Against The Square Root Of Time (√T, $H^{1/2}$).

NHT-loaded CS NPs (F1-F6) were compared with NHT-loaded BG-CS NPs (F1"-F6") to assess their Higuchi release profiles. This was done by graphing the cumulative drug release (Qt, %) versus the square root of time (√t) (Figure 4.20). F1" (R^2=0.695) and F2" (R^2=0.786) adhered more closely to the Higuchi diffusion mechanism since they were the most linear and had the least amount of dispersion around the regression lines. On the other hand, at larger √t values, F3" (R^2=0.553), F4" (R^2=0.954), F5" (R^2=0.507), and F6" (R^2=00.518) displayed small deviations from linearity.

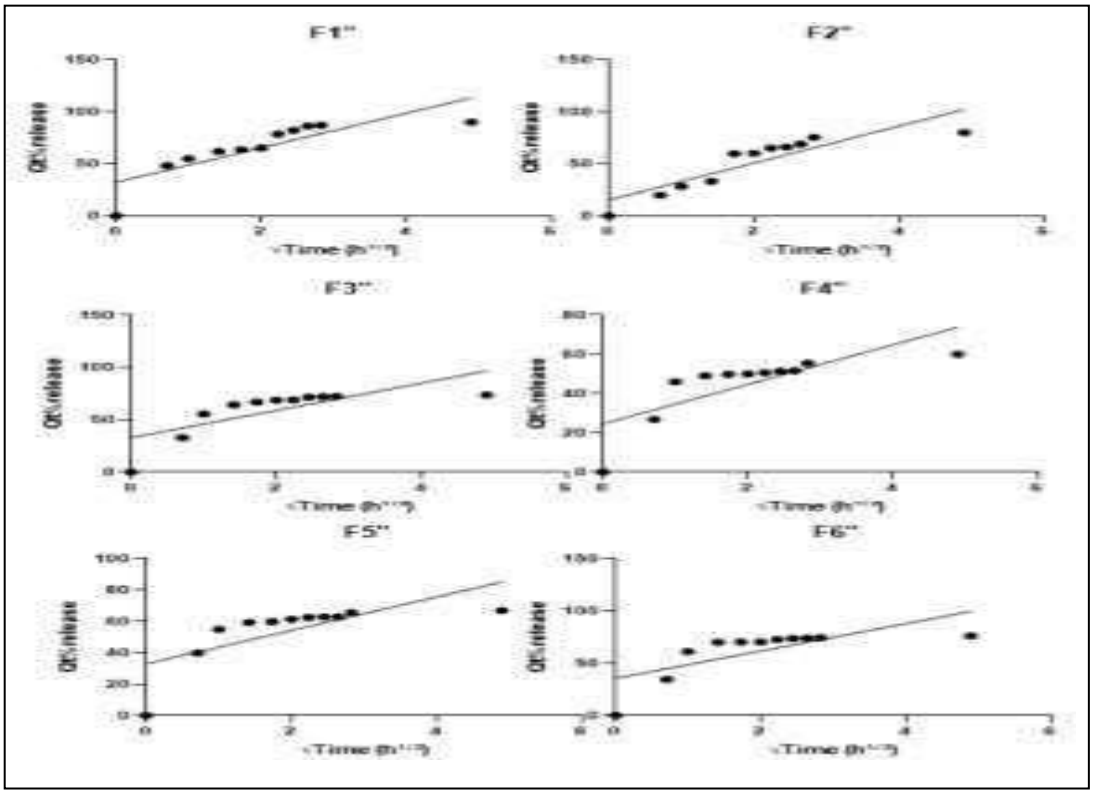

Figure 4.20Higuchi Release Model Plots Of NHT-Loaded BG-CS Nps F1"–F6". Cumulative Drug Release (Qt, %) Is Plotted Against The Square Root Of Time (√T, $H^{1/2}$).

Higuchi model was applied to NHT (Figure 4.21). The linear connection that NHT displayed (R2=0.548), intermediate for Higuchi model.

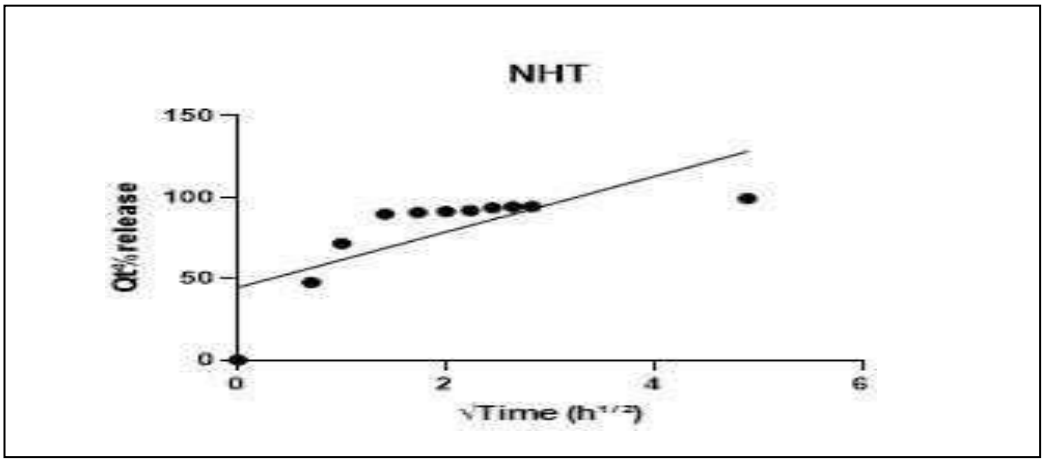

Figure 4.21Higuchi Release Model Of NHT. Cumulative Drug Release (Qt, %) Is Plotted Against The Square Root Of Time (√T, $H^{1/2}$).

4.7.3 Hixson–Crowell Release Model

Particle erosion and surface area changes were examined in relation to drug release from NHT-loaded CS NPs (F1-F6) using the Hixson-Crowell cube-root model $(100-Qt)^{1/3}$(Figure 4.22). The graphs demonstrated that the drug release was influenced by changes in particle size and surface area caused by the dissolution or erosion of the NPs matrix. All of the formulations followed a linear declining trend. A larger contribution of erosion-controlled release mechanisms was suggested by the improved linearity and reduced data dispersion around the regression lines in F2(R^2=0.703) and F4(R^2=0.722). On the other hand, F1(R^2=0.490), F3(R^2=0.476), F5(R^2=0.464), and F6(R^2=0.582) exhibited considerable non-linearities.

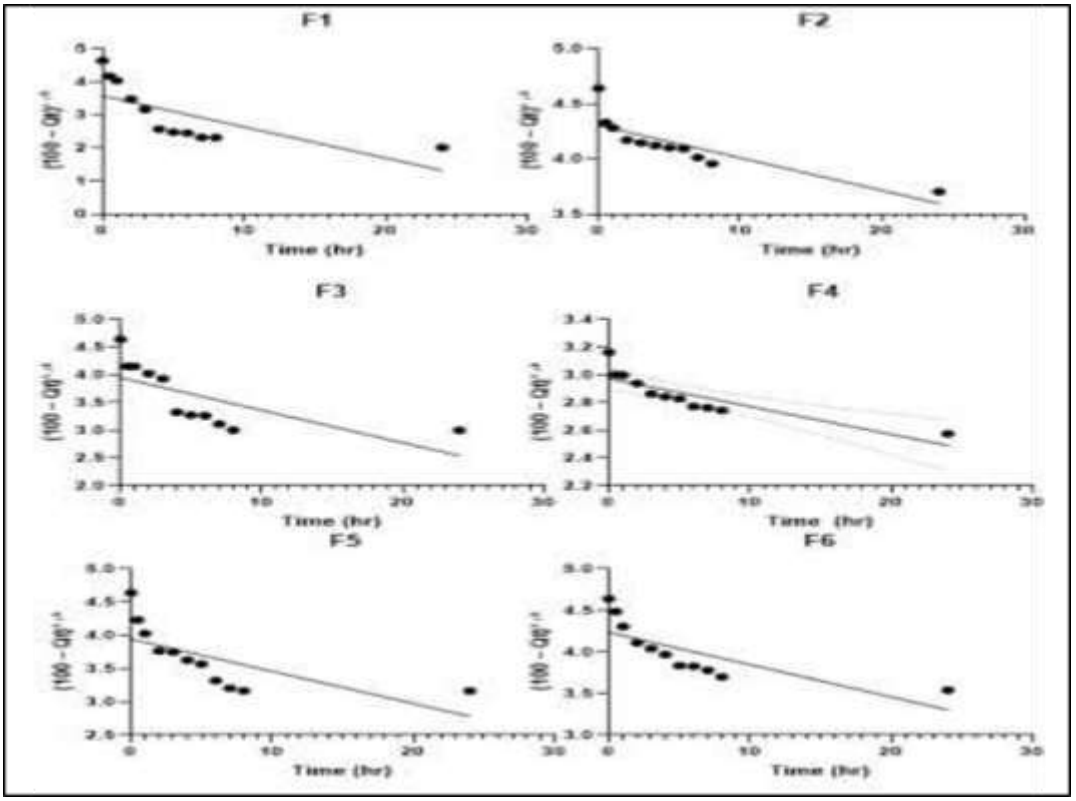

Figure 4.22Hixson–Crowell Cube-Root Model Plots Of NHT-Loaded CS Nps Formulations (F1–F6). The Cube Root Of The Remaining Drug ($100-Qt^{1/3}$) Is Plotted Against Time (Hr.)

NHT-loaded BG-CS NPs formulations (F1″-F6″) were subjected to the Hixson-Crowell cube-root model ($100-Qt^{1/3}$), which involved graphing the findings against time.

(F1″-F6″) demonstrated less data point scatter around the regression lines (Figure 4.23). F1" (R^2=0.532) and F2" (R^2=0.572), F3" (R^2=0.291), F4" (R^2=0.357), F5" (R^2=0.265), and F6" (R^2=0.266) showed small deviations from linearity.

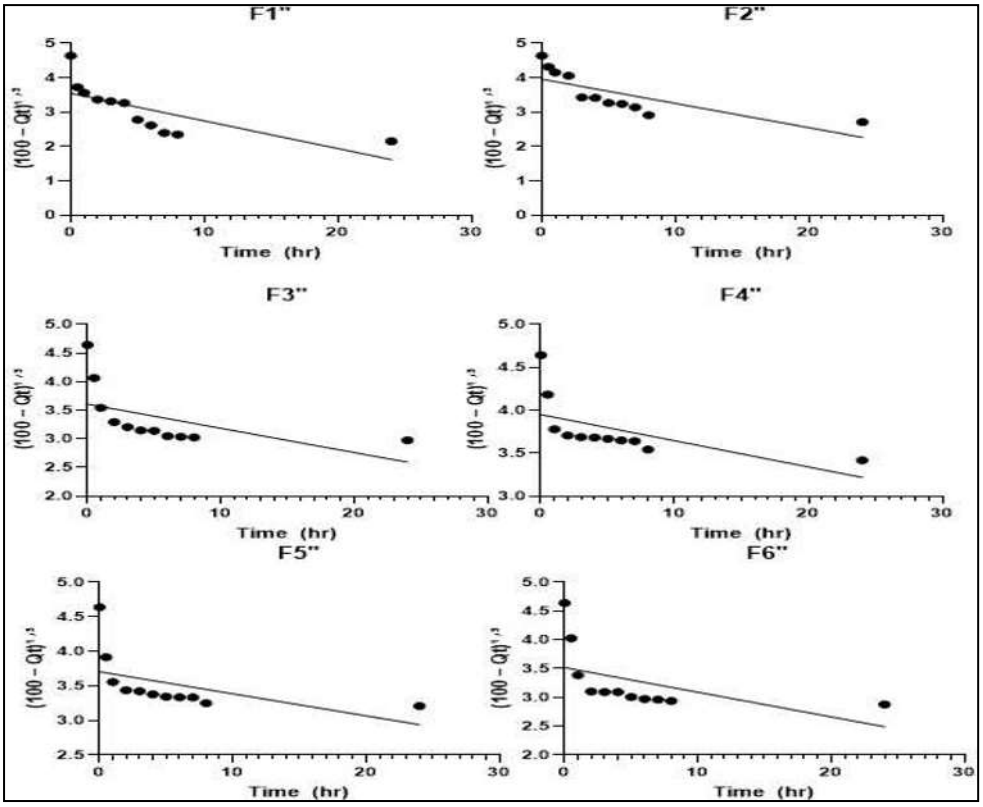

Figure 4.23Hixson–Crowell Cube-Root Model Plots Of NHT Release From NHT-Loaded BG-CS Nps Formulations (F1"–F6"). The Cube Root Of The Remaining Drug ($100\text{-}Qt^{1/3}$) Is Plotted Against Time (Hr.)

The Hixson-Crowell cube-root model was tested using NHT by plotting against time$(100\text{-}Qt)^{1/3}$(Figure 4.24). The resultant profile was not well-fit by the Hixson-Crowell model due to its poor linearity and apparent data dispersion (R^2=0.505).

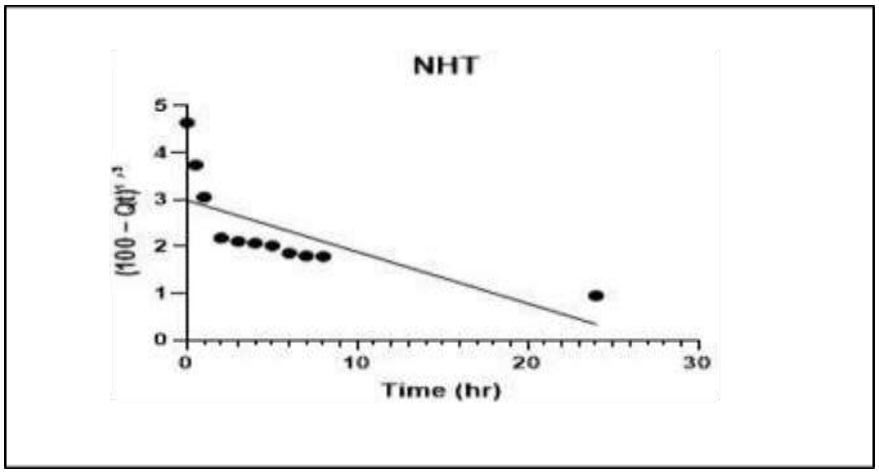

Figure 4.24Hixson–Crowell Cube Root Plot Of (NHT. The Plot Of (100-Qt1/3) Versus Time Hr.

4.7.4 Korsmeyer-Peppas Release Model

The drug-release mechanism of the NPs formulations was studied using the Korsmeyer-Peppas model, which involves graphing log (Mt/M∞) vs log(time) (Figure 4.25). NHT-loaded CS NPs (F1-F6) show linearity, which means the Korsmeyer-Peppas equation is a good fit for the release kinetics model. F1(R^2=0.941), F2(R^2=0.977), F3(R^2=0.869), F4(R^2=0.967), F5(R^2=0.952) and F6(R^2=0.874). The Korsmeyer-Peppasmodel is a good mechanistic tool for studying controlled drug release from NPs systems.

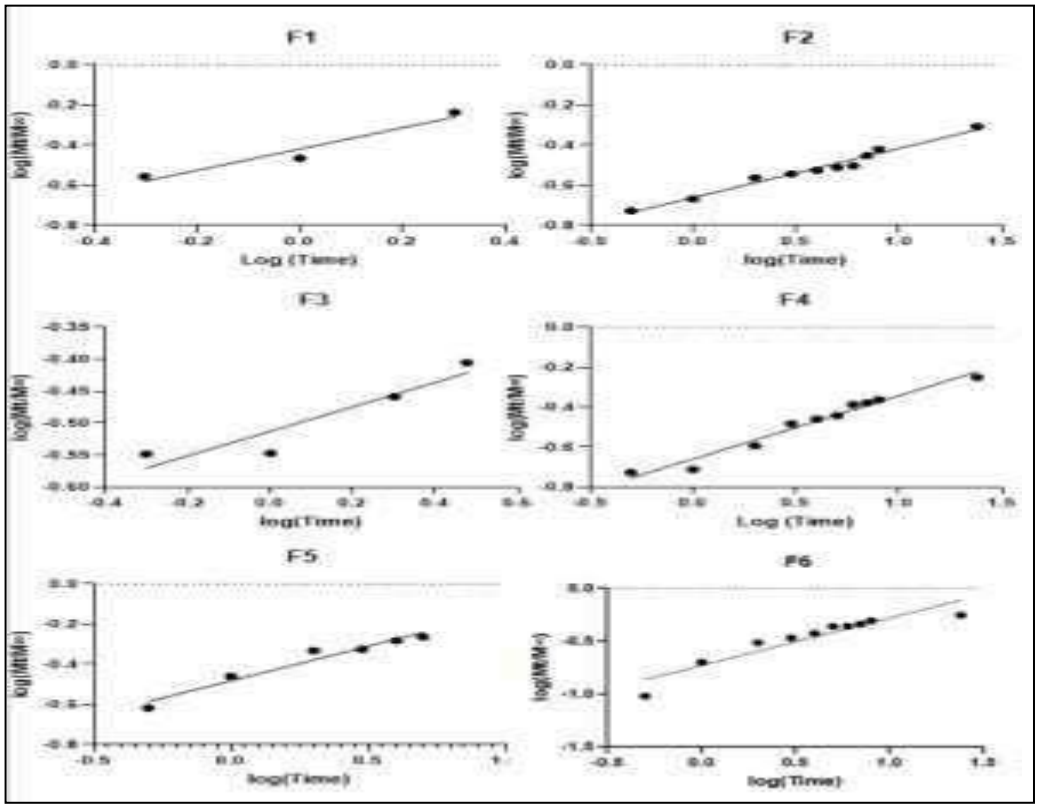

Figure 4.25Korsmeyer–Peppas Release Model Plots For Formulations F1–F6. Logarithmic Plots Of Log (Mt/M∞) Versus Log(Time).

By graphing log (Mt/M∞) with log(time) (Figure 4.26), the Korsmeyer-Peppas model was used to further understand the drug-release mechanism of the NHT-loaded BG-CS NPs formulations (F1" -F6″). The graphs confirmed that the Korsmeyer-Peppas equation adequately captures the release behavior. F1" (R^2=1.00), F2" (R^2=0.927), F3" (R^2=1.00), F4" (R^2=0.709), F5" (R^2=0.832) and F6" (R^2=1.00). The Korsmeyer-Peppas model for NHT determined not exhibit the model.

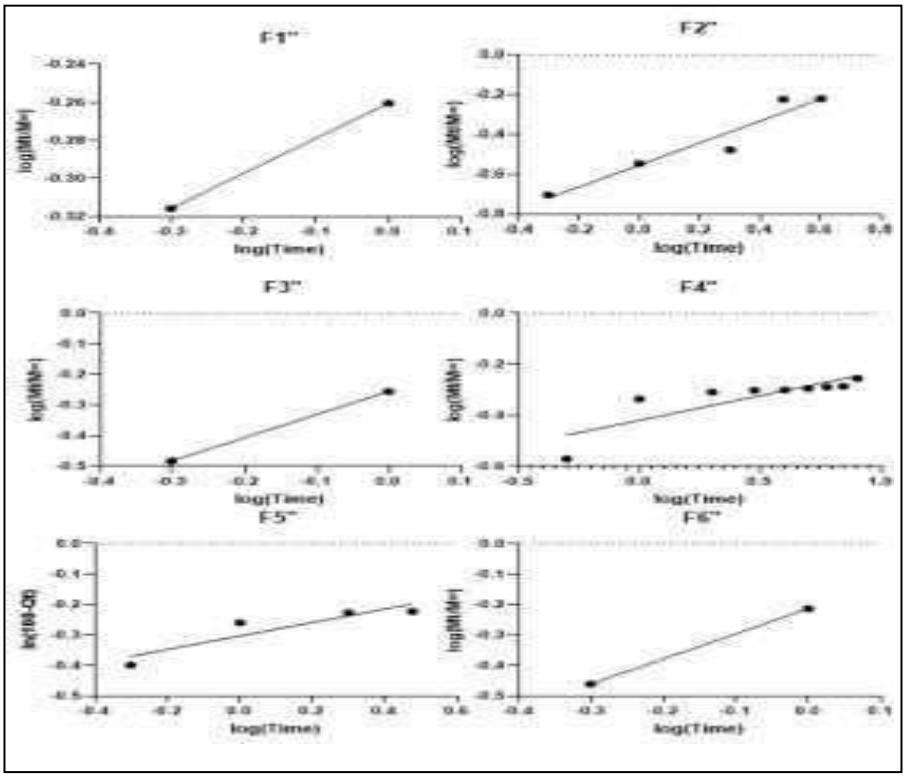

Figure 4.26Korsmeyer–Peppas Release Model Plots For Formulations F1"–F6". Logarithmic Plots Of Log (Mt/M∞) Versus Log(Time).

4.8 Stability Studies of CS and BG-CS NPs (Blank and NHT-loaded)

4.8.1 Stability Studies of CS NPs

Stability studies for blank CS and NHT-loaded CS NPs were performed at 5 ± 3°C and 25 ± 2°C with 60 ± 5% relative humidity (RH) over a period of 3 months (Table 4.10). At 25 ± 2 °C, the particle size of all formulations was evaluated over 90 days and compared with the corresponding blank CS (0.05%/0.1%). The blank NPs were used as a reference to distinguish changes caused by the NPs matrix from those potentially associated with nicotine loading, this comparison was intended to evaluate the influence of the encapsulated drug on particle size during storage under identical conditions. Blank CS (0.05%) showed a significant increase in particle size from 133.8 ± 4.4 nm (D0) to 168.2± 2.2 nm (D90) (****$p \leq 0.0001$). Compared with this blank, F1 particle size increased from 175.5 ± 2.4 nm to 185.2 ± 1.5 nm (****$p \leq 0.0001$), while F2 particle size increased from 138.5 ± 3.0 nm to 146.3 ± 3.7 nm (****$p \leq 0.0001$). F3 showed significantly larger particle sizes than blank CS (0.05%), with particle size increased from 223.7 ± 4.7 nm to 239.7 ± 3.4 nm (****$p \leq 0.0001$). Blank CS (0.1%) demonstrated relatively stable but larger particle sizes, increasing from 215.1 ± 5.2 nm to 224.1 ±

2.4 nm over 90 days (****$p \leq 0.0001$). Relative to this blank, F4 showed higher particle sizes, increasing from 269.7 ± 4.5 nm to 273.6 ± 4.2 nm (****$p \leq 0.0001$), while F5 increased from 275.2± 3.3 nm to 288.6 ± 4.6 nm (****$p \leq 0.0001$). F6 exhibited the largest particle size, increasing from 332.5 ± 4.3 nm to 337.5 ± 3.4 nm (****$p \leq 0.0001$). Overall, F2 showed particle size behavior most comparable to blank CS (0.05%), indicating superior physical stability, whereas F5 and F6 displayed the greatest size increases and comparatively lower stability. At 25 ± 2°C, the particle size of blank CS NPs (0.05%) increased significantly over the 90-day storage period, from 133.8 ± 4.4 nm at (D0) to 168.2 ± 2.2 nm at (D90) (****$p \leq 0.0001$). In contrast, blank CS NPs (0.1%) exhibited only a slight increase in particle size, from 215.1 ± 5.2 nm to 224.1 ± 2.4 nm, with no statistically significant difference ($p > 0.05$). Similarly, the nicotine-loaded formulations (F1–F6) showed only minor changes in particle size throughout the (D90) storage period. F1 increased from 175.5 ± 2.4 nm to 185.2 ± 1.5 nm, F2 from 138.5 ± 3.0 nm to 146.3 ± 3.7 nm, F3 from 223.7 ± 4.7 nm to 239.7 ± 3.4 nm, F4 from 269.7 ± 4.5 nm to 273.6 ± 4.2 nm, F5 from 275.2 ± 3.3 nm to 288.6 ± 4.6 nm, and F6 from 332.5 ± 4.3 nm to 337.5 ± 3.4 nm, with no statistically significant differences observed ($p > 0.05$). These findings indicate that all nicotine-loaded formulations remained physically stable during storage at 25 ± 2°C.

At 5 ± 3 °C (Table 4.10), blank CS (0.05%) showed a significant increase in particle size from 214.7 ± 2.3 nm (D0) to 221.2 ± 3.7 nm (D90) (****$p \leq 0.0001$). Compared with this blank, F1 exhibited larger particle sizes, remaining relatively stable from 244.6 ± 2.1 nm to 242.6 ± 2.2 nm (****$p \leq 0.0001$), whereas F2 increase from 337.6 ± 2.0 nm to 352.3 ± 4.2 nm (****$p \leq 0.0001$). F3 particle size increased from 342.8 ± 6.0 nm to 365.3 ± 2.4 nm (****$p \leq 0.0001$), blank CS (0.1%) particle size increased from 238.7 ± 5.8 nm to 243.9 ± 4.6 nm (****$p \leq 0.0001$). Relative to this blank, F4 showed consistently larger particle sizes, rising from 349.7 ± 4.6 nm to 355.5 ± 3.7 nm (****$p \leq 0.0001$), while F5 particle size increased from 351.9 ± 5.6 nm to 370.3 ± 5.5 nm (****$p \leq 0.0001$). F6 exhibited the largest particle size, increasing from 381.5 ± 3.4 nm to 405.1 ± 2.4 nm (****$p \leq 0.0001$). F6 and F5 showing the greatest size and lowest physical stability. At 5 ± 3°C, all formulations maintained good physical stability throughout the (D90) storage period. The particle size of blank CS (0.05%) increased slightly from 214.7 ± 2.3 nm at (D0) to 221.2 ± 3.7 nm at (D90), while blank CS (0.1%) showed a minor increase from 238.7 ± 5.8 nm to 243.9 ± 4.6 nm. Similarly, the NHT-loaded formulations exhibited only slight changes in particle size over the storage

period: F1 changed from 244.6 ± 2.1 nm to 242.6 ± 2.2 nm, F2 from 337.6 ± 2.0 nm to 352.3 ± 4.2 nm, F3 from 342.8 ± 6.0 nm to 365.3 ± 2.4 nm, F4 from 349.7 ± 4.6 nm to 355.5 ± 3.7 nm, F5 from 351.9 ± 5.6 nm to 370.3 ± 5.5 nm, and F6 from 381.5 ± 3.4 nm to 405.1 ± 2.4 nm. No statistically significant differences were observed between (D0) and (D90) ($p > 0.05$).

Since the stability assessment was conducted using a freshly manufactured separate batch measured expressly for the stability experiment, the particle size values given in the study deviate slightly from those in the first characterization. NPs systems generated by ionic gelation are likely to exhibit small batch-to-batch changes and may require re-measurement using a distinct preparation. However, the physicochemical properties and starting particle sizes were staying within the nanometer range. Therefore, these small differences are not expected to affect the interpretation of the stability results or the overall conclusions of the study.

Table 4.10
Average Particle Size Of Blank CS And NHT CS Nps At 25 ± 2ºC And 5 ± 3ºC (N=3)

	Particle size of CS NPs at 25 ± 2ºC							Particle size of CS NPs at 5 ± 3ºC						
	D0	D2	D5	D14	D30	D60	D90	D0	D2	D5	D14	D30	D60	D90
Blank CS (0.05%)	133.8 ± 4.4	139.9 ± 3.2	145.9 ± 3.4	158.2 ± 2.7	165.4 ± 3.5	169.8 ± 4.3	168.2 ± 2.2	214.7 ± 2.3	212.3 ± 4.4	213.3 ± 2.2	214.8 ± 1.3	218.5 ± 3.5	225.3 ± 2.6	221.2 ± 3.7
Blank CS (0.1%)	215.1 ± 5.2	218.2 ± 5.4	216.5 ± 2.1	219.7 ± 3.7	222.9 ± 4.7	226.4 ± 3.6	224.1 ± 2.4	238.7 ± 5.8	238.5 ± 3.6	239.3 ± 4.8	239.9 ± 3.6	244.0 ± 2.7	246.5 ± 3.9	243.9 ± 4.6
F1	175.5 ± 2.4	180.1 ± 3.4	176.7 ± 2.3	182.6 ± 2.9	183.8 ± 4.1	185.8 ± 2.5	185.2 ± 1.5	244.6 ± 2.1	243.5 ± 4.6	246.5 ± 2.0	243.6 ± 1.1	241.5 ± 4.5	240.3 ± 3.3	242.6 ± 2.2
F2	138.5 ± 3.0	138.9 ± 4.6	139.8 ± 3.1	142.5 ± 5.6	144.9 ± 3.4	148.2 ± 2.9	146.3 ± 3.7	337.6 ± 2.0	335.9 ± 4.9	338.4 ± 5.0	345.6 ± 3.1	349.9 ± 4.2	356.2 ± 3.3	352.3 ± 4.2
F3	223.7 ± 4.7	221.5 ± 2.5	226.9 ± 3.4	231.1 ± 2.2	235.7 ± 4.6	238.4 ± 2.3	239.7 ± 3.4	342.8 ± 6.0	346.9 ± 4.1	348.1 ± 4.8	356.2 ± 2.4	361.4 ± 6.3	363.4 ± 3.4	365.3 ± 2.4
F4	269.7 ± 4.5	265.2 ± 3.3	268.2 ± 6.6	269.9 ± 3.7	272.2 ± 2.9	275.8 ± 3.7	273.6 ± 4.2	349.7 ± 4.6	348.2 ± 2.4	346.5 ± 4.3	348.1 ± 3.5	351.6 ± 4.2	356.2 ± 2.1	355.5 ± 3.7
F5	275.2 ± 3.3	274.8 ± 4.2	275.9 ± 3.1	279.2 ± 1.1	284.6 ± 3.4	286.1 ± 4.7	288.6 ± 4.6	351.9 ± 5.6	348.2 ± 5.3	353.6 ± 2.9	357.3 ± 6.2	364.2 ± 4.1	371.4 ± 3.8	370.3 ± 5.5

Particle size of CS NPs at 25 ± 2ºC								Particle size of CS NPs at 5 ± 3ºC					
F6	332.5 ± 4.3	333.1 ± 3.7	333.6 ± 2.6	335.8 ± 1.4	338.9 ± 3.2	342.8 ± 2.1	337.5 ± 3.4	381.5 ± 3.4	383.2 ± 4.2	382.1 ± 1.2	385.6 ± 3.4	392.2 ± 5.0	403.1 ± 3.2	405.1 ± 2.4
D(Day)														

The zeta potential stability of all formulations was monitored over 90 days at 25 ± 2 °C and 5 ± 3 °C. At 25 °C (Table 4.11), Blank CS (0.05%) showed a significant decrease in zeta potential from 50.2 ± 1.0 +mV (D0) to +42.6 ± 3.4 +mV (D90) (****$p \leq 0.0001$). Compared with this blank, F1 exhibited a slight increase in zeta potential from +33.4 ± 1.6 +mV to +37.4 ± 4.5 +mV (**$p \leq 0.05$), while F3 showed mino fluctuations with an overall stable trend +24.5 ± 1.2 to +25.8 ± 4.8 +mV (**$p \leq 0.01$). In contrast, F5 presented lower absolute zeta potential values and a significant reduction from +24.0 ± 1.8 +mV to +22.6 ± 2.3 +mV (**$p \leq 0.001$). Blank CS (0.1%) decreased from +51.7 ± 2.2 mV to +47.6 ± 3.8 mV over the same period (****$p \leq 0.0001$). Relative to this blank, F2 remained the most stable, showing minimal change from +34.8 ± 2.1 +mV to +34.9 ± 2.5 +mV, but non-significant to blank CS (0.1%). F4 exhibited a slight decrease from +26.3 ± 1.4 +mV to +25.7 ± 3.2 +mV (**$p \leq 0.05$), whereas F6 showed the lowest zeta potential from +18.2 ± 2.4 +mV to +16.7 ± 3.1 +mV (****$p \leq 0.0001$). At 25 ± 2°C, the zeta potential of blank CS NPs (0.05%) decreased significantly during the (D90) storage period, from 50.2 ± 1.0 +mV at (D0) to 42.6 ± 3.4 +mV at (D90) (****$p \leq 0.0001$). In contrast, blank CS NPs (0.1%) showed a slight decrease from 51.7 ± 2.2 +mV to 47.6 ± 3.8 +mV, which was not statistically significant ($p > 0.05$). Likewise, all NHT-loaded formulations (F1–F6) exhibited only minor fluctuations in zeta potential throughout storage. F1 changed from +33.4 ± 1.6 mV to +37.4 ± 4.5 +mV, F2 from +34.8 ± 2.1 +mV to +34.9 ± 2.5 +mV, F3 from +24.5 ± 1.2 +mV to +25.8 ± 4.8 +mV, F4 from +26.3 ± 1.4 +mV to +25.7 ± 3.2 +mV, F5 from +24.0 ± 1.8 +mV to +22.6 ± 2.3 +mV, and F6 from +18.2 ± 2.4 mV to +16.7 ± 3.1 +mV, with no statistically significant differences observed between (D0) and (D90) ($p > 0.05$). These findings indicate that the surface charge of the NHT-loaded NPs remained stable during storage at 25 ± 2°C.

At 5 ± 3 °C (Table 4.8, Figure 4.42), the zeta potential of all formulations was compared with blank CS (0.05%/0.1%) over 90 days. Blank CS (0.05%) showed minimal variation, decreasing slightly from +36.5 ± 0.9 +mV (D0) to +35.8 ± 2.4 +mV (D90) (**$p \leq 0.05$). Compared with this blank, F1 exhibited significantly lower zeta potential,

decreasing from +28.6 ± 1.9 +mV to +27.4 ± 2.9 +mV (**p ≤ 0.01), while F3 decreased from +24.6 ± 4.6 +mV to +21.2 ± 2.1 +mV (**p ≤ 0.001). F5 also showed lower zeta potential compared with blank CS (0.05%), decreasing from +24.1 ± 0.5 +mV to +22.1 ± 3.3 +mV (**p ≤ 0.001), indicating reduced electrostatic stability. Blank CS (0.1%) exhibited significant decrease from +38.1 ± 1.1 +mV to +36.3 ± 3.2 +mV over 90 days (**p ≤ 0.05). Relative to this blank, F2 showed more reduction in zeta potential, decreasing from +30.9 ± 1.6 +mV to +26.9 ± 3.3 +mV (**p ≤ 0.001), while F4 decreased from +26.1 ± 1.2 +mV to +24.4 ± 2.1 +mV (**p ≤ 0.01). F6 exhibited the lowest zeta potential among all formulations, decreasing from +21.6 ± 1.3 +mV to +18.8 ± 1.3 +mV (****p ≤ 0.0001). At 5 ± 3°C, the zeta potential of both blank and NHT-loaded CS NPs remained stable throughout the 90-day storage period. Blank CS (0.05%) showed a slight decrease in zeta potential from +36.5 ± 0.9 +mV at (D0) to +35.8 ± 2.4 +mV at (D90), while blank CS (0.1%) decreased marginally from +38.1 ± 1.1 +mV to +36.3 ± 3.2 +mV. Similarly, the NHT-loaded formulations exhibited only minor fluctuations during storage: F1 changed from +28.6 ± 1.9 +mV to +27.4 ± 2.9 +mV, F2 from +30.9 ± 1.6 +mV to +26.9 ± 3.3 +mV, F3 from +24.6 ± 4.6 +mV to +21.2 ± 2.1 +mV, F4 from + 26.1 ± 1.2 +mV to +24.4 ± 2.1 +mV, F5 from +24.1 ± 0.5 +mV to +22.1 ± 3.3 +mV, and F6 from +21.6 ± 1.3 +mV to +18.8 ± 1.3 +mV (p > 0.05), indicating that refrigerated storage effectively maintained the surface charge stability of both blank and NHT -loaded CS NPs over the study period.

Table 4.11
Zeta Potential Of Blank CS And NHT CS Nps At 25 ± 2ºC And 5 ± 3ºC (N=3).

	Zeta potential of CS NPs at 25 ± 2ºC							Zeta potential of CS NPs at 5 ± 3ºC						
	D0	D2	D5	D14	D30	D60	D90	D0	D2	D5	D14	D30	D60	D90
Blank CS (0.05%)	+50.2 ±1.0	+48.6 ±1.3	+48.2 ±2.1	+46.9 ±1.1	+46.6 ±3.6	+43.8 ± 1.8	+42.6 3.4	±+36.5 ±0.9	+36.2 ±1.8	+36.5 ±2.6	+36.9 ±1.0	+36.0 ±3.1	+35.6 ±2.0	+35.8 ±2.4
Blank CS (0.1%)	+51.7 ±2.2	+53.9 ±3.7	+52.7 ±1.0	+51.1 ±3.0	+48.7 ±1.0	+44.2 ± 2.6	+47.6 3.8	±+38.1 ±1.1	+37.6 ±2.1	+37.4 ±1.0	+37.9 ±1.2	+37.1 ±2.4	+35.4 ±1.0	+36.3 ±3.2
F1	+33.4 ±1.6	+33.2 ±1.1	+34.2 ±2.6	+37.2 ±3.1	+39.5 ±3.5	+36.3 ± 2.6	+37.4 4.5	±+28.6 ±1.9	+28.9 ±3.7	+29.4 ±2.0	+29.1 ±1.3	+28.7 ±3.5	+26.1 ±2.1	+27.4 ±2.9

Zeta potential of CS NPs at 25 ± 2ºC								Zeta potential of CS NPs at 5 ± 3ºC						
F2	+34.8 ±2.1	+35.0 ±1.1	+35.8 ±1.0	+35.2 ±3.1	+34.5 ±1.8	+32.8 ± 3.4	+34.9 2.5	±+30.9 ±1.6	+31.5 ±2.0	+30.3 ±3.2	+29.9 ±3.7	+28.6 ±2.7	+26.0 ±1.0	+26.9 ±3.3
F3	+24.5 ±1.2	+24.9 ±3.1	+24.5 ±1.0	+25.8 ±3.1	+25.3 ±3.7	+25.9 ± 2.9	+25.8 4.8	±+24.6 ±4.6	+23.7 ±2.0	+23.2 ±3.4	+23.5 ±1.0	+22.7 ±2.1	+20.1 ±3.1	+21.2 ±2.1
F4	+26.3 ±1.4	+27.0 ±3.7	+27.8 ±2.4	+26.0 ±2.8	+25.4 ±4.7	+26.0 ± 1.0	+25.7 3.2	±+26.1 ±1.2	+25.7 ±2.4	+25.3 ±3.3	+26.9 ±1.0	+25.0 ±2.5	+22.5 ±3.0	+24.4 ±2.1
F5	+24.0 ±1.8	+24.0 ±2.8	+24.5 ±2.6	+24.0 ±1.1	+23.8 ±2.3	+21.1 ± 3.1	+22.6 2.3	±+24.1 ±0.5	+25.4 ±1.0	+25.7 ±3.1	+24.5 ±3.0	+23.4 ±2.0	+22.4 ±1.0	+22.1 ±3.3
F6	+18.2 ±2.4	+18.6 ±2.1	+18.4 ±1.0	+17.9 ±2.0	+18.2 ±3.2	+14.8 ± 1.0	+16.7 3.1	±+21.6 ±1.3	+20.6 ±0.9	+20.2 ±1.0	+19.6 ±1.1	+18.0 ±2.1	+17.2 ±2.0	+18.8 ±1.3

PDI for blank CS and NHT-loaded CS NPs were performed at 5 ± 3°C and 25 ± 2°C (Table 4.12). At 25 °C, blank CS (0.05%) PDI increased from 0.324 (D0) to 0.423 (D90), with a transient increase observed at D60 (0.514), indicating temporary heterogeneity. Blank CS (0.1%) exhibited a similar variable trend, increasing from 0.288 (D0) to 0.328 (D90). F1 demonstrated acceptable andimproving homogeneity, with PDI decreasing from 0.339 (D0) to 0.298 (D90) and reaching a minimum of 0.111 at D30. F2 and F6 maintained comparatively lower andmore consistent PDI values at D90 0.212 and 0.320 respectively, whereas F3 and F5 showed higher PDI values, reaching 0.395 and 0.384 at D90 respectively. F4 exhibited moderate variability, with PDI values generally between 0.164 and 0.330

At 5 ± 3 °C, all formulations generally exhibited higher PDI values compared with room temperature, suggesting increased aggregation. Blank CS (0.05%) showed a reduction from 0.457 (D0) to 0.212 (D90), while Blank CS (0.1%) decreased from 0.323 to 0.145, indicating improved dispersion uniformity at later time points. Although PDI decreased during storage reduction in zeta potential suggests that the lower PDI values do not necessarily indicate improved colloidal stability, but rather reflect narrower partic le size distribution. F1 also showed narrower particle size distribution, with PDI decreasing from 0.406 to 0.211. In contrast, NHT-loaded formulations such as F3 and F5 displayed high PDI values: 0.521 and 0.450 at D90 respectively. However, Blank CS form ulations and F2 demonstrated more stable particle size distributions, while F3, F5, and F6

showed greater heterogeneity, particularly under refrigerated storage. F4 and F6 showed intermediate PDI, with values at D90 of 0.454 and 0.411, respectively.

Table 4.12
PDI Of Blank CS And NHT CS Nps At 25 ± 2ºC And 5 ± 3ºC (N=3).

	Polydispersity index of CS NPs at 25 ± 2ºC							Polydispersity index of CS NPs at 5 ± 3ºC						
	D0	D2	D5	D14	D30	D60	D90	D0	D2	D5	D14	D30	D60	D90
Blank CS (0.05%)	0.324	0.399	0.277	0.244	0.286	0.514	0.423	0.457	0.343	0.221	0.442	0.351	0.242	0.212
Blank CS (0.1%)	0.288	0.423	0.341	0.435	0.484	0.217	0.328	0.323	0.432	0.311	0.251	0.142	0.149	0.145
F1	0.339	0.222	0.341	0.416	0.111	0.257	0.298	0.406	0.231	0.342	0.221	0.326	0.235	0.211
F2	0.323	0.444	0.121	0.322	0.321	0.222	0.212	0.376	0.265	0.258	0.467	0.346	0.257	0.291
F3	0.425	0.411	0.436	0.246	0.385	0.473	0.395	0.455	0.436	0.421	0.456	0.447	0.412	0.521
F4	0.330	0.164	0.178	0.246	0.324	0.198	0.295	0.344	0.451	0.446	0.432	0.497	0.426	0.454
F5	0.448	0.149	0.217	0.359	0.415	0.322	0.384	0.425	0.459	0.413	0.327	0.417	0.482	0.450
F6	0.408	0.167	0.233	0.122	0.346	0.223	0.320	0.436	0.417	0.328	0.311	0.473	0.327	0.411

4.8.2 Stability Studies of BG-CS NPs

Stability studies for blank BG-CS and NHT-loaded BG-CS NPs were conducted at 5 ± 3 ºC and 25 ± 2 ºC at 60 ± 5% relative humidity (RH) for a period of 3 months. The physicochemical characteristics of the NPs (size, zeta potential, and PDI) are shown in (Tables 4.13, 4.14, and 4.15). All evaluated formulations exhibited short term stability during the initial storage period, with particle size and zeta potential staying predominantly unaltered through day 1 and, in certain instances, extending to day 5. At 25 °C (Table 4.13), blank CS (0.05%) showed an average particle size increased from

72.4 ± 2.4 nm at D0 to 153.8 ± 5.05 nm at D90, while blank BG-CS (0.1%) showed an average particle size increased from 86.6 ± 0.9 nm to 109.6 ± 2.7 nm over the same period. Statistical analysis indicated that most of these changes were not statistically significant ($p > 0.05$), particularly during the early and intermediate storage periods. F1″ exhibited an increase in particle size from 64.3 ± 0.7nm at D0 to 1221± 1.8 nm at D90, and this change remained non-significantly different from the blank ($p > 0.05$). Similarly, F6″ showed a limited increase of the average particle size from 90.7 ± 0.7 nm to 109.7 ± 2.1 nm, with no statistically significant difference ($p > 0.05$). F3″ demonstrated an increased in particle size from 82.9 ± 5.2 nm at D0 to 289.8 ± 6.7 nm at D90, while F5″ increased from 127.1 ± 1.1 nm to 186.8 ± 6.7 nm. These increases were statistically significant compared with the blank (****$p \leq 0.0001$), indicating particle aggregation during prolonged storage. F2″ and F4″ showed intermediate behavior, increasing from 86.0 ± 1.2 nm to 180.8 ± 10.8 nm and from 80.5 ± 1.2 nm to 144.2 ± 5.8 nm respectively. These changes were mostly non-significant at early stages, but showed a tendency toward increased particle size at extended storage times. At 25 ± 2°C, the particle size of the blank BG-CS NPs showed a significant increase during the 90-day storage period ($p < 0.05$). Blank BG-CS (0.05%) increased from 72.4 ± 2.4 nm at D0 to 153.8 ± 5.0 nm at D90, while blank BG-CS (0.1%) increased from 86.6 ± 0.9 nm to 109.6 ± 2.7 nm. In distinction, all NHT-loaded modified formulations (F1″–F6″) exhibited only minor fluctuations in particle size throughout the study period, with no statistically significant differences between D0 and D90 ($p > 0.05$). These findings indicate that nicotine loading enhanced the physical stability of the modified CS NPs. At 5 ± 3 °C (Table 4.13), blank BG-CS (0.05%) showed an increase in particle size from 76.7 ± 0.8 nm at D0 to 152.6 ± 1.2 nm at D90, while blank BG-CS (0.1%) increased from 87.06 ± 1.8 nm to 106.9 ± 6.6 nm over the same period. According to the statistical analysis, these changes were mostly non-significant ($p > 0.05$). F1″ average particle size increased from 70.4 ± 0.6 nm at D0 to 274.2 ± 1.9 nm at D90, showing a statistically significant difference at the later storage time points (****$p \leq 0.0001$), which suggests particle growth during prolonged refrigerated storage. Similarly, F2″ average particle size increased from 92.5 ± 3.4 nm to 196.4 ± 2.9 nm, and this increase was also statistically significant compared to the blank CS NPs (****$p \leq 0.0001$). A marked increase was observed for F3″, where particle size increased from 115.9 ± 1.8 nm at D0 to 380.9 ± 7.1 nm at D90, representing the largest size growth among all formulations anda highly significant difference (****$p \leq 0.0001$), indicating substantial

particle aggregation. F4″ exhibited increasing in average particle size from 99.6 ± 3.8 nm to 168.5 ± 6.7 nm ($p > 0.05$). F5″ average particle size increased from 168.3 ± 1.1 nm at D0 to 336.3 ± 7.7 nm at D90(****$p \leq 0.0001$). F6″ showed increase in particle size from 105.6 ± 1.6 nm at D0 to 136.2 ± 3.1 nm at D90. F6″ showed no statistically significant difference in particle size increment during the early storage period of 1 day to 2 weeks ($p > 0.05$). However, a statistically significant increase in particle size was observed at the later storage times from 1–3 months (****$p \leq 0.0001$). NHT -loaded modified formulations (F1″–F6″) exhibited only minor fluctuations in particle size throughout thestorage period, with no statistically significant differences between D0 and D90 ($p > 0.05$). These findings demonstrate that nicotine loading contributed to maintaining the physical stability of the modified CS NPs during storage at 5 ± 3°C

Table 4.13
Average Particle Size Of Blank BG-CS And NHT-Loaded BG-CS Nps At 25 ± 2 ºC And 5
± 3 ºC (N = 3).

	Particle size of BG-CS NPs at 25 ± 2ºC							Particle size of BG-CS NPs at 5 ± 3ºC						
	D0	D2	D5	D14	D30	D60	D90	D0	D2	D5	D14	D30	D60	D90
Blank BG-CS (0.05%)	72.4 ± 2.4	74.9 ± 0.3	89.1 ± 1.9	101.9 ± 2.9	126.2 ± 5.5	152.1 ± 1.8	153.8 ± 5.05	76.7 ± 0.8	86.4 ± 1.6	89.6 ± 1.1	105.9 ± 4.3	138.9 ± 5.3	151.6 ± 2.6	152.6 ± 1.2
Blank BG-CS (0.1%)	86.6± 0.9	87.4± 0.8	89.2± 0.9	92.8 ± 1.9	89.4± 2.1	95.4 ± 4.6	109.6 ± 2.7	87.06± 1.8	89.6± 2.1	90.2± 0.2	92.6± 1.5	95.1± 4.3	99.9± 3.0	106.9 ± 6.6
F1”	64.3± 0.7	77.4± 2.3	76.1± 2.9	98.4 ± 4.0	103.8± 5.4	122.3± 1.1	122.1 ± 1.8	70.4 ± 0.6	74.8 ± 2.1	81.6 ± 0.7	102.6± 5.6	112.1± 2.2	144.4± 8.3	274.2 ± 1.9
F2”	86.0± 1.2	87.5± 1.2	88.4± 0.4	102.2± 5.8	138.5± 7.2	165.7± 2.7	180.8 ± 10.8	92.5 ± 3.4	95.9 ± 2.2	94.1 ± 1.9	114.1± 2.8	167.9± 4.7	166.8± 7.1	196.4 ± 2.9

F3”	82.9± 5.2	100 ± 0.6	122 ± 3.7	114.4± 2.1	121.2± 2.5	265.8± 7.6	289.8 ± 6.7	115.9± 1.8	120.5± 0.8	219.6± 5.1	226.7± 2.7	238.4± 3.4	273 ± 8.8	380.9 ± 7.1
F4”	80.5± 1.2	85.3± 0.5	87.5± 0.5	81.8 ± 0.6	93.4± 1.8	92.2 ± 3.1	144.2 ± 5.8	99.6 ± 3.8	93.2 ± 3.4	96.7 ± 4.8	112.7± 1.4	107.8± 4.7	95.2± 2.8	168.5 ± 6.7
F5”	127.1 ±1.1	137.8 ±2.9	159.2± 9.7	156.6±1 .2	161.7± 5.6	179.1± 8.4	186.8 ±6.7	168.3±1. 1	169.5± 2.1	182.2± 1.9	195.8± 1.6	202.2±1 .6	255.9± 3.9	336.3 ±7.7
F6”	90.7± 0.7	95.9± 1.6	95.5± 0.4	99.5 ± 1.6	100.9± 0.8	101.5± 1.0	109.7 ± 2.1	105.6± 1.6	105.3± 0.8	104.7± 0.3	109.5± 1.5	113.5± 3.8	125.3± 3.1	136.2 ± 3.1

At 25 ± 2 °C (Table 4.14), blank BG-CS (0.05%) showed a decrease in zeta potential from +37.7 ± 0.9 +mV at D0 to +23.6 ± 0.9 +mV at D90. F1″ exhibited decreasing zeta potential from +33.3 ± 1.4 +mV to +23.6 ± 2.7 +mV ($p > 0.05$). F3″ showed slightly lower zeta potential values from +28.7 ± 0.3 +mV at D0 to +27.9 ± 2.4 +mV at D90 ($p > 0.05$). F5″ demonstrated higher reduction in zeta potential from +25.2 ± 0.1 +mV to +14.9 ± 2.1 +mV, with statistically significant differences compared with blank BG-CS (0.05%) at the later storage times (**$p \leq 0.01$, ****$p \leq 0.0001$), indicating reduced electrostatic stability. For blank BG-CS (0.1%), the zeta potential decreased from +35.6 ±0.9 +mV at D0 to +21.3 ± 1.3 +mV at D90. F2″ showed a decreased in zeta potential from +30.7 ± 3.0 +mV to +24.6 ± 0.4 +mV ($p > 0.05$). F4″ exhibited a larger decreased in zeta potential from +26.2 ± 0.1 +mV to +17.8 ± 1.4 +mV, where significant differences (****$p \leq 0.0001$) was observed. F6″ zeta potential decreased from +27.0 ± 6.0 +mV at D0 to +20.1 ± 4.7 +mV at D90. (**$p \leq 0.01$, ***$p \leq 0.001$, ****$p \leq 0.0001$). The zeta potential of the blank BG-CS formulations (0.05% and 0.1%) showed a significant reduction during the 90-day storage period ($p < 0.05$). In contrast, the NHT-loaded formulations generally maintained their surface charge, with F1″, F2″, F4″, F5″, and F6″ showing no statistically significant changes ($p > 0.05$). Only F3″ exhibited a significant decrease in zeta potential over the storage period ($p < 0.05$).

Table 4.14
Zeta Potential Of Blank BG-CS And NHT-Loaded BG-CS At 25 ± 2 ºC And 5 ± 3 ºC (N = 3).

	Zeta potential of BG-CS NPs at 25 ± 2ºC							Zeta potential of BG-CS NPs at 5 ± 3ºC						
	D0	D2	D5	D14	D30	D60	D90	D0	D2	D5	D14	D30	D60	D90
Blank BG-CS (0.05%)	+37.7 ±0.9	+33.4 ±1.3	+32.1 ±0.1	+33.8 ±2.1	+28.9 ±0.8	+26.1 ±1.9	+23.6 ±0.9	+34.3 ±0.7	+34.4 ±1.6	+31.7 ±0.4	+29.1 ±1.1	+28.4 ±0.7	+24.1 ±0.7	+21.5 ±3.4
Blank BG-CS (0.1%)	+35.6 ±0.9	+31.8 ±0.8	+29.4 ±1.1	+25.9 ±0.4	+25.2 ±0.6	+24.5 ±1.5	+21.3 ±1.3	+31.9 ±1.2	+30.3 ±3.5	+29.4 ±0.7	+25.6 ±0.9	+25.5 ±1.5	+22.1 ±1.6	+19.3 ±1.7
F1”	+33.3 ±1.4	+30.3 ±0.4	+28.7 ±3.7	+28.5 ±0.9	+27.4 ±0.6	+25.4 ±0.2	+23.6 ±2.7	+31.9 ±0.6	+31.8 ±0.1	+26.8 ±0.6	+29.7 ±0.9	+25.6 ±0.5	+23.0 ±1.9	+22.5 ±2.1
F2”	+30.7 ±3.0	+28.1 ±0.4	+27.5 ±1.2	+27.1 ±0.2	+26.7 ±0.7	+24.9 ±1.0	+24.6 ±0.4	+29.2 ±2.5	+27.6 ±1.0	+27.3 ±0.2	+26.7 ±0.7	+25.6 ±0.4	+24.5 ±0.3	+24.3 ±0.7
F3”	+28.7 ±0.3	+27.9 ±0.2	+28.2 ±1.5	+25.8 ±1.4	+25.6 ±0.9	+25.8 ±0.6	+27.9 ±2.4	+28.1 ±0.2	+28.6 ±0.4	+25.4 ±1.1	+23.9 ±2.5	+22.9 ±0.9	+22.8 ±2.0	+20.7 ±1.9
F4”	+26.2 ±0.1	+24.6 ±2.4	+25.2 ±1.1	+24.8 ±0.6	+23.6 ±1.8	+17.9 ±1.7	+17.8 ±1.4	+25.5 ±0.2	+24.9 ±1.2	+24.5 ±0.5	+21.1 ±0.8	+21.5 ±0.2	+19.6 ±1.8	+18.5 ±1.7
F5”	+25.2 ±0.1	+25.1 ±0.9	+23.7 ±0.4	+22.9 ±0.3	+22.8 ±1.3	+20.7 ±1.6	+14.9 ±2.1	+24.1 ±0.3	+23.3 ±0.4	+24.3 ±1.7	+20.6 ±0.4	+18.9 ±1.3	+18.6 ±1.2	+12.0 ±0.9
F6”	+27.0 ±6.0	+25.3 ±0.1	+21.6 ±0.7	+21.7 ±0.2	+21.4 ±1.3	+20.9 ±0.4	+20.1 ±4.7	+23.0 ±1.1	+20.7 ±1.4	+18.7 ±2.5	+20.2 ±0.8	+18.0 ±1.1	+18.1 ±3.8	+14.6 ±1.1

At 5 ± 3 °C (Table 4.14), blank BG-CS (0.05%) showed a reduction in zeta potential from +34.3 ± 0.7 +mV at D0 to +21.5 ± 3.4 +mV at D90. F1″ exhibited decreasing zeta potential from +31.9 ± 0.6 +mV to +22.5 ± 2.1 +mV ($p > 0.05$) with significant difference

(*p ≤ 0.05) at 1 day and (**p ≤ 0.01) at 2 weeks. F3″ showed lower zeta potential values than the blank, decreasing from +28.1 ± 0.2 +mV at D0 to +20.7 ± 1.9 +mV at D90. F5″ exhibited decreasing zeta potential from +24.1 ± 0.3 +mV to +12.0 ± 0.9 +mV (****p ≤ 0.0001). For blank BG-CS (0.1%), the zeta potential decreased from +31.9 ± 1.2 +mV at D0 to +19.3 ± 1.7 +mV at D90. F2″ showed decreasing zeta potential from +29.2 ±2.5 +mV to +24.3 ± 0.7 +mV (p > 0.05). F4″ exhibited a reduction in zeta potential from +25.5 ± 0.2 +mV to +18.5 ± 1.7 +mV (****p ≤ 0.0001) at 3 months. F6″ showed a marked zeta potential decrease from +23.0 ± 1.1 +mV at D0 to +14.6 ± 1.1 +mV at D90(****p ≤ 0.0001) at 5 day and (p > 0.05) 3 months. Similarly, storage at 5 ± 3°C resulted in a significant decrease in the zeta potential of the blank BG-CS formulations (p < 0.05). However, the nicotine-loaded BG-CS NPs (F1″–F6″) maintained relatively stable zeta potential values throughout the 90-day storage period, with no statistically significant differences between Day 0 and Day 90 (p > 0.05). High positive zeta potential confersgood stability (Midekessa etal., 2020). Due to the positive charge of the NPs and the negatively charged cell membrane, with anionic glycoproteins in the nasal mucosa, strong NP adherence to the mucosal surface promotes permeation and drug deliver.

PDI results for blank BG-CS and NHT-loaded BG-CS NPs reveal variations in size distribution uniformity at 25 ± 2 °C and 5 ± 3 °C over a period of 90 days (Table 4.15). At ambient temperature, blank BG-CS (0.1%) and F6″ consistently demonstrated lower PDI values (≈0.22–0.36), indicating a more homogeneous particle size distribution in contrast to blank BG-CS (0.05%). F3″ exhibited elevated and more variable PDI values up to 0.50 and 0.49, respectively. F1″ and F5″ exhibited comparatively elevated PDI values at many time intervals reaching 0.55, signifying enhanced heterogeneity and potential particle aggregation. Formulations F1″, F3″, and F5″ exhibiteda slight increase in PDI values with time; however, these variations were minimal and not statistically significant(p>0.05).

Table 4.15
PDI Of Blank BG-CS And NHT BG-CS At 25 ± 2 ºC And 5 ± 3 ºC (N = 3).

Polydispersity index of BG-CS NPs at 25 ± 2ºC							Polydispersity index of BG-CS NPs a 5 ± 3ºC						
D0	D2	D5	D14	D30	D60	D90	D0	D2	D5	D14	D30	D60	D90

Polydispersity index of BG-CS NPs at 25 ± 2ºC							Polydispersity index of BG-CS NPs a 5 ± 3ºC							
Blank BG-CS (0.05%)	0.38	0.40	0.45	0.41	0.45	0.50	0.24	0.40	0.45	0.47	0.54	0.58	0.25	0.22
Blank BG-CS (0.1%)	0.22	0.27	0.26	0.33	0.26	0.36	0.27	0.28	0.30	0.26	0.32	0.31	0.31	0.28
F1”	0.36	0.48	0.42	0.53	0.37	0.35	0.43	0.40	0.44	0.48	0.49	0.49	0.33	0.54
F2”	0.26	0.32	0.30	0.32	0.29	0.35	0.41	0.38	0.37	0.35	0.41	0.37	0.35	0.33
F3”	0.47	0.39	0.47	0.46	0.49	0.43	0.38	0.52	0.50	0.41	0.39	0.36	0.40	0.43
F4”	0.23	0.25	0.27	0.20	0.38	0.25	0.31	0.35	0.37	0.38	0.44	0.42	0.45	0.34
F5”	0.43	0.34	0.55	0.35	0.37	0.46	0.34	0.48	0.47	0.45	0.24	0.39	0.26	0.46
F6”	0.22	0.24	0.22	0.26	0.26	0.31	0.35	0.31	0.30	0.28	0.33	0.33	0.42	0.36

4.9 Cytotoxicity Studies of CS and BG-CS NPs (Blank and NHT-loaded)

4.9.1 Cytotoxicity Studies of CS and BG-CS NPs (Blank and NHT-loaded) using Fibroblast Cells

Figure 4.27 shows the percentage viability of fibroblast cells following exposure to NHT-loaded CS NPs, blank CS NPs (0.05% and 0.1%), and free NHT. At 0.5 mM, blank CS 0.05% and blank CS 0.1% exhibited cell viabilities of 105.27 ± 0.10% and 91.62 ± 0.05%, respectively. Among the NHT-loaded formulations, F1 showed the highest cell viability (99.22 ± 0.05%, ****$p \leq 0.0001$), followed by F2 (91.10 ± 0.06%, $p > 0.05$), F4 (87.99 ± 0.07%, ***$p \leq 0.001$), F3 (85.19 ± 0.01%, ****$p \leq 0.0001$), F5 (76.62 ± 0.03%, ****$p \leq 0.0001$), and F6 (71.88 ± 0.10%, ****$p \leq 0.0001$). In contrast, free NHT showed the lowest cell viability (38.54 ± 3.11%, **$p \leq 0.0001$), indicating significantly greater cytotoxicity than all NPs formulations. Cell viability increased in

a concentration-dependent manner across all formulations at the lower values (0.25-0.03125 mM). Cell viability % was consistently high in blank CS NPs and improved with NHT-loaded formulations, reaching or above 95% viability at low doses. At all concentrations studied, NHT showed the highest cytotoxicity; however, cell survival improved with decreasing concentrations. Based on ISO 10993-5, materials are considered non-cytotoxic when cell viability is ≥70%, while cell viability <70% indicates cytotoxicity (Srivastava et al., 2018).

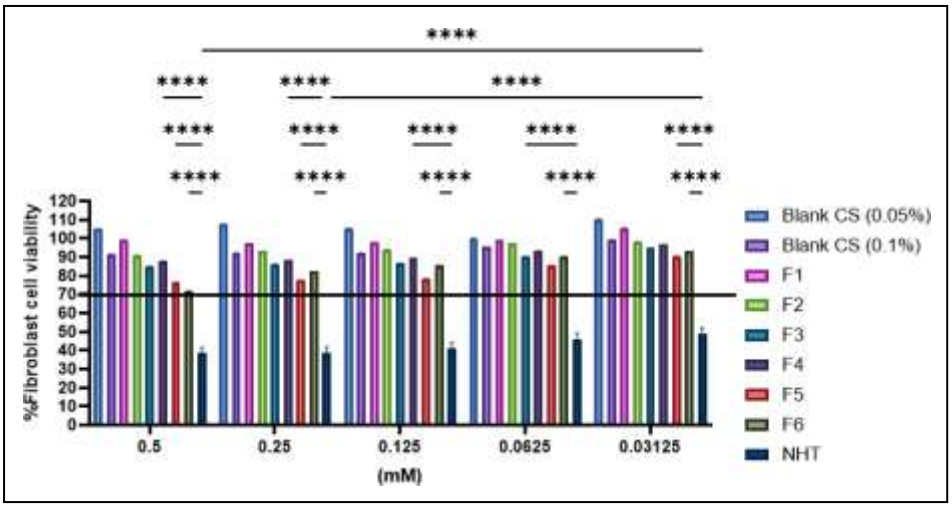

Figure 4.27Percentage Cell Viability Of Fibroblast Cell Following Exposure To Blank CS Nps, NHT-Loaded CS Nps, And NHT At Different Concentrations (0.5–0.03125 Mm).

The viability of fibroblast cells treated with NHT BG-CS NPs is summarized in Figure 4.28. Only the two best NHT BG-CS NPs formulations based on their physicochemical properties, F1″ and F2″, were selected. At 0.5 mM the viability of blank BG-CS (0.05%) and blank BG-CS (0.1%) was 99.99 ± 4.23% and 74.22 ± 4.01%, respectively. The highest cell viability was observed for F1″ (99.52 ± 2.65%) and F2″ (95.43 ± 2.73%), both of which were significantly higher than NHT, which exhibited a viability of 24.48 ± 0.81% (****$p \leq 0.0001$). Across the remaining concentrations (0.25 –0.03125 Mm) both F1″ and F2″ consistently maintained high fibroblast cell viability >95%, with only minor concentration-dependent variations. In contrast, NHT remained markedly more cytotoxic, exhibiting cell viability below 70% at all tested concentrations. According to ISO 10993-5, all BG-CS NPs formulations were classified as non-cytotoxic, as cell viability remained above the 70% (Ramakrishnan & Daly, 2026).

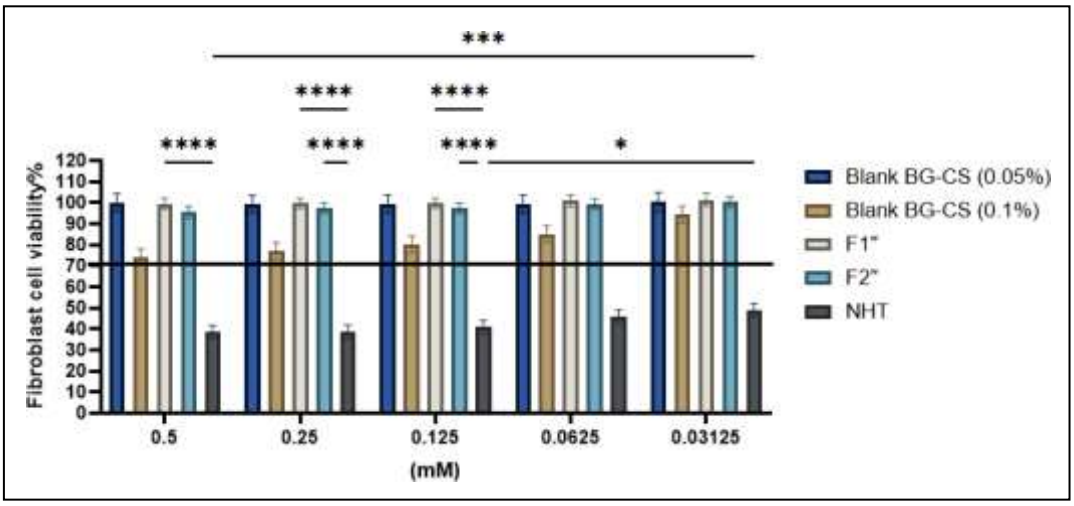

Figure 4.28Percentage Cell Viability Of Fibroblast Cell Following Exposure To Blank BG-CS Nps, F1", F2", And NHT At Different Concentrations (0.5–0.03125 Mm).

4.9.2 Cytotoxicity Studies of CS and BG-CS NPs (Blank and NHT-loaded) using Calu-3 Cells

Formulations F1 and F2 showed the highest fibroblast cells viability, hence there were further tested for cytotoxicity to Calu-3 cells, using the same the MTTtest method. Both formulations were found to produce cell viability of 80 %, which indicates non-toxicity compared the free NHT. Formulation F1 demonstrated 97.52 ± 5.60% and F2 86.73 ± 5.40% cell viability and were not significantly different from the blank at 0.5Mm. The cell vitality of F1 and F2 remained above 80% and non-cytotoxic at concentrations ranging from 0.25 to 0.31 mmol L^{-1}, in accordance with ISO 10993-5 (cell viability ≥70%), whereas the cell viability of NHT was noticeably lower. (Figure 4.29).

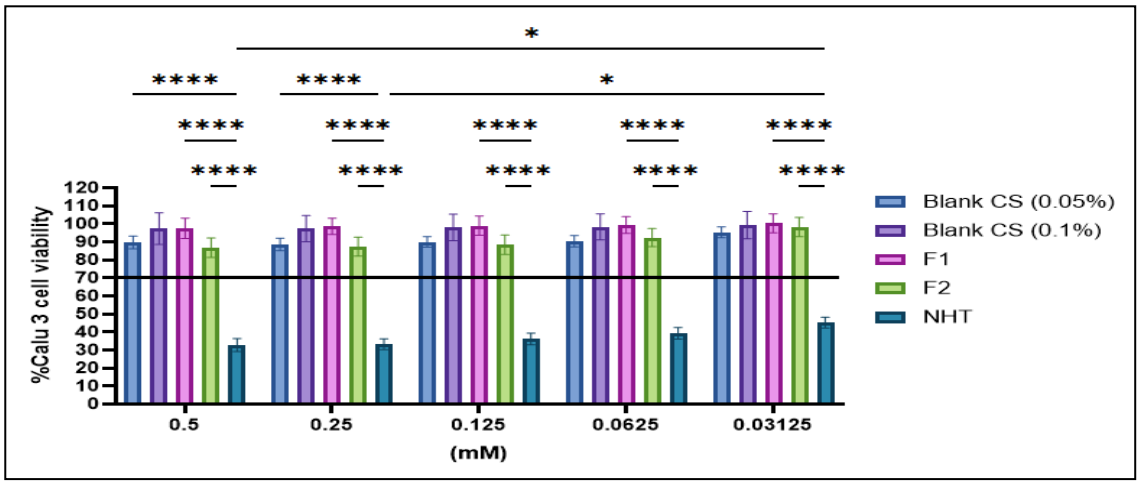

Figure 4.29Percentage Cell Viability Of Calu-3 Cells After Treatment With Blank CS Nps 0.05%, Blank CS Nps 0.1%, F1, F2 And NHT At Different Concentrations (0.5–0.03125 Mm).

Formulations NHT-loaded BG-CS NPs (F1″ and F2″) were further evaluated for cytotoxicity in Calu-3 epithelial cells using the MTT assay. As shown in Figure 4.30, both formulations demonstrated significantly higher cell viability than free NHT at all tested concentrations (***$p \leq 0.001$). At the highest concentration (0.5 mM), F1″ and F2″ exhibited cell viabilities of 66.42 ± 4.11% and 71.59 ± 6.38%, respectively. Cell viability increased with decreasing concentration, reaching 75.21 ± 4.67% for F1″ and 90.21 ± 4.12% for F2″ at 0.03125 mM. F1″ showed slight cytotoxicity only at 0.5 mM (<70% cell viability, ISO 10993-5) These findings indicate that F1" and F2", exhibited minimal cytotoxicity with free NHT at high concentration (32.77 ± 3.57 %).

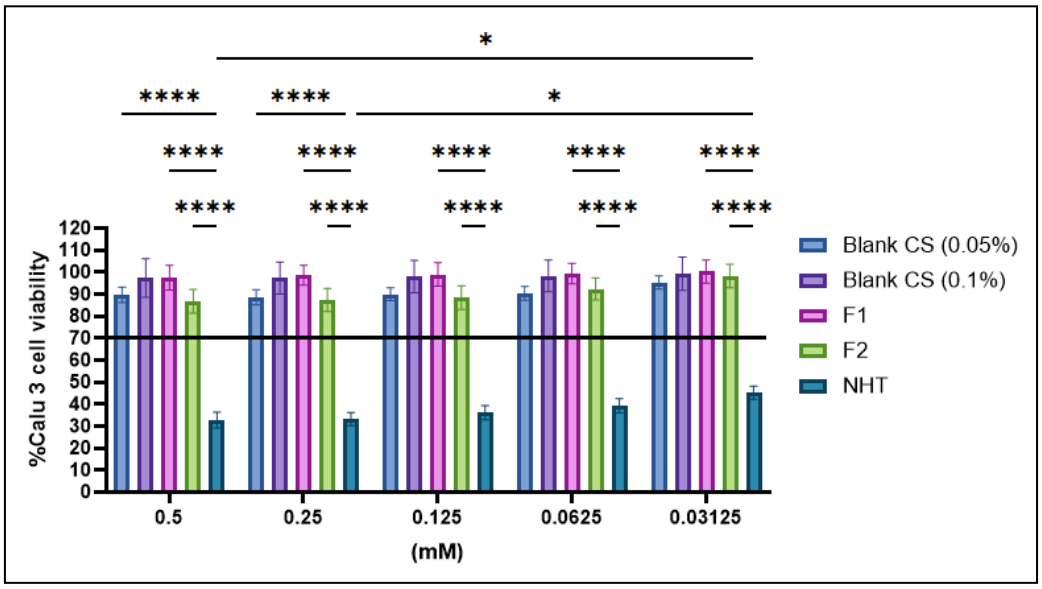

Figure 4.30Percentage Cell Viability Of Calu-3 Cells After Treatment With Blank BG-CS Nps 0.05%, Blank BG-CS Nps 0.1%, F1", F2" And NHT At Different Concentrations (0.5–0.03125 Mm).

4.10 *In Vivo* Pharmacokinetic Studies of NHT-loaded CS NPs and NHT-loaded BG-CS NPs

4.10.1 Pharmacokinetic Analysis

Table 4.16 depicts the pharmacokinetic parameters results obtained for NHT-loaded CS NPs formulations (F1, F2) and NHT. The NHT AUC is much higher than AUCs associated with both formulations, F1 and F2 (Figure 4.31). This suggests that systemic exposure to NHT is greater than that provided by F1 and F2. The AUMC of NHT is much higher than F1 and F2, indicating that the presence of NHT in the blood is longer than the NP formulations. A slow elimination rate is inferred from the long T½ of the formulations, attributable to their sustained release properties. Lower AUC values for formulations F1 and F2 show a balanced NHT delivery, reducing toxicity risk. These results corroborated with the results obtained from our previous cytotoxicity study.

Table 4.16
Pharmacokinetic Analysis Of Formulations F1, F2 And NHT (N=5).

	AUC (mg·min/mL)	AUMC (mg·min²/mL)	MRT (min)	T½ (min)
F1	191.77 ± 38.42**	16433.59±4096.78**	365.61 ± 25.19ns	548.25 ± 110.91****

	AUC (mg·min/mL)	AUMC (mg·min²/mL)	MRT (min)	T½ (min)
F2	189.15 ± 47.96**	17512.42±3754.18ns	381.38 ± 23.84ns	680.11 ± 313.34****
NHT	625.81 ± 83.23	30852.10±7098.36	295.01 ± 25.45	113.60 ± 14.91

.

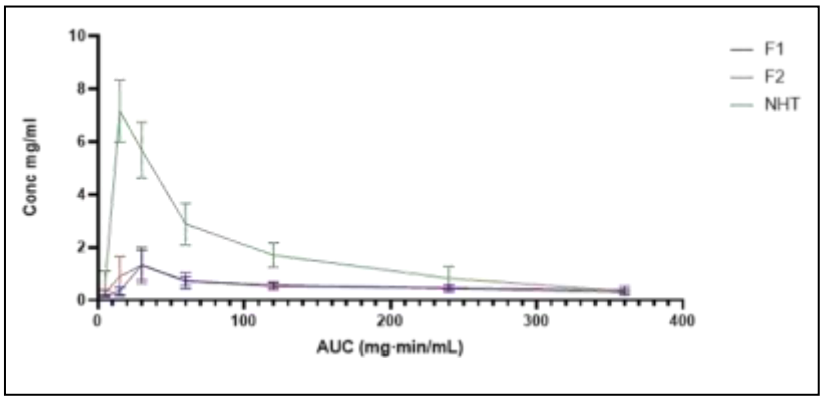

Figure 4.31AUC Of Formulations F1, F2 And NHT

Table 4.17 summarises cotinine pharmacokinetic analysis data obtained for NHT-loaded CS NPs formulations (F1, F2) and NHT. F1 exhibits the lowest AUC value, signifying less total systemic exposure to cotinine. F2 exhibits a superior AUC, signifying enhanced exposure to cotinine compared to F1. NHT exhibits the highest AUC value, indicating that this formulation yields the most significant systemic exposure to cotinine. F1 exhibits the lowest AUMC. F2 exhibits a markedly elevated AUMC, but NHT exhibits the highest AUMC value, indicating extended exposure to cotinine.

Table 4.17
Pharmacokinetic Analysis Of Cotinine In Formulations F1, F2 And NHT (N=5).

	AUC (mg·min/mL)	AUMC (mg·min²/mL)	MRT (min)	T½ (min)
F1	127.40 ±135.95	14337.18±15498.15*	416.15 ± 53.56ns	457.33 ± 236.87ns
F2	368.66 ± 69.59ns	41399.01±16184.93n	386.67 ± 84.69ns	327.88 ± 197.49ns
NHT	421.32 ± 34.22	43762.09±12756.39	404.73 ± 40.53	551.19 ± 543.63

The pharmacokinetic evaluation for NHT-loaded BG-CS NPs, F1" and F2" is summarized in Table 4.18 Lower AUC was observed for F1" and F2" (167.8 and 147.9 mg·min/mL, respectively) than NHT (625.81 mg·min/mL). The $T_{1/2}$ values of F1" (409.2 min) and F2" (278.1 min) are also markedly longer than that of NHT (113.60 min), suggesting a more extended release. The longer $T_{1/2}$ of F1" and F2", which indicates a more sustained release of NHT would be advantageous in reducing the dosing interval required for smoking cessation therapy. Formulations F1" and F2" exhibit significantly lower AUMC values of 14321.7 and 17760.39 mg·min^2/mL, respectively, which are lower than the AUMC of NHT (30852.10 mg·min2/mL), reflecting more sustained drug release. MRT values also indicate prolonged drug exposure, since the MRT for F1" (354.9 min) and F2" (513.2 min) are longer than that of NHT (295.01 min).

Table 4.18
Pharmacokinetic Analysis For Formulations, F1", F2", And NHT (N =5).

	AUC (mg·min/mL)	**AUMC (mg·min^2/mL)**	**MRT (min)**	**T½ (min)**
F1"	167.80±16.50**	14321.70± 2452.14ns	354.90±36.95ns	409.20±105.84****
F2"	147.90±2.78**	17760.39±11701.80ns	513.20±325.70ns	278.10±53.90ns
NHT	625.81 ± 83.23	30852.10±7098.36	295.01 ± 25.45	113.60 ± 14.91

Table 4.19 provides the pharmacokinetic analysis of cotinine for formulations F1", F2", and NHT. Formulations F1" and F2" show more uniform sustained release of cotinine compared to NHT. F1" has a higher AUC (346.1 mg·min/mL) than F2" (241.8 mg·min/mL), though both are lower than NHT (421.32 mg·min/mL). The AUMC of F2" (24849.5 mg·min2/mL) is significantly greater than that of F1" (2968.5 mg·min2/mL), indicative of prolonged exposure to the drug. In contrast, NHT had the highest AUMC (43762.09 mg·min2/mL), implying a faster rate of clearance. MRT values for F1" (343.5 min) and F2" (382.7 min) are somewhat lower than for NHT (404.73 min), suggesting a prolonged release, whereas the T1/2 associated with F1" (210.1 min) and F2" (204.0 min) are shorter than that of NHT (551.19 min). The results indicate that F1" and F2" also provides sustained release effects.

Table 4.19
Pharmacokinetic Analysis Of Cotinine For Formulations, F1", F2", And NHT(N=5).

	AUC (mg·min/mL)	AUMC (mg·min²/mL)	MRT (min)	$T_{1/2}$ (min)
F1"	346.1±28.7ns	2968.5±5572.08***	343.5±92.0ns	210.1±127.3ns
F2"	241.8±90.9**	24849.5±13515.9ns	382.7±45.9ns	204.0±76.9ns
NHT	421.32 ± 34.22	43762.09±12756.39	404.73 ± 40.53	551.19 ± 543.63

4.10.2 In Vivo Drug Distribution Study

The concentrations of NHT in the brain and lungs for NHT-loaded CS NPs formulations F1, F2, and NHT is depicted in Figure 4.32The brain concentration of NHT is highest at around 0.9464 ± 0.19 mg/mL, greatly exceeding that of F1 at 0.1976 ± 0.06 mg/mL (****p ≤ 0.0001) and F2 at 0.1191± 0.07 mg/mL (****p ≤ 0.0001). NHT exhibits a greater concentration in the lungs 0.7624 ± 0.45 mg/mL than F1 0.1478 ± 0.07 mg/mL (***p ≤ 0.001) and F2 0.1286 ± 0.02 mg/mL (***p ≤ 0.001).

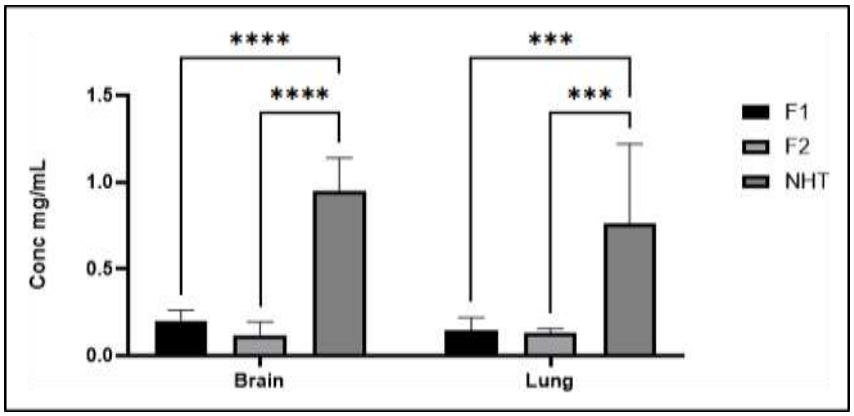

Figure 4.32NHT Concentrations In The Brain And Lungs For Formulations F1, F2, And NHT (N=5).

The cotinine concentrations in the brain and lungs (Figure 4.33) across three formulations (F1, F2, and NHT), with NHT exhibiting the greatest brain concentration 1.1880±0.04 mg/mL, much surpassing F1 0.0176 ± 0.01 mg/mL (****p ≤ 0.0001) and F2 0.0108±0.01 mg/mL (****p ≤ 0.0001). NHT exhibits a higher concentration of cotinine in the lung 0.6909 ± 0.92mg/mL than F1 0.0415±0.01 mg/mL (****p ≤ 0.0001) and F2 0.0213±0.01 mg/mL (****p ≤ 0.0001).

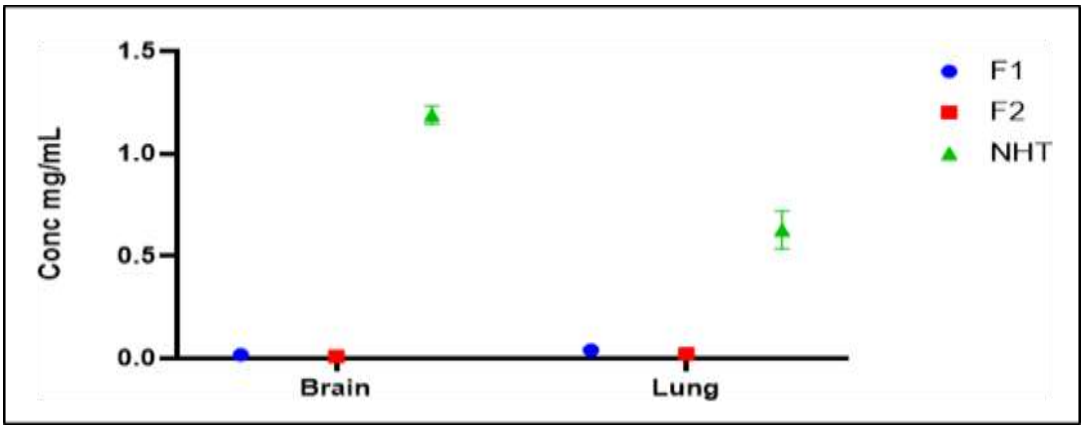

Figure 4.33Cotinine Concentrations In The Brain And Lungs For Formulations F1, F2, And NHT (N=5).

The concentrations of NHT in the brain and lungs for three distinct NHT-loaded BG-CS NPs formulations F1", F2", and NHT is depicted in Figure 4.34. The brain concentration of NHT is highest at around 0.9463 ± 0.19 mg/mL, greatly exceeding that of F1" at 0.210 ± 0.150 mg/mL (****p ≤ 0.0001) and F2" at 0.508 ± 0.160 mg/mL (*p≤ 0.05). NHT exhibits a greater concentration in the lungs 0.7624 ± 0.45 mg/mL than F1" 0.103 ± 0.06 mg/mL (***p ≤ 0.001) and F2" 0.228 ± 0.1 mg/mL (**p ≤ 0.01).

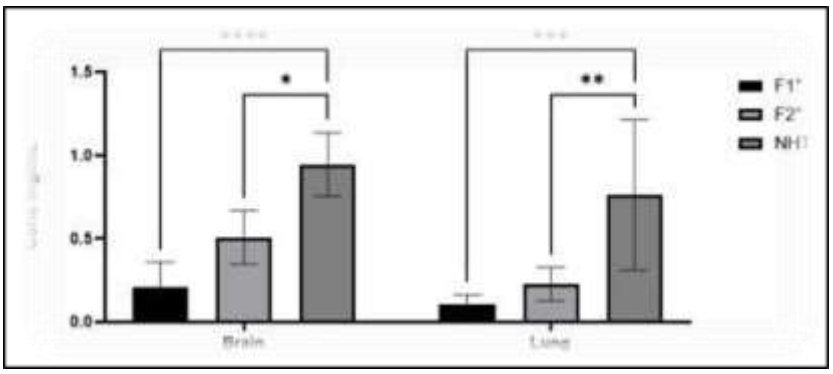

Figure 4.34NHT Concentrations In The Brain And Lungs For Formulations F1", F2", And NHT (N=5).

The cotinine concentrations in the brain and lungs (Figure 4.35) across three formulations (F1", F2", and NHT), with NHTexhibitingthe greatest brain concentration 1.1880 ± 0.04 mg/mL, much surpassing F1" 0.0186 ± 0.01 mg/mL (***p ≤ 0.001) and F2" 0.009 ± 0.01 mg/mL (***p ≤ 0.001). NHTexhibits a higher concentration of cotinine in the lung (0.6909 ± 0.92mg/mL) than F1" (0.0269 ± 0.01 mg/mL) (*p ≤ 0.05) and F2" (0.013±0.01 mg/mL) (*p ≤ 0.05). The objective of formulations F1" and F2" were to provide sustained release delivery of NHT, primarily to the brain. Although delivery of

free NHT results in a notably higher concentration in the brain, the same trend is also evident in the lungs. These findings indicate that, even though NHT facilitates the greatest accumulation in the brain and lungs, F1" and F2" formulations yielded reduced but sustained concentrations, providing more precise NHT dosing.

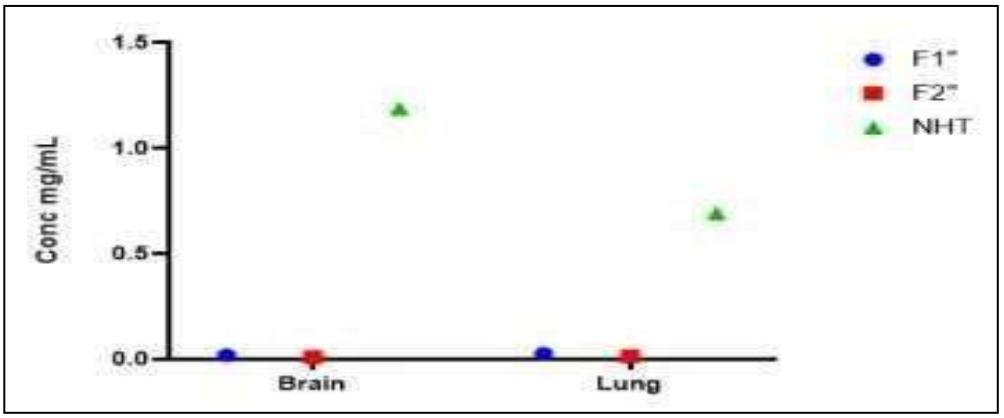

Figure 4.35Cotinine Concentrations In The Brain And Lungs For Formulations F1", F2", And NHT (N=5).

CHAPTER 5
DISCUSSION

5.1 Introduction

This chapter presents and discusses in detail the findings from the evaluation of NHT loaded CS NPs and BG-CS NPs studies. The following topics are covered in the discussion: modification of CS, synthesis of NHT loaded CS and BG-CS NPs, physicochemical properties, DL%, EE%, stability, and cytotoxicity studies of NHT loaded CS NPs and BG-CS NPs. Finally, in *vivo* pharmacokinetic studies using Sprague Dawley ratsare also discussed. Results interpretation in respect to processing and formulation parameters is the major emphasis of this chapter.

5.2 Preparation of BG-CS

5.2.1 Synthesis of Phthaloyl CS

FTIR, ^{1}H NMR, and ^{13}C NMR data confirmed that CS was successfully modified with phthaloyl groups. The FTIR spectra display a prominent peak at 1745.58 cm^{-1}, attributed to the C=O functional group stretch of the newly formed phthaloyl moiety, indicating successful phthaloylation (Kurita et al., 2000). The broad peak observed at 3587.60 cm^{-1} is attributed to O−H stretching, confirming the presence of hydroxyl groups on the CS backbone (Yoksan et al., 2001).

The presence of the phthaloyl structure is supported by the ^{1}H NMR spectrum, in which the phthaloyl group aromatic protons (7.5–7.9 ppm) and the pyranose ring protons (2.8–3.3 ppm) are clearly observed (Asgatay et al., 2013; Barooah et al., 2006; Haverkamp et al., 1975). In the ^{13}C NMR spectrum, the peak at 162.79 ppm is attributed to phthaloyl carbonyl (Mu & Fang, 2007). These combined analyses confirmed that phthaloyl CS was successfully synthesized (Molnár et al., 2010).

5.2.2 Synthesis of BG Phthaloyl CS

FTIR, ^{1}H NMR, and ^{13}C NMR characterization shows that phthaloyl group and glycerol were covalently attached to CS. The broad band at 3419.79 cm^{-1} in the FTIR spectrum

is related to the O−H stretching of glycerol, confirming its presence (Jadhav et al., 2019; Radha et al., 2020). Bands at 2918.29 and 2861.3 cm^{-1} are assigned to C−H stretching in the pyranose ring and alkyl groups, validatingpreservation of the structural integrity of CS and the presence of alkyl chains (Diem et al., 1981). The strong bands at 1774.51 and 1710.85 cm^{-1} are in the range typical of phthaloyl C=O stretching, which indicates successful phthaloylation (Babin et al., 2012). The two bands associated with C=C aromatic stretching at 1485.1 and 1442.75 cm^{-1} and amide II at 1523.76 cm^{-1} also confirm the incorporation of the phthaloyl group (Pastorova et al., 1994).

^{1}H NMR analysis confirmed the presence of alkyl chains, with signals at 0.92, 1.4, and 1.55 ppm, and an acetyl CH_3 peak in the range 2.6–4.52 ppm. Glycerol protons resonate in this same range, overlapping with pyranose proton signals, suggesting attachment of glycerol to the CS backbone. The aromatic protons of the phthaloyl moiety appear at 7.6–8.27 ppm, confirming the predicted structure. The ^{13}C NMR spectra showed the presence of alkyl carbons indicated by the signals in the range 14.19−31.8 ppm (Ramos, 2003). The peak at 40.51 ppm is associated with the acetyl group. The signals present at 69.25–70.00 ppm indicates the presence of glycerol. The signals at 166.07 and 168.51 ppm belong to the phthaloyl carbonyls. This thorough spectral examination strongly supports the successful modification of CS with both phthaloyl and glycerol moieties (Molnár et al., 2010).

5.2.3 Synthesis of BG- CS

The FTIR, ^{1}H NMR, and ^{13}C NMR analyses confirmed the successful modification of CS with glycerol and alkyl groups while maintaining its original structure. FTIR analysis showed a broad band at 3369 cm^{-1} associated with glycerol O−H stretching, also indicating its incorporation (Wei et al., 2014). A band at 2873.95 cm^{-1} for C−H stretching of both pyranose ring and alkyl chain CH_2 groups confirmed the CS structural residue and the inclusion of alkyl groups (Song et al., 2011; Rinaudo et al., 2005). The prominent bands at 1657.07 and 1592.12 cm^{-1} represent the amine group and amide group, with a signal at around 1378.13 cm^{-1} indicating acetyl groups (Ahmad et al., 2011; Walsh et al., 2003; Grant et al., 1989).

^{1}H NMR confirmed the existence of alkyl chains with signals at 0.98, 1.33, and 1.55 ppm, while the acetyl CH_3 group resonates at 1.9 ppm (Van Poucke et al., 2024; Paixão et al., 2024). The pyranose ring and glycerol protons resonate between 2.78 and 3.38

ppm (Far et al., 2023). The ^{13}C NMR spectrum reveals signals for the alkyl carbons at δ 14.25−70.58 ppm, confirming the presence of those groups. The peak at 31.78 ppm represents the acetyl CH_3 group, and the carbons of glycerol resonate at 71.90 ppm. Combined, these spectra confirm that CS was successfully modified with glycerol and alkyl groups, and that the pyranose ring structure has been preserved (Molnár et al., 2010; Mathias et al., 2025).

5.3 Preformulation Studies and Development of CS NPs

5.3.1 Varying Ratios of CS and TPP

The physicochemical parameters of the NPs are strongly affected by the concentration of CS and the ratio of CS:TPP. NPs showed improved homogeneity and colloidal stability at lower CS (0.05% and 0.1%), with smaller particle sizes, relatively low PDI values, and larger positive zeta potentials. This is because the low viscosity of the polymer solution allows the protonated amino groups of CS to efficiently ionic crosslink with the negatively charged TPP (Lusiana et al., 2017). The properties of NPs, such as their size and homogeneity, are greatly affected by the concentration of CS. Reportedly, as the concentration of CS increases, the particle size grows due to the polymer solution's higher viscosity and more intermolecular interactions. These characteristics allow for the aggregation of NPs, which results in larger NPs with less PDI (Hussain & Sahudin, 2016). A study by Kim et al. reported that reducing the concentration of reducing TPP from 0.571 mg/mL to 0.429 mg/mL altered the CS:TPP ratio from (1:1) to (1.3:1) at a constant CS concentration of 0.571 mg/mL. With (1:1), (1.1:1), and (1.2:1) ratio, the particle size stayed about the same: 505.2, 486.0, and 483.9 nm, respectively. However, particle size increased to 653.8 nm when the ratio reached (1.3:1) as a result of reduced TPP (Kim et al., 2022). When compared to this research, our current study produces NPs that are more homogeneous and stable, with smaller sizes, lower PDI, and stronger positive zeta potential. According to Calvo et al. (1997), the size of NPs is significantly affected by the amounts of CS and TPP. Concentrations of 0.05%, 0.1%, 0.5%, and 1% (w/v) of CS and 0.05%, 0.1%, 0.5%, and 1% (w/v) of TPP were utilized in their investigation. Their results indicated that the particle size increased with increasing CS content, this was likely caused by increased intermolecular interactions between polymer chains and a thicker solution. In addition, due to the higher crosslinking density and potential NPs aggregation, larger particle sizes

were also seen with increasing TPP concentration (Bangun et al., 2018; Calvo et al., 1997). A study by Dong et.al (2013) showed that by reducing the CS:TPP ratio from 7:1,5:1 and 3:1, the NPs size also decreased. Reducing the CS:TPP ratio allows more water to be involved in the gelation process since the CS/TPP system is more diluted. This is turn, speeds up the TPP anions dipersion within the CS molecules, resulting in the formation of smaller NPs (Fan et al. 2012). Lower CS concentrations generally produced NPs with smaller particle sizes, although the effects on PDI and zeta potential depended on the CS:TPP ratio. All formulations exhibited positive zeta potential, which can be attributed to the protonated amino groups of CS remaining on the NPs surface. Variations in zeta potential likely reflected differences in the degree of ionic crosslinking between CS, TPP and the number of residual surface amino groups. Following TPP addition the NPs was sonicated using a probe sonicator for 4 min. The low zeta potential (+17.6 ± 0.45 +mV) during ionic gelation could be because TPP neutralizes the positively charged amino groups of CS more effectively. The result was a decrease in the surface charge of the NPs because fewer free protonated amino groups were left on their surface. The decrease in electrostatic repulsion could perhaps account for the rise in particle size and PDI (Masoudipour et al., 2017) that accompanied this formulation.

5.3.2 Varying Sonication Time

The physicochemical characteristics of the NPs were greatly affected by the duration of sonication (Gokce et al., 2014). Minimization of particle size and PDI was observed with an increase in sonication duration from 1 to 4 min, suggesting enhanced dispersion and production of more uniform NPs. This is because the uniform dispersion of particles is enhanced by the ultrasonic energy, which breaksdown clumps of particles. Increasing the sonication time to 8 minutes caused the particle size to rise, which may indicate re-aggregation or instability caused by the increased energy input. Prolonged sonication did not appreciably alter size distribution or surface charge, since PDI and zeta potential stayed generally stable despite these alterations. Reduced particle size, PDI and stable zeta potential (>30 +mV) suggesting good colloidal stability were all outcomes of a 4 min sonication session, which struck the ideal balance. While there was no statistically significant difference between 2 and 4 minutes, the best condition was determined to be 4 minutes since it consistently produced slightly smaller particles and PDI while

keeping the zeta potential steady. The generation of cavitation forces during ultrasonication improves dispersion and reduces particle size by disrupting intermolecular connections (Nguyen et al., 2010). Additionally, by increasing the protonation of amino groups, it improves the stability of colloidal particles. On the other hand, re-aggregation or instability could result from over-fragmentation caused by excessive sonication (Vo et al., 2026). According to previous research, zeta potential is almost unaffectedby ultrasonication, butparticle size and PDI are reduced as a result of CS depolymerization and NPs fragmentation (Tang et al., 2003). Another study indicated that NPs can be better dispersed and made more homogeneous by using ultrasonication for a lengthy period of time (40 min) to achieve this goal (Nasti et al., 2009). However, in our present study, the duration of 1 -4 min successfully decreased particle size as a result of enhanced dispersion in the current investigation.

5.4 Characterization of NHT-loaded CS NPs and NHT-loaded BG-CS NPs

5.4.1 Particle size, Zeta potential and PDI

CS NPs and BG-CS NPs (blanks and NHT-loaded) were positively charged and the presence of charges decreased with increasing NHT concentration in the NPs. The decreasing surface charge with increased drug loading showed that the surface coverage of CS NPs with NHT caused the positive charge to reduce. It may be noted that the surface zeta potential of particles was reduced with increased particle size owing to drug loading, suggesting that the particle surface positive charges were masked because of the increased accumulation of NHT on the surface. Higher concentrations of drug loading showed that a significant amount of drug adheres to the particle surface (He et al., 2010). In addition, since the NHT has a net negative charge because of the presence of tartaric acid salt, the positive charge of the CS amino groups decreased with increased concentrations of NHT in the formulation (Wang et al., 2017).

In comparison to more traditional nicotine formulations, the usage of nicotine hydrogen tartrate has the benefit of a more rapid rise in plasma nicotine levels due to its quicker dissolution and absorption. Important in the fight against relapse while trying to quit smoking, this expedites the start of therapeutic benefits, most notably the alleviation of cravings (Shiffman et al., 2008). An inhaled formulation of nicotine hydrogen tartrate, encased in CS NPs, has demonstrated efficient lung transport and encouraging deposition; this suggests that it may be a viable option for the treatment of nicotine

addiction that does not cause cancer (Nikou et al., 2026). The effect of increasing the concentration of crosslinker TPP and CS in insecticide nicotine hydrochloride was studied by Yang et al., (2018). At a concentration of 0.10% for TPP and 0.05 or 0.10% for CS, the diameters of the NPs were about 300 nm. However, when either of these concentrations was higher than 0.10%, the diameters of the NPs rose quite quickly. This was also seen in our results. Another study reported the synthesis of CS NPs loaded with zidovudine (AZT) by an ionotropic gelation technique employing TPP, and the manipulation of the CS proportion led to a reduction in NPs size, with an approximate diameter of 260 nm. In addition, an increase in TPP percentage resulted in larger NPs, measuring around 330 nm. The use of AZT resulted in a significant augmentation of the NPs dimensions. The existence of a positive charge on the surface of NPs plays a vital role in their mucoadhesive qualities (Da Silva Barbi et al., 2014). Nicotine can be classified as a weak base since it has a pKa of approximately 8.0 (Govind et al., 2017). This means that, in its basic form, nicotine can readily accept protons (H^+) to become positively charged. Higher drug loading concentrations resulted in a considerable amount of drug attached to the surface of the particle (Prabaharan & Mano, 2004: Chakravarthi & Robinson, 2011). Helene Jonassen et al. (2012) stated that an increase in TPP concentration leads to an increase in the TPP to CS ratio and a consequent increase in the size of the particles due to higher CS concentrations, which increases particle aggregation and sedimentation. This becomes unfavourable for the colloidal stability of the NPs (Jonassen et al., 2012). The CS to TPP weight ratio was found to significantly affect particle size in a linear fashion, whereby, as the CS to cross-linking agent TPP ratio increased, so did particle size (Gan et al., 2005).

For nasal formulations, particle size is an important metric for managing deposition, dissolution, and possible passage outside the nasal canal. Particles of a size below 10 μm have the potential to travel beyond the nasopharynx and into other organs, such as the lungs, potentially impacting systemic exposure (Doub et al., 2023). According to earlier research, most solid lipid NPs formulations have particle sizes below 200 nm, which is ideal for transit from the nose to the brain. Particles in this size range havea larger surface area, interact better with nasal mucosa, and can penetrate the olfactory epithelium's intercellular gaps (Nguyen & Maeng, 2022). Albarki and Donovan revealed that smaller PLGA NPs (~60 nm) were internalized into nasal epithelium and submucosal tissues in greater quantities than bigger particles (~125 nm) (Albarki & Donovan, 2020). Surface properties rather than particle size alone, control the effectiveness of NPs systems for

nasal administration. Nanoscale particles can enter the nose by transcellular pathways and be taken up bythe epithelial cells there, but their ability to penetrate the nasal mucosa is still constrained by the small size of the tight junctions. Notably, compared to negatively charged nasal mucosa, positively charged NPs interact better, leading to longer nasal residency time and better local drug availability. This highlights the importance of positive zeta potential over size minimization alone, as NPs with the righ surface charge and moderate nanoscale dimensions canaccomplish successful nasal drug delivery without requiring extremely small particle sizes (Illum, 2007). Nanocarriers derived from modified CS usually have a positive zeta potential. This allows them to interact electrostatically with the negatively charged nasal mucus, which improves mucoadhesion and increases the amount of time the medication stays in the nose (Sonvico et al., 2018). It is worthy to note that formulations F1, F2, F1" and F2" had excellent particle size, PDI and zeta potential.

According to quality target product profile (QTPP) and critical quality attributes (COAs) for choosing the best formulations for intranasal delivery (Pallagi et al., 2015) is depicted in Figure 5.1 All formulations (F1-F6) and (F1"-F2") were analysed for particle size, PDI, and zeta potential (n = 3, mean ± SD). A predetermined target product profile (QTPP) for intranasal CS NPs/BG-CS NPs includes a particle size of less than 200 nm, PDI of less than 0.30, and a zeta potential exceeding 25 +mV. The particle size for F1, F2, F1" and F2" was 155.8 ± 6.28 nm ,120.36 ± 3.23 nm, 83.64 ± 1.73 nm and 69.42 ± 0.72 nm and zeta potential of +30.66 ± 2.51+mV, +36.06 ± 1.70 +mV, +31.93 ± 0.68 +mV and +36.93 ± 0.89+mV respectively. Although F1 met the zeta potential criterion, its larger particle size (155.83 ± 6.28 nm) and higher PDI (0.4 ± 0.007) reduced its compliance with QTPP. Similarly, F1" exhibited a small particle size (83.64 ± 1.73 nm) but a relatively high PDI (0.43 ± 0.020), indicating poorer homogeneity than F2". Through statistical analysis and comparison with the QTPP, F2 and F2" were selected because they exhibited the most desirable combination of particle size below 200 nm, zeta potential greater than +25 +mV, and the lowest PDI indicating better colloidal stability.

The selection of these concentrations was based on their lowest particle size, positive zeta potential, and low PDI compared to other tested formulations. Theseconcentrations also showed a spherical image in the TEM, high EE% with a sustained release method, and a higher percent cell viability in the MTT test study.

The study on ghrelin intranasal liposomes began with the establishment of the QTPP. The QTPP defined important aspects such as the following: an intranasal route for direct access to the central nervous system, a range of particle sizes (70-400 nm) for effective targeting to the nose and brain, a PDI < 0.3, a zeta potential > +20 +mV and stability for 60 days. These factors directly impact nasal deposition, mucosal penetration, formulation stability, and reproducibility of therapeutic performance (De Barros et al., 2021). The chemical alteration of CS has a considerable impact on the physicochemical properties of the NPs. The creation of more compact NPs was promoted by the BG modification, as evidenced by the substantially smaller particle size of blank BG-CS NPs compared to blank CS NPs at the 0.1% CS concentration (**p < 0.0001). At the 0.05% CS concentration, however, no such diminution in particle size was noted, indicating that the concentration plays a determining factor in the effect of BG alteration on particle size. At larger concentrations of CS, the effect of BG modification may become more apparent due to improved intermolecular interactions, which may allow for tighter packing of NPs. The differen trend after NHT loading may reflect NHT–BG-CS interactions.

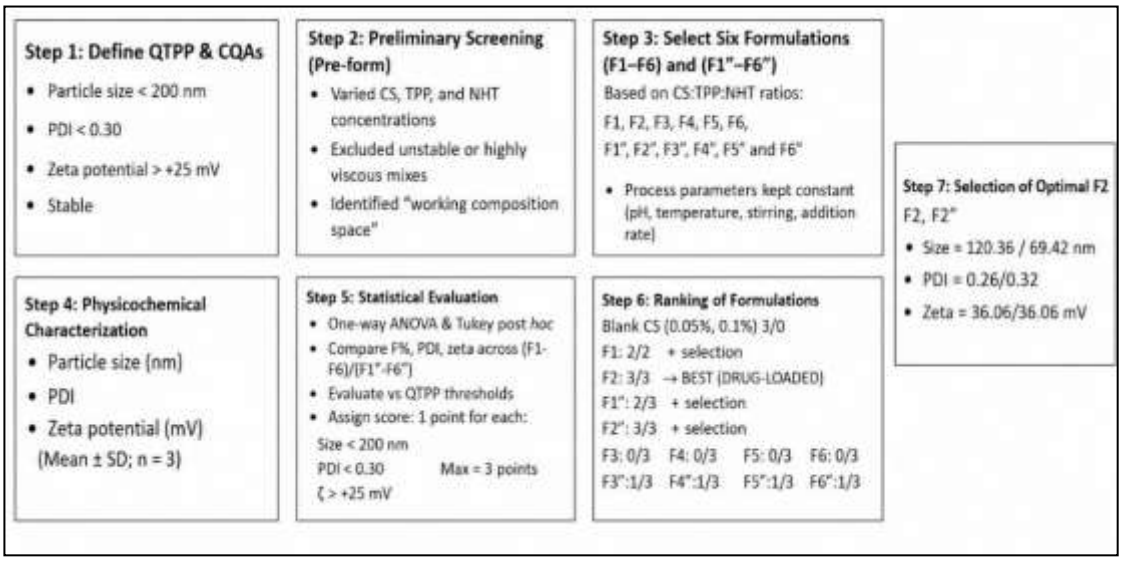

Figure 5.1 Formulation Rationale Scheme.

5.4.2 Transmission Electron Microscopy (TEM)

A nearly spherical shape is often desired for certain applications since they can have advantages in terms of their stability and interactions with biological systems (Zhang et al., 2021). Hui Liu (Liu & Gao, 2008) showed TEM observation for CS NPs in which no serious aggregation of the particles was seen. CS NPs also have a deeper color in the

core and surface, which indicates that these regions have a larger electron density distribution, since TPP contains the element phosphorus, which has a higher electron density. Furthermore, CS has a higher degree of cross-linking density with TPP in these places (Fan et al., 2011). Recent research found that NPs with sizes between 38 and 90 nm, as determined by TEM, were evenly distributed and displayed little to no aggregation, in contrast to particles with sizes more than 300 nm, which exhibited more clustering. These TEM findings were directly linked to nasal performance, since the smaller NPs showed better retention in the nose cavity and better interaction with nasal mucin. As a result, the morphological evidence presented by the TEM size analysis proved that smaller, more evenly distributed CS NPs were the best candidates for use as intranasal formulation carriers (Vega-Rojas et al., 2025). Particle size in the range of 150-200 nm was validatedby TEM analysis for xylometazoline-loaded CS NPs Particles smaller than 200 nm can improve mucosal adherence without triggering rapid mucociliary clearance, making this size range especially important for nasal formulations. Longer residence duration and better drug penetration are likely the outcomes of the homogeneous shape and consistent surface texture seen by TEM (Attri et al., 2022). These results concur with our results for NHT CS NPs and BG-CS NPs where the NPs size was less than 300nm and a nearly spherical shape of the NPs. Although the previous study involved ciprofloxacin loaded NPs rather than nicotine loaded NPs, the observed homogeneous morphology after drug loading is reliable with our TEM findings and supports successful nicotine encapsulation. Wang's TEM analysis also revealed that blank CS NPs exhibited a smooth, nearly spherical shape, while NHT-loaded particles displayed a rougher surface (Wang et al., 2017). The denser appearance detected in F5" may be attributed to differences in particle distribution On TEM grid through sample preparation rather than a change in NPs morphology.

5.4.3 Differential Scanning Calorimetry (DSC)

The endothermic peaks, which were similar to the peaks from CS transition, shifted to a lower temperature with the NHT-loaded CS NPs. It is considered that this is a proof of incorporation of NHTinto the matrix of CS NPs.The possible reasons for the absence of NHT endothermic peak were: 1) NHT was dissolved into CS NPs matrix as a solid solution and did not crystallize; 2) NHT was converted to its amorphous form within NPs (Wang et al., 2017); 3) the characteristic peaks of NHT and CS were overlap ped,

so the combined peaks shifted to lower temperature (Hancock & Zografi, 1997; Fathy et al., 2023). DSC study revealed that both CS NPs and BG-CS NPs noticeably affected the thermal properties of NHT during NPs synthesis. In all systems, the distinctive crystalline endothermic melting peak of pure NHT (~90 °C) was absent in all NHT-loaded formulations, thereby affirming the successful addition of NHT into the polymeric matrix and its transformation into a non-crystalline state. The extensive endothermic changes noted for CS NPs and BG-CS NPs were mostly linked to polymer dehydration, suggesting that NHT was molecularly disseminated inside the NPs instead of existing as a crystalline phase. Nicotine was successfully encapsulated within the NP system, it was found to be evenly distributed and not aggregated, confirming that it had been effectively incorporated into the carrier matrix. It is reasonable to assume that the NPs contain nicotine in an amorphous or molecularly dispersed form, as this behavior is usually linked to the breakdown of crystalline structure (Ike et al., 2025). A minor difference was noted between the two NPs systems regarding the onset temperature of the polymer-associated endothermic peak: BG-CS NPs demonstrated a slightly elevated start temperature for bound water loss in comparison to CS NPs, indicating improved polymer–drug and polymer–polymer interactions subsequent to BG-CS. Nonetheless, the thermal profiles of NHT-loaded CS NPs and BG-CS NPs were analogous, as both systems exhibited similar vanishing of NHT endothermic peaks and equivalent changes in peaks toward lower temperatures. The DSC data revealed that nicotine was converted into an amorphous or molecularly dispersed state in both CS NPs and BG-CS NPs, as evidenced by the lack of its crystalline melting peak. The thermal properties are beneficial for intranasal delivery, as amorphous drug forms exhibit rapid breakdown in the nasal mucosa, leading to improved absorption and more consistent drug uptake. A high-energy solid state can be generated via nanosization, leading to partial amorphization, as demonstrated in previous research. This state improves medication solubility and membrane permeability (Latif et al., 2021). Previous research has shown that intranasal medication formulations benefit from amorphization since it greatly improves solubility within the small volume of nasal mucus. Amorphization, as confirmed by DSC, facilitated rapid drug dissolution in artificial nasal fluid, enabling efficient drug release despite the brief nasal residence time constrained by mucociliary clearance (Inoue et al., 2022).

5.4.4 Thermogravimetric Analysis (TGA)

The weight losses of CS NPs were shown to be in the temperature range of 150 to 800 °C and could be attributed to the decomposition and degradation of the polymer chain of the free CS and CS cross-linked with TPP, the breakage of hydrogen bonds between the N-acetyl and free amino groups, the gradual oxidative degradation of carbonaceous residue, and byproducts formed (Elzamly et al., 2021). In general, CS NPs have higher thermal stability than CS due to the presence of phosphate groups in TPP (Jiang et al., 2012). A smaller initial weight loss was seen with BG-CS compared to unmodified CS, which may indicate that the presence of hydrophobic butylglycerol moieties that causes lower hygroscopicity. There was a noticeable contrast between the CS NPs and BG-CS NPs TGA thermograms. Because of the higher hydrophobicity brought about by the butylglycerol modification, BG-CS NPs showed less initial weight loss in the 25-150 °C range compared to CS NPs. This suggests that there was less moisture uptake. Additionally, the polymeric matrix appeared to be more thermally stable in BG-CS NPs, since their thermal breakdown profile was less abrupt. BG-CS NPs have better thermal stability and less moisture uptake than CS NPs, making them better for intranasal delivery. These properties help to keep the formulation intact and increase the amount of time the drug stays in the nose. There have been reports that CS physicochemical and thermal behaviour can be drastically changed by chemical modification. This is because the polymer chain organization and intermolecular interactions are changed. Functional groups improve heat stability and minimize moisture uptake by increasing structural cohesion and decreasing polymer hydrophilicity (Dash et al., 2011). BG-CS NPs increased thermal stability in CS, contrary to earlier findings that found decreased thermal stability after CS acylation and that disrupt intermolecular hydrogen bonding and weaken the polymeric network (Sánchez et al., 2015). The improved thermal stability in this study is due to the BG modification, which stabilizes the polymeric matrix and delays thermal breakdown through increased hydrophobic contacts and reduced moisture uptake.

5.4.5 X-ray Diffraction (XRD)

After NHT loading, the diffraction intensities became weaker, which implied decreased crystallinity within the NPs. One of the highest meltingpoints for a crystalline NHT solid that has been reported to date is possessed by the salt that was synthesized by employing

d-(−)-tartaric acid (Angevine et al., 2023). Hence, amorphous-crystalline CS samples are subjected to intensive mechanical treatment, the XRD patterns demonstrate the qualitative changes that take place in the crystal structure (Podgorbunskikh et al., 2022). However, dissolution of substances in the amorphous state does not require the consumption of energy or time in order to dissolve the crystal lattice, which results in an improvement in the pharmacokinetic parameters of the pharmacological composition (Menshutina et al., 2022). Amorphous forms often exhibit higher solubility, rapid dissolution and more flexibility in controlling drug release profiles compared to their crystalline equivalents (Peltonen & Strachan, 2020; Pandi et al., 2020).

5.4.6 Fourier Transform Infrared Spectroscopy (FTIR)

Covalent alterations have a secondary role in the creation of NPs system, and according to the FTIR spectra, ionic interactions serve as the primary governing factor. Past research has shown that ionic gelation produces CS NPs by electrostatic interactions between the positively charged phosphate groups of TPP and the protonated amino groups ($-NH_3^+$) of CS, rather than by creating new chemical bonds. It is also confirmed that the connection is ionic rather than covalent by FTIR investigations, which show peak shifting and intensity changes instead of new bands appearing in such systems (Alehosseini et al., 2022). CS functional groups are involved in intermolecular interactions, probably via electrostatic binding with TPP, as shown by the spectrum alterations, especially the broadening and minor shifting of the hydroxyl and amine bands. Studies on CS-TPP NP systems have also shown similar FTIR behaviour, with the -OH and $-NH_2$ peaks expandingandshiftingexplained by ionic crosslinking between the protonated amine groups of CS and the phosphate groupsof TPP (Shu & Zhu, 2000). All formulations show that CS/BG-CS and NHT have kept their structural integrity, since the principal functional group signatures have been preserved. Molecular level evidence suggests that the drug is not present as a distinct crystalline phase but rather strongly distributed throughout the polymeric matrix, as shown by the attenuation and overlap of distinctive peaks, particularly in the fingerprint area. NHT carboxyl peaks slightly shifted after encapsulation into CS and BG-CS and partially masked due to overlap with carbonyl bands at 1719 cm^{-1}. These changes indicate the presence of molecular interactions.

5.5 EE% and DL% of NHT-loaded CS NPs and NHT-loaded BG-CS NPs

Increasing the concentration of NHT in the mixture can lead to an increase in the liquid crystalline properties. This is because the NHT molecules may contribute to the ordering of the system, promoting DL% phase behavior. The difference in DL% between F5 and F6, despite having the same quantity of NHT, can be attributed to F6" higher CS content. An improved ionic crosslinking between CS and TPP causes a more compact and densely NPs to be formed, which in turn causes a decrease in DL% at higher CS concentrations (Nogueira-Librelotto et al., 2016). The lower DL% observed for F6 compared with F5 is consistent with the higher CS content, which increased polymer mass and crosslinking density. Factors such as hydration and crosslinking of the polymer network have a significant impact on the nicotine encapsulation in CS systems. Drug retention is enhanced by increasing hydration or crosslinking, whereas drug mobility and release are enhanced by decreasing network integrity. Therefore, the optimal intracellular network and polymer density order the efficacy of DL% and EE% (Lino et al., 2017). DL% is governed by both the amount of incorporated nicotine and the total polymer mass, increasing nicotine content tends to increase DL%. EE% was defined as the percentage of the initial nicotine that was successfully incorporated into the NPs, while DL% was determined as the mass of nicotine incorporated into the NPs relative to the total recovered mass of the nanoparticles loaded with nicotine (Shen et al., 2017).

Lower CS content means less polymer bulk around the NHT, allowing more NHT relative to polymer to be loaded into each particle, increasing DL% (Xu & Du, 2002). The EE% was high for all formulations as the cationic CS interacts tightly with the negatively charged NHT and TPP, enabling efficient encapsulation at low CS loading. On the other hand, the formulations with higher CS proportions (F2", F4", and F6") generated a thicker CS matrix leading to enhanced EE% at the expense of DL%. Consequently, formulations having lower CS ratios attain higher DL% without compromising EE% significantly. Kongala et al. designed harpin -loaded CS NPs to induce defense responses in tobacco plant at an EE% of 85% and sustained release for 4 hrs. The average bioavailability to the tobacco plant was improved with the harpin-CS mixed NPs at nanogram concentrations in comparison with harpin or CS alone (Kongala & Mamidala, 2023).

5.6 Release Studies of NHT-loaded CS NPs and NHT-loaded BG-CS NPs

Zeng et al (2021) stated that there was less than complete release in some formulations from cross-linked polymer systems with different CS:TPP ratio that may extend the release (Zeng et al., 2021). In our study, the results showed sustained release of NHT from CS particles over the first 5 hrs. Contrary, the release of free NHT was abrupt, with NHT release of 71.61 ± 1.34 indicates that CS NPs can provide sustained release of NHT. Incorporating NHT into CS NPs is a promising strategy for achieving sustained drug release, thereby enhancing patient compliance and decreasing toxicity.

Formulations F1" and F2" exhibit significant disparities in their drug release characteristics, although possessing comparably high EE% (F1": 95.27%, F2": 93.61%). F2", characterized by a greater concentration of CS and TPP, demonstrates a markedly reduced drug release in the initial hr (28.43%) compared to F1" (54.88%). This is due to the thicker CS matrix in F2", which more effectively inhibits drug diffusion. Despite F2" exhibiting a little reduced DL% (43.53%) compared to F1" (45.93%) ($p > 0.05$), the CS to drug ratio in F2" facilitates a more regulated release. F3" and F6" have essentially identical release patterns over a 24 hrs period (F3" = 73.63±0.89%, F6" = 76.15±4.31%), despite their difference in EE% and DL%. This indicates that elements beyond loading capacity such as polymer concentration and network density, significantly influence release behavior (Kamaly et al., 2016). Corroborating the assertion that elevated drug concentrations facilitate a swifter initial release. Conversely, formulations F2", F4", and F6", which contain higher CS levels, demonstrate reduced release rates, thereby supporting that increased polymer concentration increases matrix viscosity and diffusion resistance (Kasaliwal et al., 2011). The higher concentrations of CS and TPP increased the degree of ionic crosslinking, producing a denser and less porous polymeric network. This slowed nicotine diffusion from NPs, resulting in a more sustained release profile (Khoerunnisa et al., 2021).

The Korsmeyer-Peppas model considers exclusively the beginning of the release profile, which usually accounts for up to 60% cumulative drug release ($Mt/M\infty \leq 0.6$). This limitation is critical as the model's purpose is to depict the release process in its early stages, before considerable effects of matrix erosion, swelling, or depletion take center stage (Khalbas et al., 2024). The Korsmeyer-Peppas model is not applicable to

NHT because determining the release reliably needs numerous data points within this range.

The release of NHT from the NPs is likely governed primarily by diffusion through the hydrated CS matrix. An initial release phase may be attributed to NHT located near the NPs surface, followed by a slower release of the entrapped drug as it diffuses through the crosslinked polymeric network. The higher CS and TPP content in F2″ likely produced a denser matrix, increasing the diffusion pathway and consequently slowing NHT release compared with F1″. In addition, the BG-CS NPs may have reduced water penetration into the polymer matrix, further contributing to the sustained release profile (Tien et al., 2003).

The in vitro release study was conducted in PBS (pH 7.4), which is widely used as a standard release medium to maintain sink conditions. However, the physiological pH of the nasal cavity ranges from approximately 5.5 to 6.5 (Washington et al., 2000). CS is a weak polycation, its protonation, swelling, and solubility are influenced by pH (Mura et al., 2022). At the slightly acidic pH of the nasal cavity, CS is expected to remain more protonated, which may enhance polymer swelling and mucoadhesion and consequently alter the nicotine release profile. Therefore, the release behavior observed at pH 7.4 may not fully represent the in vivo nasal environment, and future studies should evaluate the release profile under simulated nasal conditions (pH 5.5 –6.5). In addition, the selection of the 500–1000 Da membrane allows free nicotine, with a molecular weight of 162.23 Da to diffuse into the release medium while keeping the CS NPs inside the dialysis bag.

For all NPs formulations, the drug release can be explained using the Korsmeyer-Peppas model. The created system release behavior could be adequately described by this model, shown by the strong correlation coefficient (R^2) values found for the majority of formulations, including F1-F6 and F1”-F6”. On the other hand, the Korsmeyer-Peppas model did not fit the release of pure NHT, indicating that the drug release was quick and unregulated. Strong R^2 values do not prove continued release, but they do show that the model was well-fit. As a result, the underlying release mechanism was deduced by looking at the slop (n values). The n values that were obtained indicated that the drug release from the NPs formulations was regulated. The results also showed that the NHT BG-CS NPs formulations are better than the NHT CS NPs in sustained drug release.

5.7 Stability Studies of NHT-loaded CS NPs and NHT-loaded BG-CS NPs

The stability of the drug-loaded NPs in terms of particle size, zeta potential, and PDI is very important for optimal nasal to brain delivery (Deruyver et al., 2023). A consistent particle size promotes adequate absorption via the nasal mucosa, since large particles may not penetrate and small particles may be rapidly cleared from the respiratory system (Yan & Sha, 2023). A high positive zeta potential means the system is electrostatically stable and prevents NP aggregation as it generates high electrostatic repulsion between particles of similar charge (Shrestha et al., 2020). A low and stable PDI value highlights the relatively narrow particle size distribution, which is critical for consistent drug delivery and absorption (Masarudin et al., 2015). In a re cent study, niosomes based CS were prepared and demonstrated high stability for the nasal to brain delivery of clonazepam (CLZ). These chitosomes had a particle size of ~200 nm and PDI < 3. They were stable for 12 weeks while stored at 4 ºC, 24 hrs in simulated nasal fluid, and after lyophilization-sonication. More importantly, the chitosomes demonstrated a controlled release of 50% of CLZ over 4 hrs, showed mucoadhesive characteristics, and enhanced drug permeability while decreasing toxicity (Nerli et al., 2023).

Disparities in colloidal stability were noted among the evaluated formulations, based on an assessment of particle size, PDI, and zeta potential at both ambient temperature (25 ± 2 °C) and refrigerated conditions (5 ± 3 °C). F6 and F6″ exhibited physical stability, particle size remained relatively stable throughout storage, minimal change in PDI throughout storage and satisfactory zeta potential profiles during the storage duration. F1 and F1″ exhibited moderate stability, marked by significant particle size enlargement (**** $p \leq 0.0001$), elevated zeta potential ($p > 0.05$) and variable PDI ($p > 0.05$), indicating diminished homogeneity with time. F2 and F2″ characterized by moderate increases in particle size (**** $p \leq 0.0001$), elevated zeta potential ($p > 0.05$) and low PDI ($p > 0.05$).Conversely, (F3/F3″), (F4/F4″), (F5/F5″) and (F6/F6”) formulations exhibited the lowest stability, characterized by notable particle aggregation (**** $p \leq 0.0001$), elevated PDI ($p > 0.05$), and substantial decreases in zeta potential ($p > 0.05$), especially during prolonged storage durations.

The ideal formulation, F2, was determined after a thorough stability evaluation throughout 90 days at both 25 ± 2 °C and 5 ± 3 °C, which included particle size, zeta potential, and PDI. When compared to the other NHT-loaded CS NPs, F2 showed the

best stability, smallest particle size, minimum change in surface charge, and low PDI. F1 was less stable than F2 due to its smaller zeta potential, but it nevertheless showed acceptable stability characteristics overall. A high positive zeta potential leads to good stability and an absence of particle aggregation (Jhaveri et al., 2021). Positively charged NPs offer benefits in drug delivery since, due to their interaction with negatively charged cell surfaces between the anionic nature of the glycoproteins in the nasal mucosa and the cationic nature of the produced NPs, the NPs can adhere to the mucosa and easily penetrate through the mucosal barrier. (Khezri et al., 2019). Although EE% was detemined after initial characterization, it was not re-evaluated during stability testing.

5.8 Cytotoxicity Studies of NHT-loaded CS NPs and NHT-loaded BG-CS NPs

Nicotine is a highly addictive and poisonous drug (Alhusban & Ata, 2020). It has been reported that CS has been most widely investigated in terms of efficiency and safety (Sonin et al., 2020). Formulations F1, F2, F1" and F2" showed high fibroblast and Calu-3 cell viability, suggesting that the CS NPs and BG-CS NPs were minimal toxicity for intranasal administration. Nicotine is passively transported across Calu-3 airway cells, and this process gets better over time. The type of nicotine salt and pH have a significant impact on permeability, with nicotine benzoate exhibiting the maximum transport (Chu et al., 2023). Researchers found that CS, when administered nasally, improves absorption without causing any side effects (Chengcheng et al., 2011).

The cytotoxicity of CS NPs is concentration-dependent (Sarangapani et al., 2018). The slight reduction in cell viability at higher concentrations may be attributed to increased NPs cell membrane interactions and enhanced cellular uptake (Behzadi et al., 2017). Conversely, lower concentrations generally exhibit improved cytocompatibility due to reduced cellular stress. This trend was observed in the present study, where higher concentrations, particularly 0.5 mM, produced lower cell viability than lower concentrations. These findings are consistent with previous studies reporting the dose-dependent cytotoxicity of CS NPs.

The increased sensitivity of epithelial cells was reflected by the continuously higher vitality of fibroblasts compared to Calu-3 cells (**$p \leq 0.01$-****$p \leq 0.0001$). Changes in the CS:TPP ratio or formulation alterations did not negatively impact cellular vitality, as indicated by the lack of statistically significant variances ($p > 0.05$) in cell viability,

even if there were small numerical fluctuations within the same cell type. Vllasaliu et al. (2012) reported that Calu-3 cell viability remained above 80% following exposure to the tested CS concentrations, indicating low cytotoxicity. It also showed a stro ng opening of tight junctions by considerably reducing transepithelial electrical resistance to about 4-5% of baseline. This confirmed its efficacy as an absorption enhancer in Calu-3 epithelial models, leading to a significant improvement in permeability (around an 11-fold increase) (Vllasaliu et al., 2012). The NPs made of CS were well-tolerated by Calu-3 cells, preserving cell viability at or above 80% without causing major damage to the membrane. However, there was a small rise in inflammatory markers (Rodrigues et al., 2015). According to numerous reports, CS NPs show minimal cytotoxicity when tested on different cell lines and under different experimental settings. In fact, the majority of these studies show that cell viability is higher than 80%. Particularly, CS NPs crosslinked with TPP exhibited low cytotoxic effects and great biocompatibility, much like the current formulation. In addition, investigations conducted intranasally showed that the nasal mucosa was not irritated or structurally damaged, providing further evidence that they are safe for nasal delivery (Frigaard et al., 2022). There have been reports of enhanced safety profiles and cell
viability levels above 85-95% when using modified CS derivatives, such as PEGylated CS. These results demonstrate that CS-based NPs, especially after optimization or chemical modification, are cytocompatible and appropriate for use in biomedical applications (Clementino et al., 2025).

5.9 *In Vivo* Studies of NHT-loaded CS NPs and NHT-loaded BG-CS NPs

5.9.1 Pharmacokinetic Analysis

NHT has a high AUC, indicating that even small doses may achieve high levels in circulation, producing rapid neuropharmacological effects that increase rewarding potential (Bourdès et al., 2022). In the development of NRT and anti-smoking medications, the AUC is an important parameter (Azzopardi et al., 2022). Teichert et al. showed that the dose in the first AUC after 10 min was higher than the product Nicorette, which indicates that in the first interval, much nicotine is absorbed (Teichert et al., 2017). Although a lower AUC generally reflects reduced systemic drug exposure, AUC should not be taken in isolation. In the present study, the reduced AUC observed for the NPs formulations should be considered together with the prolonged MRT,

extended T½, slower *in vitro* nicotine release. These findings suggest that the NPs modified the pharmacokinetic profile by releasing nicotine more gradually over time rather than producing an immediate burst of drug. Therefore, the lower plasma exposure may be attributed to altered release kinetics and drug disposition as well as possible inadequate nasal absorption alone. Nevertheless, the contribution of reduced nasal absorption or bioavailability cannot be completely excluded since it's a vital indicator with significant changes in plasma despite the nasal permeability and absolute bioavailability were limited in the present study. Furthermore, the pharmacokinetic study was limited to 6 hr to evaluate early NHT absorption and disposition. However, 24hr sampling in higher animal model is recommended to fully characterize the sustained profile and is acknowledged as a study limitation.

Our result indicates that an increased amount of NHT is converted to cotinine and accumulated in the body over time (Kim, 2019). The severity of nicotine withdrawal varies based on the dose of the drug, the length of exposure, and the type of exposure. A high AUC for nicotine indicates prolonged systemic exposure, potentially prolonging withdrawal symptoms following cessation (Skjei & Markou, 2003). Sustained nicotine release formulations may deliver more stable drug levels while reducing withdrawal symptoms, facilitating the success of smoking cessation programs.

The AUC values of all NPs formulations (F1, F2, F1″, and F2″) were significantly lower than those of free NHT, indicating reduced systemic nicotineexposure. The lower AUC observed for the NPs formulations may be attributed to the mucoadhesive properties of CS (Alcantara et al., 2022), which affects the prolonged residence time of the NPs on the nasal mucosa, thus promote gradual nicotine release rather than rapid systemic absorption (Mostafa et al., 2026). In our study, we did not look into this property due to difficulty in obtaining the nasal membrane from the mice, due to its small size. As mentioned earlier, higher animal model such as using sheeps or rabbits are better suited to allow this study to be conducted. It was observed that plasma nicotineconcentrations increased more slowly, while MRT and T½ were prolonged. Additionally, the contribution of incomplete absorption during the sampling period cannot be excluded because nasal mucoadhesion and permeation studies were not performed. However, these findings support a modified pharmacokinetic profile characterized by a more gradual nicotine release. With considerably prolonged T½, especially in F1: (548.25 min) and F2: (680 min), showing sustained release behavior, both F1 and F2 demonstrated identical AUC values of (191.77 ± 38.42 mg·min/mL) and (189.15 ±

47.96 mg·min/mL), respectively (**p ≤ 0.01). The results suggested slight differences in the pharmacokinetic behavior between F1” and F2”. However, there was a decrease in T½ when compared to F2, suggesting a less pronounced prolongation effect. Interestingly, F1″ had a very long T½ (409.2 min) than F2” :(278.1 min), which is in consistent with prolonged drug retention, whereas F2″ showed a higher MRT (513.2 min), which indicates prolonged residency even if there were no significant changes in elimination rate. In general, F1, F2, F1” and F2” show that CS NPs can lower AUC and change nicotine pharmacokinetics, while F1 and F2 show more T½ prolongation while F1" and F2" show better modulation of systemic exposure. One possible explanation for these differences is the variation in formulation composition and polymer network density (Ding et al., 2007).

Rapid absorption and fast systemic availability, which are features of nicotine free form, are reflected in the much greater AUC reported for NHT: (625.81 ± 83.23 mg·min/mL). The total accessible dose and duration of exposure are the primary determinants of nicotine AUC, according to previous research (Digard et al., 2012). Systems that provide rapid and continuous drug availability generally result in greater systemic exposure. Alternatively, the lower AUC observed for NPs formulations, may be attributed to the ability of the CS polymeric matrix to retain nicotine and slow its diffusion (Mohammed et al., 2017). Drug release from CSNPs is primarily governed by diffusion through the polymeric matrix, which acts as a diffusion barrier and provides sustained release. Consequently, the amount of nicotine available for rapid systemic absorption may be reduced despite prolonged residence time, as reflected by the increased T½ and MRT observed in the present study, slower in vitro release, is consistent with a more gradual nicotine release profile that limits peak systemic exposure, is indicated by the substantial drop in AUC found for F1, F2, F1″, and F2″. Sustained delivery systems, which control absorption kinetics and decrease burst release, are compatible with this characteristic. Additionally, the mucoadhesive qualities of CS and the prolonged nasal residence time are likely responsible for the prolonged T½ observed, which indicates delayed clearance and drug retention. In order to increase the amount of time that CS spends at the absorption site, its mucoadhesive properties allow it to form strong interactions with mucin through electrostatic binding of positively charged amino groups and negatively charged sialic acid residues. This interaction causes the drug to be released into the bloodstream at a slower rate, which could slow down the rate of absorption. Hejjaji et al. (2018) found that despite increased

retention and controlled release features, formulations based on CS NPs may show lower AUC values compared to free drug solutions.

Although MRT and AUMC did not show statistically significant differences between the NHT and NPs formulations, the overall trend supports a shift toward sustained pharmacokinetics. Collectively, these findings suggest that the NPs formulations modified pharmacokinetics by reducing systemic exposure (lower AUC) while prolonging drug residence time, which is desirable for improving safety and maintaining therapeutic effects.

NHT showed the largest AUC for cotinine (421.32 ± 34.22 mg·min/mL), suggesting that nicotine was converted into its principal metabolite. On the other hand, the cotinine exposure was reduced by the NPs formulations. F1 exhibited drop in AUC (127.40 ± 135.95 mg·min/mL, ****$p \leq 0.0001$) and F2 showed non-significant reduction (368.66 ± 69.59 mg·min/mL). Similarly, F2 demonstrated decline in AUC (241.8±90.9 mg·min/mL) (**$p \leq 0.01$), although F1 did not exhibit any significant change (346.1±28.7 mg·min/mL). AUMC also showed a declining trend, with F1 and F1″ showing a considerable decrease. The MRT and T½ values were similar across all formulations ($p > 0.05$), which means that cotinine elimination behavior was mostly unaltered.

Compared to free NHT, the AUC of cotinine was lower in NPs formulations, suggesting a reduced amount of nicotine metabolism. The amount and rate of nicotine biotransformation are reflected in the systemic exposure of cotinine, the principal metabolite of nicotine (Bao et al., 2004). The increased cotinine AUC for NHT indicates that the freely accessible nicotine is rapidly absorbed and undergoes significant first-pass metabolism (Tang et al., 2024). Contrarily, the sustained release characteristics of CS NPs are responsible for the reduced cotinine levels in F1, F2, F1″, and F2″. It can be inferred that the metabolite's elimination was unaffected since there were no notable changes in MRT and T½ of cotinine. However, the 6hrs sample time was chosen as it adequately captures the pharmacokinetic profile of NHT following intranasal treatment, while also reducing unnecessary animal usage (Yang et al., 2018; Clark & Sun, 2020). Previous study shown that the rate of absorption and the method of distribution have a significant impact on the pharmacokinetics of nicotine. To illustrate the difference, the absorption of nicotine from combustible cigarettes reaches its highest plasma concentration quickly (Tmax = 7 min), but the release profile of oral nicotine pouches is slower and more gradual (Tmax ≈ 60-65 min). Despite the fact that it takes longer for

the nicotine to enter the bloodstream after being administered orally, the (AUC_0 -6 hours) can still be as high as or higher than cigarette nicotine levels. This shows that the formulating and delivery mechanisms of a substance have a greater impact on systemic exposure than the nicotine content alone. Results from this investigation corroborate previous research showing that changes to drug delivery technologies, like NPs formulations, can affect systemic exposure and absorption kinetics (McEwan et al., 2021).

5.9.2 *In Vivo* Drug Distribution Study

The brain and lungs were selected because they are highly relevant to the pharmacological action and disposition of nicotine. The brain represents the primary target organ for nicotine, whereas the lungs represent the principal organ associated with conventional nicotine exposure through cigarette smoking. Despite the formulations demonstrating lower NHT concentrations in the brain and lungs than free NHT, this pattern may prove beneficial for smoking cessation studies, liable upon behavioral validation. The diminished availability of NHT to these essential regions results in a decreased concentration of cotinine, the principal metabolite linked to NHT adverse effects. Cotinine, as an indicator of NHT exposure, provides insight into the metabolic processing of NHT within the body (Kyerematen & Vesell, 1991). The rapid delivery is mostly attributed to the combustion process, facilitating quick absorption into the pulmonary epithelium (X. Feng et al., 2024). In contrast, NRT products are designed to provide a controlled and gradual release of NHT (Giulietti et al., 2020). Research demonstrates that reduced cotinine levels are associated with a diminished likelihood of relapse following smoking cessation efforts (Fu et al., 2022). The utilization of NRT formulations that produce diminished cotinine levels is an option to mitigate the addictive potential often associated with conventional smoking methods (Ellerbeck et al., 2018; Bowker et al., 2014). Free NHT exhibited fast brain clearance, whereas NHT-loaded CS NPs maintained sustained NHT concentrations during the first phase.

The results of the tissue distribution show that as compared to the NPs formulations, NHT showed substantially larger concentrations in the brain and lung. The results demonstrated that NHT was rapidly absorbed and distributed throughout the body, as it accumulated much more in the brain and lungs (****$p \leq 0.0001$). Statistically

significant differences were observed (*p ≤ 0.05, **p < 0.01) between the F1 and F2 formulations, which indicated significantly lower amounts, regulated release and limited immediate tissue exposure. Additionally, F1″ and F2″ demonstrated reduced accumulation. Since NHT is readily available and efficiently absorbed systemically, nicotine can penetrate biological membranes more rapidly, leading to greater amounts in the brain and lungs (Sai et al., 2019; Herman & Tarran, 2020). On the other hand, a sustained release behaviour is likely to blame for the decreased tissue dispersion seen in NPs formulations. This would explain how nicotine is slowly released from the CS matrix.

In addition, the cotinine distribution data showed that, in comparison to all NPs formulations, NHT had much larger quantities in lung and brain tissues. F1, F2, F1″, and F2″, on the other hand, exhibited extremely low amounts of cotininein both organs. According to earlier research, nicotine has a high uptake rate via the BBB (~3.1×10^{-2} ml/s/g), but its main metabolite, cotinine, has a much lower absorption rate (~2.0×10^{-3} ml/s/g), which is around ten times lower. Because of its low permeability and reliance on metabolic synthesis, cotinine is present at far lower concentrations in the brain than nicotine, which accumulates at a considerably faster rate (Lockman et al., 2005). These findings are consistent with previous reports suggesting that greater nicotine availability may increase brain exposure, whereas sustained-release formulations may reduce tissue nicotine and cotinine concentrations, while less readily available nicotine, as is the case with controlled-release devices, would lead to lower concentrations of cotinine in brain tissue. While nicotine is quickly absorbed by lung tissue, cotinine is produced by the body's metabolism and represents nicotine exposure instead of direct uptake by the tissues themselves. The quick availability and metabolism of nicotine is indicated by the higher cotinine levels in the NHT, while the regulated release and limited metabolic conversion are suggested by the low levels in the NPs formulations (Gibbs et al., 2015). It is assumed that the well-known properties such as mucoadhesion and permeation enhancing properties of CS altered tissue distribution following intranasal administration (Hassan et al., 2022; Omidian et al., 2024) which was the primary in - vivo objective of this research. However, the nasal permeability and direct nose-to-brain transport were beyond the design of in- vivo experimental scope and tissue distribution uniquely affirms the nasal deliver and future evaluations shall render additional mechanistic insights for the direct enhancement of nose to brain drug delivery.

CHAPTER 6
CONCLUSION AND RECOMMENDATION

6.1 Overall Conclusion

NHT-loaded CS NPs and NHT-loaded BG-CS NPs prepared by varying concentrations of CS and NHT, showed that ionic gelation method was a suitable method for their synthesis. The attachment of BG chains to CS via primary hydroxy groups has been achieved by protecting the free amino functionalities through phthaloylation. In DLS study, the lowest particle size was F2" with size of 69.42 ± 0.72 nm, F1" with 83.64 ± 1.73, F2 with 120.36 ± 3.23 nm, F3" with 139.4 ± 4.46 nm and F1 with 155.83 ± 6.28 nm. Higher and stable zeta potentials was found in formulations F2" with +36.93 ± 0.89 +mV, F2 with +36.06 ± 1.70 +mV, F1" with +31.93 ± 0.68 +mV and F1with +30.66 ± 2.51 +mV. Morphological analysis by TEM revealed that the NPs were spherical in shape especially for F2, F1" and F2". According to DSC analysis, the endothermic peaks, which were comparable to the peaks from the CS and BG-CS transition, moved to a lower temperature when the NHT-loaded CS NPs and NHT-loaded BG-CS NPs were present. In TGA analysis, NHT was more thermally stabilized after being encapsulated in the CS NPs and BG-CS NPs matrix. XRD and FTIR analyses indicated that NHT retransformed into its amorphous form after entrapment into CS and BG-CS particles. FTIR studies showed that the carboxyl peaks of NHT were slightly shifted due to encapsulation with CS and BG-CS but this peak was masked by the aldehyde peak. F3" gave a maximum DL% of 60.57 ± 2.06%, followed by F5" with 56.172.59%, F6 48.47 ± 0.57%, F1 46.28 ± 1.18% and F1" with 45.93 ± 7.18%. F1 had the maximum EE% 96.83 ± 0.152% followedby F2 96.16 ± 0.763%, F1" 95.27 ± 0.13% and F2" 93.61 ± 0.34%. F1 gave the maximum sustained release of 91.83% of the drug followed by F1": 87.02 % and F2" :75.39%. NHT loaded CS NPs and NHT loaded BG-CS NPs remained stable at 5 ± 3 °C and 25 ± 2 °C for 90 days. Cytotoxicity using fibroblast and Calu-3 cells showed cell viability of >70%, indicating that the NPs were minimal toxic. F1, F2, F1", and F2" demonstrated lower AUC values and prolonged T½compared with free NHT, suggesting sustained intranasal nicotine release. Hence, this present study defined CS and BG-CS NPs as potential intranasal delivery systems for NHT for sustained intranasal nicotine delivery. The chemical

modification of CS increased lipophilicity, which may promote interaction with the nasal epithelium and has the potential to improve intranasal delivery of NHT. In conclusion, this study has successfully established an effective and feasible way to develop NHT-loaded CS and NHT-loaded BG-CS NPs formulations. The outcomes of this study suggest that the developed nanoparticles have potential as sustained intranasal nicotine delivery systems. At the end of this work, it is expected that this project will provide a platform for further studies to ascertain the use of NHT loaded CS and BG-CS NPs in providing sustained intranasal nicotine delivery.

6.2 Limitation

Results from in *vitro* and animal models formed the basis of this preliminary clinical investigation. Because human physiology and reactions might vary greatly from preclinical models, additional research on the biocompatibility and long-term safety of the intranasal CS and BG-CS NHT formulation is necessary. To evaluate the potential side effects associated with formulation usage over an extended period of time, comprehensive toxicological investigations and clinical trials are required. The *in vitro* release study was performed in PBS (pH 7.4), which does not fully stimulate the physiological pH of the nasal cavity. Therefore, future studies should evaluate nicotine release under simulated nasal condition (pH 5.5-6.5) to better predict in vivo release behavior. Furthermore, the stability study focused on the physicochemical properties of the formulations. However, drug leakage or changes in EE% during storage were not evaluated. Future studies should investigate drug retention throughout storage. The 6 hr pharmacokinetic study may not have fully captured the 24hr NHT release profile; therefore, extended sampling is recommended. Lower absorption may be related to administering the formulation as nasal drops. Future studies should evaluate nasal spray administration and its effect on deposition and absorption.

In addition, mucoadhesion, permeation, and penetration studies were not performed in the present study. Mucoadhesion evaluation would have confirmed the interaction between the NPs and the nasal mucus, providing evidence of prolonged nasal residence and reduced mucociliary clearance (Largent, 1992; Dhawan et al., 2004). Likewise, permeation studies across the nasal epithelium would have clarified the extent of nicotine transport and absorption (Zhang et al., 2012), while penetration studies could have demonstrated the distribution and depth of NPs penetration within the nasal

mucosa (Watchorn et al., 2022). Collectively, these investigations would have provided valuable mechanistic insight into the intranasal delivery behavior of the developed formulation. Furthermore, these studies may help explain the lower AUC observed for NPs by distinguishing whether it resulted primarily from sustained drug release, prolonged nasal retention, or limited epithelial transport. Therefore, these evaluations should be included in future studies to establish a clearer correlation between the formulation characteristics and its pharmacokinetic performanc.

6.3 Future Directions

Research for a safe and effective nasal delivery method for nicotine addiction treatment is an ongoing and lengthy process. Investigating a more effective therapy alternative for nicotine dependence management is an ongoing process, and this study is just the beginning. The topic's complexity and the lack of accessible techniques have resulted in numerous un-answered questions. We have created a workable method for particle preparation, but there has to be more research into optimizing intranasal fo rmulation methods and animal models for intranasal drug delivery.

Further improvement is needed to maximize the translational application of CS NPs, despite their promising promise for intranasal nicotine delivery owing to their biocompatibility, mucoadhesive and sustained release behavior. Chemical modification of CS at the C2 amino group has been the subject of the majority of published studies, while modification at the C6 hydroxyl positionhas been mostly unexplored. The present work found that introducing BG to the polymer backbone increased its physicochemical properties, such as drug loading and particle size, but more research is needed to determine how dual alteration at C2 and C6 affects stability, brain targeting and permeability. The physiological variations in nasal structures make it difficult to translate results from in *vivo* animal research, which showed positive pharmacokinetic behavior and acceptablesafety profiles to humanuse. It’s also necessary to determine the modified CS derivatives long-term biodegradability.

The effectiveness of NHT-loaded CS and BG-CS NPs as an intranasal formulation has been investigated in this work, beginning with the acute response in an animal model. Examining the effectiveness of intranasal formulations of NHT-loaded CSNHT-loaded CS and BG-CS NPs particles in lowering nicotine use in rats’ model for the long term

requires future investigations to measure nicotine-mediated behaviors as well as clinically related blood levels of nicotine and cotinine.

REFERENCES

Abbas, H., Refai, H., Sayed, N. E., Rashed, L. A., Mousa, M. R., & Zewail, M. (2021). Superparamagnetic iron oxide loaded chitosan coated bilosomes for magnetic nose to brain targeting of resveratrol. *International Journal of Pharmaceutics, 610*, 121244. https://doi.org/10.1016/j.ijpharm.2021.121244

Abdelgawad, A. M., & Hudson, S. M. (2019). Chitosan nanoparticles: Polyphosphates cross-linking and protein delivery properties. *International Journal of Biological Macromolecules, 136*, 133–142. https://doi.org/10.1016/j.ijbiomac.2019.06.062

Abdelkader, R., Maabreh, R. S., Al-Dgheim, R., Altarawneh, N. S., Alrabab'a, M. H., Zaiton, H., Abdelmaksoud, A. S., Almagharbeh, W. T., Alnawafleh, K. A., Alfanash, H. A., Saleh, Z. T., & Elshatarat, R. A. (2024). The impact of tobacco use and nicotine addiction on health: A literature review of nursing interventions for smoking cessation. *Journal of Integrative Nursing, 6*(4), 218–230. https://doi.org/10.4103/jin.jin_110_24

Abeysekera, I., De Silva, R., Silva, D., Piumika, L., Jayathilaka, R., & Rajamanthri, L. (2024). Examining the influence of global smoking prevalence on stroke mortality: Insights from 27 countries across income strata. *BMC Public Health, 24*(1), Article 18250. https://doi.org/10.1186/s12889-024-18250-1

Abid, S., Hussain, T., Nazir, A., Zahir, A., & Khenoussi, N. (2019). A novel double-layered polymeric nanofiber-based dressing with controlled drug delivery for pain management in burn wounds. *Polymer Bulletin, 76*(12), 6387–6411. https://doi.org/10.1007/s00289-019-02727-w

Abioye, A. O., Issah, S., & Kola-Mustapha, A. T. (2015). Ex vivo skin permeation and retention studies on chitosan–ibuprofen–gellan ternary nanogel prepared by in situ ionic gelation technique—a tool for controlled transdermal delivery of ibuprofen. *International Journal of Pharmaceutics, 490* (1–2), 112–130. https://doi.org/10.1016/j.ijpharm.2015.05.030

Adekola, A. D., Mbata, A. O., & Ogbeta, C. P. (2023). Integrating multisectoral strategies for tobacco control: Evidence-based approaches and public health outcomes. *International Journal of Medical and All Body Health Research, 4*(1), 60–69. https://doi.org/10.54660/ijmbhr.2024.4.1.60-69

Adepu, S., & Ramakrishna, S. (2021). Controlled Drug Delivery Systems: current status and future directions. *Molecules, 26*(19), 5905. https://doi.org/10.3390/molecules26195905

Aderibigbe, B. A., & Naki, T. (2019). Chitosan-based nanocarriers for nose to brain delivery. *Applied Sciences, 9*(11), 2219. https://doi.org/10.3390/app9112219

Adivitiya, N., Kaushik, M. S., Chakraborty, S., Veleri, S., & Kateriya, S. (2021). Mucociliary Respiratory Epithelium Integrity in Molecular Defense and Susceptibility to Pulmonary Viral Infections. *Biology, 10*(2), 95. https://doi.org/10.3390/biology10020095

Adkison, S. E., O'Connor, R. J., Bansal-Travers, M., Hyland, A., Borland, R., Yong, H., Cummings, K. M., McNeill, A., Thrasher, J. F., Hammond, D., & Fong, G. T. (2013). Electronic nicotine delivery systems. *American Journal of Preventive Medicine, 44*(3), 207–215. https://doi.org/10.1016/j.amepre.2012.10.018

Adolf, L. A., & Heilbronner, S. (2022). Nutritional interactions between bacterial species colonising the human nasal cavity: Current knowledge and future prospects. *Metabolites, 12*(6), 489. https://doi.org/10.3390/metabo12060489

Ahmad, W. A., Ahmad, W. Y. W., Zakaria, Z. A., & Yusof, N. Z. (2011). Isolation of Pigment-Producing bacteria and characterization of the extracted pigments. In *Springer briefs in molecular science* (pp. 25–44). https://doi.org/10.1007/978-3-642-24520-6_2

Ainurofiq, A., Prasetya, A., Rahayu, B. G., Qadri, M. S. A., Kovusov, M., & Laksono, O. E. P. (2023). Recent developments in brain-targeted drug delivery systems via intranasal route. *Farmacja Polska, 78*(12), 695–708. https://doi.org/10.32383/farmpol/163334

Akash, M. S. H., & Rehman, K. (2025). Comprehensive Insights into Thermo Gravimetric Analysis. *In Essentials of Pharmaceutical Analysis* (pp. 899–929). https://doi.org/10.1007/978-981-96-5996-8_19

Akhtar, K., Khan, S. A., Khan, S. B., & Asiri, A. M. (2018). Scanning Electron Microscopy: Principle and Applications in Nanomaterials Characterization. *In Handbook of Materials Characterization* (pp. 113–145). https://doi.org/10.1007/978-3-319-92955-2_4

Alabsi, W., Eedara, B. B., Encinas-Basurto, D., Polt, R., & Mansour, H. M. (2022). Nose-to-brain delivery of therapeutic peptides as nasal aerosols. *Pharmaceutics, 14*(9), 1870. https://doi.org/10.3390/pharmaceutics14091870

Alastal, A., Kwaik, A. D. A., Malkawi, A. A., Baltzley, S., & Al-Ghananeem, A. M. (2023). Enhancing intranasal delivery and bioavailability of dihydroergotamine utilizing chitosan nanoparticles. *Journal of Clinical Pharmacy and Therapeutics, 2023*, Article 2284371. https://doi.org/10.1155/2023/2284371

Al-Awsi, G. R. L., Alameri, A. A., Al-Dhalimy, A. M. B., Gabr, G. A., & Kianfar, E. (2023). Application of nano-antibiotics in the diagnosis and treatment of infectious diseases. *Brazilian Journal of Biology, 84*, e264946. https://doi.org/10.1590/1519-6984.264946

Albarki, M. A., & Donovan, M. D. (2020). Bigger or smaller? Size and loading effects on nanoparticle uptake efficiency in the nasal mucosa. *AAPS PharmSciTech, 21*(8), 294. https://doi.org/10.1208/s12249-020-01837-3

Albetawi, S. (2022). Current research on spray -dried chitosan nanocomposite microparticles for pulmonary drug delivery. *Pharmaceutical Nanotechnology, 11*(2), 127–137. https://doi.org/10.2174/2211738511666221128093822

Alboksmaty, A., Agaku, I. T., Odani, S., & Filippidis, F. T. (2019). Prevalence and determinants of cigarette smoking relapse among US adult smokers: A longitudinal study. *BMJ Open, 9*(11),e031676. https://doi.org/10.1136/bmjopen-2019-031676

Alcantara, K. P., Nalinratana, N., Chutiwitoonchai, N., Castillo, A. L., Banlunara, W., Vajragupta, O., Rojsitthisak, P., & Rojsitthisak, P. (2022). Enhanced nasal deposition and Anti-Coronavirus effect of Favipiravir-Loaded mucoadhesive Chitosan–Alginate nanoparticles. Pharmaceutics, 14(12), 2680. https://doi.org/10.3390/pharmaceutics14122680

Al-Dahhan, W., Kadhom, M., Yousif, E., Mohammed, S., & Alkaim, A. (2021). Extraction and determination of nicotine in tobacco from selected local cigarette brands in Iraq. *Letters in Applied NanoBioScience, 11*(1), 3278–3290. https://doi.org/10.33263/lianbs111.32783290

Aldeek, F., Wagner, K., Haase, V., Sublette, E., & Lopez, V. (2025). Analysis and toxicological evaluation of nicotine degradants and impurities in oral tobacco products: A case study of on! PLUS nicotine pouches. *ACS Omega, 10*(6), 6267–6278. https://doi.org/10.1021/acsomega.5c00263

Alehosseini, E., Tabarestani, H. S., Kharazmi, M. S., & Jafari, S. M. (2022). Physicochemical, thermal, and morphological properties of chitosan

nanoparticles produced by ionic gelation. *Foods, 11*(23), 3841. https://doi.org/10.3390/foods11233841

Alewel, D. I., Jackson, T. W., Rentschler, K. M., Schladweiler, M. C., Astriab -Fisher, A., Gavett, S. H., Evansky, P. A., & Kodavanti, U. P. (2023). Differential transcriptomic alterations in nasal versus lung tissue of acrolein -exposed rats. *Frontiers in Toxicology, 5,* Article 1280230. https://doi.org/10.3389/ftox.2023.1280230

Alhusban, A. A., & Ata, S. A. (2020). Simple HPLC method for rapid quantification of nicotine content in e-cigarettes liquids. *Acta Chromatographica, 33*(3), 302–307. https://doi.org/10.1556/1326.2020.00832

Ali, G., Sharma, M., Salama, E., Ling, Z., & Li, X. (2022). Applications of chitin and chitosan as natural biopolymers: Potential sources, pretreatments, and degradation pathways. *Biomass Conversion and Biorefinery, 14*(4), 4567–4581. https://doi.org/10.1007/s13399-022-02684-x

Al-Nemrawi, N. K., Alsharif, S. S. M., & Dave, R. H. (2018). Preparation of chitosan-TPP nanoparticles: The influence of chitosan polymeric properties and formulation variables. *International Journal of Applied Pharmaceutics, 10* (5), 60. https://doi.org/10.22159/ijap.2018v10i5.26375

Alwahsh, W., Sahudin, S., Alkhatib, H., Bostanudin, M. F., & Alwahsh, M. (2024). Chitosan-based nanocarriers for pulmonary and intranasal drug delivery systems: A comprehensive overview of their applications. *Current Drug Targets, 25*(7), 492–511. https://doi.org/10.2174/0113894501301747240417103321

Amin, M. K., & Boateng, J. S. (2022). Enhancing stability and mucoadhesive properties of chitosan nanoparticles by surface modification with sodium alginate and polyethylene glycol for potential oral mucosa vaccine delivery. *Marine Drugs, 20*(3), 156. https://doi.org/10.3390/md20030156

Andrés, P., Alcaraz, A., Palacios, A., Rodríguez, B., Reynales-Shigematsu, L. M., Pinto, M., Castillo-Riquelme, M., Torres, E. P., Osorio, D. I., Huayanay, L., Munarriz, C. L., De Miera-Juárez, B. S., Gallegos-Rivero, V., De La Puente, C., Del Pilar Navia-Bueno, M., Caporale, J., Roberti, J., Virgilio, S. A., Augustovski, F., & Bardach, A. (2020). The health and economic burden of smoking in 12 Latin American countries and the potential effect of increasing

tobacco taxes: An economic modelling study. *The Lancet Global Health, 8*(10), e1282–e1294. https://doi.org/10.1016/s2214-109x(20)30311-9

Angevine, D. J., Camacho, K. J., Zhang, X., Rzayev, J., & Benedict, J. B. (2023). Enhancing the stability of nicotine via crystallization using enantiopure tartaric acid salt formers. *ACS Omega, 8*(17), 15535–15542. https://doi.org/10.1021/acsomega.3c00849

Angevine, D. J., Camacho, K. J., Zhang, X., Rzayev, J., & Benedict, J. B. (2023). Enhancing the stability of nicotine via crystallization using enantiopure tartaric acid salt formers. *ACS Omega, 8*(17), 15535–15542. https://doi.org/10.1021/acsomega.3c00849

Antoniraj, M. G., Leena, M. M., Moses, J., & Anandharamakrishnan, C. (2019). Cross-linked chitosan microparticles preparation by modified three fluid nozzle spray drying approach. *International Journal of Biological Macromolecules, 147*, 1268–1277. https://doi.org/10.1016/j.ijbiomac.2019.09.254

An, X., & Sha, X. (2023). Nanoparticle-mediated strategies for enhanced drug penetration and retention in the airway mucosa. Pharmaceutics, 15(10), 2457. https://doi.org/10.3390/pharmaceutics15102457

Aranaz, I., Alcántara, A. R., Civera, M. C., Arias, C., Elorza, B., Caballero, A. H., & Acosta, N. (2021). Chitosan: An overview of its properties and applications. *Polymers, 13*(19), 3256. https://doi.org/10.3390/polym13193256

Ardean, C., Davidescu, C. M., Nemeş, N. S., Negrea, A., Ciopec, M., Duteanu, N., Negrea, P., Duda-Seiman, D., & Musta, V. (2021). Factors influencing the antibacterial activity of chitosan and chitosan modified by functionalization. *International Journal of Molecular Sciences, 22* (14), 7449. https://doi.org/10.3390/ijms22147449

Arias, H. R., Feuerbach, D., Targowska-Duda, K., Kaczor, A. A., Poso, A., & Jozwiak, K. (2014). Pharmacological and molecular studies on the interaction of varenicline with different nicotinic acetylcholine receptor subtypes: Potential mechanism underlying partial agonism at human α4β2 and α3β4 subtypes. *Biochimica et Biophysica Acta (BBA) - Biomembranes, 1848*(2), 731–741. https://doi.org/10.1016/j.bbamem.2014.11.003

Arias, H. R., Targowska-Duda, K. M., García-Colunga, J., & Ortells, M. O. (2021). Is the antidepressant activity of selective serotonin reuptake inhibitors mediated

by nicotinic acetylcholine receptors? *Molecules, 26*(8), 2149. https://doi.org/10.3390/molecules26082149

Arya, S., Kumar, R., & Prakash, O. (2024). Nicotine and salts: Sedative, stimulants, and toxicological effects. In *Title of the book* (pp. 593–605). Elsevier. https://doi.org/10.1016/b978-0-323-95235-4.00084-0

Asgatay, S., Champion, C., Marloie, G., Drujon, T., Senamaud-Beaufort, C., Ceccaldi, A., Erdmann, A., Rajavelu, A., Schambel, P., Jeltsch, A., Lequin, O., Karoyan, P., Arimondo, P. B., & Guianvarc'h, D. (2013). Synthesis and evaluation of analogues of N-Phthaloyl-L-tryptophan (RG108) as inhibitors of DNA methyltransferase 1. *Journal of Medicinal Chemistry, 57*(2), 421–434. https://doi.org/10.1021/jm401419p

Askarizadeh, M., Esfandiari, N., Honarvar, B., Sajadian, S. A., & Azdarpour, A. (2023). Kinetic Modeling to Explain the Release of Medicine from Drug Delivery Systems. *ChemBioEng Reviews, 10*(6), 1006–1049. https://doi.org/10.1002/cben.202300027

Aslani, A., & Rafiei, S. (2012). Design, formulation and evaluation of nicotine chewing gum. *Advanced Biomedical Research, 1*(1), 57. https://doi.org/10.4103/2277-9175.100175

Ata, S., Rasool, A., Islam, A., Bibi, I., Rizwan, M., Azeem, M. K., Qureshi, A. U. R., & Iqbal, M. (2019). Loading of Cefixime to pH sensitive chitosan based hydrogel and investigation of controlled release kinetics. *International Journal of Biological Macromolecules, 155*, 1236–1244. https://doi.org/10.1016/j.ijbiomac.2019.11.091

Atay, H. Y. (2019). Antibacterial Activity of Chitosan-Based Systems. In *Functional Chitosan*. (pp. 457–489). https://doi.org/10.1007/978-981-15-0263-7_15

Atik, A., Günal, T., Bozkurt, P. A., Köse, S. N., Alp, B., Yandim, C., Kaleli, N. M., Kabay, G., & Kaleli-Can, G. (2023). Characterization of cisplatin loaded hydrophilic glycol chitosan modified eumelanin nanoparticles for potential controlled-release application. *Journal of Drug Delivery Science and Technology, 84*, 104440. https://doi.org/10.1016/j.jddst.2023.104440

Attri, K., Singh, M., & Bhalla, V. (2022). Xylometazoline loaded chitosan nanoparticles: Fabrication, optimization and evaluation for nasal congestion. *Indian Journal of Pharmaceutical Education and Research, 56* (3), 716–722. https://doi.org/10.5530/ijper.56.3.120

Aubin, H., Luquiens, A., & Berlin, I. (2013). Pharmacotherapy for smoking cessation: pharmacological principles and clinical practice. *British Journal of Clinical Pharmacology*, 77(2), 324–336. https://doi.org/10.1111/bcp.12116

Aziz, S. (2017). Morphological and Optical Characteristics of Chitosan(1−x) ($4 \leq x \leq 12$) Based Polymer Nano-Composites: Optical Dielectric Loss as an Alternative Method for Tauc's Model. *Nanomaterials, 7*(12), 444. https://doi.org/10.3390/nano7120444

Azzopardi, D., Ebajemito, J., McEwan, M., Camacho, O. M., Thissen, J., Hardie, G., Voisine, R., Mullard, G., Cohen, Z., & Murphy, J. (2022). A randomised study to assess the nicotine pharmacokinetics of an oral nicotine pouch and two nicotine replacement therapy products. *Scientific Reports, 12*(1), 6949. https://doi.org/10.1038/s41598-022-10544-x

Babb, S., Malarcher, A., Schauer, G. L., Asman, K., & Jamal, A. (2017). Quitting smoking among adults—United States, 2000–2015. *Morbidity and Mortality Weekly Report, 65*(52), 1457–1464. https://doi.org/10.15585/mmwr.mm6552a1

Babin, M., Ruest, A., Drouin, G., Sirois, K., Ouellet, S., & Gagnon, J. (2012). Regioselective pivaloylation of N-phthaloylchitosan: A promising soluble intermediate for chitosan chemistry. *Carbohydrate Research, 351*, 87–92. https://doi.org/10.1016/j.carres.2012.01.016

Bahadur, S., Pardhi, D. M., Rautio, J., Rosenholm, J. M., & Pathak, K. (2020). Intranasal nanoemulsions for direct nose-to-brain delivery of actives for CNS disorders. *Pharmaceutics, 12*(12), 1230. https://doi.org/10.3390/pharmaceutics12121230

Bahmanpour, A. H., Ghaffari, M., Ashraf, S., & Mozafari, M. (2020). Nanotechnology for pulmonary and nasal drug delivery. In *Elsevier eBooks* (pp. 561–579). https://doi.org/10.1016/B978-0-08-102985-5.00023-1

Bahmanpour, A., Ghaffari, M., Milan, P. B., Moztarzadeh, F., & Mozafari, M. (2020). Synthesis and characterization of thermosensitive hydrogel based on quaternized chitosan for intranasal delivery of insulin. *Biotechnology and Applied Biochemistry, 68*(2), 247–256. https://doi.org/10.1002/bab.1917

Baker, T. B., Piper, M. E., Stein, J. H., Smith, S. S., Bolt, D. M., Fraser, D. L., & Fiore, M. C. (2016). Effects of nicotine patch vs varenicline vs combination nicotine replacement therapy on smoking cessation at 26 weeks. *JAMA, 315*(4), 371–379. https://doi.org/10.1001/jama.2015.19284

Balfour, D. J. K. (2015). The role of mesoaccumbens dopamine in nicotine dependence. *Current Topics in Behavioral Neurosciences, 24* , 55–98. https://doi.org/10.1007/978-3-319-13482-6_3

Balsari, P., Gil, E., Marucco, P., Van De Zande, J., Nuyttens, D., Herbst, A., & Gallart, M. (2017). Field-crop-sprayer potential drift measured using test bench: Effects of boom height and nozzle type. *Biosystems Engineering, 154*, 3–13. https://doi.org/10.1016/j.biosystemseng.2016.10.015

Bangun, H., Tandiono, S., & Arianto, A. (2018). Preparation and evaluation of chitosan-tripolyphosphate nanoparticles suspension as an antibacterial agent. *Journal of Applied Pharmaceutical Science, 8*(12), 147–156. https://doi.org/10.7324/JAPS.2018.81217

Bansal, S., Liu, D., Mao, Q., Bauer, N., & Wang, B. (2024). Carbon monoxide as a potential therapeutic agent: A molecular analysis of its safety profiles. *Journal of Medicinal Chemistry, 67*(12), 9789–9815. https://doi.org/10.1021/acs.jmedchem.4c00823

Bao, Z., He, X., Ding, X., Prabhu, S., & Hong, J. (2004). Metabolism of nicotine and cotinine by human cytochrome P450 2A13. *Drug Metabolism and Disposition, 33*(2), 258–261. https://doi.org/10.1124/dmd.104.002105

Barooah, N., Sarma, R. J., Batsanov, A. S., & Baruah, J. B. (2006). Structural aspects of adducts of N-phthaloylglycine and its derivatives. *Journal of Molecular Structure, 791*(1–3), 122–130. https://doi.org/10.1016/j.molstruc.2006.01.025

Bashir, S. M., Rather, G. A., Patrício, A., Haq, Z., Sheikh, A. A., Shah, M. Z. U. H., Singh, H., Khan, A. A., Imtiyaz, S., Ahmad, S. B., Nabi, S., Rakhshan, R., Hassan, S., & Fonte, P. (2022). Chitosan nanoparticles: A versatile platform for biomedical applications. *Materials, 15*(19), 6521. https://doi.org/10.3390/ma15196521

Bates, S., Zografi, G., Engers, D., Morris, K., Crowley, K., & Newman, A. (2006). Analysis of amorphous and nanocrystalline solids from their X-ray diffraction patterns. *Pharmaceutical Research, 23*(10), 2333–2349. https://doi.org/10.1007/s11095-006-9086-2

Bayassi-Jakowicka, M., Lietzau, G., Czuba, E., Steliga, A., Waśkow, M., & Kowiański, P. (2021). Neuroplasticity and multilevel system of connections determine the integrative role of nucleus accumbens in the brain reward system. *International*

Journal of Molecular Sciences, 22(18), 9806. https://doi.org/10.3390/ijms22189806

Bayer, I. S. (2022). Recent advances in mucoadhesive interface materials, mucoadhesion characterization, and technologies. *Advanced Materials Interfaces, 9*(18), 2200211. https://doi.org/10.1002/admi.202200211

Behlke, L. M., Lenze, E. J., & Carney, R. M. (2020). The cardiovascular effects of newer antidepressants in older adults and those with or at high risk for cardiovascular diseases. *CNS Drugs, 34*(11), 1133–1147. https://doi.org/10.1007/s40263-020-00763-z

Behzadi, S., Serpooshan, V., Tao, W., Hamaly, M. A., Alkawareek, M. Y., Dreaden, E. C., Brown, D., Alkilany, A. M., Farokhzad, O. C., & Mahmoudi, M. (2017). Cellular uptake of nanoparticles: Journey inside the cell. *Chemical Society Reviews, 46*(14), 4218–4244. https://doi.org/10.1039/C6CS00636A

Benli, A. R., Erturhan, S., Oruc, M. A., Kalpakci, P., Sunay, D., & Demirel, Y. (2017). A comparison of the efficacy of varenicline and bupropion and an evaluation of the effect of the medications in the context of the smoking cessation programme. *Tobacco Induced Diseases, 15*(1), Article 15. https://doi.org/10.1186/s12971-017-0116-0

Benowitz, N. (2008). Clinical pharmacology of nicotine: Implications for understanding, preventing, and treating tobacco addiction. *Clinical Pharmacology & Therapeutics, 83*(4), 531–541. https://doi.org/10.1038/clpt.2008.3

Benowitz, N., Zevin, S., & Jacob, P. (1997). Sources of variability in nicotine and cotinine levels with use of nicotine nasal spray, transdermal nicotine, and cigarette smoking. *British Journal of Clinical Pharmacology, 43*(3), 259–267. https://doi.org/10.1111/j.1365-2125.1997.00566.x

Benowitz, N. L., & Liakoni, E. (2021). Tobacco use disorder and cardiovascular health. *Addiction, 117*(4), 1128–1138. https://doi.org/10.1111/add.15703

Beyazçiçek, Ö., Beyazçiçek, E., Özmerdivenli, R., & Demir, S. (2020). E-sigaralar: Yeni bir fenomen. *Sağlık Bilimlerinde Değer, 10*(3), 404–415. https://doi.org/10.33631/duzcesbed.748056

Bhatta, D. N., Bialous, S., Crosbie, E., & Glantz, S. (2019). Exceeding WHO Framework Convention on Tobacco Control (FCTC) obligations: Nepal overcoming tobacco industry interference to enact a comprehensive tobacco

control policy. *Nicotine & Tobacco Research, 22*(12), 2213–2223. https://doi.org/10.1093/ntr/ntz177

Bhumkar, D. R., & Pokharkar, V. B. (2006). Studies on effect of pH on cross -linking of chitosan with sodium tripolyphosphate: A technical note. *AAPS PharmSciTech, 7*(2), E138–E143. https://doi.org/10.1208/pt070250

Bilano, V., Gilmour, S., Moffiet, T., D'Espaignet, E. T., Stevens, G. A., Commar, A., Tuyl, F., Hudson, I., & Shibuya, K. (2015). Global trends and projections for tobacco use, 1990–2025: An analysis of smoking indicators from the WHO Comprehensive Information Systems for Tobacco Control. *The Lancet, 385*(9972), 966–976. https://doi.org/10.1016/S0140-6736(15)60264-1

Binesh, N., Babaloo, H., & Farhadian, N. (2023). Microencapsulation: Spray drying. In *Elsevier eBooks* (pp. 271–296). https://doi.org/10.1016/B978-0-323-85947-9.00010-8

Biswas, R., Mondal, S., Ansari, M. A., Sarkar, T., Condiuc, I. P., Trifas, G., & Atanase, L. I. (2025). Chitosan and its derivatives as nanocarriers for drug delivery. *Molecules*, *30*(6), 1297. https://doi.org/10.3390/molecules30061297

Blagodatskikh, I. V., Vyshivannaya, O. V., Tishchenko, N. A., Orlov, V. N., Tikhonov, V. E., Bezrodnykh, E. A., Ezernitskaya, M. A., & Khokhlov, A. R. (2023). Complexation between chitosan and carboxymethyl cellulose in weakly acidic, neutral, and weakly alkaline media. *International Journal of Biological Macromolecules*, *243*, 125277. https://doi.org/10.1016/j.ijbiomac.2023.125277

Boddu, S. H. S., & Kumari, S. (2020). A short review on the intranasal delivery of diazepam for treating acute repetitive seizures. *Pharmaceutics, 12*(12), 1167. https://doi.org/10.3390/pharmaceutics12121167

Bohrey, S., Chourasiya, V., & Pandey, A. (2016). Polymeric nanoparticles containing diazepam: Preparation, optimization, characterization, in vitro drug release and release kinetic study. *Nano Convergence, 3*(1), 3. https://doi.org/10.1186/s40580-016-0061-2

Bonasia, S., Bojanowski, M., & Robert, T. (2019). Embryology and anatomical variations of the ophthalmic artery. *Neuroradiology*, *62*(2), 139–152. https://doi.org/10.1007/s00234-019-02336-4

Boominathan, T., & Sivaramakrishna, A. (2021). Recent advances in the synthesis, properties, and applications of modified chitosan derivatives: Challenges and

opportunities. *Topics in Current Chemistry, 379*(3), 19. https://doi.org/10.1007/s41061-021-00331-z

Boonsongrit, Y., Mueller, B. W., & Mitrevej, A. (2007). Characterization of drug–chitosan interaction by 1H NMR, FTIR and isothermal titration calorimetry. *European Journal of Pharmaceutics and Biopharmaceutics, 69* (1), 388–395. https://doi.org/10.1016/j.ejpb.2007.11.008

Borkar, N. A., Thompson, M. A., Bartman, C. M., Khalfaoui, L., Sine, S., Sathish, V., Prakash, Y. S., & Pabelick, C. M. (2023). Nicotinic receptors in airway disease. *American Journal of Physiology-Lung Cellular and Molecular Physiology, 326*(2), L149–L163. https://doi.org/10.1152/ajplung.00268.2023

Bostanudin, M. F., Lalatsa, A., Górecki, D. C., & Barbu, E. (2020). Engineering butylglyceryl-modified polysaccharides towards nanomedicines for brain drug delivery. *Carbohydrate Polymers, 236,* 116060. https://doi.org/10.1016/j.carbpol.2020.116060

Bostanudin, M. F., Salam, A., Kayed, K., & Jan, N. (2023). Alkylated chitosan nanomaterials for enhanced antimicrobial activity and delivery of fusidic acid: Preparation and preliminary in vitro investigation. *Journal of Applied Polymer Science, 140*(26), e53990. https://doi.org/10.1002/app.53990

Boudieu, L., Mennetrier, M., Llorca, P., & Samalin, L. (2023). The efficacy and safety of intranasal formulations of ketamineand esketaminefor the treatment of major depressive disorder: A systematic review. *Pharmaceutics, 15*(12), 2773. https://doi.org/10.3390/pharmaceutics15122773

Bourdès, V., Dogterom, P., Aleman, A., Parmantier, P., Colas, D., Lemarchant, S., Marie, S., Chou, T., Abd-Elaziz, K., & Godfrin, Y. (2022). Safety, tolerability, pharmacokinetics and initial pharmacodynamics of a subcommissural organ-spondin-derived peptide: A randomized, placebo-controlled, double-blind, single ascending dose first-in-human study. *Neurology and Therapy, 11*(3), 1353–1374. https://doi.org/10.1007/s40120-022-00380-6

Bowker, K. A., Lewis, S., Coleman, T., Vaz, L. R., & Cooper, S. (2014). Comparison of cotinine levels in pregnant women while smoking and when using nicotine replacement therapy. *Nicotine & Tobacco Research, 16*(6), 895–898. https://doi.org/10.1093/ntr/ntu029

Brasselet, C., Pierre, G., Dubessay, P., Dols-Lafargue, M., Coulon, J., Maupeu, J., Vallet-Courbin, A., De Baynast, H., Doco, T., Michaud, P., & Delattre, C.

(2019). Modification of chitosan for the generation of functional derivatives. *Applied Sciences, 9*(7), 1321. https://doi.org/10.3390/app9071321

Brenner, S. (2010). Nanomedicine: Promises and challenges for the future of public health. *International Journal of Nanomedicine, 5*, 803–809. https://doi.org/10.2147/IJN.S13816

Brown, J., Hajek, P., McRobbie, H., Locker, J., Gillison, F., McEwen, A., Beard, E., & West, R. (2013). Cigarette craving and withdrawal symptoms during temporary abstinence and the effect of nicotine gum. *Psychopharmacology, 229*(1), 209–218. https://doi.org/10.1007/s00213-013-3100-2

Brunzell, D. H., McIntosh, J. M., & Papke, R. L. (2014). Diverse strategies targeting α7 homomeric and α6β2* heteromeric nicotinic acetylcholine receptors for smoking cessation. *Annals of the New York Academy of Sciences, 1327*(1), 27–45. https://doi.org/10.1111/nyas.12421

Büyük, N. İ., Arayici, P. P., Derman, S., Mustafaeva, Z., & Yücel, S. (2020). An optimization study for chitosan nanoparticles: Synthesis and characterization. *Celal Bayar Üniversitesi Fen Bilimleri Dergisi, 16*(2), 119–127. https://doi.org/10.18466/cbayarfbe.658921

Caldwell, B. O., & Crane, J. (2016). Combination nicotine metered dose inhaler and nicotine patch for smoking cessation: A randomized controlled trial. *Nicotine & Tobacco Research, 18*(10), 1944–1951. https://doi.org/10.1093/ntr/ntw093

Calva, C. B., & Fadel, J. R. (2018). Intranasal administration of orexin peptides: Mechanisms and therapeutic potential for age-related cognitive dysfunction. *Brain Research, 1731*, 145921. https://doi.org/10.1016/j.brainres.2018.08.024

Calvo, P., Remuñán-López, C., Vila-Jato, J. L., & Alonso, M. J. (1997). Novel hydrophilic chitosan–polyethylene oxide nanoparticles as protein carriers. *Journal of Applied Polymer Science, 63*(1), 125–132. https://doi.org/10.1002/(SICI)1097-4628(19970103)63:1

Cañas, J. E. C., Monge-Palacios, M., Grajales-González, E., & Sarathy, S. M. (2021). Early chemistry of nicotine degradation in heat-not-burn smoking devices and conventional cigarettes: Implications for users and second- and third-hand smokers. *The Journal of Physical Chemistry A, 125*(15), 3177–3188. https://doi.org/10.1021/acs.jpca.1c01650

Cao, Y., Tan, Y. F., Wong, Y. S., Liew, M. W. J., & Venkatraman, S. (2019). Recent advances in chitosan-based carriers for gene delivery. *Marine Drugs, 17*(6), 381. https://doi.org/10.3390/md17060381

Caprifico, A. E., Foot, P. J. S., Polycarpou, E., & Calabrese, G. (2020). Overcoming the blood–brain barrier: Functionalised chitosan nanocarriers. *Pharmaceutics, 12*(11), 1013. https://doi.org/10.3390/pharmaceutics12111013

Carrillo, N. (2021). Nicotine dependence and tobacco use disorder treatment. In *Psychiatry update* (pp. 101–111). https://doi.org/10.1007/978-3-030-86430-9_10

Casettari, L., & Illum, L. (2014). Chitosan in nasal delivery systems for therapeutic drugs. *Journal of Controlled Release, 190*, 189–200. https://doi.org/10.1016/j.jconrel.2014.05.003

Cellina, M., Gibelli, D., Cappella, A., Martinenghi, C., Belloni, E., & Oliva, G. (2020). Nasal cavities and the nasal septum: Anatomical variants and assessment of features with computed tomography. *The Neuroradiology Journal, 33*(4), 340–347. https://doi.org/10.1177/1971400920913763

Cha, S., Jang, J., Park, S., Ryu, S. M., Cho, S., & Yang, S. (2023). Cigarette smoke-induced respiratory response: Insights into cellular processes and biomarkers. *Antioxidants, 12*(6), 1210. https://doi.org/10.3390/antiox12061210

Chakravarthi, S. S., & Robinson, D. H. (2011). Enhanced cellular association of paclitaxel delivered in chitosan-PLGA particles. *International Journal of Pharmaceutics, 409*(1–2), 111–120. https://doi.org/10.1016/j.ijpharm.2011.02.034

Chan, G. C., Stjepanović, D., Lim, C., Sun, T., Anandan, A. S., Connor, J. P., Gartner, C., Hall, W. D., & Leung, J. (2021). A systematic review of randomized controlled trials and network meta-analysis of e-cigarettes for smoking cessation. *Addictive Behaviors, 119*, 106912. https://doi.org/10.1016/j.addbeh.2021.106912

Chatzitaki, A., Jesus, S., Karavasili, C., Andreadis, D., Fatouros, D. G., & Borges, O. (2020). Chitosan-coated PLGA nanoparticles for the nasal delivery of ropinirole hydrochloride: In vitro and ex vivo evaluation of efficacy and safety. *International Journal of Pharmaceutics, 589*, 119776. https://doi.org/10.1016/j.ijpharm.2020.119776

Chen, H., & Chen, C. (2022). Evaluation of calibration equations by using regression analysis: An example of chemical analysis. *Sensors*, *22*(2), 447. https://doi.org/10.3390/s22020447

Chen, M., Wu, Y., & Jafvert, C. T. (2017). Synthesis of cross-linked cationic surfactant nanoparticles for removing anions from water. *Environmental Science: Nano*, *4*(7), 1534–1543. https://doi.org/10.1039/C7EN00382J

Chen, Q., Qi, Y., Jiang, Y., Quan, W., Luo, H., Wu, K., Li, S., & Ouyang, Q. (2022). Progress in research of chitosan chemical modification technologies and their applications. *Marine Drugs*, *20*(8), 536. https://doi.org/10.3390/md20080536

Chen, X. (2025). Research progress on the impact of humidification therapy on mucociliary clearance in tracheostomy patients. *Discover Medicine*, *2*(1). https://doi.org/10.1007/s44337-025-00508-1

Cheng, Y. (2002). Development of a novel nasal nicotine formulation comprising an optimal pulsatile and sustained plasma nicotine profile for smoking cessation. *Journal of Controlled Release*, *79*(1–3), 243–254. https://doi.org/10.1016/S0168-3659(01)00553-3

Chengcheng, F., Xiayan, S., Chi, Z., Qingfeng, L., Jie, C., Yehong, S., Qizhi, Z., & Xinguo, J. (2011). Effect of absorption enhancers on nasal delivery of basic fibroblast growth factor. *African Journal of Pharmacy and Pharmacology*, *5* (8), 1070–1079. https://doi.org/10.5897/AJPP11.157

Chik, M. W., Affandi, M. M. R. M. M., & Singh, G. K. S. (2022). Detection of astaxanthin at different regions of the brain in rats treated with astaxanthin nanoemulsion. *Journal of Pharmacy and Bioallied Sciences*, *14* (1), 25–30. https://doi.org/10.4103/jpbs.jpbs_464_21

Choi, C., Nam, J., & Nah, J. (2015). Application of chitosan and chitosan derivatives as biomaterials. *Journal of Industrial and Engineering Chemistry*, *33* , 1–10. https://doi.org/10.1016/j.jiec.2015.10.028

Chu, M., Deng, J., Hu, H., Wang, R., Li, D., Chen, Z., Liu, X., & Lu, J. (2023). Nicotine transport across Calu-3 cell monolayer: Effect of nicotine salts and flavored e-liquids. *Drug Development and Industrial Pharmacy*, *49* (10), 628–636. https://doi.org/10.1080/03639045.2023.2263791

Chung, S., Peters, J. M., Detyniecki, K., Tatum, W., Rabinowicz, A. L., & Carrazana, E. (2022). The nose has it: Opportunities and challenges for intranasal drug

administration for neurologic conditions including seizure clusters. *Epilepsy & Behavior Reports, 21*, 100581. https://doi.org/10.1016/j.ebr.2022.100581

Cinciripini, P. M., Green, C. E., Shete, S., Minnix, J. A., Robinson, J. D., Cui, Y., Kim, S., Kypriotakis, G., Beneventi, D., Blalock, J. A., Versace, F., & Karam-Hage, M. (2024). Smoking cessation after initial treatment failure with varenicline or nicotine replacement. *JAMA, 331*(20), 1722–1730. https://doi.org/10.1001/jama.2024.4183

Ciumărnean, L., Milaciu, M. V., Negrean, V., Orasan, O. H., Vesa, Ș. C., Sălăgean, O., Ilut, S., & Vlaicu, S. (2022). Cardiovascular risk factors and physical activity for the prevention of cardiovascular diseases in the elderly. *International Journal of Environmental Research and Public Health, 19* (1), 207. https://doi.org/10.3390/ijerph19010207

Clark, A., Tate, B., Urban, B., Schroeder, R., Gennuso, S., Ahmadzadeh, S., McGregor, D., Girma, B., Shekoohi, S., & Kaye, A. D. (2023). Bupropion-mediated effects on depression, attention deficit hyperactivity disorder, and smoking cessation. *Health Psychology Research, 11*, 81043. https://doi.org/10.52965/001c.81043

Clark, J. A. M., & Sun, D. (2020). Guidelines for the ethical review of laboratory animal welfare People's Republic of China National Standard GB/T 35892-2018 [Issued 6 February 2018, effective from 1 September 2018]. *Animal Models and Experimental Medicine, 3*(1), 103–113. https://doi.org/10.1002/ame2.12111

Clayton, P. M., Vas, C. A., Bui, T. T. T., Drake, A. F., & McAdam, K. (2012). Spectroscopic investigations into the acid–base properties of nicotine at different temperatures. *Analytical Methods, 5*(1), 81–88. https://doi.org/10.1039/C2AY25678A

Clementino, A., Climani, G., Bianchera, A., Buttini, F., & Sonvico, F. (2025). Polysaccharides: New frontiers for nasal administration of medicines. *Polysaccharides, 6*(1), 6. https://doi.org/10.3390/polysaccharides6010006

Cohen, E., & Poverenov, E. (2022). Hydrophilic chitosan derivatives: Synthesis and applications. *Chemistry—A European Journal, 28*(67), e202202156. https://doi.org/10.1002/chem.202202156

Collado-González, M., Espinosa, Y. G., & Goycoolea, F. M. (2019). Interaction between chitosan and mucin: Fundamentals and applications. *Biomimetics, 4*(2), 32. https://doi.org/10.3390/biomimetics4020032

Cortés, H., Alcalá-Alcalá, S., Caballero-Florán, I. H., Bernal-Chávez, S. A., Ávalos-Fuentes, A., González-Torres, M., Carmen, M. G., Figueroa-González, G., Reyes-Hernández, O. D., Floran, B., Del Prado-Audelo, M. L., & Leyva-Gómez, G. (2020). A reevaluation of chitosan-decorated nanoparticles to cross the blood–brain barrier. *Membranes, 10*(9), 212. https://doi.org/10.3390/membranes10090212

Craft, S., Baker, L. D., Montine, T. J., Minoshima, S., Watson, G. S., Claxton, A., Arbuckle, M., Callaghan, M., Tsai, E., Plymate, S. R., Green, P. S., Leverenz, J., Cross, D., & Gerton, B. (2012). Intranasal insulin therapy for Alzheimer disease and amnestic mild cognitive impairment: A pilot clinical trial. *Archives of Neurology, 69*(1), 29–38. https://doi.org/10.1001/archneurol.2011.233

Crowe, T. P., Greenlee, M. H. W., Kanthasamy, A. G., & Hsu, W. H. (2017). Mechanism of intranasal drug delivery directly to the brain. *Life Sciences, 195*, 44–52. https://doi.org/10.1016/j.lfs.2017.12.025

Crowe, T. P., & Hsu, W. H. (2022). Evaluation of recent intranasal drug delivery systems to the central nervous system. *Pharmaceutics, 14*(3), 629. https://doi.org/10.3390/pharmaceutics14030629

Curcio, M., Cirillo, G., Rouaen, J. R. C., Saletta, F., Nicoletta, F. P., Vittorio, O., & Iemma, F. (2020). Natural polysaccharide carriers in brain delivery: Challenge and perspective. *Pharmaceutics, 12*(12), 1183. https://doi.org/10.3390/pharmaceutics12121183

Danaei, M., Dehghankhold, M., Ataei, S., Davarani, F. H., Javanmard, R., Dokhani, A., Khorasani, S., & Mozafari, M. R. (2018). Impact of particle size and polydispersity index on the clinical applications of lipidic nanocarrier systems. *Pharmaceutics, 10*(2), 57. https://doi.org/10.3390/pharmaceutics10020057

Dash, M., Chiellini, F., Ottenbrite, R., & Chiellini, E. (2011). Chitosan—A versatile semi-synthetic polymer in biomedical applications. *Progress in Polymer Science, 36*(8), 981–1014. https://doi.org/10.1016/j.progpolymsci.2011.02.001

Da Silva Barbi, M., Carvalho, F. C., Kiill, C. P., Da Silva Barud, H., Santagneli, S. H., Ribeiro, S. J. L., & Gremião, M. P. D. (2014). Preparation and characterization of chitosan nanoparticles for zidovudine nasal delivery. *Journal of Nanoscience and Nanotechnology*, *15*(1), 865–874. https://doi.org/10.1166/jnn.2015.9180

Davraj, K., Yadav, M., Chappity, P., Sharma, P., Grover, M., Sharma, S., Kataria, T., Bhawna, K., Pendakur, A., Singh, G., Irugu, D. V. K., Singh, A., & Gupta, N.

(2021). Nasal physiology and sinusitis. In *Springer eBooks* (pp. 49–101). https://doi.org/10.1007/978-981-33-6284-0_3

De Barros, C., Aranha, N., Severino, P., Souto, E. B., Zielińska, A., Lopes, A., Rios, A., Batain, F., Crescencio, K., Chaud, M., & Alves, T. (2021). Quality by design approach for the development of liposome carrying ghrelin for intranasal administration. *Pharmaceutics, 13*(5), 686. https://doi.org/10.3390/pharmaceutics13050686

De Castro, K. C., Costa, J. M., & Campos, M. G. N. (2020b). Drug-loaded polymeric nanoparticles: A review. *International Journal of Polymeric Materials and Polymeric Biomaterials, 71*(1), 1–13. https://doi.org/10.1080/00914037.2020.1798436

De La Paz, N., Fernández, M., López, O., Garcia, C., Nogueira, A., Torres, L., Turiño, W., & Heinämäki, J. (2021). Spray drying of chitosan acid salts: Process development, scaling up and physicochemical material characterization. *Marine Drugs, 19*(6), 329. https://doi.org/10.3390/md19060329

Delijewski, M., Bartoń, A., Delijewska, P., Balwierz, R., Jakubiak, G., Kośmider, L., & Pawlas, N. (2019). Genetically determined metabolism of nicotine and its clinical significance. *Acta Biochimica Polonica, 66*(3), 277–283. https://doi.org/10.18388/abp.2019_2645

Denis, J., & Gagnon, J. (2022). Determination of the degree of quaternization of N,N,N-trimethylchitosan by CP-MAS 13C NMR. *Carbohydrate Research, 523*, 108736. https://doi.org/10.1016/j.carres.2022.108736

Deruyver, L., Rigaut, C., Gomez-Perez, A., Lambert, P., Haut, B., & Goole, J. (2023). In vitro evaluation of paliperidone palmitate-loaded cubosomes effective for nasal-to-brain delivery. *International Journal of Nanomedicine, 18*, 1085–1106. https://doi.org/10.2147/IJN.S397650

Desai, N., Rana, D., Salave, S., Gupta, R., Patel, P., Karunakaran, B., Sharma, A., Giri, J., Benival, D., & Kommineni, N. (2023). Chitosan: A potential biopolymer in drug delivery and biomedical applications. *Pharmaceutics, 15*(4), 1313. https://doi.org/10.3390/pharmaceutics15041313

Dessaix, A., Jardine, E., Freeman, B., & Kameron, C. (2022). Undermining Australian controls on electronic nicotine delivery systems: Illicit imports and illegal sales. *Tobacco Control, 31*(6), 689–690. https://doi.org/10.1136/tc-2022-057772

Dhawan, S., Singla, A. K., & Sinha, V. R. (2004). Evaluation of mucoadhesive properties of chitosan microspheres prepared by different methods. *AAPS PharmSciTech, 5*(4), 122–128. https://doi.org/10.1208/pt050467

Dholakia, J., Prabhakar, B., & Shende, P. (2021). Strategies for the delivery of antidiabetic drugs via intranasal route. *International Journal of Pharmaceutics, 608*, 121068. https://doi.org/10.1016/j.ijpharm.2021.121068

Diem, M., MacDonald, B. G., & Lee, E. K. C. (1981). Photolysis and laser-excited fluorescence and phosphorescence emission of trans-glyoxal in an argon matrix at 13 K. *The Journal of Physical Chemistry, 85*(15), 2227–2232. https://doi.org/10.1021/j150615a018

Digard, H., Proctor, C., Kulasekaran, A., Malmqvist, U., & Richter, A. (2012). Determination of nicotine absorption from multiple tobacco products and nicotine gum. *Nicotine & Tobacco Research, 15*(1), 255–261. https://doi.org/10.1093/ntr/nts123

Ding, L., Huang, Y., Cai, X., & Wang, S. (2018). Impact of pH, ionic strength and chitosan charge density on chitosan/casein complexation and phase behavior. *Carbohydrate Polymers, 208*, 133–141. https://doi.org/10.1016/j.carbpol.2018.12.015

Ding, P., Huang, K., Li, G., & Liu, Y. (2007). Preparation and properties of modified chitosan as potential matrix materials for drug sustained-release beads. *International Journal of Biological Macromolecules, 41* (2), 125–131. https://doi.org/10.1016/j.ijbiomac.2006.12.008

Ding, Y., Nielsen, K. A., Nielsen, B. P., Bøje, N. W., Müller, R. H., & Pyo, S. M. (2018). Lipid-drug-conjugate (LDC) solid lipid nanoparticles (SLN) for the delivery of nicotine to the oral cavity—Optimization of nicotine loading efficiency. *European Journal of Pharmaceutics and Biopharmaceutics, 128*, 10–17. https://doi.org/10.1016/j.ejpb.2018.03.004

Disease interrupted: Tobacco reduction and cessation . (n.d.). Google Books. https://books.google.jo/books?id=1ssoEAAAQBAJ

Dong, D., Li, H., Qin, M., Tian, J., Qiao, X., Hu, H., Song, Y., Wang, C., & Zhao, Y. (2024). Alterations in nasal airflow and air conditioning after endoscopic nasopharyngectomy for recurrent nasopharyngeal carcinoma: A pilot computational fluid dynamics study. *Computer Methods in Biomechanics and*

Biomedical Engineering, 1–14. https://doi.org/10.1080/10255842.2024.2406368

Dong, Y., Ng, W. K., Shen, S., Kim, S., & Tan, R. B. (2013). Scalable ionic gelation synthesis of chitosan nanoparticles for drug delivery in static mixers. *Carbohydrate Polymers*, *94*(2), 940–945. https://doi.org/10.1016/j.carbpol.2013.02.013

Doub, W. H., Suman, J. M., Copley, M., Goodey, A. P., Hosseini, S., & Mitchell, J. P. (2023). Laboratory performance testing of aqueous nasal inhalation products for droplet/particle size distribution: An assessment from the International Pharmaceutical Aerosol Consortium on Regulation and Science (IPAC-RS). *AAPS PharmSciTech*, *24*(7), 208. https://doi.org/10.1208/s12249-023-02665-x

D'Souza, A. A., Kutlehria, S., Huang, D., Bleier, B. S., & Amiji, M. M. (2021). Nasal delivery of nanotherapeutics for CNS diseases: Challenges and opportunities. *Nanomedicine*, *16*(30), 2651–2655. https://doi.org/10.2217/nnm-2021-0311

D'Souza, A. A., & Shegokar, R. (2016). Polyethylene glycol (PEG): A versatile polymer for pharmaceutical applications. *Expert Opinion on Drug Delivery*, *13*(9), 1257–1275. https://doi.org/10.1080/17425247.2016.1182485

Du, S., Wen, Z., Yu, J., Meng, Y., Liu, Y., & Xia, X. (2024). Breath and beyond: Advances in nanomedicine for oral and intranasal aerosol drug delivery. *Pharmaceuticals*, *17*(12), 1742. https://doi.org/10.3390/ph17121742

Du Sert, N. P., Hurst, V., Ahluwalia, A., Alam, S., Avey, M. T., Baker, M., Browne, W. J., Clark, A., Cuthill, I. C., Dirnagl, U., Emerson, M., Garner, P., Holgate, S. T., Howells, D. W., Karp, N. A., Lazic, S. E., Lidster, K., MacCallum, C. J., Macleod, M., . . . Würbel, H. (2020). The ARRIVE guidelines 2.0: Updated guidelines for reporting animal research. *PLoS Biology*, *18*(7), e3000410. https://doi.org/10.1371/journal.pbio.3000410

Duarte, J. L., Di Filippo, L. D., Vilella, K. J. A., Dutra, J. A. P., Ribeiro, D. M., Da Silva, M. F., De Medeiros, A. I., & Chorilli, M. (2024). Chitosan-coated nanoemulsion for intranasal administration increases temozolomide mucosal permeation, cellular uptake, and in vitro cytotoxicity in glioblastomamultiforme cells. *Journal of Drug Delivery Science and Technology*, *102* , 106390. https://doi.org/10.1016/j.jddst.2024.106390

Dudhani, A. R., & Kosaraju, S. L. (2010). Bioadhesive chitosan nanoparticles: Preparation and characterization. *Carbohydrate Polymers, 81*(2), 243–251. https://doi.org/10.1016/j.carbpol.2010.02.026

Eaton, D. L., Kwan, L. Y., & Stratton, K. (2018). Nicotine. In *Public health consequences of e-cigarettes*. National Academies Press.

Egorov, A. R., Kirichuk, A. A., Rubanik, V. V., Tskhovrebov, A. G., & Kritchenkov, A. S. (2023). Chitosan and its derivatives: Preparation and antibacterial properties. *Materials, 16*(18), 6076. https://doi.org/10.3390/ma16186076

Eker Fidan, E. B., Bal, K., & Pabuccuoğlu, S. K. (2025). A review on basic principles of mucoadhesion: The importance of chitosan as a mucoadhesive biopolymer. *ALKÜ Fen Bilimleri Dergisi, 6*(3), 174–194. https://doi.org/10.46740/alku.1511772

Ekpu, V. U., & Brown, A. K. (2015). The economic impact of smoking and of reducing smoking prevalence: Review of evidence. *Tobacco Use Insights, 8*, 1–35. https://doi.org/10.4137/TUI.S15628

Elabd, M. A., & Saleh, M. N. (2025). Sustainable strategies for extending strawberry shelf life: A comparative efficacy of ultrasonic, sonochemical, and chitosan-based coatings. *Food and Bioprocess Technology, 18*(11), 9706–9724. https://doi.org/10.1007/s11947-025-03994-4

Eliyan, Y., Varga-Huettner, V. E., & Pinto, J. M. (2023). Physiology of the aging nose and geriatric rhinitis. In *Springer eBooks* (pp. 157–178). https://doi.org/10.1007/978-3-031-12386-3_14

Ellerbeck, E. F., Nollen, N., Hutcheson, T. D., Phadnis, M., Fitzgerald, S. A., Vacek, J., Sharpe, M. R., Salzman, G. A., & Richter, K. P. (2018). Effect of long-term nicotine replacement therapy vs standard smoking cessation for smokers with chronic lung disease. *JAMA Network Open, 1*(5), e181843. https://doi.org/10.1001/jamanetworkopen.2018.1843

Elzamly, R. A., Mohamed, H. M., Mohamed, M. I., Zaky, H. T., Harding, D. R., & Kandile, N. G. (2021). New sustainable chemically modified chitosan derivatives for different applications: Synthesis and characterization. *Arabian Journal of Chemistry, 14*(8), 103255. https://doi.org/10.1016/j.arabjc.2021.103255

Erdlenbruch, B., Alipour, M., Fricker, G., Miller, D. S., Kugler, W., Eibl, H., & Lakomek, M. (2003). Alkylglycerol opening of the blood–brain barrier to small

and large fluorescence markers in normal and C6 glioma-bearing rats and isolated rat brain capillaries. *British Journal of Pharmacology*, *140*(7), 1201–1210. https://doi.org/10.1038/sj.bjp.0705554

Ezzaki, C., Chaari, A., & Al-Othman, A. (2025). Recent advances on chitosan-based nanoparticles for brain drug delivery. *Polymers*, *17*(22), 3055. https://doi.org/10.3390/polym17223055

Fan, W., Yan, W., Xu, Z., & Ni, H. (2011). Formation mechanism of monodisperse, low molecular weight chitosan nanoparticles by ionic gelation technique. *Colloids and Surfaces B: Biointerfaces*, *90* , 21–27. https://doi.org/10.1016/j.colsurfb.2011.09.042

Far, B. F., Omrani, M., Jamal, M. R. N., & Javanshir, S. (2023). Multi-responsive chitosan-based hydrogels for controlled release of vincristine. *Communications Chemistry*, *6*(1), 28. https://doi.org/10.1038/s42004-023-00829-1

Farcher, R., Syleouni, M. E., Vinci, L., & Mattli, R. (2023). Burden of smoking on disease-specific mortality, DALYs, and costs: The case of a high-income European country. *BMC Public Health*, *23*(1), 698. https://doi.org/10.1186/s12889-023-15535-9

Farsalinos, K., & Le Houezec, J. (2015). Regulation in the face of uncertainty: The evidence on electronic nicotine delivery systems (e-cigarettes). *Risk Management and Healthcare Policy*, *8*, 157–167. https://doi.org/10.2147/RMHP.S62116

Fathi, J. T., & Kathuria, H. (2023). Tobacco prevalence and treatment. In *Respiratory medicine* (pp. 49–69). Springer. https://doi.org/10.1007/978-3-031-38412-7_3

Fathy, M. M., Hassan, A. A., Elsayed, A. A., & Fahmy, H. M. (2023). Controlled release of silica-coated insulin-loaded chitosan nanoparticles as a promising oral administration system. *BMC Pharmacology and Toxicology*, *24*(1), 21. https://doi.org/10.1186/s40360-023-00662-1

Feng, C., Li, J., Kong, M., Liu, Y., Cheng, X. J., Li, Y., Park, H. J., & Chen, X. G. (2015). Surface charge effect on mucoadhesion of chitosan-based nanogels for local anti-colorectal cancer drug delivery. *Colloids and Surfaces B: Biointerfaces*, *128*, 439–447. https://doi.org/10.1016/j.colsurfb.2015.02.042

Feng, X., Shi, Y., Zhang, Y., Lei, F., Ren, R., & Tang, X. (2024b). Opportunities and challenges for inhalable nanomedicine formulations in respiratory diseases: A

review. *International Journal of Nanomedicine, 19*, 1509–1538. https://doi.org/10.2147/IJN.S446919

Feyisa, Z., Gupta, N. K., Edossa, G. D., Sundaramurthy, A., Kapoor, A., & Inki, L. G. (2023). Fabrication of pH-sensitive double cross-linked sodium alginate/chitosan hydrogels for controlled release of amoxicillin. *Polymer Engineering & Science, 63*(8), 2546–2564. https://doi.org/10.1002/pen.26395

Fidan, E. B. E., Bal, K., & Pabuccuoğlu, S. K. (2024). A review on basic principles of mucoadhesion: The importance of chitosan as a mucoadhesive biopolymer.

Flowers, L. (2016). Nicotine replacement therapy. *American Journal of Psychiatry Residents' Journal, 11*(6), 4–7. https://doi.org/10.1176/appi.ajp-rj.2016.110602

Folkow, L., & Nord, A. (2022, May 27). *The structure of nasal conchae in Svalbard rock ptarmigan (Lagopus muta hyperborea) with comparisons to three other Galliform birds*. https://hdl.handle.net/10037/25555

Foll, B. L., Piper, M. E., Fowler, C. D., Tonstad, S., Bierut, L., Lu, L., Jha, P., & Hall, W. D. (2022). Tobacco and nicotine use. *Nature Reviews Disease Primers, 8*(1), 19. https://doi.org/10.1038/s41572-022-00346-w

Fortuna, A., Schindowski, K., & Sonvico, F. (2022). Editorial: Intranasal drug delivery: Challenges and opportunities. *Frontiers in Pharmacology, 13*, 868986. https://doi.org/10.3389/fphar.2022.868986

Fouz-Rosón, N., Montemayor-Rubio, T., Almadana-Pacheco, V., Montserrat-García, S., Gómez-Bastero, A. P., Romero-Muñoz, C., & Polo-Padillo, J. (2017). Effect of 0.5 mg versus 1 mg varenicline for smoking cessation: A randomized controlled trial. *Addiction, 112*(9), 1610–1619. https://doi.org/10.1111/add.13855

Frigaard, J., Jensen, J. L., Galtung, H. K., & Hiorth, M. (2022). The potential of chitosan in nanomedicine: An overview of the cytotoxicity of chitosan-based nanoparticles. *Frontiers in Pharmacology, 13*, 880377. https://doi.org/10.3389/fphar.2022.880377

Fröhlich, E. (2012). The role of surface charge in cellular uptake and cytotoxicity of medical nanoparticles. *International Journal of Nanomedicine, 7*, 5577–5591. https://doi.org/10.2147/IJN.S36111

Fröhlich, E. (2022). Non-cellular layers of the respiratory tract: Protection against pathogens and target for drug delivery. *Pharmaceutics, 14*(5), 992. https://doi.org/10.3390/pharmaceutics14050992

Fu, Z., Qi, G., Qu, Z., Lin, X., Xu, L., Shen, B., Dong, F., & Ge, S. (2022). Higher blood cotinine level is associated with worse cognitive functioning in non-smoking older adults. *Frontiers in Neuroscience, 16*, 1080066. https://doi.org/10.3389/fnins.2022.1080066

Gagliardi, M., Chiarugi, S., De Cesari, C., Di Gregorio, G., Diodati, A., Baroncelli, L., Cecchini, M., & Tonazzini, I. (2023). Crosslinked chitosan nanoparticles with muco-adhesive potential for intranasal delivery applications. *International Journal of Molecular Sciences, 24*(7), 6590. https://doi.org/10.3390/ijms24076590

Galge, A. G., & Pagire, D. (2022). A review on transdermal patches. *International Journal of Research Publication and Reviews*, 1810–1824. https://doi.org/10.55248/gengpi.2022.3.10.60

Gandhi, S., Shastri, D. H., Shah, J., Nair, A. B., & Jacob, S. (2024). Nasal delivery to the brain: Harnessing nanoparticles for effective drug transport. *Pharmaceutics, 16*(4), 481. https://doi.org/10.3390/pharmaceutics16040481

Gan, Q., Wang, T., Cochrane, C., & McCarron, P. (2005). Modulation of surface charge, particle size and morphological properties of chitosan–TPP nanoparticles intended for gene delivery. *Colloids and Surfaces B: Biointerfaces, 44*(2–3), 65–73. https://doi.org/10.1016/j.colsurfb.2005.06.001

Gänger, S., & Schindowski, K. (2018). Tailoring formulations for intranasal nose-to-brain delivery: A review on architecture, physico-chemical characteristics and mucociliary clearance of the nasal olfactory mucosa. *Pharmaceutics, 10*(3), 116. https://doi.org/10.3390/pharmaceutics10030116

Gao, X., Liu, N., Wang, Z., Gao, J., Zhang, H., Li, M., Du, Y., Gao, X., & Zheng, A. (2021). Development and optimization of chitosan nanoparticle-based intranasal vaccine carrier. *Molecules, 27*(1), 204. https://doi.org/10.3390/molecules27010204

Gausterer, J. C., Schlager, M., Ahmadi, N., Nieratschker, M., Dahm, V., Wirth, M., Arnoldner, C., Honeder, C., & Gabor, F. (2023). A novel preparation technique for human nasal respiratory mucosa to disclose its glycosylation pattern for bioadhesive drug delivery. *Pharmaceutics, 15*(3), 973. https://doi.org/10.3390/pharmaceutics15030973

George, M., & Abraham, T. E. (2006). Polyionic hydrocolloids for the intestinal delivery of protein drugs: Alginate and chitosan—A review. *Journal of Controlled Release, 114*(1), 1–14. https://doi.org/10.1016/j.jconrel.2006.04.017

Georgieva, D., Nikolova, D., Vassileva, E., & Kostova, B. (2023). Chitosan-based nanoparticles for targeted nasal galantamine delivery as a promising tool in Alzheimer's disease therapy. *Pharmaceutics, 15*(3), 829. https://doi.org/10.3390/pharmaceutics15030829

Ghanbari, E., Picken, S. J., & Van Esch, J. H. (2023). Analysis of differential scanning calorimetry (DSC): Determining the transition temperatures, and enthalpy and heat capacity changes in multicomponent systems by analytical model fitting. *Journal of Thermal Analysis and Calorimetry, 148*(22), 12393–12409. https://doi.org/10.1007/s10973-023-12356-1

Gholap, V. V., Kosmider, L., Golshahi, L., & Halquist, M. S. (2020). Nicotine forms: Why and how do they matter in nicotine delivery from electronic cigarettes? *Expert Opinion on Drug Delivery, 17*(12), 1727–1736. https://doi.org/10.1080/17425247.2020.1814736

Gibbs, K., Collaco, J. M., & McGrath-Morrow, S. A. (2015). Impact of tobacco smoke and nicotine exposure on lung development. *CHEST Journal, 149*(2), 552–561. https://doi.org/10.1378/chest.15-1858

Gierszewska, M., & Ostrowska-Czubenko, J. (2016). Chitosan-based membranes with different ionic crosslinking density for pharmaceutical and industrial applications. *Carbohydrate Polymers, 153*, 501–511. https://doi.org/10.1016/j.carbpol.2016.07.126

Giratallah, H. K., Chenoweth, M. J., Addo, N., Ahluwalia, J. S., Cox, L. S., Lerman, C., George, T. P., Benowitz, N. L., & Tyndale, R. F. (2021). Nicotine metabolite ratio: Comparison of the three urinary versions to the plasma version and nicotine clearance in three clinical studies. *Drug and Alcohol Dependence, 223*, 108708. https://doi.org/10.1016/j.drugalcdep.2021.108708

Gisleskog, P. O. O., Ruixo, J. J. P., Westin, Å., Hansson, A. C., & Soons, P. A. (2020). Nicotine population pharmacokinetics in healthy smokers after intravenous, oral, buccal and transdermal administration. *Clinical Pharmacokinetics, 60*(4), 541–561. https://doi.org/10.1007/s40262-020-00960-5

Giulietti, F., Filipponi, A., Rosettani, G., Giordano, P., Iacoacci, C., Spannella, F., & Sarzani, R. (2020). Pharmacological approach to smoking cessation: An updated

review for daily clinical practice. *High Blood Pressure & Cardiovascular Prevention, 27*(5), 349–362. https://doi.org/10.1007/s40292-020-00396-9

Glantz, S. A., & Bareham, D. W. (2018). E-cigarettes: Use, effects on smoking, risks, and policy implications. *Annual Review of Public Health, 39*(1), 215–235. https://doi.org/10.1146/annurev-publhealth-040617-013757

Gokce, Y., Cengiz, B., Yildiz, N., Calimli, A., & Aktas, Z. (2014). Ultrasonication of chitosan nanoparticle suspension: Influence on particle size. *Colloids and Surfaces A: Physicochemical and Engineering Aspects, 462* , 75–81. https://doi.org/10.1016/j.colsurfa.2014.08.028

Goldberger, B. A., & Karch, S. (2022). *Karch's drug abuse handbook*. CRC Press. https://doi.org/10.4324/9781315155159

Gómez-Coronado, N., Walker, A. J., Berk, M., & Dodd, S. (2017). Current and emerging pharmacotherapies for cessation of tobacco smoking. *Pharmacotherapy: The Journal of Human Pharmacology and Drug Therapy, 38*(2), 235–258. https://doi.org/10.1002/phar.2073

Gong, Y., Chen, X., & Wu, W. (2024). Application of Fourier transform infrared (FTIR) spectroscopy in sample preparation: Material characterization and mechanism investigation. *Advances in Sample Preparation, 11*, 100122. https://doi.org/10.1016/j.sampre.2024.100122

González, M. M. (2023). CNS compartments: The anatomy and physiology of the cerebrospinal fluid. In *Liquorpheresis* (pp. 1–19). https://doi.org/10.1007/978-3-031-43482-2_1

Goodchild, M., Nargis, N., & D'Espaignet, E. T. (2017). Global economic cost of smoking-attributable diseases. *Tobacco Control, 27*(1), 58–64. https://doi.org/10.1136/tobaccocontrol-2016-053305

Gooneh-Farahani, S., Naghib, S. M., & Naimi-Jamal, M. R. (2020). A novel and inexpensive method based on modified ionic gelation for pH-responsive controlled drug release of homogeneously distributed chitosan nanoparticles with a high encapsulation efficiency. *Fibers and Polymers, 21*(9), 1917–1926. https://doi.org/10.1007/s12221-020-1095-y

Govind, A. P., Vallejo, Y. F., Stolz, J. R., Yan, J., Swanson, G. T., & Green, W. N. (2017). Selective and regulated trapping of nicotinic receptor weak base ligands and relevance to smoking cessation. *eLife, 6*, e25651. https://doi.org/10.7554/eLife.25651

Grant, D., Long, W. F., Moffat, C. F., & Williamson, F. B. (1989). Infrared spectroscopy of chemically modified heparins. *Biochemical Journal, 261*(3), 1035–1038. https://doi.org/10.1042/bj2611035

Grenha, A., Grainger, C. I., Dailey, L. A., Seijo, B., Martin, G. P., Remuñán-López, C., & Forbes, B. (2007). Chitosan nanoparticles are compatible with respiratory epithelial cells in vitro. *European Journal of Pharmaceutical Sciences, 31* (2), 73–84. https://doi.org/10.1016/j.ejps.2007.02.008

Grossman-Giron, A., Maoz, H., Nitzan, U., Kivity, Y., Zilcha-Mano, S., Bloch, Y., Mendlovic, S., & Bitan, D. T. (2023). Intranasal oxytocin as add-on treatment for inpatients with severe mental illness: A randomized clinical trial. *Neuropsychobiology, 82*(1), 14–23. https://doi.org/10.1159/000528314

Gu, D., Sung, H., Calfee, C. S., Wang, Y., Yao, T., & Max, W. (2024). Smoking-attributable health care expenditures for US adults with chronic lower respiratory disease. *JAMA Network Open, 7*(5), e2413869. https://doi.org/10.1001/jamanetworkopen.2024.13869

Guillén, J., Prins, J., Smith, D., & Degryse, A. (2013). The European framework on research animal welfare regulations and guidelines. In *Laboratory animals* (pp. 117–188). https://doi.org/10.1016/B978-0-12-397856-1.00005-2

Guo, H., Wang, G., Zhai, Z., Huang, J., Huang, Z., Zhou, Y., Xia, X., Yao, Z., Huang, Y., Zhao, Z., Wu, C., & Zhang, X. (2024). Rivastigmine nasal spray for the treatment of Alzheimer's disease: Olfactory deposition and brain delivery. *International Journal of Pharmaceutics, 652*, 123809. https://doi.org/10.1016/j.ijpharm.2024.123809

Gupta, K. C., & Kumar, M. N. V. R. (2000). An overview on chitin and chitosan applications with an emphasis on controlled drug release formulations. *Journal of Macromolecular Science, Part C: Polymer Reviews, 40* (4), 273–308. https://doi.org/10.1081/MC-100102399

Gupta, N., & Qanungo, K. (2023). Cigarette smoking and its association with lung cancer. *AIP Conference Proceedings, 2773*, 020004. https://doi.org/10.1063/5.0116996

Hamidi, F., Aghdam, M. A., Johar, F., Mehdinejad, M. H., & Baghani, A. N. (2021). Ionic gelation synthesis, characterization and adsorption studies of cross-linked chitosan-tripolyphosphate (CS-TPP) nanoparticles for removal of As(V) ions

from aqueous solution: Kinetic and isotherm studies. *Toxin Reviews, 41*(3), 795–805. https://doi.org/10.1080/15569543.2021.1933532

Hamman, J. H., Stander, M. W., & Kotzé, A. (2002). Effect of the degree of quaternisation of N-trimethyl chitosan chloride on absorption enhancement: In vivo evaluation in rat nasal epithelia. *International Journal of Pharmaceutics, 232*(1–2), 235–242. https://doi.org/10.1016/S0378-5173(01)00914-0

Hampsher-Monk, S. C., Prieger, J. E., & Patwardhan, S. (2024). Who is (still) smoking? In *Tobacco regulation, economics, and public health, Volume I* (pp. 31–146). Springer. https://doi.org/10.1007/978-3-031-41312-4_2

Hancock, B. C., & Zografi, G. (1997). Characteristics and significance of the amorphous state in pharmaceutical systems. *Journal of Pharmaceutical Sciences, 86*(1), 1–12. https://doi.org/10.1021/js9601896

Hansen, M. E., Ibrahim, Y., Desai, T. A., & Koval, M. (2024). Nanostructure-mediated transport of therapeutics through epithelial barriers. *International Journal of Molecular Sciences, 25*(13), 7098. https://doi.org/10.3390/ijms25137098

Hansson, A., Rasmussen, T., & Kraiczi, H. (2017). Single-dose and multiple-dose pharmacokinetics of nicotine 6 mg gum. *Nicotine & Tobacco Research, 19*(4), 477–483. https://doi.org/10.1093/ntr/ntw211

Haokip, H. R., Kumar, R., Rawat, V. S., & Sharma, S. K. (2020). Efficacy of standard nicotine replacement therapy (NRT) versus video-assisted nurse-led NRT on tobacco cessation: A randomized controlled pilot trial. *Clinical Epidemiology and Global Health, 9*, 141–146. https://doi.org/10.1016/j.cegh.2020.08.004

Hard, S. A. A. A., Shivakumar, H. N., & Redhwan, M. A. M. (2023). Development and optimization of in-situ gel containing chitosan nanoparticles for possible nose-to-brain delivery of vinpocetine. *International Journal of Biological Macromolecules, 253*(Pt. 6), 127217. https://doi.org/10.1016/j.ijbiomac.2023.127217

Harrell, P. T., Simmons, V. N., Correa, J. B., Padhya, T. A., & Brandon, T. H. (2014). Electronic nicotine delivery systems (e-cigarettes): Review of safety and smoking cessation efficacy. *Otolaryngology–Head and Neck Surgery, 151*(3), 381–393. https://doi.org/10.1177/0194599814536847

Hartmann-Boyce, J., Chepkin, S. C., Ye, W., Bullen, C., & Lancaster, T. (2018). Nicotine replacement therapy versus control for smoking cessation. *Cochrane*

Database of Systematic Reviews, 2018(5), Article CD000146. https://doi.org/10.1002/14651858.CD000146.pub5

Hassan, P. A., Rana, S., & Verma, G. (2014). Making sense of Brownian motion: Colloid characterization by dynamic light scattering. *Langmuir, 31*(1), 3–12. https://doi.org/10.1021/la501789z

Hassan, R. H., Gad, H. A., El-Din, S. B., Shaker, D. S., & Ishak, R. A. (2022). Chitosan nanoparticles for intranasal delivery of olmesartan medoxomil: Pharmacokinetic and pharmacodynamic perspectives. *International Journal of Pharmaceutics, 628*, 122278. https://doi.org/10.1016/j.ijpharm.2022.122278

Hatsukami, D. K., & Carroll, D. M. (2020). Tobacco harm reduction: Past history, current controversies and a proposed approach for the future. *Preventive Medicine, 140*, 106099. https://doi.org/10.1016/j.ypmed.2020.106099

Haverkamp, J., de Bie, M. J., & Vliegenthart, J. F. G. (1975). 13C- and 1H-N.M.R. spectroscopy of permethylated gluco-, galacto-, and manno-pyranoses and their 6-deoxy analogues. *Carbohydrate Research, 39*(2), 201–211. https://doi.org/10.1016/S0008-6215(00)86130-3

Hawari, F. I. (2018). Tobacco dependence: The whole story. *International Journal of Human and Health Sciences, 2*(3), 112. https://doi.org/10.31344/ijhhs.v2i3.38

He, C., Hu, Y., Yin, L., Tang, C., & Yin, C. (2010). Effects of particle size and surface charge on cellular uptake and biodistribution of polymeric nanoparticles. *Biomaterials, 31*(13), 3657–3666. https://doi.org/10.1016/j.biomaterials.2010.01.065

Hecht, S. S., & Hatsukami, D. K. (2022). Smokeless tobacco and cigarette smoking: Chemical mechanisms and cancer prevention. *Nature Reviews Cancer, 22*(3), 143–155. https://doi.org/10.1038/s41568-021-00423-4

Hejjaji, E. M., Smith, A. M., & Morris, G. A. (2018). Evaluation of the mucoadhesive properties of chitosan nanoparticles prepared using different chitosan to tripolyphosphate (CS:TPP) ratios. *International Journal of Biological Macromolecules, 120*(Pt. B), 1610–1617. https://doi.org/10.1016/j.ijbiomac.2018.09.185

Heng, P. P., Daud, F., Lim, K. H., & Yusoff, M. M. (2021). Susceptibility to e-cigarette initiation among tobacco product-naïve adolescents in Malaysia: Findings from the Tobacco and E-Cigarette Survey among Malaysian Adolescents (TECMA). *Tobacco Induced Diseases, 19*, 1–9. https://doi.org/10.18332/tid/142900

Herdiana, Y., Febrina, E., Nurhasanah, S., Gozali, D., Elamin, K. M., & Wathoni, N. (2024). Drug loading in chitosan-based nanoparticles. *Pharmaceutics, 16*(8), 1043. https://doi.org/10.3390/pharmaceutics16081043

Herdiana, Y., Wathoni, N., Shamsuddin, S., & Muchtaridi, M. (2022). Drug release study of the chitosan-based nanoparticles. *Heliyon, 8*(1), e08674. https://doi.org/10.1016/j.heliyon.2021.e08674

Herman, M., & Tarran, R. (2020). E-cigarettes, nicotine, the lung and the brain: Multi-level cascading pathophysiology. *The Journal of Physiology, 598*(22), 5063–5071. https://doi.org/10.1113/JP278388

Hewitt, R. J., & Lloyd, C. M. (2021). Regulation of immune responses by the airway epithelial cell landscape. *Nature Reviews Immunology, 21*(6), 347–362. https://doi.org/10.1038/s41577-020-00477-9

Hikisz, P., & Jacenik, D. (2023). The tobacco smoke component, acrolein, as a major culprit in lung diseases and respiratory cancers: Molecular mechanisms of acrolein cytotoxic activity. *Cells, 12*(6), 879. https://doi.org/10.3390/cells12060879

Hill, D. B., Button, B., Rubinstein, M., & Boucher, R. C. (2022). Physiology and pathophysiology of human airway mucus. *Physiological Reviews, 102*(4), 1757–1836. https://doi.org/10.1152/physrev.00004.2021

Hirlekar, R. S., & Momin, A. M. (2018). Advances in drug delivery from nose to brain: An overview. *Current Drug Therapy, 13*(1), 4–24. https://doi.org/10.2174/1574885512666170921145204

Ho, D., Frisch, S., Biehl, A., Terriac, E., de Rossi, C., Schwarzkopf, K., Lautenschläger, F., Loretz, B., Murgia, X., & Lehr, C.-M. (2018). Farnesylated glycol chitosan as a platform for drug delivery: Synthesis, characterization, and investigation of mucus–particle interactions. *Biomacromolecules, 19*(8), 3489–3501. https://doi.org/10.1021/acs.biomac.8b00795

Hoang, N. H., Thanh, T. L., Sangpueak, R., Treekoon, J., Saengchan, C., Thepbandit, W., Papathoti, N. K., Kamkaew, A., & Buensanteai, N. (2022). Chitosan nanoparticles-based ionic gelation method: A promising candidate for plant disease management. *Polymers, 14*(4), 662. https://doi.org/10.3390/polym14040662

Homayoonfal, M., Malekjani, N., Baeghbali, V., Ansarifar, E., Hedayati, S., & Jafari, S. M. (2022). Optimization of spray drying process parameters for the food

bioactive ingredients. *Critical Reviews in Food Science and Nutrition, 64* (17), 5631–5671. https://doi.org/10.1080/10408398.2022.2156976

Hong, P., Li, S., Ou, C., Li, C., Yang, L., & Zhang, C. (2007). Thermogravimetric analysis of chitosan. *Journal of Applied Polymer Science, 105* (2), 547–551. https://doi.org/10.1002/app.25920

Huang, H., Huang, S., Wang, T., Lin, T., Huang, N., Shih, O., Jeng, U., Chu, C., & Chiang, W. (2022). Clay nanosheets simultaneously intercalated and stabilized by PEGylated chitosan as drug delivery vehicles for cancer chemotherapy. *Carbohydrate Polymers, 302*, 120390. https://doi.org/10.1016/j.carbpol.2022.120390

Huang, Y., & Lapitsky, Y. (2016). On the kinetics of chitosan/tripolyphosphate micro- and nanogel aggregation and their effects on particle polydispersity. *Journal of Colloid and Interface Science, 486*, 27–37. https://doi.org/10.1016/j.jcis.2016.09.050

Hughes, J. R. (2016). Varenicline as a cause of suicidal outcomes. *Nicotine & Tobacco Research*, *18*(1), 2–9. https://doi.org/10.1093/ntr/ntu275

Husson, M., Harrington, L., Tochon, L., Cho, Y., Ibañez-Tallon, I., Maskos, U., & David, V. (2020). β4-nicotinic receptors are critically involved in reward-related behaviors and self-regulation of nicotine reinforcement. *Journal of Neuroscience*, *40*(17), 3465–3477. https://doi.org/10.1523/JNEUROSCI.0356-19.2020

Hussain, Z., & Sahudin, S. (2016). Preparation, characterisation and colloidal stability of chitosan-tripolyphosphate nanoparticles: Optimisation of formulation and process parameters. *International Journal of Pharmacy and Pharmaceutical Sciences, 8*(3), 297–308. https://innovareacademics.in/journals/index.php/ijpps/article/view/9450

Iacob, A. T., Lupascu, F. G., Apotrosoaei, M., Vasincu, I. M., Tauser, R. G., Lupascu, D., Giusca, S. E., Caruntu, I., & Profire, L. (2021). Recent biomedical approaches for chitosan-based materials as drug delivery nanocarriers. *Pharmaceutics, 13*(4), 587. https://doi.org/10.3390/pharmaceutics13040587

Ike, B. W., Nwabuife, J. C., Alake, J., Adu, D. K., Miya, L., Chauhan, R., Nate, Z., Karpoormath, R., & Faya, M. (2025). Release monitoring and detection of formulated solid nanoparticle–conjugated nicotine in blood and urine using

electrochemical technique. *Analytical Science Advances, 6*(1), e70018. https://doi.org/10.1002/ansa.70018

Ilahi, N. T., & Perry, M. (2021). The nose and associated structures: Part I. In *Springer eBooks* (pp. 1413–1432). https://doi.org/10.1007/978-3-030-53099-0_3

Illum, L. (2007). Nanoparticulate systems for nasal delivery of drugs: A real improvement over simple systems? *Journal of Pharmaceutical Sciences, 96*(3), 473–483. https://doi.org/10.1002/jps.20718

Inoue, D., Yamashita, A., & To, H. (2022). Formulation and *in vitro* characterization of a vacuum-dried drug–polymer thin film for intranasal application. *Polymers, 14*(14), 2954. https://doi.org/10.3390/polym14142954

Isfahani, M. N., Shokoohi, O., & Golshani, K. (2022). Intranasal ketamine versus intranasal fentanyl on pain management in isolated traumatic patients. *Journal of Research in Medical Sciences, 27*(1), 1. https://doi.org/10.4103/jrms.jrms_505_20

Islam, N. (2012). Improved treatment of nicotine addiction and emerging pulmonary drug delivery. *Drug Discoveries & Therapeutics, 6*(3), 123–131. https://doi.org/10.5582/ddt 2012.v6.3.123

Islam, S. U., Shehzad, A., Ahmed, M. B., & Lee, Y. S. (2020). Intranasal delivery of nanoformulations: A potential way of treatment for neurological disorders. *Molecules, 25*(8), 1929. https://doi.org/10.3390/molecules25081929

Jackson, S. E., Kotz, D., West, R., & Brown, J. (2019). Moderators of real-world effectiveness of smoking cessation aids: A population study. *Addiction, 114*(9), 1627–1638. https://doi.org/10.1111/add.14656

Jadhav, J. V., Anbu, P., Yadav, S., Pratap, A. P., & Kale, S. B. (2019). Sunflower acid oil-based production of rhamnolipid using Pseudomonas aeruginosa and its application in liquid detergents. *Journal of Surfactants and Detergents, 22*(3), 463–476. https://doi.org/10.1002/jsde.12255

Jafernik, K., Ładniak, A., Blicharska, E., Czarnek, K., Ekiert, H., Wiącek, A. E., & Szopa, A. (2023). Chitosan-based nanoparticles as effective drug delivery systems—A review. *Molecules, 28*(4), 1963. https://doi.org/10.3390/molecules28041963

Jain, A., & Jain, S. K. (2016). In vitro release kinetics model fitting of liposomes: An insight. *Chemistry and Physics of Lipids, 201*, 28–40. https://doi.org/10.1016/j.chemphyslip.2016.10.005

Jain, D., Chaudhary, P., Varshney, N., Razzak, K. S. B., Verma, D., Zahra, T. R. K., Janmeda, P., Sharifi-Rad, J., Daştan, S. D., Mahmud, S., Docea, A. O., & Calina, D. (2021). Tobacco smoking and liver cancer risk: Potential avenues for carcinogenesis. *Journal of Oncology, 2021*, 1–11. https://doi.org/10.1155/2021/5905357

Jain, R., Majumder, P., & Gupta, T. (2013). Pharmacological intervention of nicotine dependence. *BioMed Research International, 2013*, 1–8. https://doi.org/10.1155/2013/278392

Janes, K. A., & Alonso, M. J. (2003). Depolymerized chitosan nanoparticles for protein delivery: Preparation and characterization. *Journal of Applied Polymer Science, 88*(12), 2769–2776. https://doi.org/10.1002/app.12016

Janes, K. A., Fresneau, M. P., Marazuela, A., Fabra, A., & Alonso, M. J. (2001). Chitosan nanoparticles as delivery systems for doxorubicin. *Journal of Controlled Release, 73*(2–3), 255–267. https://doi.org/10.1016/S0168-3659(01)00294-2

Javed, H., Shah, S. N. H., & Iqbal, F. M. (2018). Formulation development and evaluation of diphenhydramine nasal nano-emulgel. *AAPS PharmSciTech, 19*(4), 1730–1743. https://doi.org/10.1208/s12249-018-0985-4

Jayakumar, R., Prabaharan, M., Nair, S., & Tamura, H. (2009). Novel chitin and chitosan nanofibers in biomedical applications. *Biotechnology Advances, 28*(1), 142–150. https://doi.org/10.1016/j.biotechadv.2009.11.001

Jennings, J. A. (2017). Controlling chitosan degradation properties in vitro and in vivo. In *Chitosan based biomaterials: Volume 1* (pp. 159–182). Elsevier. https://doi.org/10.1016/B978-0-08-100230-8.00007-8

Jeong, M. H., Kim, H. R., Bang, I. J., Yoo, S. H., Lee, S. J., Lee, K. H., & Chung, K. H. (2019). In vitro model for predicting acute inhalation toxicity by using a Calu-3 epithelium cytotoxicity assay. *Journal of Pharmacological and Toxicological Methods, 98*, 106576. https://doi.org/10.1016/j.vascn.2019.04.002

Jeong, S., Jang, J., & Lee, Y. (2022). Drug delivery to the brain via the nasal route of administration: Exploration of key targets and major consideration factors. *Journal of Pharmaceutical Investigation, 53*(1), 119–152. https://doi.org/10.1007/s40005-022-00589-5

Jha, P. (2020). The hazards of smoking and the benefits of cessation: A critical summation of the epidemiological evidence in high-income countries. *eLife, 9*, Article e49979. https://doi.org/10.7554/eLife.49979

Jha, R., & Mayanovic, R. A. (2023). A review of the preparation, characterization, and applications of chitosan nanoparticles in nanomedicine. *Nanomaterials, 13*(8), 1302. https://doi.org/10.3390/nano13081302

Jhaveri, J., Raichura, Z., Khan, T., Momin, M., & Omri, A. (2021). Chitosan nanoparticles—Insight into properties, functionalization and applications in drug delivery and theranostics. *Molecules, 26*(2), 272. https://doi.org/10.3390/molecules26020272

Jiang, W., Hao, J., & Han, Z. (2012). Study on the thermal degradation of mixtures of ammonium polyphosphate and a novel caged bicyclic phosphate and their flame retardant effect in polypropylene. *Polymer Degradation and Stability, 97*(4), 632–637. https://doi.org/10.1016/j.polymdegradstab.2012.01.001

Jiao, J., & Zhang, L. (2022). Nasal mucociliary clearance. In L. Zhang & C. Bachert (Eds.), *Chronic rhinosinusitis* (pp. 89–96). Springer. https://doi.org/10.1007/978-981-16-0784-4_11

Jiménez-Ruiz, C. A., Rabade-Castedo, C., de Higes Martinez, E., & de Granda-Orive, J. I. (2023). Some problems for smoking cessation. *Open Respiratory Archives, 6*(2), 100297. https://doi.org/10.1016/j.opresp.2023.100297

Jintapattanakit, A., Peungvicha, P., Sailasuta, A., Kissel, T., & Junyaprasert, V. B. (2010). Nasal absorption and local tissue reaction of insulin nanocomplexes of trimethyl chitosan derivatives in rats. *Journal of Pharmacy and Pharmacology, 62*(5), 583–591. https://doi.org/10.1211/jpp.62.05.0004

Jonassen, H., Kjøniksen, A.-L., & Hiorth, M. (2012). Stability of chitosan nanoparticles cross-linked with tripolyphosphate. *Biomacromolecules, 13*(11), 3747–3756. https://doi.org/10.1021/bm301207a

Jordan, C. J., & Xi, Z.-X. (2018). Discovery and development of varenicline for smoking cessation. *Expert Opinion on Drug Discovery, 13*(7), 671–683. https://doi.org/10.1080/17460441.2018.1458090

Jozanikohan, G., & Abarghooei, M. N. (2022). The Fourier transform infrared spectroscopy (FTIR) analysis for the clay mineralogy studies in a clastic reservoir. *Journal of Petroleum Exploration and Production Technology, 12*(8), 2093–2106. https://doi.org/10.1007/s13202-021-01449-y

Kabiri, M., Bolourian, H., Dehghan, S., & Tafaghodi, M. (2021). The dry powder formulation of mixed cross-linked dextran microspheres and tetanus toxoid-loaded trimethyl chitosan nanospheres as a potent adjuvant for nasal delivery system. *Iranian Journal of Basic Medical Sciences, 24* (1), 116–122. https://doi.org/10.22038/ijbms.2020.49486.11313

Kahdestani, S. A., Shahriari, M. H., & Abdouss, M. (2021). Synthesis and characterization of chitosan nanoparticles containing teicoplanin using sol–gel. *Polymer Bulletin, 78*(2), 1133–1148. https://doi.org/10.1007/s00289-020-03134-2

Kamala, K., Sankethguddad, S., & Sujith, S. (2019). An update on nicotine replacement therapy. *Journal of Oral Research and Review, 11*(2), 41. https://doi.org/10.4103/jorr.jorr_9_18

Kamaly, N., Yameen, B., Wu, J., & Farokhzad, O. C. (2016). Degradable controlled-release polymers and polymeric nanoparticles: Mechanisms of controlling drug release. *Chemical Reviews, 116*(4), 2602–2663. https://doi.org/10.1021/acs.chemrev.5b00346

Kamiloglu, S., Sari, G., Ozdal, T., & Capanoglu, E. (2020b). Guidelines for cell viability assays. *Food Frontiers, 1*(3), 332–349. https://doi.org/10.1002/fft2.44

Kang, D. S., Lee, N., Shin, D. Y., Jang, Y. J., Lee, S., Lim, K., Ahn, Y., Lee, C. M., & Seo, Y. R. (2022). Network-based integrated analysis for toxic effects of high-concentration formaldehyde inhalation exposure through the toxicogenomic approach. *Scientific Reports, 12*, 5645. https://doi.org/10.1038/s41598-022-09673-0

Karoyo, A. H., & Wilson, L. D. (2021). A review on the design and hydration properties of natural polymer-based hydrogels. *Materials, 14*(5), 1095. https://doi.org/10.3390/ma14051095

Kasaliwal, G. R., Göldel, A., Pötschke, P., & Heinrich, G. (2011). Influences of polymer matrix melt viscosity and molecular weight on MWCNT agglomerate dispersion. *Polymer, 52*(4), 1027–1036. https://doi.org/10.1016/j.polymer.2011.01.007

Kashyap, K., & Shukla, R. (2019). Drug delivery and targeting to the brain through nasal route: Mechanisms, applications and challenges. *Current Drug Delivery, 16*(10), 887–901. https://doi.org/10.2174/1567201816666191029122740

Kaur, A., Nigam, K., Bhatnagar, I., Sukhpal, H., Awasthy, S., Shankar, S., Tyagi, A., & Dang, S. (2020). Treatment of Alzheimer's disease using donepezil nanoemulsion: An intranasal approach. *Drug Delivery and Translational Research, 10*(6), 1862–1875. https://doi.org/10.1007/s13346-020-00754-z

Kaushal, A. M., Gupta, P., & Bansal, A. K. (2004). Amorphous drug delivery systems: Molecular aspects, design, and performance. *Critical Reviews in Therapeutic Drug Carrier Systems, 21*(3), 133–193. https://doi.org/10.1615/CritRevTherDrugCarrierSyst.v21.i3.10

Keane, H. (2013). Making smokers different with nicotine: NRT and quitting. *International Journal of Drug Policy, 24*(3), 189–195. https://doi.org/10.1016/j.drugpo.2013.01.011

Keller, L. A., Merkel, O., & Popp, A. (2022). Intranasal drug delivery: Opportunities and toxicologic challenges during drug development. *Drug Delivery and Translational Research, 12*, 735–757. https://doi.org/10.1007/s13346-020-00891-鼻

Khadam, V. K. R., Singh, R. P., Prajapati, D., Yunus, M., Prajapat, B., Rai, S. K., Kumari, P., & Gogoi, D. (2024). An updated comprehensive review on novel drug delivery systems (NDDS) in the pharmaceuticals. *Asian Journal of Pharmaceutical Research and Development, 12* (1), 55–64. https://doi.org/10.22270/ajprd.v12i1.1349

Khafagy, E., Soliman, G. A., Shahba, A. A., Aldawsari, M. F., Alharthy, K. M., Abdel-Kader, M. S., & Zaatout, H. H. (2023). Brain targeting by intranasal drug delivery: Effect of different formulations of the biflavone "cupressuflavone" from *Juniperus sabina* L. on the motor activity of rats. *Molecules, 28*(3), 1354. https://doi.org/10.3390/molecules28031354

Khalbas, A. H., Albayati, T. M., Ali, N. S., & Salih, I. K. (2024). Drug loading methods and kinetic release models using mesoporous silica nanoparticles as a drug delivery system: A review. *South African Journal of Chemical Engineering, 50*, 261–280. https://doi.org/10.1016/j.sajce.2024.08.013

Khan, H., Yerramilli, A. S., D'Oliveira, A., Alford, T. L., Boffito, D. C., & Patience, G. S. (2020). Experimental methods in chemical engineering: X-ray diffraction spectroscopy—XRD. *The Canadian Journal of Chemical Engineering, 98* (6), 1255–1266. https://doi.org/10.1002/cjce.23747

Khan, S., Berendt, R., Ellison, C., Ciavarella, A., Asafu-Adjaye, E., Khan, M., & Faustino, P. (2016). Bupropion hydrochloride. *Profiles of Drug Substances, Excipients, and Related Methodology*, *41*, 1–30. https://doi.org/10.1016/bs.podrm.2015.12.001

Khanna, K., Sharma, N., Karwasra, R., Kumar, A., Nishad, D. K., Janakiraman, A. K., Mani, R. R., Rajagopal, M., Tayyab, S., & Goel, B. (2025). Exploring nalbuphine-loaded chitosan nanoparticles for effective pain management through intranasal administration: A comparative study. *Journal of Drug Targeting*, *33*(1), 99–110. https://doi.org/10.1080/1061186X.2024.2397800

Khezri, F. A. N. Z., Lakshmi, C., Bukka, R., Nidhi, M., & Nargund, S. L. (2019). Pharmacokinetic study and brain tissue analysis of zolmitriptan-loaded chitosan nanoparticles in rats by LC–MS method. *International Journal of Biological Macromolecules*, *142*, 52–62. https://doi.org/10.1016/j.ijbiomac.2019.08.236

Khoerunnisa, F., Nurhayati, M., Dara, F., Rizki, R., Nasir, M., Aziz, H. A., Hendrawan, H., Poh, N. E., Kaewsaneha, C., & Opaprakasit, P. (2021). Physicochemical properties of TPP-crosslinked chitosan nanoparticles as potential antibacterial agents. *Fibers and Polymers*, *22*(11), 2954–2964. https://doi.org/10.1007/s12221-021-0397-z

Khunt, D., & Misra, M. (2021). An overview of anatomical and physiological aspects of the nose and the brain. In *Direct nose-to-brain drug delivery* (pp. 3–14). Elsevier. https://doi.org/10.1016/B978-0-12-822522-6.00029-1

Kienitz, R., Kay, L., Beuchat, I., Gelhard, S., von Brauchitsch, S., Mann, C., Lucaciu, A., Schäfer, J., Siebenbrodt, K., Zöllner, J., Schubert-Bast, S., Rosenow, F., Strzelczyk, A., & Willems, L. M. (2022). Benzodiazepines in the management of seizures and status epilepticus: A review of routes of delivery, pharmacokinetics, efficacy, and tolerability. *CNS Drugs*, *36*(9), 951–975. https://doi.org/10.1007/s40263-022-00940-2

Kim, S., Kim, H., Rhee, J., & Park, K. (2017). Versatile chemical derivatizations to design glycol chitosan-based drug carriers. *Molecules*, *22*(10), 1662. https://doi.org/10.3390/molecules22101662

Kim, S. (2019). Overview of cotinine cutoff values for smoking status classification. In *Preanalytics of biomedical diagnostics* (pp. 419–431). Elsevier. https://doi.org/10.1016/B978-0-12-813035-3.00051-4

Kim, E. S., Baek, Y., Yoo, H., Lee, J., & Lee, H. G. (2022). Chitosan-tripolyphosphate nanoparticles prepared by ionic gelation improve the antioxidant activities of astaxanthin in the *in vitro* and *in vivo* model. *Antioxidants, 11*(3), 479. https://doi.org/10.3390/antiox11030479

Kim, K., & Picciotto, M. R. (2023). Nicotine addiction: More than just dopamine. *Current Opinion in Neurobiology, 83*, 102797. https://doi.org/10.1016/j.conb.2023.102797

King, D. P., Paciga, S., Pickering, E., Benowitz, N. L., Bierut, L. J., Conti, D. V., Kaprio, J., Lerman, C., & Park, P. W. (2012). Smoking cessation pharmacogenetics: Analysis of varenicline and bupropion in placebo-controlled clinical trials. *Neuropsychopharmacology, 37*(3), 641–650. https://doi.org/10.1038/npp.2011.232

Klebe, S., Leigh, J., Henderson, D. W., & Nurminen, M. (2019). Asbestos, smoking and lung cancer: An update. *International Journal of Environmental Research and Public Health, 17*(1), 258. https://doi.org/10.3390/ijerph17010258

Klein, L. W. (2022). Pathophysiologic mechanisms of tobacco smoke producing atherosclerosis. *Current Cardiology Reviews, 18*(6), e110422203585. https://doi.org/10.2174/1573403X18666220411113112

Kolli, A. R., Kuczaj, A. K., Martin, F., Hayes, A. W., Peitsch, M. C., & Hoeng, J. (2019). Bridging inhaled aerosol dosimetry to physiologically based pharmacokinetic modeling for toxicological assessment: Nicotine delivery systems and beyond. *Critical Reviews in Toxicology, 49*(9), 725–741. https://doi.org/10.1080/10408444.2019.1692780

Kolli, A. R. (2023). Plasma protein binding and tissue retention kinetics influence the rate and extent of nicotine delivery to the brain. *Toxicology Letters, 380*, 69–74. https://doi.org/10.1016/j.toxlet.2023.04.006

Kongala, S. I., & Mamidala, P. (2023). Harpin-loaded chitosan nanoparticles induced defense responses in tobacco. *Carbohydrate Polymer Technologies and Applications, 5*, 100293. https://doi.org/10.1016/j.carpta.2023.100293

Koo, J., Lim, C., & Oh, K. T. (2024). Recent advances in intranasal administration for brain-targeting delivery: A comprehensive review of lipid-based nanoparticles and stimuli-responsive gel formulations. *International Journal of Nanomedicine, 19*, 1767–1807. https://doi.org/10.2147/IJN.S439181

Koukaras, E. N., Papadimitriou, S. A., Bikiaris, D. N., & Froudakis, G. E. (2012). Insight on the formation of chitosan nanoparticles through ionotropic gelation with tripolyphosphate. *Molecular Pharmaceutics, 9*(10), 2856–2862. https://doi.org/10.1021/mp300162j

Kruczkowska, W., Gałęziewska, J., Grabowska, K., Liese, G., Buczek, P., Kłosiński, K. K., Kciuk, M., Pasieka, Z., Kałuzińska-Kołat, Ż., & Kołat, D. (2024). Biomedical trends in stimuli-responsive hydrogels with emphasis on chitosan-based formulations. *Gels, 10*(5), 295. https://doi.org/10.3390/gels10050295

Kuen, C. Y., & Masarudin, M. J. (2022). Chitosan nanoparticle-based system: A new insight into the promising controlled release system for lung cancer treatment. *Molecules, 27*(2), 473. https://doi.org/10.3390/molecules27020473

Kumar, A., Cherian, S. V., Vassallo, R., Yi, E. S., & Ryu, J. H. (2018). Current concepts in pathogenesis, diagnosis, and management of smoking-related interstitial lung diseases. *Chest, 154*(2), 394–408. https://doi.org/10.1016/j.chest.2017.11.023

Kumar, M., Mandal, U. K., & Mahmood, S. (2023). Novel drug delivery system. In *Advances and challenges in pharmaceutical technology* (pp. 1–32). Elsevier. https://doi.org/10.1016/B978-0-323-91668-4.00012-5

Kumar, M. N. V. R., Muzzarelli, R. A. A., Muzzarelli, C., Sashiwa, H., & Domb, A. J. (2004). Chitosan chemistry and pharmaceutical perspectives. *Chemical Reviews, 104*(12), 6017–6084. https://doi.org/10.1021/cr030441b

Kumari, S., & Kishor, R. (2020). Chitin and chitosan: Origin, properties, and applications. In *Handbook of chitin and chitosan* (pp. 1–33). Elsevier. https://doi.org/10.1016/B978-0-12-817970-3.00001-8

Kurita, K., Kojima, T., Nishiyama, Y., & Shimojoh, M. (2000). Synthesis and some properties of nonnatural amino polysaccharides: Branched chitin and chitosan. *Macromolecules, 33*(13), 4711–4716. https://doi.org/10.1021/ma992113c

Kyerematen, G. A., & Vesell, E. S. (1991). Metabolism of nicotine. *Drug Metabolism Reviews, 23*(1–2), 3–41. https://doi.org/10.3109/03602539109029754

L, J. P., B, D. A., & B, S. R. (2017). A recent review on nasal microemulsion for treatment of CNS disorder. *International Journal of Current Pharmaceutical Research, 9*(4), 5. https://doi.org/10.22159/ijcpr.2017v9i4.20963

Latif, R., Makar, R. R., Hosni, E. A., & El-Gazayerly, O. N. (2021). The potential of intranasal delivery of nanocrystals in powder form on the improvement of zaleplon performance: In vitro and in vivo assessment. *Drug Development and*

Industrial Pharmacy, 47(2), 268–279. https://doi.org/10.1080/03639045.2021.1879834

Le, T. T., Méndez, D., & Warner, K. E. (2023). New estimates of smoking-attributable mortality in the U.S. from 2020 through 2035. *American Journal of Preventive Medicine, 66*(5), 877–882. https://doi.org/10.1016/j.amepre.2023.12.017

Leader, P., Alvarez, R., & Geiger, Z. (2023, June 5). Anatomy, head and neck, sphenopalatine artery. In *StatPearls*. StatPearls Publishing. https://www.ncbi.nlm.nih.gov/books/NBK539758/

Lee, P. I. (2011). Modeling of drug release from matrix systems involving moving boundaries: Approximate analytical solutions. *International Journal of Pharmaceutics, 418*(1), 18–27. https://doi.org/10.1016/j.ijpharm.2011.01.019

Leung, M. K. W., Bai, D., Yip, B. H. K., Fong, M. Y., Lai, P. M. H., Lai, P., Lai, I. S. Y., Lam, Z. H. W., Leung, A. T. F., To, D. K. Y., Wong, M. T., Wong, T. K., & Chao, D. V. K. (2019). Combined nicotinepatch with gum versus nicotine patch alone in smoking cessation in Hong Kong primary care clinics: A randomized controlled trial. *BMC Public Health, 19*, Article 1302. https://doi.org/10.1186/s12889-019-7634-z

Li, L., Zhang, H., Wen, J., Shen, Y., Li, D., Luo, C., Zheng, J., & Yang, J. (2022). Direct determination of free nicotine content in tobacco. *ACS Omega, 7*(27), 23061–23068. https://doi.org/10.1021/acsomega.2c00089

Li, X., Wang, Y., Feng, C., Chen, H., & Gao, Y. (2022). Chemical modification of chitosan for developing cancer nanotheranostics. *Biomacromolecules, 23*(6), 2197–2218. https://doi.org/10.1021/acs.biomac.2c00184

Li, Y., Giovannini, S., Wang, T., Fang, J., Li, P., Shao, C., Wang, Y., Agostini, M., Bove, P., Mauriello, A., Novelli, G., Piacentini, M., Rovella, V., Scimeca, M., Sica, G., Sun, Q., Tisone, G., Shi, Y., Candi, E., … Bernassola, F. (2023). p63: A crucial player in epithelial stemness regulation. *Oncogene, 42*(46), 3371–3384. https://doi.org/10.1038/s41388-023-02859-4

Lim, C., Hwang, D. S., & Lee, D. W. (2021). Intermolecular interactions of chitosan: Degree of acetylation and molecular weight. *Carbohydrate Polymers, 259*, 117782. https://doi.org/10.1016/j.carbpol.2021.117782

Lim, K. H., Teh, C. H., Pan, S., Ling, M. Y., Yusoff, M. F. M., Ghazali, S. M., Kee, C. C., Lim, K. K., Chong, K. H., & Lim, H. L. (2018). Prevalence and factors associated with smoking among adults in Malaysia: Findings from the National

Health and Morbidity Survey (NHMS) 2015. *Tobacco Induced Diseases, 16*, 1–11. https://doi.org/10.18332/tid/82190

Lima, R., Fernandes, C., & Pinto, M. M. M. (2022). Molecular modifications, biological activities, and applications of chitosan and derivatives: A recent update. *Chirality, 34*(9), 1166–1190. https://doi.org/10.1002/chir.23477

Lino, M. E. S., Ruela, A. L. M., Trevisan, M. G., & Pereira, G. R. (2017). Influence of hydration and crosslinking in transdermal delivery of nicotine from chitosan-based gels by thermal analysis. *Journal of Thermal Analysis and Calorimetry, 130*(3), 1455–1461. https://doi.org/10.1007/s10973-017-6129-3

Liu, H., & Gao, C. (2008). Preparation and properties of ionically cross-linked chitosan nanoparticles. *Polymers for Advanced Technologies, 20*(7), 613–619. https://doi.org/10.1002/pat.1306

Liu, X., & Yu, W. (2005). Evaluating the thermal stability of high performance fibers by TGA. *Journal of Applied Polymer Science, 99*(3), 937–944. https://doi.org/10.1002/app.22305

Liu, Z., Jiao, Y., Wang, Y., Zhou, C., & Zhang, Z. (2008). Polysaccharides -based nanoparticles as drug delivery systems. *Advanced Drug Delivery Reviews, 60*(15), 1650–1662. https://doi.org/10.1016/j.addr.2008.09.001

Lochhead, J. J., & Davis, T. P. (2019). Perivascular and perineural pathways involved in brain delivery and distribution of drugs after intranasal administration. *Pharmaceutics, 11*(11), 598. https://doi.org/10.3390/pharmaceutics11110598

Lockman, P. R., McAfee, G., Geldenhuys, W. J., Van der Schyf, C. J., Abbruscato, T. J., & Allen, D. D. (2005b). Brain uptake kinetics of nicotine and cotinine after chronic nicotine exposure. *Journal of Pharmacology and Experimental Therapeutics, 314*(2), 636–642. https://doi.org/10.1124/jpet.105.085381

Lombardo, R., Musumeci, T., Carbone, C., & Pignatello, R. (2021). Nanotechnologies for intranasal drug delivery: An update of literature. *Pharmaceutical Development and Technology, 26*(8), 824–845. https://doi.org/10.1080/10837450.2021.1950186

Lombardo, R., Ruponen, M., Rautio, J., Ghelardini, C., Di Cesare Mannelli, L., Calosi, L., Bani, D., Lampinen, R., Kanninen, K. M., Koivisto, A. M., Penttilä, E., Löppönen, H., & Pignatello, R. (2023). Development of lyophilised Eudragit® Retard nanoparticles for the sustained release of clozapine via intranasal

administration. *Pharmaceutics, 15*(5), 1554. https://doi.org/10.3390/pharmaceutics15051554

López-León, T., Carvalho, E. L. S., Seijo, B., Ortega-Vinuesa, J. L., & Bastos-González, D. (2004). Physicochemical characterization of chitosan nanoparticles: Electrokinetic and stability behavior. *Journal of Colloid and Interface Science, 283*(2), 344–351. https://doi.org/10.1016/j.jcis.2004.08.186

Lovinger, D. M., Mateo, Y., Johnson, K. A., Engi, S. A., Antonazzo, M., & Cheer, J. F. (2022). Local modulation by presynaptic receptors controls neuronal communication and behaviour. *Nature Reviews Neuroscience, 23*(4), 191–203. https://doi.org/10.1038/s41583-022-00561-0

Lowry, G. V., Hill, R. J., Harper, S., Rawle, A. F., Hendren, C. O., Klaessig, F., Nobbmann, U., Sayre, P., & Rumble, J. (2016). Guidance to improve the scientific value of zeta-potential measurements in nanoEHS. *Environmental Science: Nano, 3*(5), 953–965. https://doi.org/10.1039/C6EN00136J

Lu, B., Lv, X., & Le, Y. (2019). Chitosan-modified PLGA nanoparticles for controlled drug delivery. *Polymers, 11*(2), 304. https://doi.org/10.3390/polym11020304

Lucio, D., & Martínez-Ohárriz, M. C. (2017). Chitosan: Strategies to increase and modulate drug release rate. In *Chitosan-based systems for biopharmaceuticals: Delivery, targeting and polymer therapeutics*. IntechOpen. https://doi.org/10.5772/65714

Luppi, B., Bigucci, F., Cerchiara, T., & Zecchi, V. (2010). Chitosan-based hydrogels for nasal drug delivery: From inserts to nanoparticles. *Expert Opinion on Drug Delivery, 7*(7), 811–828. https://doi.org/10.1517/17425247.2010.495981

Lusiana, R. A., Protoningtyas, W. P., Wijaya, A. R., Siswanta, D., Mudasir, M., & Santosa, S. J. (2017). Chitosan-tripolyphosphate (CS-TPP) synthesis through cross-linking process: The effect of concentration towards membrane mechanical characteristic and urea permeation. *Oriental Journal of Chemistry, 33*(6), 2913–2919. https://doi.org/10.13005/ojc/330626

Macchi, M., Bambini, L., Franceschini, S., Alexa, I. D., & Agostoni, C. (2020). The effect of tobacco smoking during pregnancy and breastfeeding on human milk composition—A systematic review. *European Journal of Clinical Nutrition, 75*(5), 736–747. https://doi.org/10.1038/s41430-020-00784-3

Mahmoudi, M., Pakpour, S., & Perry, G. (2018). Drug-abuse nanotechnology: Opportunities and challenges. *ACS Chemical Neuroscience, 9*(10), 2288–2298. https://doi.org/10.1021/acschemneuro.8b00127

Maiyo, A. K., Kibet, J. K., & Kengara, F. O. (2022). A review of the characteristic properties of selected tobacco chemicals and their associated etiological risks. *Reviews on Environmental Health, 38*(3), 479–491. https://doi.org/10.1515/reveh-2022-0013

Makate, M., Whetton, S., Tait, R. J., Dey, T., Scollo, M., Banks, E., Norman, R., Pidd, K., Roche, A. M., & Allsop, S. (2019). Tobacco cost of illness studies: A systematic review. *Nicotine & Tobacco Research, 22*(4), 458–465. https://doi.org/10.1093/ntr/ntz038

Malik, A., Gupta, M., Gupta, V., Gogoi, H., & Bhatnagar, R. (2018). Novel application of trimethyl chitosan as an adjuvant in vaccine delivery. *International Journal of Nanomedicine, 13*, 7959–7970. https://doi.org/10.2147/IJN.S165876

Mamand, D. M., Hadi, J. M., Omer, R. A., & Aziz, S. B. (2024). FTIR, UV–Vis, and DFT approach to study the structural, optical and thermal properties of chitosan biopolymer. *Doklady Physical Chemistry, 518*(1–2), 137–154. https://doi.org/10.1134/S001250162460030X

Mandal, U., Mahmood, S., & Taher, M. (2014). Experimental design and optimization of raloxifene hydrochloride-loaded nanotransfersomes for transdermal application. *International Journal of Nanomedicine, 9*, 4331–4346. https://doi.org/10.2147/IJN.S65408

Manna, S., Seth, A., Gupta, P., Nandi, G., Dutta, R., & Jana, S. (2023). Chitosan derivatives as carriers for drug delivery and biomedical applications. *ACS Biomaterials Science & Engineering, 9*(5), 2181–2202. https://doi.org/10.1021/acsbiomaterials.2c01297

Marcela, S., & Agamennoni, O. (2024). Drug abuse: From biological to psychological dynamics. In *Psychiatry and neuroscience update—Vol. V* (pp. 141–155). Springer. https://doi.org/10.1007/978-3-031-72219-6_12

Marcello, E., & Chiono, V. (2023). Biomaterials-enhanced intranasal delivery of drugs as a direct route for brain targeting. *International Journal of Molecular Sciences, 24*(4), 3390. https://doi.org/10.3390/ijms24043390

Marcham, C. L., & Springston, J. P. (2019). Electronic cigarettes in the indoor environment. *Reviews on Environmental Health, 34*(2), 105–124. https://doi.org/10.1515/reveh-2019-0012

Marques, P., Piqueras, L., & Sanz, M. (2021). An updated overview of e-cigarette impact on human health. *Respiratory Research, 22*(1), Article 151. https://doi.org/10.1186/s12931-021-01737-5

Marsalek, R. (2014). Particle size and zeta potential of ZnO. *APCBEE Procedia, 9*, 13–17. https://doi.org/10.1016/j.apcbee.2014.01.003

Masarudin, M. J., Cutts, S. M., Evison, B. J., Phillips, D. R., & Pigram, P. J. (2015). Factors determining the stability, size distribution, and cellular accumulation of small, monodisperse chitosan nanoparticles as candidate vectors for anticancer drug delivery: Application to the passive encapsulation of [14C]-doxorubicin. *Nanotechnology, Science and Applications, 8* , 67–78. https://doi.org/10.2147/NSA.S91785

Masoudipour, E., Kashanian, S., Azandaryani, A. H., Omidfar, K., & Bazyar, E. (2017). Surfactant effects on the particle size, zeta potential, and stability of starch nanoparticles and their use in a pH-responsive manner. *Cellulose, 24*(10), 4217–4234. https://doi.org/10.1007/s10570-017-1426-3

Mathias, S. L., Pereira, R. V., de Menezes, A. J., & Dufresne, A. (2025). Synthesis of a chitosan derivative via conjugate addition-elimination with diethylethoxymethylenemalonate and its physicochemical properties. *Reactive and Functional Polymers, 208*, 106167. https://doi.org/10.1016/j.reactfunctpolym.2025.106167

Maurya, R., Vikal, A., Patel, P., Narang, R. K., & Kurmi, B. D. (2024). Enhancing oral drug absorption: Overcoming physiological and pharmaceutical barriers for improved bioavailability. *AAPS PharmSciTech, 25*(7), Article 228. https://doi.org/10.1208/s12249-024-02940-5

Mazurov, A., & Yohannes, D. (2014). Nicotinic acetylcholine receptor modulators. In *Topics in medicinal chemistry* (pp. 213–253). Springer. https://doi.org/10.1007/7355_2014_56

McEwan, M., Azzopardi, D., Gale, N., Camacho, O. M., Hardie, G., Fearon, I. M., & Murphy, J. (2021). A randomised study to investigate the nicotine pharmacokinetics of oral nicotine pouches and a combustible cigarette.

European Journal of Drug Metabolism and Pharmacokinetics, 47 (2), 211–221. https://doi.org/10.1007/s13318-021-00742-9

McKinney, D. L., & Vansickel, A. R. (2016). Nicotine chemistry, pharmacology, and pharmacokinetics. In V. R. Preedy (Ed.), *Neuropathology of drug addictions and substance misuse: Volume 1* (pp. 93–103). Elsevier. https://doi.org/10.1016/B978-0-12-800213-1.00009-2

McRobbie, H., & Kwan, B. (2020). Tobacco use disorder and the lungs. *Addiction, 116*(9), 2559–2571. https://doi.org/10.1111/add.15309

Mendonça, C., Rocha, S., Meireles, J., Pestana, P., Teixeira, C., & Aragão, I. (2015). Sustained-release bupropion overdose: A case report. *International Journal of Medical and Pharmaceutical Case Reports, 3*(2), 38–43. https://doi.org/10.9734/IJMPCR/2015/14703

Menku, B., Altiparmak, T., Genis, B., & Cosar, B. (2021). Adverse neuropsychiatric events associated with varenicline: A case series. *Psychiatry and Behavioral Sciences, 11*(1), 80. https://doi.org/10.5455/PBS.20201231094830

Menshawy, A., Ahmed, H., Ismail, A., Abushouk, A. I., Ghanem, E., Pallanti, R., & Negida, A. (2017). Intranasal sumatriptan for acute migraine attacks: A systematic review and meta-analysis. *Neurological Sciences, 39*(1), 31–44. https://doi.org/10.1007/s10072-017-3119-y

Menshutina, N., Majouga, A., Uvarova, A., Lovskaya, D., Tsygankov, P., Mochalova, M., Abramova, O., Ushakova, V., Morozova, A., & Silantyev, A. (2022b). Chitosan aerogel particles as nasal drug delivery systems. *Gels, 8*(12), 796. https://doi.org/10.3390/gels8120796

Mhlanga, N., & Ray, S. S. (2014). Kinetic models for the release of the anticancer drug doxorubicin from biodegradable polylactide/metal oxide-based hybrids. *International Journal of Biological Macromolecules, 72* , 1301–1307. https://doi.org/10.1016/j.ijbiomac.2014.10.038

Mi, F., Shyu, S., & Peng, C. (2005). Characterization of ring-opening polymerization of genipin and pH-dependent cross-linking reactions between chitosan and genipin. *Journal of Polymer Science Part A: Polymer Chemistry, 43*(10), 1985–2000. https://doi.org/10.1002/pola.20669

Midekessa, G., Godakumara, K., Ord, J., Viil, J., Lättekivi, F., Dissanayake, K., Kopanchuk, S., Rinken, A., Andronowska, A., Bhattacharjee, S., Rinken, T., & Fazeli, A. (2020). Zeta potential of extracellular vesicles: Toward understanding

the attributes that determine colloidal stability. *ACS Omega, 5*(27), 16701–16710. https://doi.org/10.1021/acsomega.0c01582

Mignani, S., Shi, X., Karpus, A., & Majoral, J. (2020). Non-invasive intranasal administration route directly to the brain using dendrimer nanoplatforms: An opportunity to develop new CNS drugs. *European Journal of Medicinal Chemistry, 209*, 112905. https://doi.org/10.1016/j.ejmech.2020.112905

Mikušová, V., & Mikuš, P. (2021). Advances in chitosan-based nanoparticles for drug delivery. *International Journal of Molecular Sciences, 22* (17), 9652. https://doi.org/10.3390/ijms22179652

Mills, E. J., Wu, P., Lockhart, I., Wilson, K., & Ebbert, J. O. (2010). Adverse events associated with nicotine replacement therapy (NRT) for smoking cessation: A systematic review and meta-analysis of one hundred and twenty studies involving 177,390 individuals. *Tobacco Induced Diseases, 8*(1), 8. https://doi.org/10.1186/1617-9625-8-8

Mills, E. J., Wu, P., Lockhart, I., Thorlund, K., Puhan, M., & Ebbert, J. O. (2012). Comparisons of high-dose and combination nicotine replacement therapy, varenicline, and bupropion for smoking cessation: A systematic review and multiple treatment meta-analysis. *Annals of Medicine, 44*(6), 588–597. https://doi.org/10.3109/07853890.2012.705016

Mircioiu, C., Voicu, V., Anuta, V., Tudose, A., Celia, C., Paolino, D., Fresta, M., Sandulovici, R., & Mircioiu, I. (2019). Mathematical modeling of release kinetics from supramolecular drug delivery systems. *Pharmaceutics, 11*(3), 140. https://doi.org/10.3390/pharmaceutics11030140

Mitchison, H. M., & Valente, E. M. (2016). Motile and non-motile cilia in human pathology: From function to phenotypes. *The Journal of Pathology, 241*(2), 294–309. https://doi.org/10.1002/path.4843

Mittal, D., Md, S., Hasan, Q., Fazil, M., Ali, A., Baboota, S., & Ali, J. (2014). Brain-targeted nanoparticulate drug delivery system of rasagiline via intranasal route. *Drug Delivery, 23*(1), 130–139. https://doi.org/10.3109/10717544.2014.907372

Mizoguchi, H., Wang, T., Kusaba, M., Fukumoto, K., & Yamada, K. (2018). Nicotine and varenicline ameliorate changes in reward-based choice strategy and altered decision-making in methamphetamine-treated rats. *Behavioural Brain Research, 359*, 935–941. https://doi.org/10.1016/j.bbr.2018.06.016

Mohammed, M. A., Syeda, J. T. M., Wasan, K. M., & Wasan, E. K. (2017). An overview of chitosan nanoparticles and its application in non-parenteral drug delivery. *Pharmaceutics, 9*(4), 53. https://doi.org/10.3390/pharmaceutics9040053

Molander, L., & Lunell, E. (2001). Pharmacokinetic investigation of a nicotine sublingual tablet. *European Journal of Clinical Pharmacology, 56* (11), 813–819. https://doi.org/10.1007/s002280000223

Molnár, É., Barbu, E., Lien, C., Górecki, D. C., & Tsibouklis, J. (2010). Toward drug delivery into the brain: Synthesis, characterization, and preliminary in vitro assessment of alkylglyceryl-functionalized chitosan nanoparticles. *Biomacromolecules, 11*(11), 2880–2889. https://doi.org/10.1021/bm100577x

Mostafa, H. G., Sheta, N. M., Farag, M. M., El-Dahmy, R. M., & Halim, S. A. A. (2026). Surface engineering of nanocarriers with polymer coatings: Materials, strategies, functional outcomes, and clinical translation. *Pharmaceutical Development and Technology, 31*(5), 877–905. https://doi.org/10.1080/10837450.2026.2693861

Mourya, V. K., & Inamdar, N. N. (2008). Chitosan-modifications and applications: Opportunities galore. *Reactive and Functional Polymers, 68*(6), 1013–1051. https://doi.org/10.1016/j.reactfunctpolym.2008.03.002

Mucha, M., & Pawlak, A. (2004b). Thermal analysis of chitosan and its blends. *Thermochimica Acta, 427*(1–2), 69–76. https://doi.org/10.1016/j.tca.2004.08.014

Mula, M. (2014). The safety and tolerability of intranasal midazolam in epilepsy. *Expert Review of Neurotherapeutics, 14*(7), 735–740. https://doi.org/10.1586/14737175.2014.925398

Mundorf, N., Redding, C. A., & Paiva, A. L. (2018). Sustainable transportation attitudes and health behavior change: Evaluation of a brief stage-targeted video intervention. *International Journal of Environmental Research and Public Health, 15*(1), 150. https://doi.org/10.3390/ijerph15010150

Mura, P., Maestrelli, F., Cirri, M., & Mennini, N. (2022). Multiple roles of chitosan in mucosal drug delivery: An updated review. *Marine Drugs, 20*(5), 335. https://doi.org/10.3390/md20050335

N, V., Sk, A. P., Yadala, P. C., & M, S. (2025). UV spectrophotometric method for the estimation of pure nicotine. *Journal of Innovations in Applied Pharmaceutical Science, 10*(3), 37–45. https://doi.org/10.37022/jiaps.v10i3.766

Naki, T., Peter, S., & Alven, S. (2025). Polymeric nanocarrier-based drug formulations for enhancing nose-to-brain delivery. *Pharmaceutics, 17*(10), 1242. https://doi.org/10.3390/pharmaceutics17101242

Nalini, T., Basha, S. K., Sadiq, A. M. M., Kumari, V. S., & Kaviyarasu, K. (2019). Development and characterization of alginate/chitosan nanoparticulate system for hydrophobic drug encapsulation. *Journal of Drug Delivery Science and Technology, 52*, 65–72. https://doi.org/10.1016/j.jddst.2019.04.002

Naskar, S., Kuotsu, K., & Sharma, S. (2018). Chitosan-based nanoparticles as drug delivery systems: A review on two decades of research. *Journal of Drug Targeting, 27*(4), 379–393. https://doi.org/10.1080/1061186X.2018.1512112

Nasti, A., Zaki, N. M., De Leonardis, P., Ungphaiboon, S., Sansongsak, P., Rimoli, M. G., & Tirelli, N. (2009). Chitosan/TPP and chitosan/TPP-hyaluronic acid nanoparticles: Systematic optimisation of the preparative process and preliminary biological evaluation. *Pharmaceutical Research, 26*(8), 1918–1930. https://doi.org/10.1007/s11095-009-9908-0

Nelson, V. A., Goniewicz, M. L., Beard, E., Brown, J., Sheals, K., West, R., & Shahab, L. (2015). Comparison of the characteristics of long-term users of electronic cigarettes versus nicotine replacement therapy: A cross-sectional survey of English ex-smokers and current smokers. *Drug and Alcohol Dependence, 153*, 300–305. https://doi.org/10.1016/j.drugalcdep.2015.05.005

Nerli, G., Robla, S., Bartalesi, M., Luceri, C., D'Ambrosio, M., Csaba, N., & Maestrelli, F. (2023). Chitosan-coated niosomes for nose-to-brain delivery of clonazepam: Formulation, stability and permeability studies. *CarCarbohydrate Polymer Technologies and Applications, 6*, 100332. https://doi.org/10.1016/j.carpta.2023.100332

Nestler, E. J., & Lüscher, C. (2019). The molecular basis of drug addiction: Linking epigenetic to synaptic and circuit mechanisms. *Neuron, 102*(1), 48–59. https://doi.org/10.1016/j.neuron.2019.01.016

Neto, C., Giacometti, J., Job, A., Ferreira, F., Fonseca, J., & Pereira. (2005b). Thermal analysis of chitosan-based networks. *Carbohydrate Polymers, 62*(2), 97–103. https://doi.org/10.1016/j.carbpol.2005.02.022

Nguyen, C., Mondoloni, S., Le Borgne, T., Centeno, I., Come, M., Jehl, J., Solié, C., Reynolds, L. M., Cuttoli, R. D., Tolu, S., Valverde, S., Didienne, S., Hannesse, B., Fiancette, J., Pons, S., Maskos, U., Deroche-Gamonet, V., Dalkara, D., Hardelin, J., . . . Faure, P. (2021). Nicotine inhibits the VTA-to-amygdala dopamine pathway to promote anxiety. *Neuron, 109*(16), 2604–2615.e9. https://doi.org/10.1016/j.neuron.2021.06.013

Nguyen, T., & Maeng, H. (2022). Pharmacokinetics and pharmacodynamics of intranasal solid lipid nanoparticles and nanostructured lipid carriers for nose-to-brain delivery. *Pharmaceutics, 14*(3), 572. https://doi.org/10.3390/pharmaceutics14030572

Nguyen, V. S., Rouxel, D., Hadji, R., Vincent, B., & Fort, Y. (2011). Effect of ultrasonication and dispersion stability on the cluster size of alumina nanoscale particles in aqueous solutions. *Ultrasonics Sonochemistry, 18*(1), 382–388. https://doi.org/10.1016/j.ultsonch.2010.07.003

Nikou, M., Chountoulesi, M., Pispas, S., & Pippa, N. (2026). From classics to nano-excipients and biopolymers: Pulmonary drug delivery formulations. *Pharmaceutics, 18*(1), 108. https://doi.org/10.3390/pharmaceutics18010108

Nogueira-Librelotto, D. R., Scheeren, L. E., Vinardell, M. P., Mitjans, M., & Rolim, C. M. (2016). Chitosan-tripolyphosphate nanoparticles functionalized with a pH-responsive amphiphile improved the *in vitro* antineoplastic effects of doxorubicin. *Colloids and Surfaces B: Biointerfaces*, *147*, 326–335. https://doi.org/10.1016/j.colsurfb.2016.08.014

Obeidat, W. M., Gharaibeh, S. F., & Jaradat, A. (2022). The influence of drugs solubilities and chitosan-TPP formulation parameters on the mean hydrodynamic diameters and drugs entrapment efficiencies into chitosan-TPP nanoparticles. *AAPS PharmSciTech, 23*(7), 262. https://doi.org/10.1208/s12249-022-02420-8

Obeidat, W. M., & Lahlouh, I. K. (2025). Chitosan nanoparticles: Approaches to preparation, key properties, drug delivery systems, and developments in therapeutic efficacy. *AAPS PharmSciTech, 26*, 108. https://doi.org/10.1208/s12249-025-03100-z

Ojeda-Hernández, D. D., Canales-Aguirre, A. A., Matias-Guiu, J., Gomez-Pinedo, U., & Mateos-Díaz, J. C. (2020). Potential of chitosan and its derivatives for biomedical applications in the central nervous system. *Frontiers in*

Bioengineering and Biotechnology, 8, 389. https://doi.org/10.3389/fbioe.2020.00389

Okorare, O., Evbayekha, E. O., Adabale, O. K., Daniel, E., Ubokudum, D., Olusiji, S. A., & Antia, A. U. (2023). Smoking cessation and benefits to cardiovascular health: A review of the literature. *Cureus, 15*(3), e35966. https://doi.org/10.7759/cureus.35966

Omidian, H., Gill, E. J., Chowdhury, S. D., & Cubeddu, L. X. (2024). Chitosan nanoparticles for intranasal drug delivery. *Pharmaceutics, 16*(6), 746. https://doi.org/10.3390/pharmaceutics16060746

Ong, H. X., Traini, D., & Young, P. M. (2013). Pharmaceutical applications of the Calu-3 lung epithelia cell line. *Expert Opinion on Drug Delivery, 10*(9), 1287–1302. https://doi.org/10.1517/17425247.2013.805743

Onor, I. O., Stirling, D., Williams, S. R., Bediako, D., Borghol, A., Harris, M. B., Darensburg, T. B., Clay, S. D., Okpechi, S. C., & Sarpong, D. F. (2017). Clinical effects of cigarette smoking: Epidemiologic impact and review of pharmacotherapy options. *International Journal of Environmental Research and Public Health, 14*(10), 1147. https://doi.org/10.3390/ijerph14101147

Onwuzo, C. N., Olukorode, J., Sange, W., Orimoloye, D. A., Udojike, C., Omoragbon, L., Hassan, A. E., Falade, D. M., Omiko, R., Odunaike, O. S., Adams-Momoh, P. A., Addeh, E., Onwuzo, S., & Joseph-Erameh, U. (2024). A review of smoking cessation interventions: Efficacy, strategies for implementation, and future directions. *Cureus*. https://doi.org/10.7759/cureus.5210

Ostrowska-Czubenko, J., Gierszewska, M., & Pieróg, M. (2015). pH-responsive hydrogel membranes based on modified chitosan: Water transport and kinetics of swelling. *Journal of Polymer Research, 22*(8). https://doi.org/10.1007/s10965-015-0786-3

Ottaviano, G. (2023). Physiology: Nasal airflow. In *Nasal airway obstruction* (pp. 33–42). Springer. https://doi.org/10.1007/978-3-031-28690-2_3

Oudih, S. B., Tahtat, D., Khodja, A. N., Mahlous, M., Hammache, Y., Guittoum, A., & Gana, S. K. (2023). Chitosan nanoparticles with controlled size and zeta potential. *Polymer Engineering & Science, 63*(3), 1011–1021. https://doi.org/10.1002/pen.26261

Pagano, A. S., & Márquez, S. (2022). The nasopharynx as a window to half a billion years of evolutionary change to the upper respiratory tract. *The Anatomical Record, 305*(8), 1829–1841. https://doi.org/10.1002/ar.25020

Paixão, B. A. L., Sá, N. B., da Encarnação, J. R., Batista, J. D. S., Laier, L. O., Neiva, E. G. C., Souza, E. A., de Siqueira Melo, R., Novato, W. T. G., Bellettini, I. C., da Cruz, J. W., & Maia, P. J. S. (2024). Electrocatalyst for ethanol oxidation reaction based on isatin-modified chitosan. *Journal of Applied Electrochemistry, 54*, 1235–1247. https://doi.org/10.1007/s10800-024-02228-3

Pal, R., Pandey, P., Koli, M., Srivastava, K., Tiwari, V., Gaur, A. K., & Dutta, P. (2024). Exploring future potential of nasopulmonary drug delivery systems for nasal route drug administration. *Journal of Drug Delivery and Therapeutics, 14* (3), 126–136. https://doi.org/10.22270/jddt.v14i3.6444

Pallagi, E., Ambrus, R., Szabó-Révész, P., & Csóka, I. (2015). Adaptation of the quality by design concept in early pharmaceutical development of an intranasal nanosized formulation. *International Journal of Pharmaceutics, 491*(1–2), 384–392. https://doi.org/10.1016/j.ijpharm.2015.06.018

Pan, C., Qian, J., Zhao, C., Yang, H., Zhao, X., & Guo, H. (2020). Study on the relationship between crosslinking degree and properties of TPP-crosslinked chitosan nanoparticles. *Carbohydrate Polymers, 241*, 116349. https://doi.org/10.1016/j.carbpol.2020.116349

Pandi, P., Bulusu, R., Kommineni, N., Khan, W., & Singh, M. (2020). Amorphous solid dispersions: An update for preparation, characterization, mechanism on bioavailability, stability, regulatory considerations and marketed products. *International Journal of Pharmaceutics, 586*, 119560. https://doi.org/10.1016/j.ijpharm.2020.119560

Pandian, S., Jeevanesan, V., Ponnusamy, C., & Natesan, S. (2016). RES-loaded PEGylated CS NPs: For efficient ocular delivery. *IET Nanobiotechnology, 11*(1), 32–39. https://doi.org/10.1049/iet-nbt.2016.0069

Pankow, J. F. (2001). A consideration of the role of gas/particle partitioning in the deposition of nicotine and other tobacco smoke compounds in the respiratory tract. *Chemical Research in Toxicology, 14*(11), 1465–1481. https://doi.org/10.1021/tx0100901

Parashar, A. K., Saraogi, G. K., & Sethi, V. A. (2025). Characterization and evaluation techniques for core-shell nanoconstructs for cancer theragnostics. In *Core-shell*

nano constructs for cancer theragnostic (pp. 179–214). Springer. https://doi.org/10.1007/978-981-96-3025-7_8

Parchen, G. P., Quaillet, M., De Freitas, R. A., & Hillaireau, H. (2025). Chitosan-based nano-objects for drug delivery: A review of their chemical modifications, supramolecular organization and biological fate. *RSC Pharmaceutics, 2*(6), 1292–1322. https://doi.org/10.1039/d5pm00095e

Pardeshi, C. V., & Belgamwar, V. S. (2019). Improved brain pharmacokinetics following intranasal administration of N,N,N-trimethyl chitosan tailored mucoadhesive NLCs. *Materials Technology, 35*(5), 249–266. https://doi.org/10.1080/10667857.2019.1674522

Pardeshi, S., More, M., Patil, P., Pardeshi, C., Deshmukh, P., Mujumdar, A., & Naik, J. (2021). A meticulous overview on drying-based (spray-, freeze-, and spray-freeze) particle engineering approaches for pharmaceutical technologies. *Drying Technology, 39*(11), 1447–1491. https://doi.org/10.1080/07373937.2021.1893330

Parhi, R. (2020). Drug delivery applications of chitin and chitosan: A review. *Environmental Chemistry Letters, 18*(3), 577–594. https://doi.org/10.1007/s10311-020-00963-5

Park, E., Lee, J., Huh, K. M., Lee, S. H., & Lee, H. (2019). Toxicity-attenuated glycol chitosan adhesive inspired by mussel adhesion mechanisms. *Advanced Healthcare Materials, 8*(14), Article 1900275. https://doi.org/10.1002/adhm.201900275

Parrilla, C., Bussu, F., Turra, N., Gallus, R., Fonnesu, C., Tsatsaris, N., & Montella, A. (2023). Anatomy of the nose vestibule. In *The nasal vestibule* (pp. 1–9). Springer. https://doi.org/10.1007/978-3-031-32850-3_1

Pastorova, I., Botto, R. E., Arisz, P. W., & Boon, J. J. (1994). Cellulose char structure: A combined analytical Py-GC-MS, FTIR, and NMR study. *Carbohydrate Research, 262*(1), 27–47. https://doi.org/10.1016/0008-6215(94)84003-2

Patel, K., Allen, S., Haque, M. N., Angelescu, I., Baumeister, D., & Tracy, D. K. (2016). Bupropion: A systematic review and meta-analysis of effectiveness as an antidepressant. *Therapeutic Advances in Psychopharmacology, 6* (2), 99–144. https://doi.org/10.1177/2045125316629071

Patel, M. M., & Patel, B. M. (2017). Crossing the blood–brain barrier: Recent advances in drug delivery to the brain. *CNS Drugs, 31*(2), 109–133. https://doi.org/10.1007/s40263-016-0405-9

Patel, R., Barker, J., & ElShaer, A. (2020). Pharmaceutical excipients and drug metabolism: A mini-review. *International Journal of Molecular Sciences, 21*(21), 8224. https://doi.org/10.3390/ijms21218224

Pathak, K., & Akhtar, N. (2016). Nose-to-brain delivery of nanoformulations for neurotherapeutics in Parkinson's disease: Defining the preclinical, clinical and toxicity issues. *Current Drug Delivery, 13*(8), 1205–1221. https://doi.org/10.2174/1567201813666160607123409

Patidar, N., Navale, A. M., Parsaila, N., Sharma, D., Nahar, P., Shinde, S., Solanki, N., & Shelke, A. (2025). Nicotine replacement therapy: Insights into the mechanisms and potential of nicotine receptor pathway. *American Journal of Translational Research, 17*(4), 2396–2410. https://doi.org/10.62347/mobz7773

Patil, G. B., Singh, S. S., Ramani, K. P., Chatap, V. K., & Deshmukh, P. K. (2013). Design and development of novel dual-compartment capsule for improved gastroretention. *ISRN Pharmaceutics, 2013*, 1–7. https://doi.org/10.1155/2013/752471

Pednekar, D. D., Liguori, M. A., Marques, C. N. H., Zhang, T., Zhang, N., Zhou, Z., Amoako, K., & Gu, H. (2022). From static to dynamic: A review on the role of mucus heterogeneity in particle and microbial transport. *ACS Biomaterials Science & Engineering, 8*(7), 2825–2848. https://doi.org/10.1021/acsbiomaterials.2c00182

Pedroso-Santana, S., & Fleitas-Salazar, N. (2020). Ionotropic gelation method in the synthesis of nanoparticles/microparticles for biomedical purposes. *Polymer International, 69*(5), 443–447. https://doi.org/10.1002/pi.5970

Pellis, A., Guebitz, G. M., & Nyanhongo, G. S. (2022). Chitosan: Sources, processing and modification techniques. *Gels, 8*(7), 393. https://doi.org/10.3390/gels8070393

Peltonen, L., & Strachan, C. J. (2020). Degrees of order: A comparison of nanocrystal and amorphous solids for poorly soluble drugs. *International Journal of Pharmaceutics, 586*, 119492. https://doi.org/10.1016/j.ijpharm.2020.119492

Peng, X., Li, Z., Li, H., Peng, W., Zhou, X., Song, D., Zhou, B., & Lv, C. (2019). The clinical application of mental nerve dissection in transoral endoscopic

thyroidectomy via an oral vestibular approach. *Surgical Endoscopy, 34*(1), 153–158. https://doi.org/10.1007/s00464-019-06743-9

Perez-Paramo, Y. X., Watson, C. J., Chen, G., Thomas, C. E., Adams-Haduch, J., Wang, R., Khor, C. C., Koh, W., Nelson, H. H., Yuan, J., & Lazarus, P. (2022). Impact of genetic variants in the nicotine metabolism pathway on nicotine metabolite levels in smokers. *Cancer Epidemiology, Biomarkers & Prevention, 32*(1), 54–65. https://doi.org/10.1158/1055-9965.EPI-22-0868

Perrigue, P. M., Murray, R. A., Mielcarek, A., Henschke, A., & Moya, S. E. (2021). Degradation of drug delivery nanocarriers and payload release: A review of physical methods for tracing nanocarrier biological fate. *Pharmaceutics, 13*(6), 770. https://doi.org/10.3390/pharmaceutics13060770

Petkova, A. I., Kubajewska, I., Vaideanu, A., Schätzlein, A. G., & Uchegbu, I. F. (2022). Gene targeting to the cerebral cortex following intranasal administration of polyplexes. *Pharmaceutics, 14*(6), 1136. https://doi.org/10.3390/pharmaceutics14061136

Pickworth, W. B., Rosenberry, Z. R., Gold, W., & Koszowski, B. (2014). Nicotine absorption from smokeless tobacco modified to adjust pH. *Journal of Addiction Research & Therapy, 5*(3), Article 1000184. https://doi.org/10.4172/2155-6105.1000184

Piñón-Balderrama, C. I., Leyva-Porras, C., Terán-Figueroa, Y., Espinosa-Solís, V., Álvarez-Salas, C., & Saavedra-Leos, M. Z. (2020). Encapsulation of active ingredients in food industry by spray-drying and nano spray-drying technologies. *Processes, 8*(8), 889. https://doi.org/10.3390/pr8080889

Pinto, C. A., Saripella, K. K., Loka, N. C., & Neau, S. H. (2017). Development and characterization of chitosan cross-linked with tripolyphosphate as a sustained release agent in tablets, part I: Design of experiments and optimization. *Journal of Pharmaceutical Sciences, 107*(4), 1063–1075. https://doi.org/10.1016/j.xphs.2017.11.018

Pipe, A. L., Evans, W., & Papadakis, S. (2022). Smoking cessation: Health system challenges and opportunities. *Tobacco Control, 31*(2), 340–347. https://doi.org/10.1136/tobaccocontrol-2021-056575

Pochapski, D. J., Santos, C. C. D., Leite, G. W., Pulcinelli, S. H., & Santilli, C. V. (2021). Zeta potential and colloidal stability predictions for inorganic nanoparticle dispersions: Effects of experimental conditions and electrokinetic

models on the interpretation of results. *Langmuir, 37*(45), 13379–13389. https://doi.org/10.1021/acs.langmuir.1c02056

Podgorbunskikh, E., Kuskov, T., Rychkov, D., Lomovskii, O., & Bychkov, A. (2022). Mechanical amorphization of chitosan with different molecular weights. *Polymers, 14*(20), 4438. https://doi.org/10.3390/polym14204438

Popescu, R., Ghica, M. V., Dinu-Pîrvu, C., Anuța, V., Lupuliasa, D., & Popa, L. (2020). New opportunity to formulate intranasal vaccines and drug delivery systems based on chitosan. *International Journal of Molecular Sciences, 21*(14), 5016. https://doi.org/10.3390/ijms21145016

Prabaharan, M., & Mano, J. F. (2004). Chitosan-based particles as controlled drug delivery systems. *Drug Delivery, 12*(1), 41–57. https://doi.org/10.1080/10717540590889781

Priprem, A., Johns, J. R., Limsitthichaikoon, S., Limphirat, W., Mahakunakorn, P., & Johns, N. P. (2017). Intranasal melatonin nanoniosomes: Pharmacokinetics, pharmacodynamics and toxicity studies. *Therapeutic Delivery, 8*(6), 373–390. https://doi.org/10.4155/tde-2017-0005

Prochaska, J. J., & Benowitz, N. L. (2019). Current advances in research in treatment and recovery: Nicotine addiction. *Science Advances, 5*(10), Article aay9763. https://doi.org/10.1126/sciadv.aay9763

Qian, J., Zhao, C., Ding, J., Chen, Y., & Guo, H. (2020). Preparation of nano-enzyme aggregates by crosslinking lipase with sodium tripolyphosphate. *Process Biochemistry, 97*, 19–26. https://doi.org/10.1016/j.procbio.2020.06.026

Qin, M., Du, G., & Sun, X. (2021). Recent advances in the noninvasive delivery of mRNA. *Accounts of Chemical Research, 54*(23), 4262–4271. https://doi.org/10.1021/acs.accounts.1c00493

Qin, R., Liu, Z., Cheng, A., Zhou, X., Su, Z., Cui, Z., Li, J., Wei, X., Zhao, L., Chung, K. F., Xiao, D., & Wang, C. (2024). Efficacy of varenicline or bupropion and its association with nicotine metabolite ratio among smokers with COPD. *Respirology, 29*(6), 479–488. https://doi.org/10.1111/resp.14702

Raith, M., & Swoboda, I. (2023). Birch pollen—The unpleasant herald of spring. *Frontiers in Allergy, 4*, 1181675. https://doi.org/10.3389/falgy.2023.1181675

Rajput, A., Pingale, P., & Dhapte-Pawar, V. (2022). Nasal delivery of neurotherapeutics via nanocarriers: Facets, aspects, and prospects. *Frontiers in Pharmacology, 13*, 979682. https://doi.org/10.3389/fphar.2022.979682

Ramakrishnan, R., & Daly, A. C. (2026). Revisiting ISO 10993-5 *in vitro* cytotoxicity standard tests for evaluation of extracellular matrix-based biomaterials. *International Journal of Biomaterials, 2026* (1), 7395612. https://doi.org/10.1155/ijbm/7395612

Ramos, V. (2003). Modified chitosan carrying phosphonic and alkyl groups. *Carbohydrate Polymers, 51*(4), 425–429. https://doi.org/10.1016/S0144-8617(02)00211-4

Rao, P., Han, D. D., Tan, K., Mohammadi, L., Derakhshandeh, R., Navabzadeh, M., Goyal, N., & Springer, M. L. (2022). Comparable impairment of vascular endothelial function by a wide range of electronic nicotine delivery devices. *Nicotine & Tobacco Research, 24*(7), 1055–1062. https://doi.org/10.1093/ntr/ntac019

Rasmussen, S., Horkan, K. H., & Kotler, M. (2018). Pharmacokinetic evaluation of two nicotine patches in smokers. *Clinical Pharmacology in Drug Development, 7*(5), 506–512. https://doi.org/10.1002/cpdd.431

Rauf, M. A., Rehman, F. U., Zheng, M., & Shi, B. (2019). The strategies of nanomaterials for traversing blood-brain barrier. In *Nanomedicine in brain diseases* (pp. 29–57). Springer. https://doi.org/10.1007/978-981-13-8731-9_2

Renukuntla, J., Peterson-Sockwell, S., Clark, B. A., Godage, N. H., Gionfriddo, E., Bolla, P. K., & Boddu, S. H. S. (2023). Design and preclinical evaluation of nicotine–stearic acid conjugate-loaded solid lipid nanoparticles for transdermal delivery: A technical note. *Pharmaceutics, 15*(4), 1043. https://doi.org/10.3390/pharmaceutics15041043

Ribeiro, E. F., de Barros-Alexandrino, T. T., Assis, O. B. G., Cruz, A., Junior, Q. A., Hernando, I., & Nicoletti, V. R. (2020). Chitosan and crosslinked chitosan nanoparticles: Synthesis, characterization and their role as Pickering emulsifiers. *Carbohydrate Polymers, 250,* 116878. https://doi.org/10.1016/j.carbpol.2020.116878

Riegger, B. R., Bäurer, B., Mirzayeva, A., Tovar, G. E., & Bach, M. (2018). A systematic approach of chitosan nanoparticle preparation via emulsion crosslinking as potential adsorbent in wastewater treatment. *Carbohydrate Polymers, 180,* 46–54. https://doi.org/10.1016/j.carbpol.2017.10.002

Riggs, D., & Perfetti, T. (2001). Thermochemical properties of nicotine salts. *Beiträge zur Tabakforschung International, 19*(6), 289–295. https://doi.org/10.2478/cttr-2013-0715

Rigotti, N. A. (2012). Strategies to help a smoker who is struggling to quit. *JAMA, 308*(15), 1573–1580. https://doi.org/10.1001/jama.2012.13043

Rigotti, N. A., Benowitz, N. L., Prochaska, J., Leischow, S., Nides, M., Blumenstein, B., Clarke, A., Cain, D., & Jacobs, C. (2023). Cytisinicline for smoking cessation. *JAMA, 330*(2), 152–160. https://doi.org/10.1001/jama.2023.10042

Rinaudo, M., Auzely, R., Vallin, C., & Mullagaliev, I. (2005). Specific interactions in modified chitosan systems. *Biomacromolecules, 6*(5), 2396–2407. https://doi.org/10.1021/bm0580025

Rizeq, B. R., Younes, N. N., Rasool, K., & Nasrallah, G. K. (2019). Synthesis, bioapplications, and toxicity evaluation of chitosan-based nanoparticles. *International Journal of Molecular Sciences, 20* (22), 5776. https://doi.org/10.3390/ijms20225776

Rodrigues, C., De Mello, J. M. M., Dalcanton, F., Macuvele, D. L. P., Padoin, N., Fiori, M. A., Soares, C., & Riella, H. G. (2020). Mechanical, thermal and antimicrobial properties of chitosan-based nanocomposite with potential applications for food packaging. *Journal of Polymers and the Environment, 28* (4), 1216–1236. https://doi.org/10.1007/s10924-020-01678-y

Rodrigues, S., Cardoso, L., Da Costa, A., & Grenha, A. (2015). Biocompatibility and stability of polysaccharide polyelectrolyte complexes aimed at respiratory delivery. *Materials, 8*(9), 5647–5670. https://doi.org/10.3390/ma8095268

Ruiz, M. E., & Scioli-Montoto, S. (2024). Routes of drug administration. In *ADME processes in pharmaceutical sciences* (pp. 129–172). Springer. https://doi.org/10.1007/978-3-031-50419-8_7

Sacco, P., Pedroso-Santana, S., Kumar, Y., Joly, N., Martin, P., & Bocchetta, P. (2021). Ionotropic gelation of chitosan flat structures and potential applications. *Molecules, 26*(3), 660. https://doi.org/10.3390/molecules26030660

Saei, A. A., Yazdani, M., Lohse, S. E., Bakhtiary, Z., Serpooshan, V., Ghavami, M., Asadian, M., Mashaghi, S., Dreaden, E. C., Mashaghi, A., & Mahmoudi, M. (2017). Nanoparticle surface functionality dictates cellular and systemic toxicity. *Chemistry of Materials, 29*(16), 6578–6595. https://doi.org/10.1021/acs.chemmater.7b01979

Safarov, R., Fedotova, O., Uvarova, A., Gordienko, M., & Menshutina, N. (2024). Review of intranasal active pharmaceutical ingredient delivery systems. *Pharmaceuticals, 17*(9), 1180. https://doi.org/10.3390/ph17091180

Safiri, S., Nejadghaderi, S. A., Abdollahi, M., Carson-Chahhoud, K., Kaufman, J. S., Bragazzi, N. L., Moradi-Lakeh, M., Mansournia, M. A., Sullman, M. J. M., Almasi-Hashiani, A., Taghizadieh, A., Collins, G. S., & Kolahi, A. (2022). Global, regional, and national burden of cancers attributable to tobacco smoking in 204 countries and territories, 1990–2019. *Cancer Medicine, 11*(13), 2662–2678. https://doi.org/10.1002/cam4.4647

Sai, K. K. S., Zuo, Y., Rose, J. E., Garg, P. K., Garg, S., Nazih, R., Mintz, A., & Mukhin, A. G. (2019). Rapid brain nicotine uptake from electronic cigarettes. *Journal of Nuclear Medicine, 61*(6), 928–930. https://doi.org/10.2967/jnumed.119.230748

Sailer, S., Sebastiani, G., Andreu-Fernández, V., & Garcia-Algar, O. (2019). Impact of nicotine replacement and electronic nicotine delivery systems on fetal brain development. *International Journal of Environmental Research and Public Health, 16*(24), 5113. https://doi.org/10.3390/ijerph16245113

Salvi, S. S., Brashier, B. B., Londhe, J., Pyasi, K., Vincent, V., Kajale, S. S., Tambe, S., Mandani, K., Nair, A., Mak, S. M., Madas, S., Juvekar, S., Donnelly, L. E., & Barnes, P. J. (2020). Phenotypic comparison between smoking and non-smoking chronic obstructive pulmonary disease. *Respiratory Research, 21*(1), Article 1310. https://doi.org/10.1186/s12931-020-1310-9

Sanap, S. N., Bisen, A. C., Kedar, A., Agrawal, S., & Bhatta, R. S. (2023). Recent update on pharmacokinetics and drug metabolism in CNS-based drug discovery. *Current Pharmaceutical Design, 29*(20), 1602–1616. https://doi.org/10.2174/1381612829666230707121415

Sánchez, R., Alonso, G., Valencia, C., & Franco, J. (2015). Rheological and TGA study of acylated chitosan gel-like dispersions in castor oil: Influence of acyl substituent and acylation protocol. *Process Safety and Environmental Protection, 100,* 170–178. https://doi.org/10.1016/j.cherd.2015.05.022

Sansone, L., Milani, F., Fabrizi, R., Belli, M., Cristina, M., Zagà, V., De Iure, A., Cicconi, L., Bonassi, S., & Russo, P. (2023). Nicotine: From discovery to biological effects. *International Journal of Molecular Sciences, 24*(19), 14570. https://doi.org/10.3390/ijms241914570

Sarangapani, S., Patil, A., Ngeow, Y. K., Mohan, R. E., Asundi, A., & Lang, M. J. (2018). Chitosan nanoparticles' functionality as redox active drugs through cytotoxicity, radical scavenging and cellular behaviour. *Integrative Biology, 10*(5), 313–324. https://doi.org/10.1039/c8ib00038g

Satitsri, S., & Muanprasat, C. (2020). Chitin and chitosan derivatives as biomaterial resources for biological and biomedical applications. *Molecules, 25*(24), 5961. https://doi.org/10.3390/molecules25245961

Savva, M. (2019). Rates and orders of reactions. In *Pharmaceutical calculations* (pp. 269–299). Springer. https://doi.org/10.1007/978-3-030-20335-1_12

Schmidt, H. D., Rupprecht, L. E., & Addy, N. A. (2018). Neurobiological and neurophysiological mechanisms underlying nicotine seeking and smoking relapse. *Complex Psychiatry, 4*(4), 169–189. https://doi.org/10.1159/000494799

Schnoll, R. A., Wileyto, E. P., Leone, F. T., Tyndale, R. F., & Benowitz, N. L. (2012). High-dose transdermal nicotine for fast metabolizers of nicotine: A proof-of-concept placebo-controlled trial. *Nicotine & Tobacco Research, 15*(2), 348–354. https://doi.org/10.1093/ntr/nts129

Scholze, P., & Huck, S. (2020). The α5 nicotinic acetylcholine receptor subunit differentially modulates α4β2* and α3β4* receptors. *Frontiers in Synaptic Neuroscience, 12*, Article 607959. https://doi.org/10.3389/fnsyn.2020.607959

Schrag, M., & Regal, K. (2013b). Pharmacokinetics and toxicokinetics. In *Elsevier eBooks* (pp. 69–106). Elsevier. https://doi.org/10.1016/B978-0-12-803620-4.00004-9

Seak, Y. S., Nor, J., Kamauzaman, T. H. T., Arithra, A., & Islam, M. A. (2021). Efficacy and safety of intranasal ketamine for acute pain management in the emergency setting. *American Journal of Emergency Medicine, 44*, 1–6. https://doi.org/10.1016/j.ajem.2020.02.001

Secades-Villa, R., González-Roz, A., García-Pérez, Á., & Becoña, E. (2017). Psychological, pharmacological, and combined smoking cessation interventions for smokers with current depression: A systematic review and meta-analysis. *PLOS ONE, 12*(12), e0188849. https://doi.org/10.1371/journal.pone.0188849

Shahab, L., Beard, E., Brown, J., & West, R. (2014). Prevalence of NRT use and associated nicotine intake in smokers, recent ex-smokers and longer-term ex-smokers. *PLOS ONE, 9*(11), e113045. https://doi.org/10.1371/journal.pone.0113045

Shahab, L., Brose, L. S., & West, R. (2013). Novel delivery systems for nicotine replacement therapy as an aid to smoking cessation and for harm reduction: Rationale and evidence for advantages over existing systems. *CNS Drugs, 27*(12), 1007–1019. https://doi.org/10.1007/s40263-013-0116-4

Shaik, F. B., Nagajothi, G., Swarnalatha, K., Kumar, C. S., & Maddu, N. (2019). Quantification of nicotine and cotinine in plasma, saliva, and urine by HPLC method in chewing tobacco users. *Asian Pacific Journal of Cancer Prevention, 20*(12), 3617–3623. https://doi.org/10.31557/APJCP.2019.20.12.3617

Shang, X., E, F., Guo, K., Yang, C., Zhou, L., Wu, Y., Yang, K., & Li, X. (2023). Effectiveness and safety of varenicline for smoking cessation: An overview and meta-analysis. *Journal of Addiction Medicine, 17*(5), 536–543. https://doi.org/10.1097/ADM.0000000000001171

Sharifi-Rad, J., Quispe, C., Butnariu, M., et al. (2021). Chitosan nanoparticles as a promising tool in nanomedicine with particular emphasis on oncological treatment. *Cancer Cell International*, *21*, 318. https://doi.org/10.1186/s12935-021-02025-4

Sharma, M., Waghela, S., Mhatre, R., & Saraogi, G. K. (2021). A recent update on intranasal delivery of high molecular weight proteins, peptides, and hormones. *Current Pharmaceutical Design, 27*(42), 4279–4299. https://doi.org/10.2174/1381612827666210820100723

Sharma, R., Gartner, C. E., & Hall, W. D. (2016). The challenge of reducing smoking in people with serious mental illness. *The Lancet Respiratory Medicine, 4*(10), 835–844. https://doi.org/10.1016/S2213-2600(16)30228-4

Sharma, S., & Bhende, M. (2024). An overview: Non-toxic and eco-friendly polysaccharides—Its classification, properties, and diverse applications. *Polymer Bulletin, 81*(14), 12383–12429. https://doi.org/10.1007/s00289-024-05307-9

Sharma, V., Ambekar, A., & Singh, K. (2025). Exploring chitosan nanoparticles: Preparation methods, cross-linking strategies and potential therapeutic applications. *Polymer Bulletin, 82*(16), 10671–10720. https://doi.org/10.1007/s00289-025-05979-x

Shehata, S. A., Toraih, E. A., Ismail, E. A., Hagras, A. M., Elmorsy, E., & Fawzy, M. S. (2023). Vaping, environmental toxicants exposure, and lung cancer risk. *Cancers, 15*(18), 4525. https://doi.org/10.3390/cancers15184525

Shen, S., Wu, Y., Liu, Y., & Wu, D. (2017). High drug-loading nanomedicines: Progress, current status, and prospects. *International Journal of Nanomedicine, 12*, 4085–4109. https://doi.org/10.2147/IJN.S132780

Shete, A., Chavan, A., Potekar, P., Yadav, G., & Shah, N. (2024). Modification of physicochemical properties of chitosan to improve its pharmaceutical and agrochemical potential applications. *International Journal of Biological Macromolecules, 267*, 131404. https://doi.org/10.1016/j.ijbiomac.2024.131404

Shete, A., Shete, M., & Lolage, V. (2024). Nicotine replacement therapy: A clinical approach. In *Title of the book* (pp. 147–157). Publisher. https://doi.org/10.9734/bpi/nvmms/v6/8426e

Shewale, A. R., Borse, M. S., Brown, J. D., & Li, C. (2015). Mental health status of varenicline and bupropion users during a quit attempt compared to current smokers, other quitters, and non-smokers. *Drug and Alcohol Dependence, 154*, 132–138. https://doi.org/10.1016/j.drugalcdep.2015.06.028

Shetty, S. M., & Archana, S. (2023). Anatomy and physiology of the airway: Applied aspects. In *Anatomy and physiology of the airway: Applied aspects* (pp. 21–43). Springer. https://doi.org/10.1007/978-981-19-4747-6_2

Shi, A., Guan, Y., & Zhang, Y. (2020). A new emulsification-crosslinking technique for preparation of physically crosslinked chitosan microspheres. *Journal of Bioactive and Compatible Polymers, 35*(4–5), 289–300. https://doi.org/10.1177/0883911520933921

Shiffman, S., Cone, E. J., Buchhalter, A. R., Henningfield, J. E., Rohay, J. M., Gitchell, J. G., Pinney, J. M., & Chau, T. (2008). Rapid absorption of nicotine from new nicotine gum formulations. *Pharmacology Biochemistry and Behavior, 91*(3), 380–384. https://doi.org/10.1016/j.pbb.2008.08.012

Shim, S., & Yoo, H. S. (2020). The application of mucoadhesive chitosan nanoparticles in nasal drug delivery. *Marine Drugs, 18*(12), 605. https://doi.org/10.3390/md18120605

Shoufy, N. M. A., Danaf, N. N., Jebawi, N. K. A., Aboudaher, N. S. S., Ayash, N. A., Kadi, N. A. A., Shokor, N. B., Zeidan, N. F., Kanso, N. N., Salha, N. R., Mehta, N. S. P., Shamseddine, N. M., & Nasrallah, N. J. (2024). Cascading defenses: A multifaceted narrative of immune responses in head and neck physiology. *Magna Scientia Advanced Research and Reviews, 10* (1), 194–222. https://doi.org/10.30574/msarr.2024.10.1.0018

Shoyaib, A. A., Archie, S. R., & Karamyan, V. T. (2019). Intraperitoneal route of drug administration: Should it be used in experimental animal studies? *Pharmaceutical Research, 37*(1), 12. https://doi.org/10.1007/s11095-019-2745-x

Shrestha, N., Khan, S., Neupane, Y. R., Dang, S., Md, S., Fahmy, U. A., Kotta, S., Alhakamy, N. A., Baboota, S., & Ali, J. (2020). Tailoring midazolam-loaded chitosan nanoparticulate formulation for enhanced brain delivery via intranasal route. *Polymers, 12*(11), 2589. https://doi.org/10.3390/polym12112589

Shrestha, S., Wang, B., & Dutta, P. (2020). Nanoparticle processing: Understanding and controlling aggregation. *Advances in Colloid and Interface Science, 279*, 102162. https://doi.org/10.1016/j.cis.2020.102162

Shrewsbury, S. B. (2023). The upper nasal space: Option for systemic drug delivery, mucosal vaccines and "nose-to-brain." *Pharmaceutics, 15*(6), 1720. https://doi.org/10.3390/pharmaceutics15061720

Shu, X., & Zhu, K. (2000). A novel approach to prepare tripolyphosphate/chitosan complex beads for controlled-release drug delivery. *International Journal of Pharmaceutics, 201*(1), 51–58. https://doi.org/10.1016/S0378-5173(00)00403-8

Shu, X., & Zhu, K. (2002). The influence of multivalent phosphate structure on the properties of ionically cross-linked chitosan films for controlled drug release. *European Journal of Pharmaceutics and Biopharmaceutics, 54*(2), 235–243. https://doi.org/10.1016/S0939-6411(02)00052-8

Siddiqi, K., Elsey, H., Khokhar, M. A., Marshall, A., Pokhrel, S., Arora, M., Crankson, S., Mehra, R., Morello, P., Collin, J., & Fong, G. T. (2023). Framework Convention on Tobacco Control 2030—A program to accelerate the implementation of World Health Organization Framework Convention for Tobacco Control in low- and middle-income countries: A mixed-methods evaluation. *Nicotine & Tobacco Research, 25*(6), 1074–1081. https://doi.org/10.1093/ntr/ntad022

Siepmann, J., & Peppas, N. A. (2011). Higuchi equation: Derivation, applications, use and misuse. *International Journal of Pharmaceutics, 418*(1), 6–12. https://doi.org/10.1016/j.ijpharm.2011.03.051

Siersbaek, R., Kavanagh, P., Ford, J., Burke, S., & Parker, S. (2024). How and why do financial incentives contribute to helping people stop smoking? A realist review.

BMC Public Health, *24*(1), Article 17967. https://doi.org/10.1186/s12889-024-17967-3

Silva, D. S., Santos, D. M. D., Almeida, A., Marchiori, L., Campana-Filho, S. P., Ribeiro, S. J. L., & Sarmento, B. (2018). N-(2-Hydroxy)-propyl-3-trimethylammonium, O-myristoyl chitosan enhances the solubility and intestinal permeability of anticancer curcumin. *Pharmaceutics, 10*(4), 245. https://doi.org/10.3390/pharmaceutics10040245

Silvestro, I., Francolini, I., Di Lisio, V., Martinelli, A., Pietrelli, L., D'Abusco, A. S., Scoppio, A., & Piozzi, A. (2020). Preparation and characterization of TPP-chitosan crosslinked scaffolds for tissue engineering. *Materials, 13*(16), 3577. https://doi.org/10.3390/ma13163577

Simukoko, H. (2021). Refocusing functional anatomy and immunology of the respiratory mucosa in the advent of COVID-19. In *IntechOpen eBooks*. IntechOpen. https://doi.org/10.5772/intechopen.96251

Singh, R., Verma, H., Paul, S., Bhagat, S., & Sharma, V. (2021). Septum, adenoid, and epistaxis. In *Springer eBooks* (pp. 309–328). Springer. https://doi.org/10.1007/978-981-33-6284-0_9

Singh, S. K., Hidau, M. K., Gautam, S., Gupta, K., Singh, K. P., Singh, S. K., & Singh, S. (2017). Glycol chitosan functionalized asenapine nanostructured lipid carriers for targeted brain delivery: Pharmacokinetic and teratogenic assessment. *International Journal of Biological Macromolecules, 108* , 1092–1100. https://doi.org/10.1016/j.ijbiomac.2017.11.031

Sinha, S., Devi, R., Barman, D., Hazarika, S., & Das, S. (2020). Nicotine replacement therapy: A friend or foe. *Journal of Family Medicine and Primary Care, 9*(6), 2615–2620. https://doi.org/10.4103/jfmpc.jfmpc_313_20

Sivaramakrishnan, G., Alsobaiei, M., & Sridharan, K. (2022). Oral side effects of locally delivered nicotine replacement therapy: A meta-analysis of randomized controlled trials. *International Journal of Dental Hygiene, 21* (1), 3–17. https://doi.org/10.1111/idh.12594

Sivaramakrishnan, G., & Sridharan, K. (2024). Nicotine replacement therapy and oral health: A network meta-analysis of adverse effects in randomized trials. *Evidence-Based Dentistry*. https://doi.org/10.1038/s41432-024-01064-w

Sivashankari, P., & Prabaharan, M. (2016). Deacetylation modification techniques of chitin and chitosan. In *Elsevier eBooks* (pp. 117–133). Elsevier. https://doi.org/10.1016/B978-0-08-100230-8.00005-4

Skjei, K. L., & Markou, A. (2003). Effects of repeated withdrawal episodes, nicotine dose, and duration of nicotine exposure on the severity and duration of nicotine withdrawal in rats. *Psychopharmacology, 168*(3), 280–292. https://doi.org/10.1007/s00213-003-1414-1

Smail, K. (2024). Perspective chapter: Nasal septum—A review of the pathology, clinical presentation and management. In *IntechOpen eBooks*. IntechOpen. https://doi.org/10.5772/intechopen.112424

Smith, D. H., Brook, C. D., Virani, S., & Platt, M. P. (2018). The inferior turbinate: An autonomic organ. *American Journal of Otolaryngology, 39*(6), 771–775. https://doi.org/10.1016/j.amjoto.2018.08.009

Smith, J., Wood, E., & Dornish, M. (2004). Effect of chitosan on epithelial cell tight junctions. *Pharmaceutical Research, 21*(1), 43–49. https://doi.org/10.1023/B:PHAM.0000012150.60180.E3

Sogias, I. A., Williams, A. C., & Khutoryanskiy, V. V. (2008). Why is chitosan mucoadhesive? *Biomacromolecules, 9*(7), 1837–1842. https://doi.org/10.1021/bm800276d

Soltanzadeh, M., Peighambardoust, S. H., Ghanbarzadeh, B., Mohammadi, M., & Lorenzo, J. M. (2021). Chitosan nanoparticles as a promising nanomaterial for encapsulation of pomegranate (*Punica granatum* L.) peel extract as a natural source of antioxidants. *Nanomaterials, 11*(6), 1439. https://doi.org/10.3390/nano11061439

Song, R., Wang, X., Zhang, G., Zhao, L., Sun, X., Wang, S., & Gao, B. (2011). Simulation of equilibrium system and release behaviors of both oxytetracycline and copper on aerobic granules in a sequencing batch reactor. *Biochemical Engineering Journal, 56*(3), 198–204. https://doi.org/10.1016/j.bej.2011.06.009

Sonin, D., Pochkaeva, E., Zhuravskii, S., Postnov, V., Korolev, D., Vasina, L., Kostina, D., Mukhametdinova, D., Zelinskaya, I., Skorik, Y., Naumysheva, E., Malashicheva, A., Somov, P., Istomina, M., Rubanova, N., Aleksandrov, I., Vasyutina, M., & Galagudza, M. (2020). Biological safety and biodistribution of chitosan nanoparticles. *Nanomaterials, 10*(4), 810. https://doi.org/10.3390/nano10040810

Sonvico, F., Clementino, A., Buttini, F., Colombo, G., Pescina, S., Stanisçuaski Guterres, S., Raffin Pohlmann, A., & Nicoli, S. (2018). Surface -modified nanocarriers for nose-to-brain delivery: From bioadhesion to targeting. *Pharmaceutics, 10*(1), 34. https://doi.org/10.3390/pharmaceutics10010034

Sreekumar, S., Goycoolea, F. M., Moerschbacher, B. M., & Rivera-Rodriguez, G. R. (2018). Parameters influencing the size of chitosan-TPP nano- and microparticles. *Scientific Reports, 8*(1), 4695. https://doi.org/10.1038/s41598-018-23064-4

Srivastava, G. K., Alonso-Alonso, M. L., Fernandez-Bueno, I., Garcia-Gutierrez, M. T., Rull, F., Medina, J., Coco, R. M., & Pastor, J. C. (2018). Comparison between direct contact and extract exposure methods for PFO cytotoxicity evaluation. *Scientific Reports, 8*(1), 1425. https://doi.org/10.1038/s41598-018-19428-5

Stanton, C. A., Keith, D. R., Gaalema, D. E., Bunn, J. Y., Doogan, N. J., Redner, R., Kurti, A. N., Roberts, M. E., & Higgins, S. T. (2016). Trends in tobacco use among US adults with chronic health conditions: National Survey on Drug Use and Health 2005–2013. *Preventive Medicine, 92*, 160–168. https://doi.org/10.1016/j.ypmed.2016.04.008

Stetefeld, J., McKenna, S. A., & Patel, T. R. (2016). Dynamic light scattering: A practical guide and applications in biomedical sciences. *Biophysical Reviews, 8*(4), 409–427. https://doi.org/10.1007/s12551-016-0218-6

St.Helen, G., Havel, C., Dempsey, D. A., Jacob, P., & Benowitz, N. L. (2015). Nicotine delivery, retention and pharmacokinetics from various electronic cigarettes. *Addiction, 111*(3), 535–544. https://doi.org/10.1111/add.13183

Stielow, M., Witczyńska, A., Kubryń, N., Fijałkowski, Ł., Nowaczyk, J., & Nowaczyk, A. (2023). The bioavailability of drugs—The current state of knowledge. *Molecules, 28*(24), 8038. https://doi.org/10.3390/molecules28248038

Subramaniyan, M., & Dani, J. A. (2015). Dopaminergic and cholinergic learning mechanisms in nicotine addiction. *Annals of the New York Academy of Sciences, 1349*(1), 46–63. https://doi.org/10.1111/nyas.12871

Sultan, Y., Salman, Z., Alzaatreh, M., Edilbi, A., Alani, R., Sultan, I., Alfaar, A., & Qaddoumi, I. (2024). Smoking-related disease impact in the Eastern Mediterranean region: A comprehensive assessment using Global Burden of Disease data. *Asian Pacific Journal of Cancer Prevention, 25* (2), 495–505. https://doi.org/10.31557/APJCP.2024.25.2.495

Sun, L., Du, Y., Shi, X., Chen, X., Yang, J., & Xu, Y. (2006). A new approach to chemically modified carboxymethyl chitosan and study of its moisture - absorption and moisture-retention abilities. *Journal of Applied Polymer Science, 102*(2), 1303–1309. https://doi.org/10.1002/app.23718

Sung, H., Sonaje, K., Liao, Z., Hsu, L., & Chuang, E. (2012). pH-responsive nanoparticles shelled with chitosan for oral delivery of insulin: From mechanism to therapeutic applications. *Accounts of Chemical Research, 45*(4), 619–629. https://doi.org/10.1021/ar200234q

Svensson, O., Lindh, L., Cárdenas, M., & Arnebrant, T. (2006). Layer-by-layer assembly of mucin and chitosan—Influence of surface properties, concentration and type of mucin. *Journal of Colloid and Interface Science, 299*(2), 608–616. https://doi.org/10.1016/j.jcis.2006.02.027

Szczap, J. P., & Jacobs, I. C. (2022). Atomization and spray drying processes. In *Elsevier eBooks* (pp. 59–71). Elsevier. https://doi.org/10.1016/B978-0-12-821683-5.00017-0

Szekely, D., Zara, F., Patrascu, R., Dumitru, C. S., Novacescu, D., Manole, A., Mogoanta, C. A., Iovanescu, D., & Iovanescu, G. (2025). Histopathological and molecular insights into chronic nasopharyngeal and otic disorders in children: Structural and immune mechanisms underlying disease chronicity. *Life, 15*(8), 1228. https://doi.org/10.3390/life15081228

Taghavi, T., Arger, C. A., Heil, S. H., Higgins, S. T., & Tyndale, R. F. (2017). Longitudinal influence of pregnancy on nicotine metabolic pathways. *Journal of Pharmacology and Experimental Therapeutics, 364* (2), 238–245. https://doi.org/10.1124/jpet.117.245126

Tai, J., Han, M., Lee, D., Park, I., Lee, S. H., & Kim, T. H. (2022). Different methods and formulations of drugs and vaccines for nasal administration. *Pharmaceutics, 14*(5), 1073. https://doi.org/10.3390/pharmaceutics14051073

Takeda, N., Hirata, K., Tsuruta, K., Santis, G. D., Xantheas, S. S., Ishiuchi, S., & Fujii, M. (2021). Gas phase protonated nicotine is a mixture of pyridine - and pyrrolidine-protonated conformers: Implications for its native structure in the nicotinic acetylcholine receptor. *Physical Chemistry Chemical Physics, 24*(10), 5786–5793. https://doi.org/10.1039/d1cp05175j

Talevi, A., & Ruiz, M. E. (2021). Zero-order drug release. In *The ADME encyclopedia* (pp. 1–6). Springer. https://doi.org/10.1007/978-3-030-51519-5_33-1

Tan, A. K. (2012). Distinguishing between non-smokers, casual smokers, and compulsive smokers: Evidence from Malaysia. *Atlantic Economic Journal, 40*(2), 173–184. https://doi.org/10.1007/s11293-012-9309-3

Tang, E., Huang, M., & Lim, L. (2003). Ultrasonication of chitosan and chitosan nanoparticles. *International Journal of Pharmaceutics, 265*(1–2), 103–114. https://doi.org/10.1016/S0378-5173(03)00408-3

Tang, J., Cai, L., Xu, C., Sun, S., Liu, Y., Rosenecker, J., & Guan, S. (2022). Nanotechnologies in delivery of DNA and mRNA vaccines to the nasal and pulmonary mucosa. *Nanomaterials, 12*(2), 226. https://doi.org/10.3390/nano12020226

Tang, Y. (2020). Vascular emergency of the head and neck. In *Learning vascular and interventional radiology* (pp. 127–141). Springer. https://doi.org/10.1007/978-3-030-43654-4_10

Tang, Y., Bryant, M. S., Li, M., Min, S., Pellar, G., Wu, Q., Yang, D., Kang, H., Sepehr, E., He, X., McLellen, F., Lewis, S. M., Greenhaw, J., Fisher, J., Yang, X., Chemerynski, S., Yee, S. B., Rosenfeldt, H., Yeager, R. P., & Yi, J. (2024). Pharmacokinetic analysis of nicotine and its metabolites (cotinine and trans-3′-hydroxycotinine) in male Sprague-Dawley rats following nose-only inhalation, oral gavage, and intravenous infusion of nicotine. *Toxicological Sciences, 202*(2), 196–209. https://doi.org/10.1093/toxsci/kfae120

Tanner, J., & Tyndale, R. (2017). Variation in CYP2A6 activity and personalized medicine. *Journal of Personalized Medicine, 7*(4), 18. https://doi.org/10.3390/jpm7040018

Tao, X., Zhang, Y., Zhou, Y., Liu, Z., & Feng, X. (2023). Nicotine in complex samples: Recent updates on the pretreatment and analysis method. *Critical Reviews in Analytical Chemistry, 53*(6), 1209–1238. https://doi.org/10.1080/10408347.2021.2016365

Teichert, A., Brossard, P., Medlin, L. F., Sandalic, L., Franzon, M., Wynne, C., Laugesen, M., & Lüdicke, F. (2017). Evaluation of nicotine pharmacokinetics and subjective effects following use of a novel nicotine delivery system. *Nicotine & Tobacco Research, 20*(4), 458–465. https://doi.org/10.1093/ntr/ntx093

Terrier, L., Hadjikhani, N., & Destrieux, C. (2022). The trigeminal pathways. *Journal of Neurology, 269*(7), 3443–3460. https://doi.org/10.1007/s00415-022-11002-4

Thakur, J., & Choudhari, S. G. (2024). Effectiveness of healthcare interventions on smoking cessation in adolescents in low- and middle-income countries: A narrative review. *Cureus, 16*(2), Article e54051. https://doi.org/10.7759/cureus.54051

Thambiliyagodage, C., Jayanetti, M., Mendis, A., Ekanayake, G., Liyanaarachchi, H., & Vigneswaran, S. (2023). Recent advances in chitosan-based applications—A review. *Materials, 16*(5), 2073. https://doi.org/10.3390/ma16052073

Tian, J., Venn, A., Otahal, P., & Gall, S. (2015). The association between quitting smoking and weight gain: A systematic review and meta-analysis of prospective cohort studies. *Obesity Reviews, 16*(10), 883–901. https://doi.org/10.1111/obr.12304

Tien, C. L., Lacroix, M., Ispas-Szabo, P., & Mateescu, M. (2003). N-acylated chitosan: Hydrophobic matrices for controlled drug release. *Journal of Controlled Release, 93*(1), 1–13. https://doi.org/10.1016/S0168-3659(03)00327-4

Tiwari, R. K., Sharma, V., Pandey, R. K., & Shukla, S. S. (2020). Nicotine addiction: Neurobiology and mechanism. *Journal of Pharmacopuncture, 23*(1), 1–7. https://doi.org/10.3831/kpi.2020.23.001

Tobacco & public health. (n.d.). Google Books. https://books.google.jo/books?id=yXQZEQAAQBAJ

Tolentino, S., Pereira, M. N., De Sousa, M. C., Cunha-Filho, M., Gelfuso, G. M., & Gratieri, T. (2020). The influence of sebaceous content on the performance of nanosystems designed for the treatment of follicular diseases. *Journal of Drug Delivery Science and Technology, 59*, 101895. https://doi.org/10.1016/j.jddst.2020.101895

Tonstad, S., Arons, C., Rollema, H., Berlin, I., Hajek, P., Fagerström, K., Els, C., McRae, T., & Russ, C. (2020). Varenicline: Mode of action, efficacy, safety and accumulated experience salient for clinical populations. *Current Medical Research and Opinion, 36*(5), 713–730. https://doi.org/10.1080/03007995.2020.1729708

Torres, J., Silva, R., Farias, G., Lobo, J. M. S., Ferreira, D. C., & Silva, A. C. (2024). Enhancing acute migraine treatment: Exploring solid lipid nanoparticles and nanostructured lipid carriers for the nose-to-brain route. *Pharmaceutics, 16*(10), 1297. https://doi.org/10.3390/pharmaceutics16101297

Tran, A. X., Ho, T. T., & Gupta, S. V. (2018). Role of CYP2B6 pharmacogenomics in bupropion-mediated smoking cessation. *Journal of Clinical Pharmacy and Therapeutics, 44*(2), 174–179. https://doi.org/10.1111/jcpt.12783

Trotsko, N., Miroslaw, B., Jasiński, R., Długosz, M., Sadczuk, M., & Demchuk, O. M. (2024). Efficient method of (S)-nicotine synthesis. *Molecules, 29*(23), 5731. https://doi.org/10.3390/molecules29235731

Tufail, A., Jiang, Y., & Cui, X. (2024). A review on the mucus dynamics in the human respiratory airway. *Biomechanics and Modeling in Mechanobiology*. Advance online publication. https://doi.org/10.1007/s10237-024-01898-4

Tulen, C. B. M., Opperhuizen, A., Van Schooten, F., & Remels, A. H. V. (2023). Disruption of the molecular regulation of mitochondrial metabolism in airway and lung epithelial cells by cigarette smoke: Are aldehydes the culprit? *Cells, 12*(2), 299. https://doi.org/10.3390/cells12020299

Turton, S., & Lingford-Hughes, A. (2020). Neurobiology and principles of addiction and tolerance. *Medicine, 48*(12), 749–753. https://doi.org/10.1016/j.mpmed.2020.09.012

Uemura, N., Onishi, T., Mitaniyama, A., Kaneko, T., Ninomiya, K., Nakamura, K., & Tateno, M. (2005). Bioequivalence and rapid absorption of zolmitriptan nasal spray compared with oral tablets in healthy Japanese subjects. *Clinical Drug Investigation, 25*(3), 199–208. https://doi.org/10.2165/00044011-200525030-00006

Ullah, F., Shah, K. U., Shah, S. U., Nawaz, A., Nawaz, T., Khan, K. A., Alserihi, R. F., Tayeb, H. H., Tabrez, S., & Alfatama, M. (2022). Synthesis, characterization and in vitro evaluation of chitosan nanoparticles physically admixed with lactose microspheres for pulmonary delivery of montelukast. *Polymers, 14*(17), 3564. https://doi.org/10.3390/polym14173564

Uskoković, V. (2012). Dynamic light scattering based microelectrophoresis: Main prospects and limitations. *Journal of Dispersion Science and Technology, 33*(12), 1762–1786. https://doi.org/10.1080/01932691.2011.625523

Vaezifar, S., Razavi, S., Golozar, M. A., Karbasi, S., Morshed, M., & Kamali, M. (2013). Effects of some parameters on particle size distribution of chitosan nanoparticles prepared by ionic gelation method. *Journal of Cluster Science, 24*(3), 891–903. https://doi.org/10.1007/s10876-013-0583-2

Vallés, A. S., & Barrantes, F. J. (2023). Nicotinic acetylcholine receptor dysfunction in addiction and in some neurodegenerative and neuropsychiatric diseases. *Cells, 12*(16), 2051. https://doi.org/10.3390/cells12162051

Van Amsterdam, J., Sleijffers, A., Van Spiegel, P., Blom, R., Witte, M., Van de Kassteele, J., Blokland, M., Steerenberg, P., & Opperhuizen, A. (2011). Effect of ammonia in cigarette tobacco on nicotine absorption in human smokers. *Food and Chemical Toxicology, 49*(12), 3025–3030. https://doi.org/10.1016/j.fct.2011.09.037

Van Poucke, C., Verdegem, E., Mangelinckx, S., & Stevens, C. V. (2024). Synthesis and unambiguous NMR characterization of linear and branched N-alkyl chitosan derivatives. *Carbohydrate Polymers, 337*, 122131. https://doi.org/10.1016/j.carbpol.2024.122131

Wagner, C., Wheeler, K., & Ribbeck, K. (2018). Mucins and their role in shaping the functions of mucus barriers. *Annual Review of Cell and Developmental Biology, 34*(1), 189–215. https://doi.org/10.1146/annurev-cellbio-100617-062818

Walsh, S. T., Cheng, R. P., Wright, W. W., Alonso, D. O., Daggett, V., Vanderkooi, J. M., & DeGrado, W. F. (2003). The hydration of amides in helices: A comprehensive picture from molecular dynamics, IR, and NMR. *Protein Science, 12*(3), 520–531. https://doi.org/10.1110/ps.0223003

Wang, B., He, C., Tang, C., & Yin, C. (2011). Effects of hydrophobic and hydrophilic modifications on gene delivery of amphiphilic chitosan-based nanocarriers. *Biomaterials, 32*(20), 4630–4638. https://doi.org/10.1016/j.biomaterials.2011.03.003

Wang, H., George, G., Bartlett, S., Gao, C., & Islam, N. (2017). Nicotine hydrogen tartrate-loaded chitosan nanoparticles: Formulation, characterization and in vitro delivery from dry powder inhaler formulation. *European Journal of Pharmaceutics and Biopharmaceutics, 113*, 118–131. https://doi.org/10.1016/j.ejpb.2016.12.023

Wang, H., Holgate, J., Bartlett, S., & Islam, N. (2020). Assessment of nicotine release from nicotine-loaded chitosan nanoparticles dry powder inhaler formulations via locomotor activity of C57BL/6 mice. *European Journal of Pharmaceutics and Biopharmaceutics, 154*, 175–185. https://doi.org/10.1016/j.ejpb.2020.07.011

Wang, L., Shi, Y., Jiang, J., Li, C., Zhang, H., Zhang, X., Jiang, T., Wang, L., Wang, Y., & Feng, L. (2022). Micro-nanocarriers-based drug delivery technology for blood–brain barrier crossing and brain tumor-targeting therapy. *Small, 18*(45), Article 2203678. https://doi.org/10.1002/smll.202203678

Wang, L. C., Chen, X. G., Liu, C. S., Li, P. W., & Zhou, Y. M. (2008). Dissociation behaviors of carboxyl and amine groups on carboxymethyl-chitosan in aqueous system. *Journal of Polymer Science Part B: Polymer Physics, 46* (14), 1419–1429. https://doi.org/10.1002/polb.21475

Wang, W., Meng, Q., Li, Q., Liu, J., Zhou, M., Jin, Z., & Zhao, K. (2020). Chitosan derivatives and their application in biomedicine. *International Journal of Molecular Sciences, 21*(2), 487. https://doi.org/10.3390/ijms21020487

Wang, Z. (2003). New developments in transmission electron microscopy for nanotechnology. *Advanced Materials, 15*(18), 1497–1514. https://doi.org/10.1002/adma.200300384

Washington, N., Steele, R., Jackson, S., Bush, D., Mason, J., Gill, D., Pitt, K., & Rawlins, D. (2000). Determination of baseline human nasal pH and the effect of intranasally administered buffers. *International Journal of Pharmaceutics, 198*(2), 139–146. https://doi.org/10.1016/S0378-5173(99)00442-1

Watchorn, J., Clasky, A. J., Prakash, G., Johnston, I. A. E., Chen, P. Z., & Gu, F. X. (2022). Untangling mucosal drug delivery: Engineering, designing, and testing nanoparticles to overcome the mucus barrier. *ACS Biomaterials Science & Engineering, 8*(4), 1396–1426. https://doi.org/10.1021/acsbiomaterials.2c0004

Wei, W., Zhou, Y., Chang, H., & Yeh, J. (2014). Antibacterial and miscibility properties of chitosan/collagen blends. *Journal of Macromolecular Science, Part B, 54*(2), 143–158. https://doi.org/10.1080/00222348.2014.987097

Wen, P., & Ren, C. (2024). Research progress on intranasal treatment for Parkinson's disease. *Neuroprotection, 2*(2), 79–99. https://doi.org/10.1002/nep3.42

Weng, J., Durand, A., & Desobry, S. (2023). Chitosan-based particulate carriers: Structure, production and corresponding controlled release. *Pharmaceutics, 15*(5), 1455. https://doi.org/10.3390/pharmaceutics15051455

Whitsett, J. A. (2018). Airway epithelial differentiation and mucociliary clearance. *Annals of the American Thoracic Society, 15*(Suppl. 3), S143–S148. https://doi.org/10.1513/AnnalsATS.201802-128AW

Williams, M., To, A., Bozhilov, K., & Talbot, P. (2015). Strategies to reduce tin and other metals in electronic cigarette aerosol. *PLOS ONE, 10*(9), e0138933. https://doi.org/10.1371/journal.pone.0138933

Williams, R. O., Reynolds, T. D., Cabelka, T. D., Sykora, M. A., & Mahaguna, V. (2002). Investigation of excipient type and level on drug release from controlled-release tablets containing HPMC. *Pharmaceutical Development and Technology, 7*(2), 181–193. https://doi.org/10.1081/PDT-120003486

Wills, L., & Kenny, P. J. (2021). Addiction-related neuroadaptations following chronic nicotine exposure. *Journal of Neurochemistry, 157*(5), 1652–1673. https://doi.org/10.1111/jnc.15356

Wilson, B., Alobaid, B. N. M., Geetha, K. M., & Jenita, J. L. (2020). Chitosan nanoparticles to enhance nasal absorption and brain targeting of sitagliptin to treat Alzheimer's disease. *Journal of Drug Delivery Science and Technology, 61*, 102176. https://doi.org/10.1016/j.jddst.2020.102176

Wolff, K., White, J., & Karch, S. (Eds.). (2016). *The SAGE handbook of drug & alcohol studies*. SAGE Publications. https://doi.org/10.4135/9781473922143

World Health Organization. (2018). *WHO global report on trends in prevalence of tobacco smoking 2000–2025*. https://escholarship.org/uc/item/4dc4t5d9

World Health Organization. (2021). *WHO report on the global tobacco epidemic, 2021: Addressing new and emerging products*. https://www.who.int/publications/i/item/9789240032095

World Health Organization. (2024, June 2). *Global investment case for tobacco control: Summary of evidence*. https://fctc.who.int/docs/librariesprovider12/side-events/global-investment-case-presentation-02-06-2024.pdf

World Health Organization. (2025, June 25). *Tobacco*. https://www.who.int/news-room/fact-sheets/detail/tobacco

Wu, A. D., Gao, M., Aveyard, P., & Taylor, G. (2023). Smoking cessation and changes in anxiety and depression in adults with and without psychiatric disorders. *JAMA Network Open, 6*(5), e2316111. https://doi.org/10.1001/jamanetworkopen.2023.16111

Wu, D., Chen, Q., Chen, X., Han, F., Chen, Z., & Wang, Y. (2023). The blood–brain barrier: Structure, regulation and drug delivery. *Signal Transduction and Targeted Therapy, 8*(1), Article 217. https://doi.org/10.1038/s41392-023-01481-w

Wu, J., Wang, Y., Yang, H., Liu, X., & Lu, Z. (2017). Preparation and biological activity studies of resveratrol-loaded ionically cross-linked chitosan-TPP nanoparticles. *Carbohydrate Polymers*, *175*, 170–177. https://doi.org/10.1016/j.carbpol.2017.07.058

Wu, M., Long, Z., Xiao, H., & Dong, C. (2017). Preparation of N,N,N-trimethyl chitosan via a novel approach using dimethyl carbonate. *Carbohydrate Polymers*, *169*, 83–91. https://doi.org/10.1016/j.carbpol.2017.03.043

Xiao, C., Zhou, C., Jiang, J., & Yin, C. (2020). Neural circuits and nicotinic acetylcholine receptors mediate the cholinergic regulation of midbrain dopaminergic neurons and nicotine dependence. *Acta Pharmacologica Sinica*, *41*(1), 1–9. https://doi.org/10.1038/s41401-019-0299-4

Xu, J., Liu, L., Yu, J., Zou, Y., Wang, Z., & Fan, Y. (2019). DDA (degree of deacetylation) and pH-dependent antibacterial properties of chitin nanofibers against *Escherichia coli*. *Cellulose*, *26*(4), 2279–2290. https://doi.org/10.1007/s10570-019-02287-2

Xu, X., Shrestha, S. S., Trivers, K. F., Neff, L. J., Armour, B. S., & King, B. A. (2021). U.S. healthcare spending attributable to cigarette smoking in 2014. *Preventive Medicine*, *150*, 106529. https://doi.org/10.1016/j.ypmed.2021.106529

Xu, Y., & Du, Y. (2002). Effect of molecular structure of chitosan on protein delivery properties of chitosan nanoparticles. *International Journal of Pharmaceutics*, *250*(1), 215–226. https://doi.org/10.1016/S0378-5173(02)00548-3

Xu, Z., Zhang, T., Hu, H., Liu, W., Xu, P., & Tang, H. (2023). Characterization on nicotine degradation and research on heavy metal resistance of a strain *Pseudomonas* sp. NBB. *Journal of Hazardous Materials*, *459*, 132145. https://doi.org/10.1016/j.jhazmat.2023.132145

Yang, J., Patel, M., Nikanjam, M., Capparelli, E. V., Tsunoda, S. M., Greenberg, H. E., Penzak, S. R., Stoch, S. A., Bertino, J. S., Nafziger, A. N., & Greenblatt, D. J. (2018). Midazolam single time point concentrations to estimate exposure and cytochrome P450 (CYP) 3A constitutive activity utilizing limited sampling strategy with a population pharmacokinetic approach. *The Journal of Clinical Pharmacology*, *58*(9), 1205–1213. https://doi.org/10.1002/jcph.1125

Yang, Y., Cheng, J., Garamus, V. M., Li, N., & Zou, A. (2018). Preparation of an environmentally friendly formulation of the insecticide nicotine hydrochloride through encapsulation in chitosan/tripolyphosphate nanoparticles. *Journal of*

Agricultural and Food Chemistry, 66(5), 1067–1074. https://doi.org/10.1021/acs.jafc.7b04147

Yeap, S. P., Lim, J., Ngang, H. P., Ooi, B. S., & Ahmad, A. L. (2018). Role of particle–particle interaction towards effective interpretation of Z-average and particle size distributions from dynamic light scattering (DLS) analysis. *Journal of Nanoscience and Nanotechnology, 18*(10), 6957–6964. https://doi.org/10.1166/jnn.2018.15458

Yeh, T., Hsu, L., Tseng, M. T., Lee, P., Sonjae, K., Ho, Y., & Sung, H. (2011). Mechanism and consequence of chitosan-mediated reversible epithelial tight junction opening. *Biomaterials, 32*(26), 6164–6173. https://doi.org/10.1016/j.biomaterials.2011.03.056

Yen, S., & Tan, A. (2021). Cigarette consumption patterns of non-smokers, occasional smokers, and daily smokers in selected ASEAN countries. *Asian Pacific Journal of Cancer Prevention, 22*(7), 1997–2004. https://doi.org/10.31557/APJCP.2021.22.7.1997

Yoksan, R., Akashi, M., Biramontri, S., & Chirachanchai, S. (2001). Hydrophobic chain conjugation at hydroxyl group onto γ-ray irradiated chitosan. *Biomacromolecules, 2*(3), 1038–1044. https://doi.org/10.1021/bm0155569

Yousfan, A., Rubio, N., Natouf, A. H., Daher, A., Al-Kafry, N., Venner, K., & Kafa, H. (2020). Preparation and characterisation of PHT-loaded chitosan lecithin nanoparticles for intranasal drug delivery to the brain. *RSC Advances, 10*(48), 28992–29009. https://doi.org/10.1039/D0RA04890A

Yu, L. (2001). Amorphous pharmaceutical solids: Preparation, characterization and stabilization. *Advanced Drug Delivery Reviews, 48*(1), 27–42. https://doi.org/10.1016/S0169-409X(01)00098-9

Yun, H. J., Lim, J., Fuhr, A. S., Makarov, N. S., Keene, S., Law, M., Pietryga, J. M., & Klimov, V. I. (2018). Charge-transport mechanisms in $CuInSe_xS_{2-x}$ quantum-dot films. *ACS Nano, 12*(12), 12587–12596. https://doi.org/10.1021/acsnano.8b07179

Yun, P., Devahastin, S., & Chiewchan, N. (2021). Microstructures of encapsulates and their relations with encapsulation efficiency and controlled release of bioactive constituents: A review. *Comprehensive Reviews in Food Science and Food Safety, 20*(2), 1768–1799. https://doi.org/10.1111/1541-4337.12701

Yie., Ranaweera, S., Zou, D., Cameron, A. P., Chen, X., Song, H., & Zhao, C. (2022). Improved enzyme thermal stability, loading and bioavailability using alginate encapsulation. *Food Hydrocolloids, 137*, 108385. https://doi.org/10.1016/j.foodhyd.2022.108385

Zawadzki, J., & Kaczmarek, H. (2009). Thermal treatment of chitosan in various conditions. *Carbohydrate Polymers, 80*(2), 394–400. https://doi.org/10.1016/j.carbpol.2009.11.037

Zbar, A. (2024). The arterial circulation. In *Anatomy—Head and neck* (pp. 187–208). Springer. https://doi.org/10.1007/978-3-031-69538-4_9

Zeng, L., An, L., & Wu, X. (2011). Modeling drug–carrier interaction in the drug release from nanocarriers. *Journal of Drug Delivery, 2011*, 1–15. https://doi.org/10.1155/2011/370308

Zeng, W., Hui, H., Liu, Z., Chang, Z., Wang, M., He, B., & Hao, D. (2021). TPP ionically cross-linked chitosan/PLGA microspheres for the delivery of NGF for peripheral nerve system repair. *Carbohydrate Polymers, 258*, 117684. https://doi.org/10.1016/j.carbpol.2021.117684

Zhang, H., Bahamondez-Canas, T. F., Zhang, Y., Leal, J., & Smyth, H. D. (2018). PEGylated chitosan for nonviral aerosol and mucosal delivery of the CRISPR/Cas9 system *in vitro*. *Molecular Pharmaceutics, 15*(11), 4814–4826. https://doi.org/10.1021/acs.molpharmaceut.8b00434

Zhang, H., Lin, C., & Donovan, M. D. (2012). Correlation between nasal membrane permeability and nasal absorption rate. *AAPS PharmSciTech, 14*(1), 60–63. https://doi.org/10.1208/s12249-012-9884-2

Zhang, J., Chen, Z. K., Triatin, R. D., Snieder, H., Thio, C. H. L., & Hartman, C. A. (2024). Mediating pathways between attention deficit hyperactivity disorder and type 2 diabetes mellitus: Evidence from a two-step and multivariable Mendelian randomization study. *Epidemiology and Psychiatric Sciences, 33*, Article e0593. https://doi.org/10.1017/S2045796024000593

Zhang, J., Ou, J., & Bai, C. (2011). Tobacco smoking in China: Prevalence, disease burden, challenges, and future strategies. *Respirology, 16*(8), 1165–1172. https://doi.org/10.1111/j.1440-1843.2011.02062.x

Zhang, R., Zhang, L., Li, P., Pang, K., Liu, H., & Tian, L. (2023). Epithelial barrier in the nasal mucosa, related risk factors and diseases. *International Archives of Allergy and Immunology, 184*(5), 481–501. https://doi.org/10.1159/000528969

Zhang, S., Arshad, M., & Ullah, A. (2015). Drug encapsulation and release behavior of telechelic nanoparticles. *Nanotechnology, 26*(41), 415703. https://doi.org/10.1088/0957-4484/26/41/415703

Zhang, S., Fu, Q., Zhang, Y., Pan, J., Zhang, L., Zhang, Z., & Liu, Z. (2021). Surface loading of nanoparticles on engineered or natural erythrocytes for prolonged circulation time: Strategies and applications. *Acta Pharmacologica Sinica, 42*(7), 1040–1054. https://doi.org/10.1038/s41401-020-00606-z

Zhang, X., Sun, Y., Cheung, Y. T. D., Wang, M. P., Wu, Y. S., Chak, K. Y., Chen, J., Leung, L. T., Lam, T. H., & Ho, S. Y. (2023). Cigarettes, heated tobacco products and dual use: Exhaled carbon monoxide, saliva cotinine and total tobacco consumed by Hong Kong tobacco users. *Tobacco Control, 33*(4), 457–463. https://doi.org/10.1136/tc-2022-057598

Zhang, Y., Xu, D., Bai, L., Zhou, Y., Zhang, H., & Cui, Y. (2022). A review of non-invasive drug delivery through respiratory routes. *Pharmaceutics, 14*(9), 1974. https://doi.org/10.3390/pharmaceutics14091974

Zhao, J., Li, J., Jiang, Z., Tong, R., Duan, X., Bai, L., & Shi, J. (2020). Chitosan, N,N,N-trimethyl chitosan (TMC) and 2-hydroxypropyltrimethyl ammonium chloride chitosan (HTCC): The potential immune adjuvants and nanocarriers. *International Journal of Biological Macromolecules, 154* , 339–348. https://doi.org/10.1016/j.ijbiomac.2020.03.065

Zhou, W., Li, C., Wang, Z., Zhang, W., & Liu, J. (2016). Factors affecting the stability of drug-loaded polymeric micelles and strategies for improvement. *Journal of Nanoparticle Research, 18*(9), Article 3583. https://doi.org/10.1007/s11051-016-3583-y

Zhu, D., Zhao, G., & Wang, X. (2021). Association of smoking and smoking cessation with overall and cause-specific mortality. *American Journal of Preventive Medicine, 60*(4), 504–512. https://doi.org/10.1016/j.amepre.2020.11.003

Zia, K. M. (2025). Characterization techniques for chitosan nanoparticles and derivatives. In *Smart nanomaterials technology* (pp. 135–176). Springer. https://doi.org/10.1007/978-981-96-2629-8_6

Ziedonis, D., Cimpeanu, C., Bachyrycz, A., Morelli, E., & Rancans, E. (2024). Disorders due to substance use: Nicotine. In *Textbook of addiction treatment: International perspectives* (pp. 2729–2779). Springer. https://doi.org/10.1007/978-3-030-51366-5_13

APPENDICES

APPENDIX 1

FTIR Phthaloyl CS

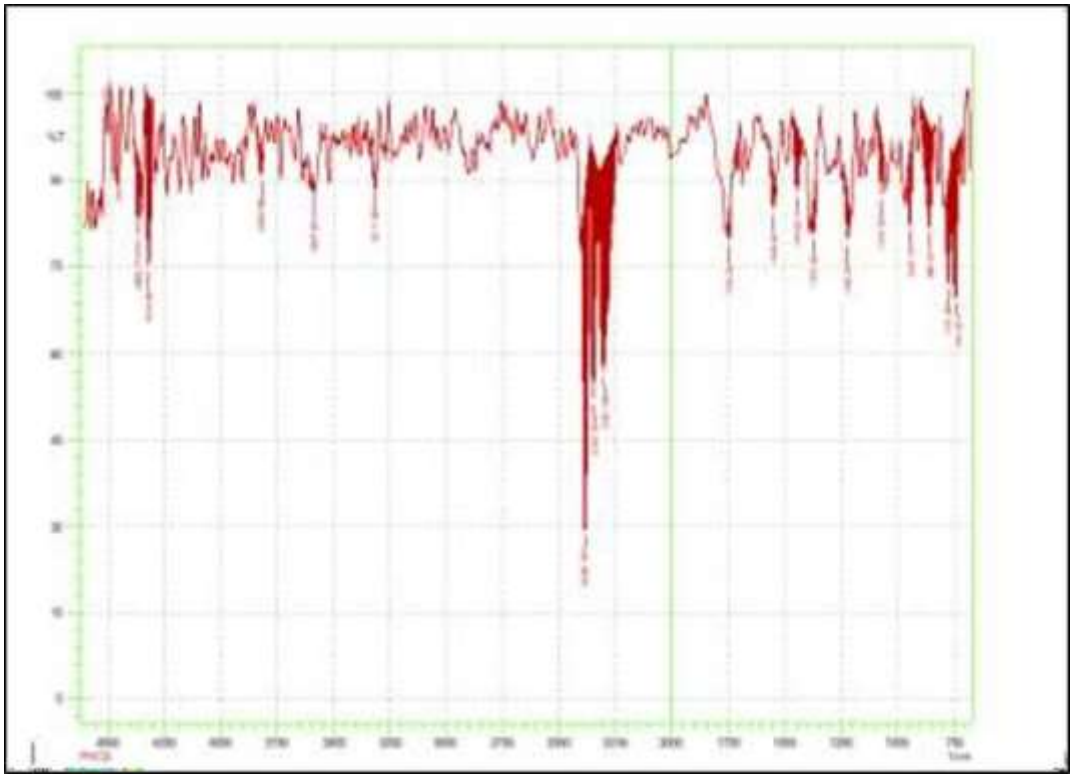

APPENDIX 2

^{1}H NMR Phythaloyl CS

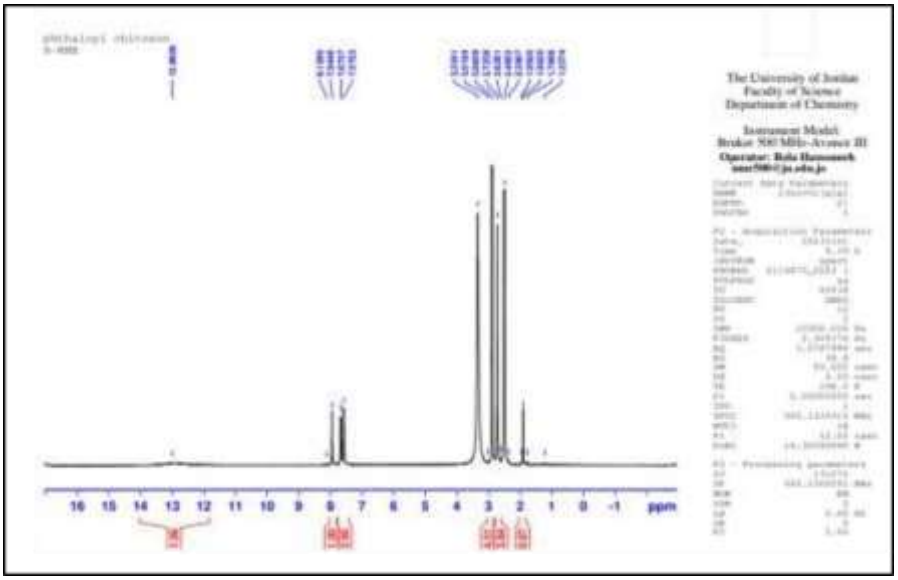

APPENDIX 3

^{13}C NMR Phthaloyl CS

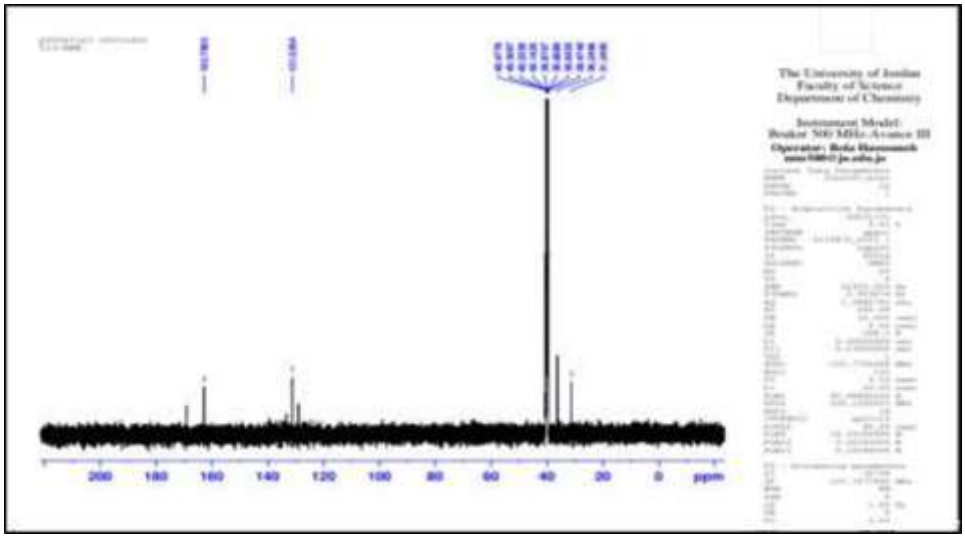

APPENDIX 4

FTIR BG Phthaloyl CS

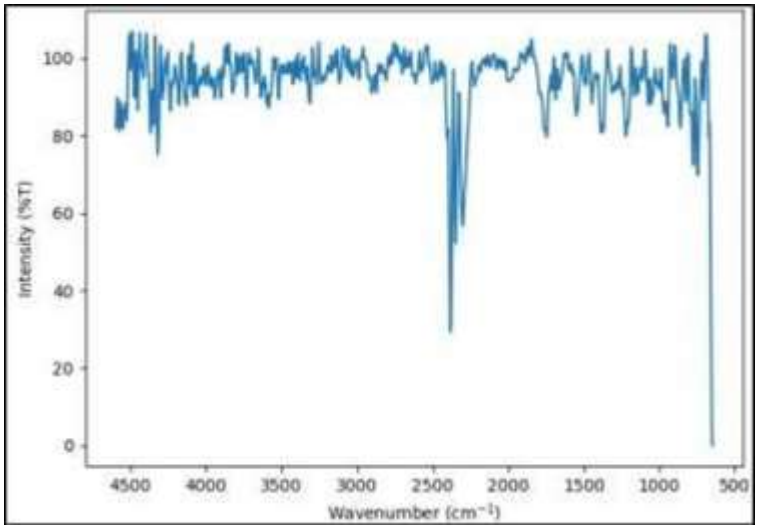

APPENDIX 5

^{1}H NMR BG Phthaloyl CS

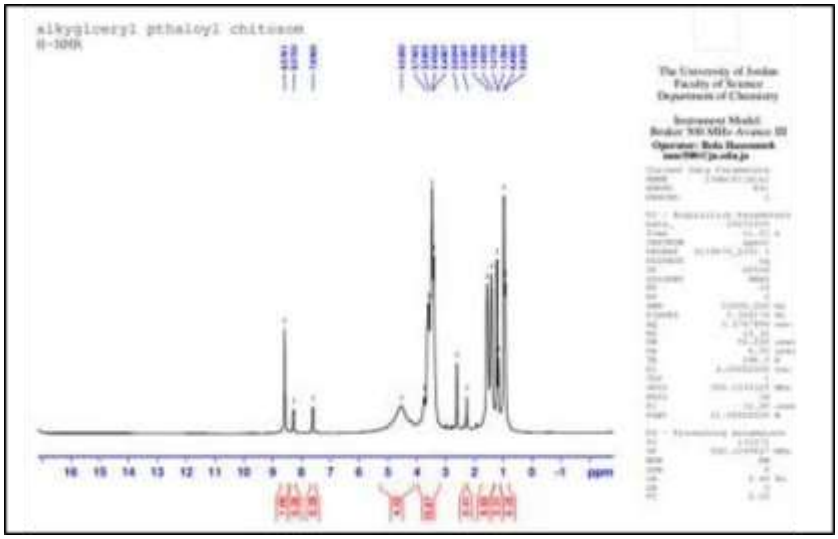

APPENDIX 6

^{13}C NMR BG Phthaloyl CS

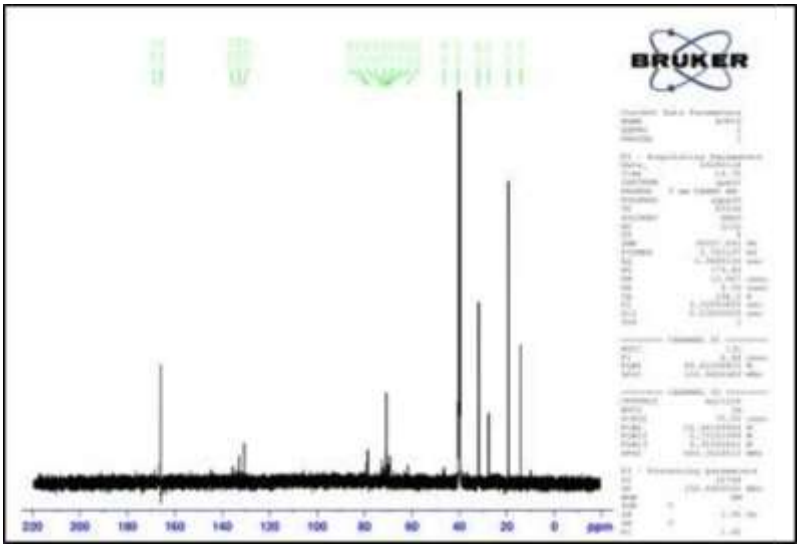

APPENDIX 7

FTIR BG-CS

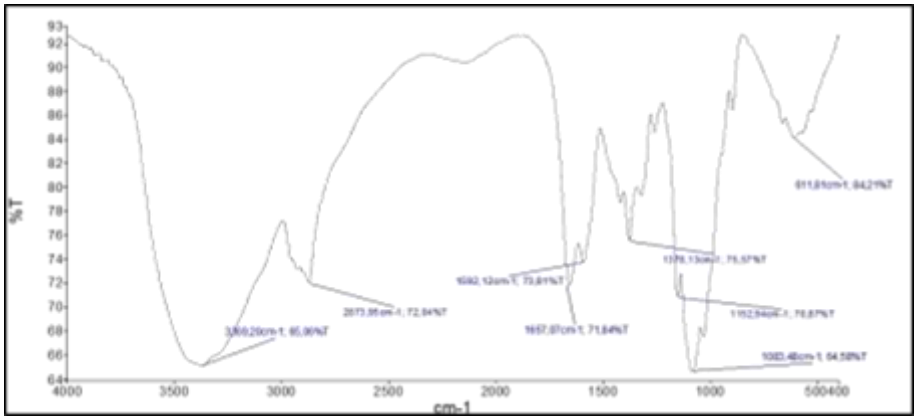

APPENDIX 8

^{1}H NMR BG-CS

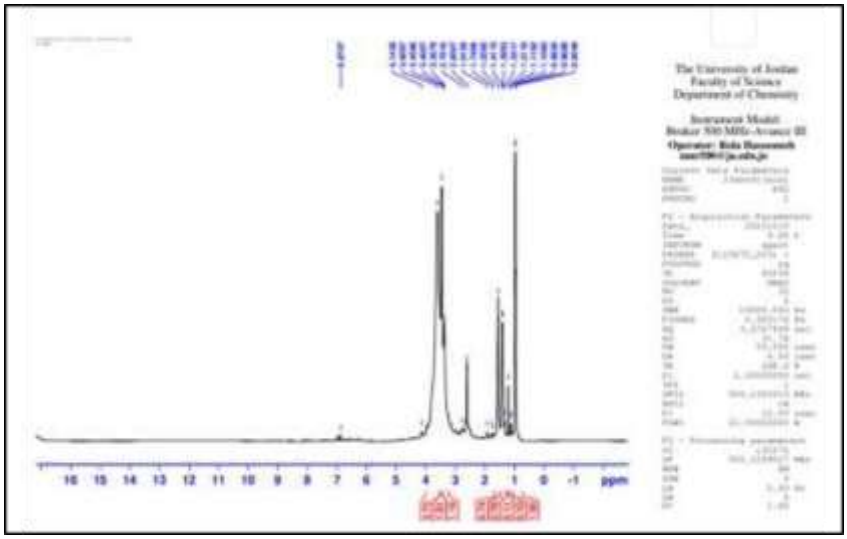

APPENDIX 9

^{13}C NMR BG-CS

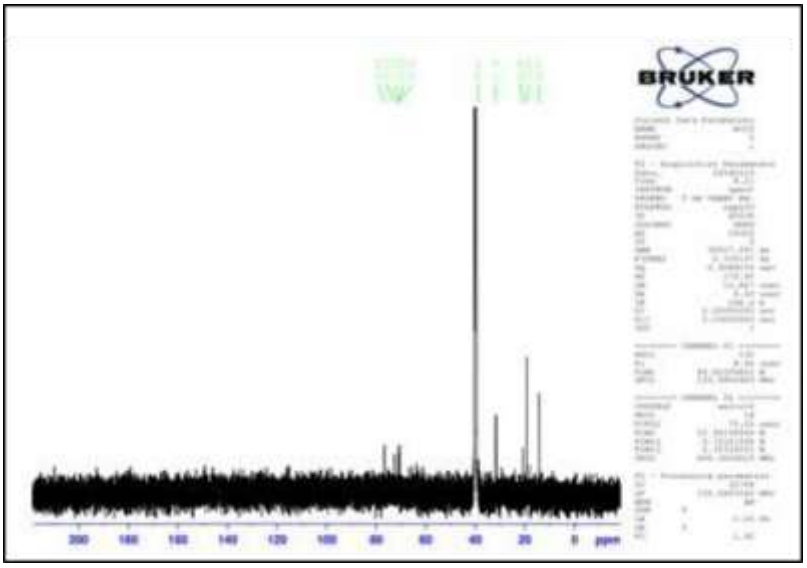

AUTHOR'S PROFILE



Wasan Ibrahim Alwahsh obtained her Bachelor of Pharmacy in 2007 from Alzaytoonah University Amman, Jordan. She obtained her MSc in Pharmacutical Science in 2020 from the same university. She attended the summer school students for polymer chemistry research in Isas College Dortmund in Germany from 2018-2019. She is a trained pharmacist in Jordan Pharmacutical Association, particularly in the critical area of asthma control management within the respiratory system. She is also a researcher at the School of Pharmacy, University of Jordan in the field of controlled drug delivery, chitosan beads, and the characterization of pharmaceutical materials.

LIST OF PUBLICATIONS:

Alwahsh, W., Sahudin, S., Alkhatib, H. *et al.* Nicotine Chitosan Nanoparticles for Sustained Release Intranasal Delivery: Development, Evaluation and Pharmacokinetics Studies. *J Pharm Innov* ; 21, 114 (2026). https://doi.org/10.1007/s12247-025-10308-w . (WoS Q2)

Alwahsh, W., Sahudin, S., Alkhatib, H., Bostanudin, M. F., & Alwahsh, M. (2024). Chitosan-Based Nanocarriers for Pulmonary and Intranasal Drug Delivery Systems: A Comprehensive Overview of their Applications. *Current Drug Targets,* *25*(7), 492–511. https://doi.org/10.2174/0113894501301747240417103321 . (WoS Q3)

Alwahsh, W., Sahudin, S., Alkhatib, H. et al. “Modified Butylglycerol Nanoparticle for Intranasal Sustained Delivery of Nicotine” (Under review in PLOS ONE Journal) (WoS Q2)